DEGREE PROJECT

Accessibility Studies of Potentially Hazardous Asteroids from the Sun-Earth L2 Libration Point

GAUTHAM GANESAN

Space Engineering, master's level (120 credits)
2020

Luleå University of Technology
Department of Computer Science, Electrical and Space Engineering

LULEÅ UNIVERSITY OF TECHNOLOGY

CRANFIELD UNIVERSITY

GAUTHAM GANESAN

ACCESSIBILITY STUDIES OF POTENTIALLY HAZARDOUS ASTEROIDS FROM THE SUN-EARTH L2 LIBRATION POINT

SCHOOL OF AEROSPACE, TRANSPORT AND MANUFACTURING
MSc in Astronautics and Space Engineering

MSc
Academic Year: 2019 – 2020

Supervisor: Dr. Marta Ceccaroni
September 2020

CRANFIELD UNIVERSITY

SCHOOL OF AEROSPACE, TRANSPORT AND MANUFACTURING
MSc in Astronautics and Space Engineering

MSc

Academic Year 2019 - 2020

GAUTHAM GANESAN

Accessibility studies of Potentially Hazardous Asteroids from the Sun – Earth L2 Libration Point

Supervisor: Dr. Marta Ceccaroni
September 2020

This thesis is submitted in partial (45%) fulfilment of the requirements for the degree of MSc in Astronautics and Space Engineering

© Cranfield University 2020. All rights reserved. No part of this publication may be reproduced without the written permission of the copyright owner.

ABSTRACT

A newly proposed F-class mission by the European Space Agency (ESA) in 2019, Comet Interceptor, aims to dynamically intercept a New Solar System Object such as a Dynamically New Comet (DNC). The Spacecraft will be placed in a periodic (Halo) orbit around the Sun-Earth L2 Lagrangian point, waiting for further instructions about the passage of a comet or an asteroid, which could well be reached within the stipulated mission constraints.

A major part of the detection of these bodies will be owed to the Large Synoptic Survey Telescope (Currently under construction in Chile), which hopes to vastly increase the ability to discover a possible target using the catalogue of Long Period Comets and a set of its orbits. It is suggested that, in a mission length of <5 years, discoveries and warnings are possible so that optimization of the trajectory and characterisation of the object are done within the set windows.

This thesis is aimed at facilitating a transfer to a Potentially Hazardous Asteroid (PHA), a subset of the Near-Earth Objects (NEO), as a secondary choice on the off-chance that the discovered comet could not be reached from the L2 Libration point within the mission constraints.

The first section of this thesis deals with the selection of a Potentially Hazardous Asteroid for our mission from the larger database of the Near-Earth Objects, based on a measure of impact hazard called the Palermo Scale, while the second section of the thesis aims to obtain a suitable Halo orbit around L2 through an analytical construction method. After a desired orbit is found, the invariant manifolds around the Halo orbit are constructed and analysed in an attempt to reduce the ΔV, where from the spacecraft can intercept the Potentially Hazardous Asteroid through the trajectory demanding the least energy.

Keywords:

Near-Earth Objects, Potentially Hazardous Asteroids, Halo Orbit, Invariant Manifolds, Analytical construction, Palermo Scale, Low-Energy transfer

ACKNOWLEDGEMENTS

Firstly, I would like to thank Luleå University of Technology and Cranfield University for being a part of the SpaceMaster consortium, and for giving me the opportunity to pursue a dual Master’s degree in Space Science and Technology and Astronautics and Space Engineering.

I would like to thank my family and everyone involved in the 2 Universities and their administrations for paving a smooth passage to pursue my studies.

Lastly, I would like to acknowledge with gratitude and thanks, the support and contributions of my supervisor, Dr. Marta Ceccaroni, without whom this project would not have taken its final shape.

TABLE OF CONTENTS

ABSTRACT ii
ACKNOWLEDGEMENTS........ iv
LIST OF FIGURES........ vii
LIST OF TABLES........ x
LIST OF TABLES (APPENDIX)........ xi
LIST OF ABBREVIATIONS........ xii
1 Introduction........ 13
1.1 ESA Comet Interceptor........ 14
1.1.1 Mission Specifications and Constraints........ 14
1.2 Introduction to Halo Orbits 15
1.3 Thesis Breakdown 17
2 . Potentially Hazardous Asteroids........ 19
3 . Background 22
3.1 N-Body Problem........ 22
3.2 Circular Restricted Three-Body Problem 24
3.2.1 Non-Dimensionalisation of measured quantities 25
3.2.2 Reference Frames 27
3.2.3 Equations of motion in the CR3BP........ 32
3.3 Libration Points........ 36
3.3.1 Jacobi constant and Zero-velocity curves 41
4 Construction of Halo Orbits and Invariant manifolds 45
4.1 Third-Order Approximation for Halo orbits 45
4.2 State Transition Matrix (STM) 52
4.3 Differential Correction 55
4.3.1 Single Shooting Method 58
4.4 Generation of Halo orbit........ 61
4.5 Stablility of the Halo orbit 65
4.6 Creation of Invariant Manifolds 70
5 Delta-V results and Transfer Trajectories........ 76
5.1 Direct Transfer from the Halo orbit........ 77
5.2 Manifold to Asteroid transfer 84
5.2.1 Unstable Manifold 1 (Away from the Sun-Earth system)........ 84
5.2.2 Unstable Manifold 2 (Towards from the Sun-Earth system)........ 89
6 Conclusions........ 92
6.1 Future Work 93
REFERENCES........ 95
7 APPENDICES 99

LIST OF FIGURES

Figure 1.1: Family of Halo orbits around Sun-Earth L2 Libration point 16

Figure 2.1: Number of NEAs discovered from 1990 by different surveys; Source: [18] 19

Figure 2.2: PHAs split according the values of its Palermo Scale 20

Figure 3.1: Representation of the N-Body Problem; Source: [22]..................... 23

Figure 3.2: Heliocentric Reference Frame 28

Figure 3.3: Barycentric Inertial Reference Frame 29

Figure 3.4: Rotating Reference Frame 30

Figure 3.5: Representation of a Circular Restricted 3 Body Problem (CR3BP); Source: [22] 33

Figure 3.6: Representation of the libration points in the Sun-Earth system 40

Figure 3.7: A zoomed-in view of the L1 and L2 Lagrangian points with Earth .. 40

Figure 3.8: Zero-Velocity curves for conditions $C>C_{L1}$ (Left) and $C = C_{L1}$ (Right); Source: [31] 43

Figure 3.9: Zero-Velocity curves for conditions $C_{L1} > C > C_{L2}$ (Left) and $C_{L2} > C > C_{L3}$ (Right); Source: [31] 44

Figure 3.10: Zero-Velocity curves for conditions $C_{L3} = C$ (Left) and $C_{L3} > C > C_{L4,5}$ (Right); Source: [31] 45

Figure 4.1: The X-Y plane of the trajectory obtained using the initial guess from the Richardson method.. 51

Figure 4.2: The 3D view of the trajectory obtained using the initial guess from the Richardson method 51

Figure 4.3: The initial conditions propagated for half the time-period (T/2), resulting in a partial halo.. 64

Figure 4.4: The 3D view of the complete periodic halo orbit of $\boldsymbol{Az = 611000\ km}$ 64

Figure 4.5: The desired halo orbit in the X-Y plane 65

Figure 4.6: The X-Z (Left) and Y-Z (Right) views of the complete Halo orbit.... 65

Figure 4.7: Unstable manifolds in the X-Y plane, for a halo orbit of A_z = 611000 km... 72

Figure 4.8: Three-Dimensional view of the unstable manifolds, for a halo orbit of A_z = 611000 km 73

Figure 4.9: Stable manifolds in the X-Z plane, for a halo orbit of A_z = 611000 km 74

Figure 4.10: Three-Dimensional view of the stable manifolds, for a halo orbit of A_z = 611000 km 74

Figure 4.11: The invariant manifolds of the halo orbit in the Y-Z axis (Left) and X-Y axis (Right) 75

Figure 4.12:The Three-Dimensional view of the invariant manifolds of the halo orbit 75

Figure 5.1: Halo orbit in the Heliocentric Reference Frame for 1 complete rotation of the halo (179 days) (3D view) 79

Figure 5.2: Halo orbit in the Heliocentric Reference Frame for 1 complete rotation of the halo (179 days) 80

Figure 5.3: Halo orbit in the Heliocentric Reference Frame for the first departure window (359 days) 80

Figure 5.4: Halo orbit in the Heliocentric Reference Frame for the first departure window (359 days) (Demonstrating the shape) 81

Figure 5.5: Halo orbit in the Heliocentric Reference Frame for the first departure window (359 days) (View of the start and end of window) 81

Figure 5.6: The transfer trajectory, along with the orbits of the Halo and Earth around the sun; (In picture: Blue star – Departure point at Halo orbit; Green star – Arrival point at Asteroid; Pink – Asteroid's orbit) 83

Figure 5.7: The transfer trajectory in the X-Y plane 83

Figure 5.8: The unstable manifold of a point in the halo orbit in the Heliocentric Reference Frame (In picture: Red – Halo point from where the manifold is propagated; Green – Unstable manifold) 85

Figure 5.9: The 3D view of the unstable manifold of a point in the halo orbit in the Heliocentric Reference Frame 85

Figure 5.10: The Y-Z view of the unstable manifolds from 5 points of the Halo orbit in the Heliocentric Reference Frame 86

Figure 5.11: The 3D view of the unstable manifolds from 5 points of the Halo orbit in the Heliocentric Reference Frame 86

Figure 5.12: The transfer trajectory, along with the orbits of the Halo and Earth around the sun; (In picture: Blue star – Departure point at a point in the Unstable Manifold 1; Green star – Arrival point at Asteroid; Pink – Asteroid's orbit) 88

Figure 5.13: The transfer trajectory in the 3D view 88

Figure 5.14: The unstable manifold of a point in the halo orbit in the Heliocentric Reference Frame (In picture: Red – Halo point from where the manifold is propagated; Pink – Unstable manifold 2) 89

Figure 5.15: The 3D view of the unstable manifold 2 of a point in the halo orbit in the Heliocentric Reference Frame 90

Figure 5.16: The Y-Z view of the unstable manifolds 2 from 5 points of the Halo orbit in the Heliocentric Reference Frame 90

Figure 5.17: The 3D view of the unstable manifolds 2 from 5 points of the Halo orbit in the Heliocentric Reference Frame 91

LIST OF TABLES

Table 2-1: PHAs sorted based on the Palermo Scale 21

Table 2-2: PHAs with the ∆V in km/s... 22

Table 3-1: Normalized parameters for a CR3BP in the Sun-Earth system....... 27

Table 3-2: Positions of the 5 libration points in the Sun-Earth system (Units: Non-Dimensional).. 39

Table 3-3: Effective Potentials and Jacobi Constants of the Libration points in the Sun-Earth system 42

Table 4-1: Initial conditions for a Halo orbit of $\boldsymbol{Az}$=611000 km, computed from the Third-order approximation method 49

Table 4-2: Initial conditions of the Halo orbit after conversion from the L2-centered reference frame to the Rotating Reference Frame 50

Table 4-3: Initial conditions of the required Halo orbit after using differential correction (Single Shooting Method) 63

Table 4-4: The [6x6] monodromy matrix for the desired halo orbit near the L2 system 68

Table 4-5: The eigenvectors of the [6x6] monodromy matrix for the desired halo orbit near the L2 system 69

Table 5-1: Values of the $\boldsymbol{\Delta v}$ and the corresponding departure and arrival dates for transfer between the halo orbit and Asteroid for the 6 departure windows 82

Table 5-2: The calculated minimum values of $\boldsymbol{\Delta v}$, the associated departure and arrival dates for the points in the Unstable manifold 1, for every departure window... 87

Table 5-3: The calculated minimum values of $\boldsymbol{\Delta v}$, the associated departure and arrival dates for the points in the Unstable manifold 2, for every departure window... 91

LIST OF TABLES (APPENDIX)

Table A-1: Values of the constants in the Richardson method for a halo orbit of A_z= 611000 km in the Sun-Earth system 104

Table B-1: Potentially Hazardous Asteroid properties database 137

Table B-2: PHAs with their Keplerian Elements 170

LIST OF ABBREVIATIONS

AU	Astronomical Unit
CR3BP	Circular Restricted 3-Body Problem
ESA	European Space Agency
GMAT	General Mission Analysis Tool
IP	Impact Probability
ISEE-3	International Sun-Earth Explorer-3
JD	Julian Day
LSST	Large Synoptic Survey Telescope
MJD	Modified Julian Day
MOID	Minimum Orbit Intersection Distance
NASA	National Aeronautics and Space Administration
ND	Non-Dimensional
NEA	Near-Earth Asteroid
NEO	Near-Earth Object
PHA	Potentially Hazardous Asteroid
STK	System ToolKit

1 Introduction

The number of asteroids and comets orbiting the sun is enormous, and only a tiny fraction of this group has paths that get them closer to our Earth. This collection of planetary bodies, called the Near Earth Objects, range in size from small pebbles to mountains [1]. Exploration of planet Earth has led to several findings regarding the topology of its surface, including the discovery of surfaces scarred with craters, which serve as proof of projectile bombardment. [2] states that while the initial planetary accretion with heavy bombardment ended around 3.8×10^9 years ago, a rain of impacts has always been there ever since at a steady rate, testifying for the impact scars that are distinguishable from the cracks and scars caused by erosion and tectonics. The findings have grown every year due to improvements in searching methodologies and telescopic techniques and this continues to serve as an evidence that the Earth is surrounded by a swarm of Asteroids [3].

The repercussions of the projectile impacts on the topology, ecosphere and geological history of the Earth has undoubtedly become a topic of current interdisciplinary interest since [4], who ties the mass extinction during the cretaceous period to an Asteroid or a comet. These impacts pose a significant risk to life on Earth and the discussion of the means to mitigate these risks is imperative. As [1] and [3] suggest, the issues concerning these Near Earth Objects are the dearth of current knowledge, risk assessment, mitigation (Deflection techniques) and disaster management, few of which can be answered after the introduction of the Large Synoptic Survey Telescope in Chile.

Adding to the above mentioned cause, the study of the Population of NEAs and other objects in new light after LSST might pave way for opportunities to study the dynamics of the Earth-Moon system, the production and evolution of the small asteroids from the asteroid belt, fast low ΔV transfers to the NEAs, and the in-situ resource utilization and asteroid deflection techniques [5].

1.1 ESA Comet Interceptor

In response to the European Space Agency's (ESA) call for F- class missions, the mission proposal for the comet interceptor spacecraft was submitted in March, 2019 and was selected by ESA as part of its Cosmic Vision programme [6]. Discovering comets approaching the sun from far enough is now possible with the advent of powerful survey telescopes such as the Large Synoptic Survey Telescope and these as-yet undiscovered comets make for exciting new frontiers as they are uncharted. Besides, the comets which have been encountered by a spacecraft till now are short-period comets and have therefore undergone several changes on their surfaces [7]. This mission focusses on a new, pristine long-period comet entering the Solar System from the Oort cloud for the first time, implying a presence of pure, unprocessed material since the dawn of the solar system which would make it an ideal place to know more about the evolution of comets as they migrate to the centre of the Solar System and how the solar system evolves [8].

1.1.1 Mission Specifications and Constraints

Launching in 2028, the Comet Interceptor is seen as a co-passenger with the ESA ARIEL spacecraft, which will be delivered to the Sun-Earth L2 Lagrangian point. From there on, upon the discovery of a suitable comet, the comet interceptor will go on a trajectory to intercept it using its own propulsion systems [8]. This mission, being a F-class mission as mentioned in 1.1, has its constraints as mentioned in [9], some of which are:

- Launcher: The mission (ARIEL + Comet Interceptor) will be launched using the Ariane 6.2 launcher; Launch with PLATO is also possible
- Spacecraft wet mass: <1000 kgs, which encompasses the scientific instruments, propulsion systems, daughtercrafts
- Spacecraft Operations: The duration for science operations is less than 2 years
- ΔV required to reach target orbit (NEAs with maximum distance to the sun < 1.5 Astronomical Units): 3 – 5 km/s, while ESA in December 2018 has restricted the budget to a 1 km/s

Detection of comets, selection of a suitable comet, design of the trajectory for an interception/rendezvous and finally, the optimization of the trajectory in order to reduce the ΔV to fit the mission constraints are the major parts of the mission. However, since the long period comets have orbital periods more than 200 years and random inclinations around the celestial sphere, they have much more unpredictability in their orbital patterns i.e., they can retrace the trajectory after thousands or millions of years or not at all, making them difficult objects to detect and catalogue [10].

Hence, this thesis evaluates transfer trajectories to equally interesting and important bodies called PHAs as a potential back-up plan, hoping to help causes discussed in 1. The ΔV constraint and optimization is also discussed, involving how its value changes from various departure positions such as the L2 point, the prescribed halo orbit and the unstable manifolds.

1.2 Introduction to Halo Orbits

A study of the trajectories of spacecrafts in the gravitational field generated by more than two bodies was referred to as the Restricted Three-Body Problem and results arising from that state that there exist these libration points around the system of 2 massive bodies rotating around their common barycenter [11]. The 3 libration points, L1, L2, and L3, are the collinear libration points and the rest, L4 and L5, are the triangular libration points.

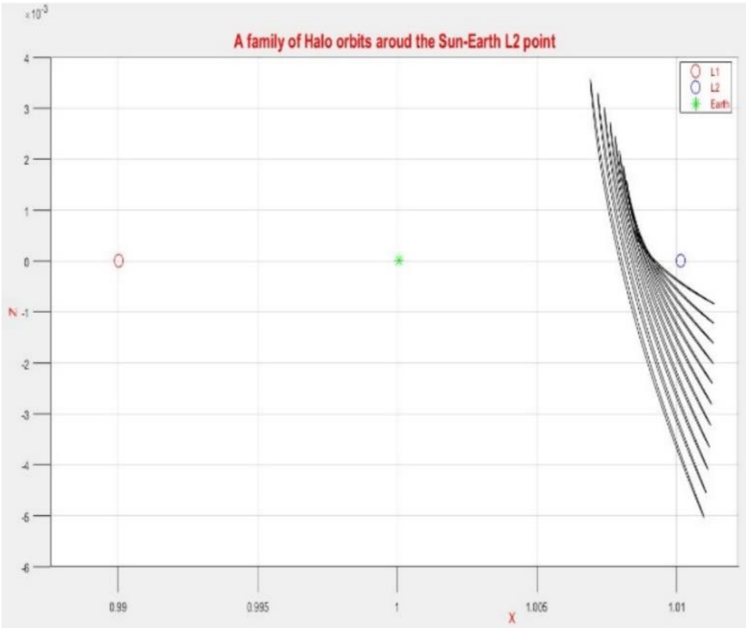

Figure 1.1: Family of Halo orbits around Sun-Earth L2 Libration point

As seen in Figure 1.1, A halo orbit is a three-dimensional periodic orbit near one of the 3 collinear libration points and different families of periodic orbits can be observed in the vicinity of each collinear libration point [12]. A halo orbit has relatively constant distances and orientation with respect to the 2 primary bodies, which makes it favourable for uses such as communication, thermal control and scientific observation [13]. Further studies and research about spacecrafts in and around the collinear points have shown that halo orbits can potentially be used as a space hub for the exploration of asteroids, communication relay spot for exploring the far side of the moon in the Earth-Moon system and as a repair and construction facility for future missions [14]. One of the first missions to utilise this was the International Sun-Earth Explorer-3 (ISEE-3) in the Sun-Earth L1 system. While it gathered valuable data in solar physics and astrophysics due to its unhindered view of the sun, it is also credited with the exemplification of libration point orbits as prime locations for space missions, as mentioned in [11]. Following the success of ISEE-3, utilizing the manifold associated with the halo orbit in order to create a low-energy transfer has resulted in many missions in the L1 and L2 of the Sun-Earth and Sun-Moon systems, where the possibility of an interplanetary trajectory and an asteroid-bound mission has been discussed [13].

This thesis aims to create a halo orbit and its invariant manifolds around the Sun-Earth L2 point, as discussed in 1.1.1, from where different scenarios for transfer trajectories to the selected PHA will be evaluated, analysed and presented.

1.3 Thesis Breakdown

The thesis is aimed at generating trajectories which require a ΔV lower than 1 Km/s within the departure and arrival windows to go from the Sun-Earth L2 point to the selected Potentially hazardous asteroid. In order to do that, the thesis is split accordingly into sections which consist of the following:

- Sorting the database of NEO based on the Palermo Scale and selecting a PHA based on a general ΔV needed to go from the L2 point
- Delving into the creation of a suitable halo orbit based on an analytical approximation method
- Computing the manifolds of the created halo orbit to check for points of departure
- Finally, generating and comparing the ΔVs required for the transfer from the Halo orbit and its manifolds, and finding the suitable departure and arrival dates within the stipulated timeframe

The thesis is organised into chapters as mentioned below:

CHAPTER 2:

This chapter deals with the extraction of the required data from the NEO database available at [15], which provides information and services about all NEAs, including their Palermo Technical scale, Keplerian elements, daily ephemeris, MOID, and animated orbit diagrams to visualise the orbit. Gathering the Keplerian elements for the PHAs in order to zero in on the target asteroid is also discussed.

CHAPTER 3:

This chapter deals with the background needed to construct orbits in the vicinity of the libration points, while specifically dealing with Sun-Earth L2 lagrangian point. The N-body problem has been discussed, succeeded by an explanation of the Circular Restricted Three Body problem, with the derivation of the equations of motion closely following. The locations of the 5 libration points are found, along with their zero-velocity curves, aiding in understanding the motion around these points in the CRTBP. The reference frames that are used to represent the Sun-Earth dynamical systems have been presented, which will be used in Chapters 4 and 5 for the construction of Halo orbit and its manifolds.

CHAPTER 4:

Chapter 4 involves the creation of a suitable halo orbit of a particular amplitude, with the help of a third-order analytical construction method in order to provide the initial guess for the orbit in the Sun-Earth L2 system. A Differential correction scheme involving the concept of State-transition Matrix, coupled with the reference frame tools from chapter 3, is employed in conjunction with the analytical construction method, thereby generating the required Halo orbit.

After generating the Halo orbit, the concept of invariant manifolds is also explored in order to identify potential trajectories with lower ΔV. The information about the suitable Jacobian and monodromy matrices, and the process of finding the stable and unstable manifolds utilising the eigenvectors are being discussed here in Chapter 4. Finally, the frame conversion techniques from Chapter 3 have been utilised in order to get the manifolds in the Inertial reference frame

CHAPTER 5:

Chapter 5 is the results and analysis section where the different cases of departure (L2 point, Halo, and the manifolds) are presented, compared and analysed based on the ΔV each case required. The thesis is summarized in the conclusion and scope for future work is also discussed.

CHAPTER 6:

Chapter 6 contains the conclusion of the thesis, along with the future work that can be carried out as an extension.

2 . Potentially Hazardous Asteroids

Asteroids and comets with a perihelion distance of less than 1.3 AU ($1.945*10^8$ kms Approx.) are put in a category called the Near-Earth Objects. The vast majority of NEOs are asteroids and are termed Near-Earth Asteroids, which are subsequently divided into groups (Amor, Apollo, Aten, and Atira) based on Semi-major axes, perihelion and aphelion distances [16]. Further classification based on the Asteroid's potential to be threateningly close to the Earth gives rise to the group of Asteroids called Potentially Hazardous Asteroids, which this thesis explores. All asteroids whose Earth Minimum Orbit Intersection Distance (MOID), which is the distance between the closest points of the orbits of Earth and the Asteroid, is less than 0.05 AU or less ($< 7.479*10^6$ kms) and absolute magnitude (A measure of the luminosity based on size and albedo) is 22 or less are called PHAs [17]. The number of known PHAs has continuously increased since the end of the 1990s, as seen below in Figure 2.1, due to advancements in the astronomical surveys and will only increase in the future with the advent of the LSST [18] . Therefore, there is an ever growing need to know more about the dynamics and the formation of these newly found bodies as it is a direct reflection on the properties of the solar system.

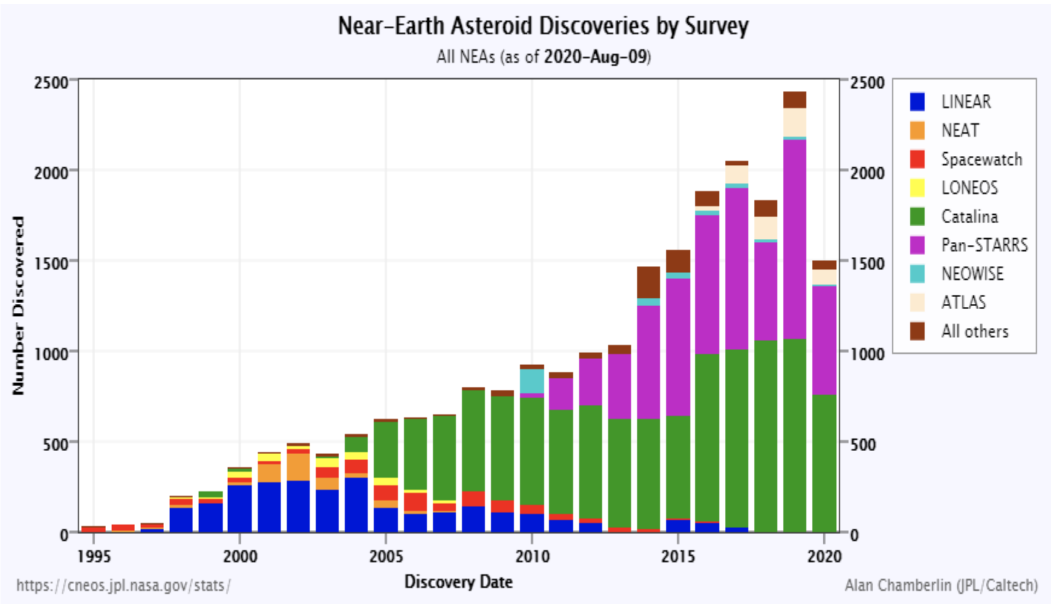

Figure 2.1: Number of NEAs discovered from 1990 by different surveys; Source: [18]

As a primary objective, this thesis will look at one particular group of PHAs, sorted based on the Palermo scale and check, under the constraints of the Comet Interceptor mission, whether a potential mission could be feasible from a Halo orbit and its manifolds.

The Palermo Technical Impact Hazard Scale is a logarithmic potential hazard impact detection scale which prioritizes and categorizes potential impacts spanning a huge range of energies, impact dates, and probabilities. It compares the likelihood of the detected impact with the average risk posed by objects of the same size or larger over the years until the date of potential impact. A scale of more than -2 means that the subject requires careful monitoring and has some level of concern while a scale of less than -2 implies that there are likely no consequences [19]. A bar graph depicting the number of PHAs under every Palermo Scale range has been shown below.

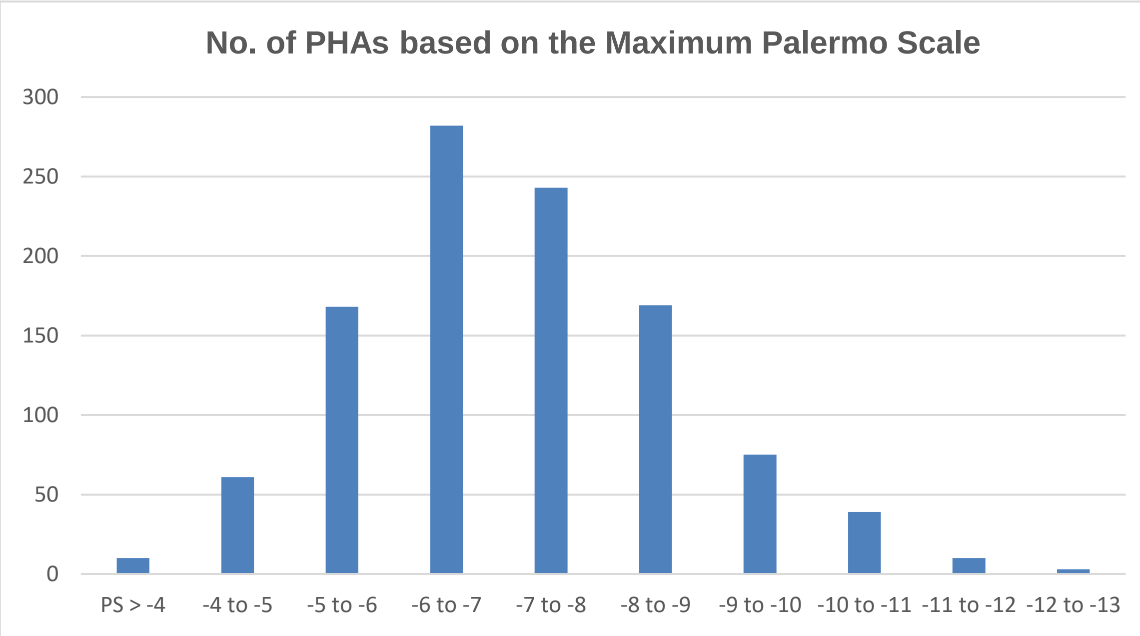

Figure 2.2: PHAs split according the values of its Palermo Scale

And going by the definition of Palermo scale, this thesis will evaluate an object from the left-most group of the above-mentioned bar graph, containing 10 PHAs with a Palermo Scale greater than -4.

Object Name	Diameter [m]	IP max	PS max
2010RF12	8	1/14	-3.20
1979XB	700	1/1.79E6	-3.27
2000SG344	40	1/1183	-3.38
99942	375	1/531914	-3.67
2008JL3	30	1/6993	-3.68
2009JF1	13	1/4166	-3.72
2018VP1	2.4	1/193	-3.77
2007KE4	30	1/10834	-3.82
2012QD8	90	1/172117	-3.91
2011DU9	16	1/1742	-3.98

Table 2-1: PHAs sorted based on the Palermo Scale

The Table 2-1 contains the name and diameter of the PHAs for further analysis, its Palermo scale values, and the impact probability (IP), which was gotten from a larger set containing 1061 PHAs, available in 7B.1. After obtaining this required set of PHAs based on their Palermo scale, there is a need to further prune this set based on the ΔV required for a transfer from the L2 point to the vicinity of the Asteroid.

In order to accomplish this, a preliminary orbit determination algorithm called the Lambert's problem, which deals with the determination of an orbital trajectory given the initial and final position vectors and the time of flight, has been used. The solution provides quite good estimates of the required energy (A reflection of ΔV) and of the manoeuvres needed for the interception/rendezvous with the PHA [20]. Therefore, using a computational software such as MATLAB, the techniques to solve the Lambert's Arc problem were implemented and the ΔV to go from the L2 point was determined so that we could weed out PHAs which require more than 1.5 km/s. To facilitate this, the Keplerian elements of the PHAs, available in 7B.2, were gathered from [21], and basic ΔVs which were calculated are presented below in Table 2-2.

Object Name	∆v FROM L2 (km/s)
2010RF12	5.8759
1979XB	21.3285
2000SG344	1.1274
99942	5.0899
2008JL3	8.2690
2009JF1	12.7377
2018VP1	8.2617
2007KE4	9.8356
2012QD8	12.4415
2011DU9	6.9569

Table 2-2: PHAs with the ∆V in km/s

The values were calculated for each PHA for the departure window, 2028-2033, while the arrival window was taken from 2028-2036. From these values, it can be seen that the PHA '2000SG344' requires the least amount of energy possible to go from the L2 point. Hence, this PHA was selected for further optimization and analysis using the halo orbit and the manifolds, to check whether there can be a reduction in ∆V less than 1 km/s, thereby creating more efficient transfer trajectories.

3 . Background

3.1 N-Body Problem

The general N-Body problem is the problem of determining the motion of 'N' number of particles which interact classically through Newton's Laws of Motion and Newton's inverse square law of Gravitation [22]. A representation of the problem has been given in Figure 3.1, where $\hat{X}$, $\hat{Y}$, and $\hat{Z}$ complete the set of orthogonal triplet making up the Inertial Reference Frame.

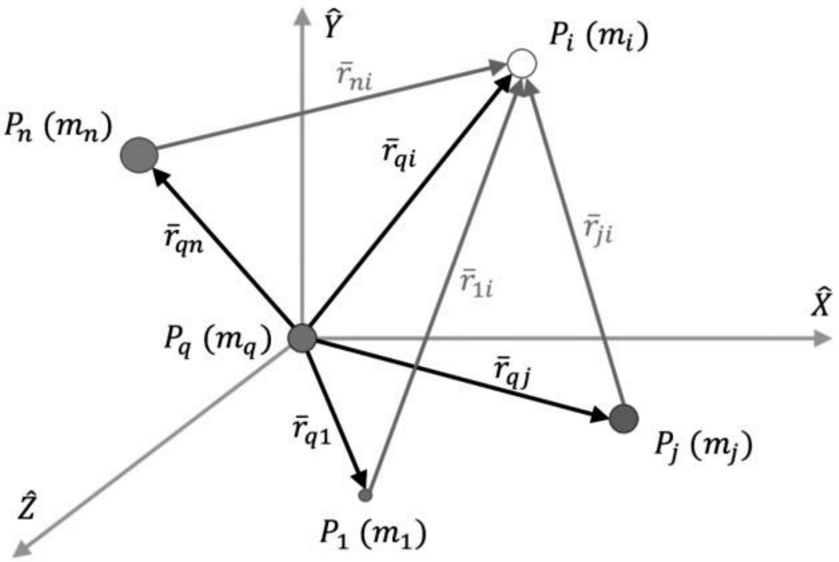

Figure 3.1: Representation of the N-Body Problem; Source: [22]

By Newton's second law, the equations of motion for 'N' particles P_n moving under mutual gravitational forces, where n = {1,2,i,j,...n} , with masses m_n respectively are given by equation (3-1).

$$m_i \frac{d^2 \bar{r}_i}{dt^2} = -G \sum_{\substack{j=1 \\ j \neq i}}^{n} \frac{m_i m_j}{r_{ji}^3} (\bar{r}_{ji}) \tag{3-1}$$

It can be further simplified into equation (3-2),

$$\ddot{\bar{r}}_i = -G \sum_{\substack{j=1 \\ j \neq i}}^{n} \frac{m_j}{\left|\bar{r}_i - \bar{r}_j\right|^3} \left(\bar{r}_i - \bar{r}_j\right) \tag{3-2}$$

Where $\bar{r}_i$ and $\bar{r}_j$ are the position vectors of particles P_i and P_j relative to the inertial reference frame, m_i and m_j are the masses of particles P_i and P_j, and G is the Universal constant of gravitation. The distance between 2 particles is given by their difference in position vectors, represented by $\left|\bar{r}_i - \bar{r}_j\right|$. The Left-Hand Side of equation (3-2) gives us the second order derivative of the position vector, which can be split into 2 first-order equations. Therefore, the dynamics of a point in the reference frame is defined by 6 first-order differential equations, implying the existence of (6*N) degrees of freedom for a total of N particles [23]. These equations provide an approximate mathematical model with many applications from astrodynamics all the up to astrophysical and cosmological level. including the motion of planets, moons and asteroids. Solving such a system would thereby require (6*N) integrals of motion. This is a time-consuming and complex procedure which cannot be solved analytically and calls for heavy dependence on computerized numerical simulations [23] .

For purposes of simplicity, the number of particles in the N-body problem are usually limited to 2 (Two-Body Problem) and 3 (Three-Body Problem) in problems of astrophysics. The Two-Body problem deals with the motion of two bodies due solely to their own mutual gravitation [24].It is extremely useful for initial analyses of trajectories due to the existence of an analytical solution, and is usually the starting point for a more complex system such as a three-body system, which does not have a closed-form analytical solution [25]. The Three body problem involves determining the dynamics of a body with respect to 2 primary bodies and can be represented by,

$$m_{body}\frac{d^2\bar{r}_{body}}{dt^2} = -G\frac{m_{body}m_{P1}}{r^3_{body-P1}}\left(\bar{r}_{body-P1}\right) - G\frac{m_{body}m_{P2}}{r^3_{body-P2}}\left(\bar{r}_{body-P2}\right) \tag{3-3}$$

Where the dynamics of the body is dependent on G, the masses on the primary bodies, $m_{P1}$and m_{P2}, and the distances of the body from the primaries, $\bar{r}_{body-P1}$ and $\bar{r}_{body-P2}$.

Since the three-body problem has no analytical solution, in order to get accurate results and save time, a simplified model of it is used, called the Circular Restricted Three-Body Problem (CR3BP) [26]. This thesis concentrates on one of the applications of CR3BP.

3.2 Circular Restricted Three-Body Problem

As mentioned in 3.1, the Circular Restricted Three-Body Problem is a scenario suited for modelling the trajectories of a spacecraft in the gravitational potential of 2 massive bodies. Because it stems from the complex 3-body problem, certain assumptions are to be made in order to formulate its equations [27].

The first assumption places a comparison on the masses of the 3 studied bodies. It states that the mass of the spacecraft is negligible when compared to the masses of the 2 primary bodies. As the thesis deals with a spacecraft in the Sun-Earth system, it is apparent that the spacecraft with mass M_B is the smaller body, while the Sun with mass M_S and Earth with mass M_E are the larger primary bodies which affect the motion of the spacecraft. It is also important to note that this effect of primary bodies, Sun and Earth, on the spacecraft far outweighs the effect the spacecraft has on the motion of the big primaries. The second assumption is related to the word 'Circular', in the sense that the 2 primary masses (M_S and M_E) move in circular, coplanar orbits around their centre of mass, also called the Barycentre. With these 2 simplifications made to the general three-body problem, it becomes more tractable and applicable to orbits and trajectories in the real world [27].

3.2.1 Non-Dimensionalisation of measured quantities

In an attempt to further simplify the study of CR3BP, different quantities are generalised and analysed as non-dimensional units. This makes the equations of motions easier to work with as it normalizes the quantities such as distances, masses, and velocities in the 3-body system.

The characteristic length is defined as the distance between the 2 primary bodies. For the Sun-Earth system, the length is given in equation (3-4)

$$l^* = D_{S-E} = |\bar{R}_s| + |\bar{R}_E| = 1\,AU \quad \textbf{(3-4)}$$

Where $|\bar{R}_E|$ and $|\bar{R}_S|$ are the distances of the Earth and the Sun from their barycentre respectively.

The mass ratio μ allows the normalization of the total mass in the system, $m^* = (m_S + m_E)$, which in turn helps in knowing the distances of the primaries from their barycentre in non-dimensionalised units. The mass ratio for the Sun-Earth system is given by,

$$\mu = \frac{m_E}{m_S + m_E} = 3.0032 * 10^{-6} \tag{3-5}$$

Including the Moon as a part of the Earth changes the value of μ and in turn slightly improves the efficiency of calculations in the CR3BP due to the consideration of an extra mass in the system ($m^* = m_S + m_E + m_M$), which makes for a deeper analysis i.e.,

$$\mu = \frac{(m_E + m_M)}{m_S + (m_E + m_M)} = 3.0542 * 10^{-6} \tag{3-6}$$

This can be directly related to the non-dimensional masses of the primaries as,

$$\mu_E = \frac{m_E}{m_S + m_E + m_M} = \mu = 3.0542 * 10^{-6} \tag{3-7}$$

$$\mu_S = \frac{m_S}{m_S + m_E + m_M} = 1 - \mu = 0.9999969 \tag{3-8}$$

The normalized value of time in this CR3BP, t^*, is given by the formula for orbital time period by Kepler's third law, as mentioned in the below-mentioned equation (3-9).

$$t^* = \sqrt{\frac{(l^*)^3}{Gm^*}} = 5.0224 * 10^6 \ (s) \tag{3-9}$$

Using the above-mentioned formula for normalized time, the characteristic value of the angular velocity, ω^*, can be found as,

$$\omega^* = \frac{1}{t^*} = \sqrt{\frac{Gm^*}{(l^*)^3}} = 1.9910 * 10^{-7} \ (\frac{rad}{s}) \tag{3-10}$$

With the values of normalized time and distance, the value of the normalized velocity determined is given by,

$$v^* = \frac{l^*}{t^*} = 29.7861\ \left(\frac{km}{s}\right) \tag{3-11}$$

Finally, another important normalization utilized throughout the system is for the Universal Gravitational constant, G.

$$G = 6.6726 * 10^{-20} \left(\frac{km^3}{kg(s^2)}\right);\quad G^* = \frac{G(l^*)^3}{m^*(t^*)^2} = 1 \tag{3-12}$$

These are the values which are used henceforth in the calculations involving CR3BP and they are recorded in Table 3-1.

Parameter	**Symbol**	**Value**	**Units**
Characteristic Mass	m^*	$1.9891 * 10^{30}$	kg
Characteristic Distance	l^*	$1.4960 * 10^{8}$	km
Characteristic Time	t^*	$5.0224 * 10^{6}$	s
Characteristic Velocity	v^*	29.7861	km/s
Characteristic Angular Velocity	ω^*	$1.9910 * 10^{-7}$	rad/s
Mass parameter	μ	$3.0542 * 10^{-6}$	-
Dimensionless Gravitational Parameter	G^*	1	-

Table 3-1: Normalized parameters for a CR3BP in the Sun-Earth system

3.2.2 Reference Frames

Before writing the equations of motion of the CR3BP, it is imperative to get to know the basic frames under which these systems are studied. This thesis uses a variety of reference frames at various instances in time, and it is important to define these sets of coordinate reference systems due to the fact that the equations of motion of a particular body in the CR3BP can be particular to a single reference frame. Also, the visualisation and analysis of certain parameters such as position and velocity are only applicable and preferable in their own coordinate systems. For example, a Rotating Reference Frame is the preferred system to deal with CR3BP, while an Inertial Reference Frame is used for Heliocentric orbits. This section covers the 3 main reference frames used in this thesis, the parameters suited to that frame and the conversion from one frame to another.

3.2.2.1 Heliocentric Reference Frame

As shown in Figure 3.2, the Heliocentric reference frame is centered around the Sun, with inertial axes x_h and y_h on the plane of rotation and z_h axis completing the right-handed coordinate system. The Earth and the barycentre are positioned according to their respective distances, $\bar{r}_{E-h}$ and $\bar{r}_{B-h}$, from the Sun in this fixed reference frame and have velocities $\bar{V}_{E-h}$ and $\bar{V}_{B-h}$,. The Positions of the Sun, Earth, and a point are given by,

$$\bar{r}_S = [\,0\;0\;0]\;(AU)\;;\;\bar{r}_{E-h} = [1\;\;0\;0]\;(AU)\;;\;\bar{r}_{point} = [\,x\;y\;z]\;(AU) \qquad \textbf{(3-13)}$$

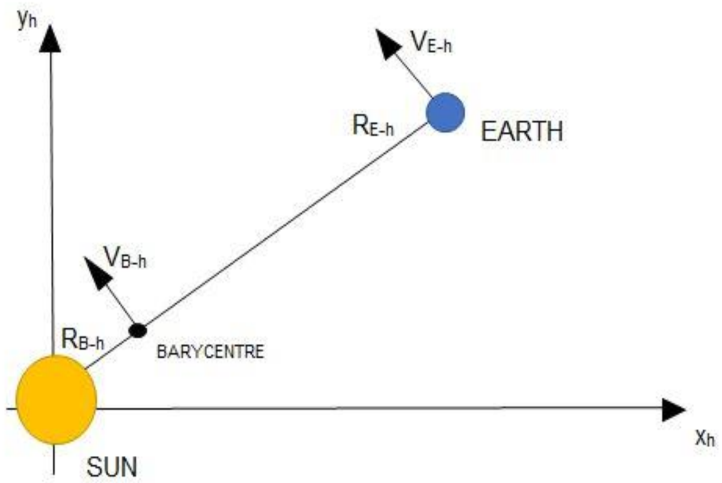

Figure 3.2: Heliocentric Reference Frame

3.2.2.2 Barycentric Inertial Frame

A barycentric Inertial reference frame is similar to the Heliocentric Reference Frame except for the fact that the centre of this coordinate system is the Barycentre. The 2 primaries, Sun and the Earth are present on the opposite sides of the x_b axis, making it easier for conversion from the rotating reference frame to the Heliocentric reference frame, which will be seen in the next section. The positions of the primaries are defined using the normalized value of the mass ratio, μ, as explained in 3.2.1. At instant t=0,

$$\bar{r}_{S-b} = [-\mu\ 0\ 0]\ ;\ \bar{r}_{E-b} = [1-\mu\ \ 0\ 0]\ ;\ \bar{r}_{point} = [x_b\ y_b\ z_b] \quad \textbf{(3-14)}$$

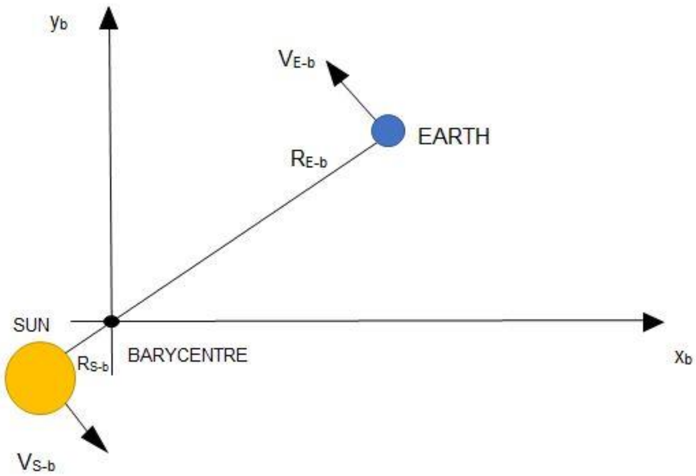

Figure 3.3: Barycentric Inertial Reference Frame

3.2.2.3 Rotating Reference Frame

The rotating reference frame is a non-inertial frame which is centred in the barycentre of the 2 primary bodies, Sun and Earth. Unlike the Barycentric inertial reference frame where the positions of the Sun and the Earth constantly changes, in this system of reference, the Sun and the Earth are fixed at their respective distances. This implies that both the bodies will be stationary with respect to the axes, while the entire reference frame rotates with the constant angular velocity (ω_r) of Earth around the Sun. This is the system of reference desired for a CR3BP, where the relative motion of a spacecraft is needed with respect to the 2 primary bodies. Hence, this is the reference frame we use in sections down the line, in order to create the halo orbit and its manifolds.

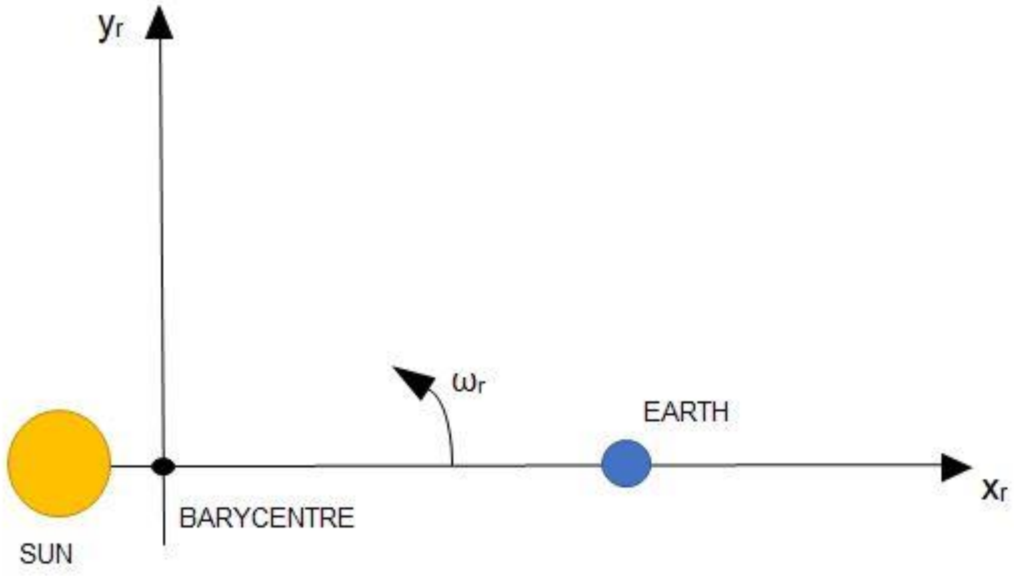

Figure 3.4: Rotating Reference Frame

3.2.2.4 Conversion of reference frames

This basically deals with the transformation of coordinates from the Rotating Reference Frame to the Heliocentric Inertial Reference Frame. This is done in order to know the relative position of spacecraft or any secondary body with respect to the primaries, whose values of position and velocity are what is needed to compute the Lambert's problem between the Asteroid and the L2 point. The process of conversion has been mentioned below.

The position and the velocity vectors, together called the state vector of a spacecraft in the Rotating Reference Frame are written as:

$$RV = \begin{bmatrix} x_r \\ y_r \\ z_r \end{bmatrix}; \tag{3-15}$$

$$VV = \begin{bmatrix} \dot{x}_r \\ \dot{y}_r \\ \dot{z}_r \end{bmatrix}$$

A transformation matrix dependant on the angle θ (Number of time steps which have passed) is first used to convert the rotational coordinates into barycentric coordinates.

$$T = \begin{bmatrix} cos\theta & -sin\theta & 0 \\ sin\theta & cos\theta & 0 \\ 0 & 0 & 1 \end{bmatrix} \quad \textbf{(3-16)}$$

The change of coordinates takes the form,

$$x_b = \cos(\theta)x_r - \sin(\theta)\, y_r \; ; \quad \textbf{(3-17)}$$

$$y_b = \sin(\theta)x_r + \cos(\theta)\, y_r \; ;$$

$$z_b = \quad z_r \; ;$$

$$\dot{x}_b = -\sin(\theta)\, \omega^* * x_r + cos(\theta)\dot{x}_r - \cos\,(\theta)\omega^* * y_r - sin(\theta)\, \dot{y}_r \; ; \quad \textbf{(3-18)}$$

$$\dot{y}_b = \cos(\theta)\, \omega^* * x_r + sin(\theta)\dot{x}_r - sin\,(\theta)\omega^* * y_r - \cos(\theta)\, \dot{y}_r \; ;$$

$$\dot{z}_b = \dot{z}_r$$

The new position and velocity coordinates in the barycentric inertial reference system are given by matrices $[x_b \;\; y_b \;\; z_b]$ and $[\dot{x}_b \;\; \dot{y}_b \;\; \dot{z}_b]$. The parameter ω^* is the angular velocity of the Rotating reference frame whose value is $1.991 * 10^{-7}$ rad/s, the calculation of which is shown in 3.2.1.

Since the main aim of our thesis circles around L2, there is a need to convert these Barycentric Inertial coordinates into the final Heliocentric Inertial coordinates. This is done by translating our system of reference to the required point in the system (Sun), aided by the non-dimensionalized mass parameter, μ. The required matrices are given below.

$$\bar{r}_{B-h} = [\cos(\theta)\, \mu \;\;\; \sin(\theta)\, \mu \;\;\; 0] \quad \textbf{(3-19)}$$

$$\bar{V}_{B-h} = [-\sin\,(\theta)\mu \;\;\; \cos(\theta)\mu \;\;\; 0]$$

The above-mentioned matrices help in converting the barycentric coordinates into the heliocentric coordinates. The final stage in conversion is to add the position and velocity vectors in the barycentric inertial system of coordinates with the respective vectors from equation (3-19).

$$\bar{r}_h = [x_b \;\; y_b \;\; z_b] + [\cos(\theta)\,\mu \;\; \sin(\theta)\,\mu \;\; 0] \tag{3-20}$$

$$\bar{V}_h = [\dot{x}_b \;\; \dot{y}_b \;\; \dot{z}_b] + [-\sin(\theta)\mu \;\; \cos(\theta)\mu \;\; 0]$$

Equation (3-20) represents the required final value of the heliocentric system obtained after conversion from the state vector in the Rotating reference frame.

3.2.3 Equations of motion in the CR3BP

This part deals with the system dynamics of the model in the CR3BP by deriving the equations of motion. It is done via the Newtonian method, where the final result of the time evolution of position and velocity are computed [24]. In this analysis, since Sun and Earth are the 2 primary bodies, only their gravitational forces are considered for further calculations. The equation of motion in the Inertial reference frame, relating the forces acting on the spacecraft with its acceleration is given by,

$$\sum F_{ext} = m_{s/c} * \ddot{\bar{r}}_{s/c} \tag{3-21}$$

where s/c stands for spacecraft and the external forces can be simplified into the gravitational forces, as seen in (3-22).

$$\ddot{\bar{r}}_{s/c} = \frac{-Gm_S\bar{r}_{S-s/c}}{r_{S-s/c}^3} - \frac{Gm_E\bar{r}_{E-s/c}}{r_{E-s/c}^3} \tag{3-22}$$

where $\bar{r}_{S-s/c}$ and $\bar{r}_{E-s/c}$ are the vectors denoting the distance between the sun and the spacecraft, and the Earth and the spacecraft respectively.

Non-dimensionalising the above equation for usage in the CR3BP yields,

$$\ddot{\bar{r}}_{s/c} = \frac{-(1-\mu) * \bar{r}_{S-s/c}}{r_{S-s/c}^3} - \frac{\mu * \bar{r}_{E-s/c}}{r_{E-s/c}^3} \tag{3-23}$$

Now, defining suitable vectors for the secondary body in the CR3BP system paves way for further analysis in the equations of motion.

$$\bar{r}_{s/c} = x\hat{i} + y\hat{j} + z\hat{k} \tag{3-24}$$

$$\overline{V}_{s/c} = \overline{v}_G + \Omega \times \overline{r}_{s/c} + \overline{v}_{REL} \tag{3-25}$$

The position vector of the spacecraft with respect to the barycentre in the CR3BP system is $\overline{r}_{s/c}$. It is aptly represented using the i, j, and k coordinates, which are basically the x, y, and z-axis, where the x-axis is the line connecting the barycenter with the Earth, the y-axis lies in the Sun-Earth orbital plane and z-axis completes the triad. The representation is given in Figure 3.5.

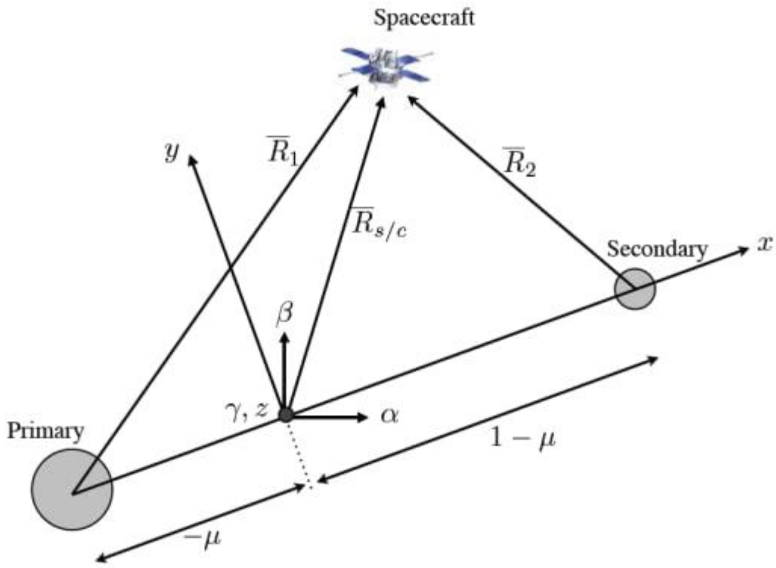

Figure 3.5: Representation of a Circular Restricted 3 Body Problem (CR3BP); Source: [22]

After knowing the position vector, the inertial velocity of the spacecraft is found by taking the time-derivative of the position vector and that is represented as $\overline{V}_{s/c.}$ The angular velocity vector Ω accounts for the rotating frame, and it is a major part of this velocity since the (i, j, k) coordinate system is rotating with a constant angular velocity ω^*. This vector is represented as,

$$\Omega = \omega^* \hat{k} \tag{3-26}$$

The component $\bar{v}_G$ is the inertial velocity of the barycentre and the component $\bar{v}_{REL}$ is the velocity of the spacecraft measure in the moving (i, j, k) frame, i.e.,

$$\bar{v}_{REL} = \dot{x}\hat{\imath} + \dot{y}\hat{\jmath} + \dot{z}\hat{k} \qquad \textbf{(3-27)}$$

The acceleration of the spacecraft is now expressed in the inertial frame of reference by differentiating the velocity vector.

$$\ddot{\bar{r}}_{s/c} = \bar{a}_G + \dot{\Omega} \times \bar{r}_{s/c} + \Omega \times \left(\Omega \times \bar{r}_{s/c}\right) + 2\Omega * \bar{v}_{REL} + \bar{a}_{REL} \qquad \textbf{(3-28)}$$

Since the velocity of the barycentre is a constant, it can be inferred that the acceleration of the barycentre, $\bar{a}_G$, is 0. Also, since the reference frame is rotating at a constant angular velocity, the term, $\dot{\Omega}$, is also 0. Therefore, the equation (3-28) reduces to,

$$\ddot{\bar{r}}_{s/c} = \Omega \times \left(\Omega \times \bar{r}_{s/c}\right) + 2\Omega * \bar{v}_{REL} + \bar{a}_{REL} \qquad \textbf{(3-29)}$$

Where the term $\Omega \times \left(\Omega \times \bar{r}_{s/c}\right)$ corresponds to the centrifugal acceleration, and $2\Omega * \bar{v}_{REL}$ corresponds to the Coriolis acceleration. The term $\bar{a}_{REL}$ depicts the acceleration with respect to the rotating frame and is given by,

$$\bar{a}_{REL} = \ddot{x}\hat{\imath} + \ddot{y}\hat{\jmath} + \ddot{z}\hat{k} \qquad \textbf{(3-30)}$$

Substituting equations (3-24), (3-26), (3-27), (3-30) into (3-29), we get the expression for the inertial acceleration in terms of the parameters measured in the rotating reference frame as,

$$\ddot{\bar{r}}_{s/c} = (\ddot{x} - 2\omega^{*}\dot{y} - {\omega^{*}}^{2}x)\hat{\imath} + (\ddot{y} + 2\omega^{*}\dot{x} - {\omega^{*}}^{2}y)\hat{\jmath} + \ddot{z}\hat{k} \qquad \textbf{(3-31)}$$

Now, in equation (3-23), if the values for $\bar{r}_{S-s/c}$ and $\bar{r}_{E-s/c}$, as mentioned in equation (3-32) are substituted as vectors in the reference frame, then the equation transforms into the equation (3-33).

$$\bar{r}_{S-s/c} = (x + \mu)\hat{\imath} + y\hat{\jmath} + z\hat{k} \qquad \textbf{(3-32)}$$

$$\bar{r}_{E-s/c} = (x - 1 + \mu)\hat{\imath} + y\hat{\jmath} + z\hat{k}$$

$$\ddot{\vec{r}}_{s/c} = \frac{-(1-\mu)*[(x+\mu)\hat{\imath} + y\hat{\jmath} + z\hat{k}]}{r^3_{S-s/c}} - \frac{\mu * [(x-1+\mu)\hat{\imath} + y\hat{\jmath} + z\hat{k}]}{r^3_{E-s/c}} \quad \textbf{(3-33)}$$

Comparing equations (3-31) and (3-33) and equating the coefficients of $\hat{\imath}$, $\hat{\jmath}$, and $\hat{k}$ furnishes the 3 equations of motion for the CR3BP.The final equations are mentioned as,

$$\left(\ddot{x} - 2\omega^*\dot{y} - \omega^{*2}x\right) = \frac{-(1-\mu)*(x+\mu)}{r^3_{S-s/c}} - \frac{\mu*(x-1+\mu)}{r^3_{E-s/c}} \quad \textbf{(3-34)}$$

$$\left(\ddot{y} + 2\omega^*\dot{x} - \omega^{*2}y\right) = \frac{-(1-\mu)*y}{r^3_{S-s/c}} - \frac{\mu*y}{r^3_{E-s/c}} \quad \textbf{(3-35)}$$

$$\ddot{z} = \frac{-(1-\mu)*z}{r^3_{S-s/c}} - \frac{\mu*z}{r^3_{E-s/c}} \quad \textbf{(3-36)}$$

Where the magnitudes of vector distances $r_{S-s/c}$ and $r_{E-s/c}$ are given by,

$$r_{S-s/c} = \sqrt{(x+\mu)^2 + y^2 + z^2} \quad \textbf{(3-37)}$$

$$r_{E-s/c} = \sqrt{(x-1+\mu)^2 + y^2 + z^2} \quad \textbf{(3-38)}$$

Another form of these equations can be derived using the help of a pseudo potential function, U, defined as,

$$U = \frac{1}{2}\omega^{*2}(x^2+y^2) + \frac{1-\mu}{r_{S-s/c}} + \frac{\mu}{r_{E-s/c}} \quad \textbf{(3-39)}$$

Differentiating U with respect to the 3 components in the rotating frame [x,y,z], we get,

$$\frac{\partial U}{\partial x} = \omega^{*2}x - \frac{(1-\mu)*(x+\mu)}{r^3_{S-s/c}} - \frac{\mu*(x-1+\mu)}{r^3_{E-s/c}} \quad \textbf{(3-40)}$$

$$\frac{\partial U}{\partial y} = \omega^{*2} y - \frac{(1-\mu) * y}{r_{S-s/c}^3} - \frac{\mu * y}{r_{E-s/c}^3} \tag{3-41}$$

$$\frac{\partial U}{\partial z} = \frac{-(1-\mu) * z}{r_{S-s/c}^3} - \frac{\mu * z}{r_{E-s/c}^3} \tag{3-42}$$

Using these equations, equations (3-34) - (3-36) can be transformed to a function of the pseudo-potential function, U, which are given by,

$$\ddot{x} - 2\omega^* \dot{y} = \frac{\partial U}{\partial x} \tag{3-43}$$

$$\ddot{y} + 2\omega^* \dot{x} = \frac{\partial U}{\partial y} \tag{3-44}$$

$$\ddot{z} = \frac{\partial U}{\partial z} \tag{3-45}$$

Using the equations given in this section, computations for the system of libration points can be made including defining and analysing the Jacobi constant and the zero-velocity curves.

3.3 Libration Points

Libration points or Lagrange points are positions in space where the gravitational forces of the 2 large primary bodies equals the centripetal force the small secondary body needs to move with them. Hence, a secondary mass placed at a lagrangian point would have zero velocity and zero acceleration. These regions provide enhanced attraction and repulsion, due to which the spacecrafts sent there use a reduced level of fuel consumption, so they can remain in positions relative to the 2 large primaries [28]. There are 5 libration points, L1 to L5, present in a system of 2 primary bodies and these are obtained as analytical solutions of the equations of motion for a CR3BP represented in equations (3-43) to (3-45) [29].

This thesis deals with the Sun-Earth L2 libration point, present at 1.5 million kms on the opposite side of Earth from the Sun. The first step in finding the positions of these 5 lagrange points would be to set the velocities and accelerations to 0 in equations (3-43) to (3-45), which gives rise to the following conditions.

$$\frac{\partial U}{\partial x} = 0 \tag{3-46}$$

$$\frac{\partial U}{\partial y} = 0 \tag{3-47}$$

$$\frac{\partial U}{\partial z} = 0 \tag{3-48}$$

This can be further expanded by substituting the values of the partial derivatives of U from equations (3-40) to (3-42).

$$\omega^{*2} x - \frac{(1-\mu) * (x+\mu)}{r_{S-s/c}^3} - \frac{\mu * (x-1+\mu)}{r_{E-s/c}^3} = 0 \tag{3-49}$$

$$\omega^{*2} y - \frac{(1-\mu) * y}{r_{S-s/c}^3} - \frac{\mu * y}{r_{E-s/c}^3} = 0 \tag{3-50}$$

$$\frac{-(1-\mu) * z}{r_{S-s/c}^3} - \frac{\mu * z}{r_{E-s/c}^3} = 0 \tag{3-51}$$

From equation (3-51), it can be inferred that z = 0, since all the other parameters have definite values. This means that all the lagrangian points are in the plane of motion of the 2 primary bodies.

From equation (3-50), there exists 2 possible solutions, one where y = 0, and another where $y \neq 0$. Analysing the second case, $y \neq 0$, implies that the rest of the equation is 0 as shown by,

$$(\omega^{*2} - \frac{(1-\mu)}{r_{S-s/c}^3} - \frac{\mu}{r_{E-s/c}^3}) = 0 \quad \textbf{(3-52)}$$

If all the values are normalized, then it can be observed from this equation that $r_{S-s/c}$ and $r_{E-s/c}$ are both equal to 1, the normalized distance. This gives rise to the 2 libration points L4 and L5, which are vertices of 2 equilateral triangles with Sun and Earth as the other 2 vertices. The position coordinates for the 2 triangular libration points are mentioned below after calculation.

$$x_{L_4} = \frac{1}{2} - \mu \; ; \; y_{L_4} = \frac{\sqrt{3}}{2} \; ; \; z_{L_4} = 0 \quad \textbf{(3-53)}$$

$$x_{L_5} = \frac{1}{2} - \mu \; ; \; y_{L_5} = -\frac{\sqrt{3}}{2} \; ; \; z_{L_5} = 0 \quad \textbf{(3-54)}$$

Analysing the case where y = 0 yields the other 3 lagrangian points L1, L2 and L3 in the same line as the Sun, Earth and the barycentre. These are termed the collinear lagrangian points and the position coordinates can be found by analysing equation (3-49) for the 3 different points.

$$L_1: (x+\mu) > 0 \; and \; (x-1+\mu) < 0 \quad \textbf{(3-55)}$$

$$L_2: (x+\mu) > 0 \; and \; (x-1+\mu) > 0 \quad \textbf{(3-56)}$$

$$L_3: (x+\mu) < 0 \; and \; (x-1+\mu) < 0 \quad \textbf{(3-57)}$$

Hence due to these conditions, the final equations to be valuated are found to be,

$$L1: x - \frac{(1-\mu)}{(x+\mu)^2} + \frac{\mu}{(x-1+\mu)^2} = 0 \quad \textbf{(3-58)}$$

$$L2: x - \frac{(1-\mu)}{(x+\mu)^2} - \frac{\mu}{(x-1+\mu)^2} = 0 \quad \textbf{(3-59)}$$

$$L3: x + \frac{(1-\mu)}{(x+\mu)^2} + \frac{\mu}{(x-1+\mu)^2} = 0 \quad \textbf{(3-60)}$$

These 3 above-mentioned equations can be solved numerically to find the positions of the 3 collinear libration points, given the value of the mass ratio for a 3-body system. For the Sun-Earth system, the positions are as follows:

$$L1: x = 0.98997 \, ; y = 0 \, ; z = 0 \quad \textbf{(3-61)}$$

$$L2: x = 1.01009 \, ; y = 0 \, ; z = 0 \quad \textbf{(3-62)}$$

$$L3: x = -1.0000012 \, ; y = 0 \, ; z = 0 \quad \textbf{(3-63)}$$

The table here contains the non-dimensionalised positions of all the 5 libration points of the Sun-Earth system, whose μ can be found in Table 3-1.

Libration Point	X-position	Y-position	Z-position
L1	0.989970869	0	0
L2	1.0100904892	0	0
L3	-1.0000012726	0	0
L4	0.49999694575	0.86602540378	0
L5	0.49999694575	- 0.86602540378	0

Table 3-2: Positions of the 5 libration points in the Sun-Earth system (Units: Non-Dimensional)

Finally, a graphical representation of the Lagrange points and their positions in the Sun – Earth system are shown in the below figure.

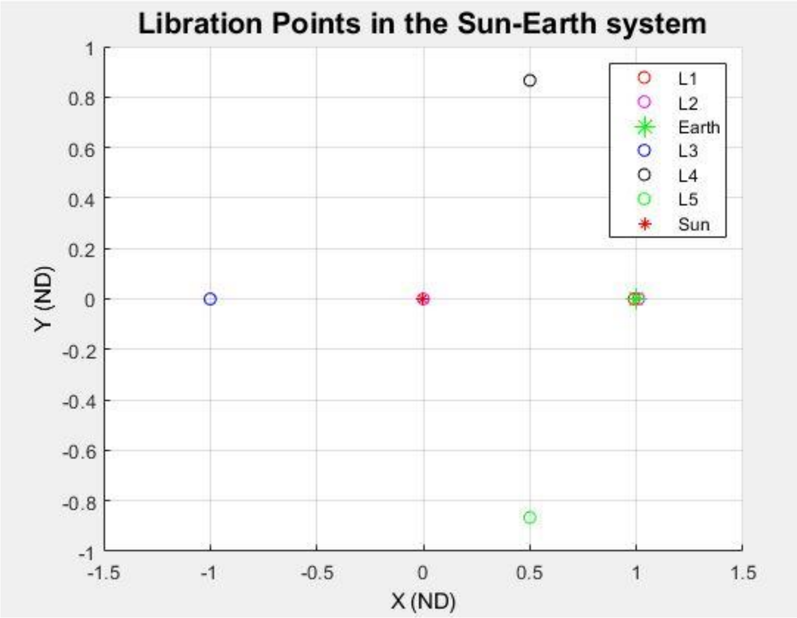

Figure 3.6: Representation of the libration points in the Sun-Earth system

In Figure 3.6, since L1, L2, and the Earth are closely packed in the system, it is not visible quite clearly. Hence, Figure 3.7 shown below presents a zoomed in, clearer view of the 2 Lagrange points with Earth.

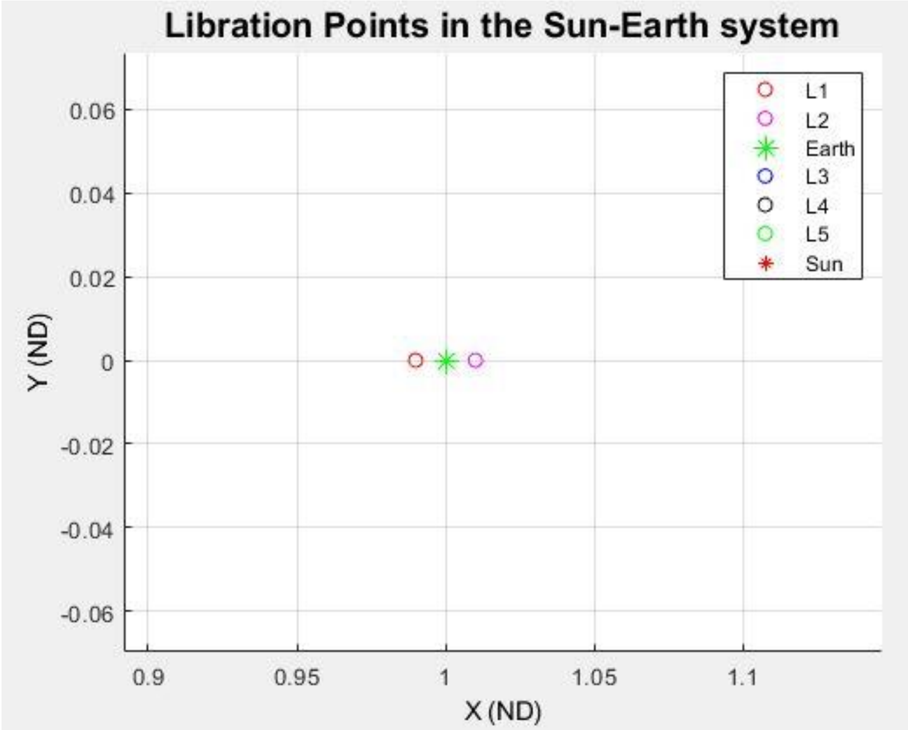

Figure 3.7: A zoomed-in view of the L1 and L2 Lagrangian points with Earth

3.3.1 Jacobi constant and Zero-velocity curves

Jacobi constant, also known as Jacobi integral is a quantity which defines the energy of a body in the CR3BP, and it exists only in the synodic reference frame (as seen in Figure 3.5) for the CR3BP [27]. Since the energy and the momentum of the system are not conserved in a CR3BP, the possibility of obtaining a general analytical solution is ruled out, but the Jacobi constant is used in special cases to derive numerous solutions [30]. Those are mentioned below with the help of equations and representations.

Multiplying equations (3-34) to (3-36) by $2\dot{x}$, $2\dot{y}$, $2\dot{z}$ respectively and adding them gives rise to the following equation.

$$2\dot{x}\ddot{x} + 2\dot{y}\ddot{y} + 2\dot{z}\ddot{z} - 2\omega^{*2}(x\dot{x} + y\dot{y}) = 2\dot{x}\frac{d}{\partial x}\left(\frac{1-\mu}{\mu_{s-s/c}} + \frac{\mu}{\mu_{E-s/c}}\right) + 2\dot{y}\frac{d}{\partial y}\left(\frac{1-\mu}{\mu_{s-s/c}} + \frac{\mu}{\mu_{E-s/c}}\right) + 2\dot{z}\frac{d}{\partial z}\left(\frac{1-\mu}{\mu_{s-s/c}} + \frac{\mu}{\mu_{E-s/c}}\right) \quad \textbf{(3-64)}$$

This equation can be integrated in order to get the final Jacobian Integral equation, which is given by,

$$\dot{x}^2 + \dot{y}^2 + \dot{z}^2 - \omega^{*2}(x^2 + y^2) = \frac{2(1-\mu)}{\mu_{s-s/c}} + \frac{2(\mu)}{\mu_{s-s/c}} - C \quad \textbf{(3-65)}$$

where C, the constant of integration, is the Jacobi constant. This equation is simplified further by involving the pseudo-potential, U.

$$\dot{x}^2 + \dot{y}^2 + \dot{z}^2 = 2U - C \quad \textbf{(3-66)}$$

Since $v^2 = \dot{x}^2 + \dot{y}^2 + \dot{z}^2$, the final equation in its simplest form is given as,

$$v^2 = 2U - C \quad \textbf{(3-67)}$$

An analysis involving this equation is the calculation of the Jacobi constant at all the libration points in the Sun-Earth system. Since a libration point has the property of having zero velocity and acceleration as explained in section 3.3, 2U – C = 0, i.e.,

$$As\ v = 0\ , 2U - C = 0 \quad \textbf{(3-68)}$$

Therefore, the jacobi constant at each of the libration points will be equal to twice the effective potential, U. A table comprising the values of the Jacobi constant and the potential for the Sun-Earth system is given below.

Libration Point	**Effective Potential, U (km^2/s^2)**	**Jacobi Integral, C (km^2/s^2)**
L1	1.500450323033066	3.000900646066
L2	1.500448286846647	3.000896573693
L3	1.500001527124101	3.000003054248
L4	1.499998472880466	2.999996945761
L5	1.499998472880466	2.999996945761

Table 3-3: Effective Potentials and Jacobi Constants of the Libration points in the Sun-Earth system

The above table is helpful in characterising the dynamics of a spacecraft in the Sun-Earth system by analysing possible motion in the system, including points of stability and instability [24]. It is used to determine the possible regions of motion of a secondary body of a particular energy level, reflected by its Jacobi constant.

It can be said that, for a spacecraft in the Sun-Earth system, $v^2 \geq 0$, implying that 2U is greater than the Jacobi constant, from equation (3-67). There exists a range of coordinates in the system where the inequality $2U \geq C$ is violated and these regions where the spacecraft cannot enter with the existing conditions are termed forbidden regions. The boundary between the allowed region and the forbidden region where $v^2 = 0$ is called the zero-velocity curve. A general representation and explanation of the zero-velocity curves for different conditions are given below.

It is important to note that the Jacobi constant is analogous to the two-body energy and therefore, a spacecraft with higher jacobi constant will be restricted in its motion whereas the spacecraft can travel farther away from the starting point with lower values of the Jacobi constant [29].

Case 1: When $C > C_{L1}$: When a spacecraft has a higher jacobi constant than that of the L1 point, its motion is restricted to the circles surrounding the 2 primaries, as shown in Figure 3.8 (left). If $C = C_{L1}$, then the spacecraft can just cross over from one primary to the other. This is shown in Figure 3.8 (right).

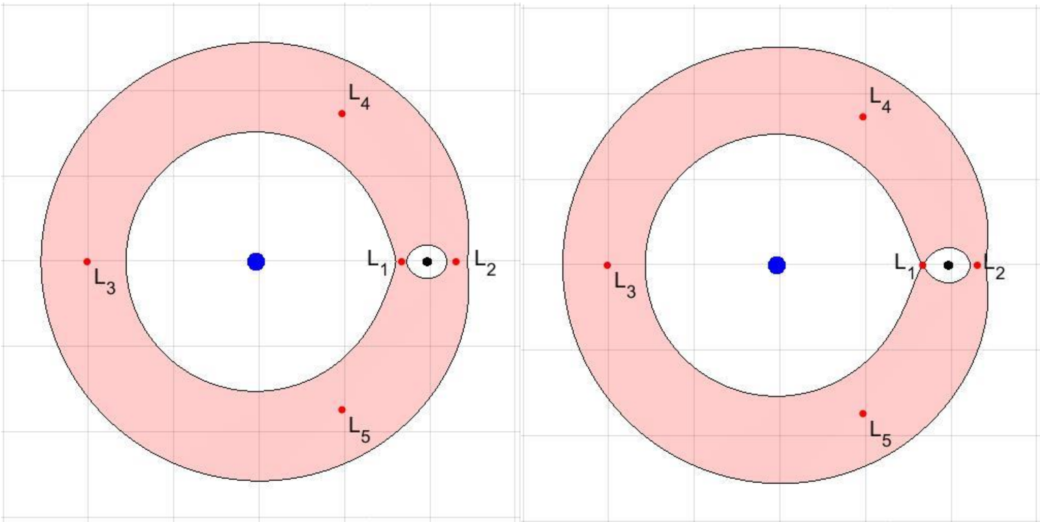

Figure 3.8: Zero-Velocity curves for conditions $C>C_{L1}$ (Left) and $C = C_{L1}$ (Right); Source: [31]

Case 2: When $C_{L1} > C > C_{L2}$: As the spacecraft successively reaches a lower value of the jacobi constant than L1, the zones around the 2 primaries can now be accessible and connected. Besides, the spacecraft still cannot escape the system since $C > C_{L2}$.This is represented by the left image of Figure 3.9.

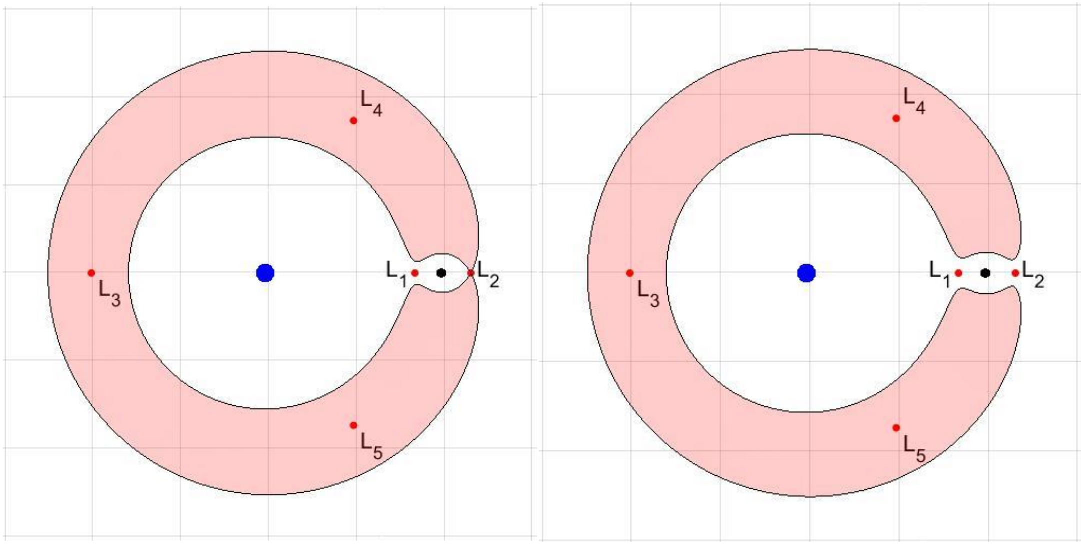

Figure 3.9: Zero-Velocity curves for conditions $C_{L1} > C > C_{L2}$ (Left) and $C_{L2} > C > C_{L3}$ (Right); Source: [31]

Case 3: When $C_{L2} > C > C_{L3}$: When the jacobi constant is lower than its value at L2, it is seen that it is possible for a spacecraft to escape the system via the neck/opening at L2. It is seen in Figure 3.9 (right).

Case 4: When $C_{L3} > C > C_{L4,5}$: When the spacecraft attains the jacobi constant of the L3 point, the spacecraft can travel beyond the bigger primary, but still cannot escape the system at L3. But when $C < C_{L3}$, the zero velocity curves are entirely separated from the X-axis and escape becomes possible in the opposite direction of the smaller primary (Ex: Earth in the Sun-Earth system and Moon in the Earth-Moon system). These are represented in the left and right images of Figure 3.10. respectively.

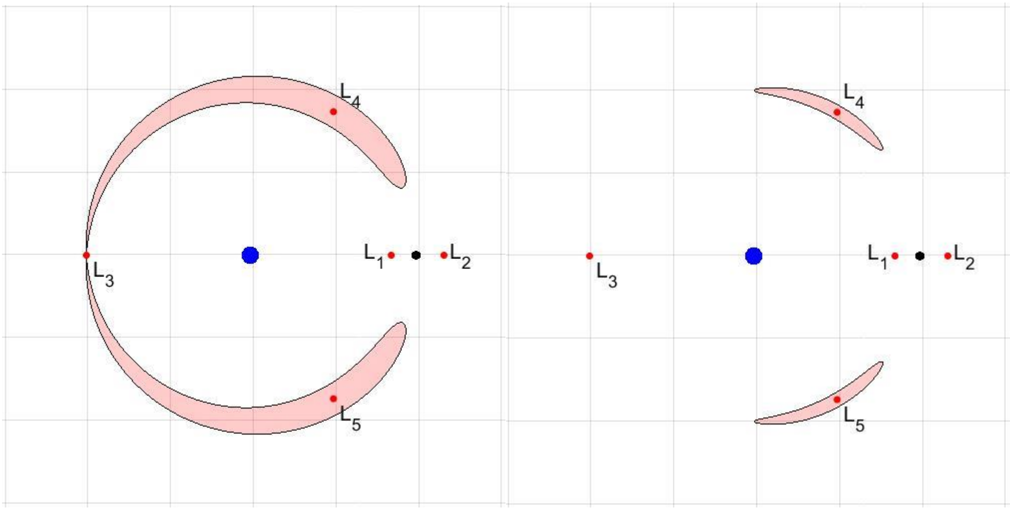

Figure 3.10: Zero-Velocity curves for conditions $C_{L3} = C$ (Left) and $C_{L3} > C > C_{L4,5}$ (Right); Source: [31]

Case 5: Further reduction in the value of the jacobi constant allows the spacecraft to essentially travel anywhere in this system and beyond, without any forbidden regions.

4 Construction of Halo Orbits and Invariant manifolds

As mentioned in the section 1.1.1, the comet Interceptor mission aims to place the spacecraft in a Halo orbit around the Sun-Earth L2 lagrangian point in order to conduct operations when a suitable asteroid/comet is detected. This chapter deals with the analytical development of a local approximation for a three-dimensional periodic orbit around the collinear lagrangian point L2, using the methods of first and third order analytical approximations to receive an initial guess for the starting point of the orbit. This is further used in conjunction with a differential correction method involving the state Transition Matrix, in order to prune the obtained initial guess.

4.1 Third-Order Approximation for Halo orbits

While the first-order approximation method is accurate in the neighbourhood of the lagrangian points, the initial conditions obtained from that method are not accurate enough for the computation of some halo orbits in the CR3BP [31].

Therefore, the third order analytical approximation method is employed in an attempt to obtain more precise values of the initial conditions. This is done with the help of the algorithm presented in [32], generally termed the Richardson method, which has been explained below.

The equations of motion of a spacecraft in the vicinity of the collinear lagrangian points can be obtained by the lagrangian, L, given by,

$$L = \frac{1}{2}\left(\dot{\bar{r}}_{s/c-L}.\dot{\bar{r}}_{s/c-L}\right) + (1-\mu)\left(\frac{1}{\left|\bar{r}_{S-L} - \bar{r}_{s/c-L}\right|} - \frac{\bar{r}_{S-L}.\bar{r}_{s/c-L}}{|\bar{r}_{S-L}|^3}\right) + (\mu)\left(\frac{1}{\left|\bar{r}_{E-L} - \bar{r}_{s/c-L}\right|} - \frac{\bar{r}_{E-L}.\bar{r}_{s/c-L}}{|\bar{r}_{E-L}|^3}\right) \tag{4-1}$$

where $\bar{r}_{S-L}$, $\bar{r}_{E-L}$, and $\bar{r}_{s/c-L}$ are the position vectors of the Sun, the Earth, and the spacecraft with respect to the lagrangian point. For the purposes of this thesis, the collinear lagrangian point L2 is being used for further calculations.

The system of normalized units utilized in CR3BP is used in order to further simplify the lagrangian, along with few additional units especially for the vicinity of the libration points. Some of the non-dimensionalized values used are mentioned below.

The units of distance and mass for motion about the L2 lagrangian point are taken as:

$$r_1 = 1 \;; \quad \mu = \frac{m_E}{m_S + m_E} \tag{4-2}$$

Another important dimensionless quantity useful in deriving other quantities is the ratio γ_L, defined by,

$$\gamma_L = \frac{r_1}{a_1} \;\; (For\ L2) \tag{4-3}$$

Where a_1 is the mean distance of Earth in its orbit around the Sun.

Using the above-mentioned non-dimensional values, the lagrangian L can be reduced to the following equation, with the notations and usage of Legendre polynomial, $P_n(x/\rho)$.

$$L = \frac{1}{2}(\rho^{*}.\rho^{*}) + \sum_{n=2}^{\infty} c_n \rho^n P_n(x/\rho) \tag{4-4}$$

Where the constant c_n is dependant on the normalized values of γ_L and μ, as given in the below-mentioned equation.

$$c_n = \frac{1}{{\gamma_L}^3}[(-1)^n\mu + (-1)^n \frac{(1-\ \mu){\gamma_L}^{n+1}}{(1+\gamma_L)^{n+1}}] \tag{4-5}$$

The three-dimensional equations of motion derived from the application of this lagrangian L are given by,

$$(\ddot{x} - 2\dot{y} - (1 + 2c_2)x) = \sum_{n=2}^{\infty}(n+1)c_{n+1}\rho^n P_n(x/\rho) \tag{4-6}$$

$$(\ddot{y} + 2\dot{x} + (c_2 - 1)y) = \sum_{n=3}^{\infty} c_n y \rho^{n-2} \tilde{P}_n(x/\rho) \tag{4-7}$$

$$(\ddot{z} + (c_2 z) = \sum_{n=3}^{\infty} c_n z \rho^{n-2} \tilde{P}_n(x/\rho) \tag{4-8}$$

where,

$$\tilde{P}_n\left(\frac{x}{\rho}\right) = \sum_{n=0}^{(n-2)/2} (3 + 4k - 2n) P_{n-2k-2}(x/\rho) \tag{4-9}$$

A new independent variable, $\tau = \omega nt$, where n is the orbital mean motion of the primary mass, is introduced to remove terms which appear because of the successive approximation method. This is in turn useful for rewriting the equations (4-6), (4-7), and (4-8) as,

$$(\omega^2\ddot{x} - 2\omega\dot{y} - (1 + 2c_2)x) = 1.5c_3(2x^2 - y^2 - z^2) + 2c_4(2x^2 - 3y^2 - 3z^2) \tag{4-10}$$

$$(\omega^2\ddot{y} + 2\omega\dot{x} + (c_2 - 1)y) = -3c_3xy - 1.5c_4y(4x^2 - y^2 - z^2) \tag{4-11}$$

$$(\omega^2\ddot{z} + c_2 z) = -3c_3 xz - 1.5c_4 z(4x^2 - y^2 - z^2) \quad \textbf{(4-12)}$$

where the frequency correction term ω is written in terms of ω_n, whose values are chosen accordingly so that the secular terms are removed.

$$\omega = 1 + \sum_{n\geq 1} \omega_n \quad \textbf{(4-13)}$$

The above-mentioned equations are used in a method similar to the Lindstedt-Poincaré method for a series of successive approximations [32]. Hence, the complete third-order solution for a periodic orbit around the collinear lagrangian points is found to be,

$$x = a_{21}A_x^2 + a_{22}A_z^2 - A_x\cos(\tau_1) + (a_{23}A_x^2 - a_{24}A_z^2)\cos(2\tau_1) + (a_{31}A_x^3 - a_{32}A_xA_z^2)\cos(3\tau_1) \quad \textbf{(4-14)}$$

$$y = kA_x\sin(\tau_1) + ((b_{21}A_x^2 - b_{22}A_z^2)\sin(2\tau_1) + (b_{31}A_x^3 - b_{32}A_xA_z^2)\sin(3\tau_1) \quad \textbf{(4-15)}$$

$$z = \delta_n A_z\cos(\tau_1) + \delta_n d_{21}A_xA_z(\cos(2\tau_1) - 3) + \delta_n(d_{32}A_zA_x^2 - d_{31}A_z^3)\cos(3\tau_1) \quad \textbf{(4-16)}$$

Where τ_1 is determined using its relationship with the phase angle ϕ like,

$$\tau_1 = \lambda t + \phi \quad \textbf{(4-17)}$$

The values of the different coefficients $(a_{ij}, b_{ij}, d_{ij,}\delta_n, \tau_1, etc.)$ present in the above-mentioned equations are provided in 7Appendix A, along with the associated techniques of determination. It can be seen from the formulations in 7Appendix A that it is possible to obtain the values of the initial position vector of the spacecraft (x, y, z) in the vicinity of the libration point, given only the amplitude in the Z-direction (A_z). Furthermore, in order to complete the initial state vector, the position vector equations (4-14), (4-15), and (4-16) are differentiated to obtain the initial velocity vectors $(\dot{x}, \dot{y}, \dot{z})$, whose expressions are also found in 7Appendix A.

For the purposes of this thesis, a halo orbit with amplitude A_z of 611,000 km has been selected and worked with, and the initial conditions have been obtained using the Richardson method and its techniques presented above. The coefficients used in the third order approximation method have been recorded in Table A-1 in 7Appendix A.

The below-mentioned table contains the initial guess (State Vector) of the trajectory of the halo orbit around the L2 lagrangian point in the Sun-Earth system. The values represented are normalized and have been done so in order to pave way for less complex calculations in the CR3BP.

State Vector components (L2-centered)	Values (Non-Dimensional)
x_0	-0.297136770570493
y_0	0
z_0	0.356938560885605
x'_0	0
y'_0	1.430582985888843
z'_0	0

Table 4-1: Initial conditions for a Halo orbit of A_z=611000 km, computed from the Third-order approximation method

Since the values represented in the above table pertain to a reference frame centred at the lagrangian point L2, it is imperative to convert those values into the rotating system of coordinates, which is the preferred reference frame for systems in the CR3BP. It is done by shifting the centre of the system from the L2 point to the barycenter, implying an addition in the position vector of the initial guess in Table 4-1. It is represented in the following equations.

$$(SV)_{L2} = \begin{bmatrix} x_0 \\ y_0 \\ z_0 \\ x'_0 \\ y'_0 \\ z'_0 \end{bmatrix} ; \ (SV)_{RRF} = d_{L2-Earth} \begin{bmatrix} x_0 \\ y_0 \\ z_0 \\ x'_0 \\ y'_0 \\ z'_0 \end{bmatrix} + B_{L2-RRF} \tag{4-18}$$

Where $d_{L2-Earth}$ is the distance between the Earth and the L2 point, and the matrix B_{L2-RRF} contains the position and velocity vectors of the L2 point in the rotating reference frame, given by,

$$B_{L2-RRF} = \begin{bmatrix} x_{L2} \\ y_{L2} \\ z_{L2} \\ x'_{L2} \\ y'_{L2} \\ z'_{L2} \end{bmatrix}_{RRF} = \begin{bmatrix} x_{L2} \\ 0 \\ 0 \\ 0 \\ 0 \\ 0 \end{bmatrix}_{RRF} = \begin{bmatrix} 1.010090489225235 \\ 0 \\ 0 \\ 0 \\ 0 \\ 0 \end{bmatrix}_{RRF} \quad \textbf{(4-19)}$$

Therefore, the initial guess obtained from the Richardson method, after conversion from the L2-centered reference frame, is recorded in Table 4-2.

State Vector components (RRF)	Values (Non-Dimensional)
$\boldsymbol{x_0}$	1.007119121519530
$\boldsymbol{y_0}$	0
$\boldsymbol{z_0}$	0.003569385608856
$\boldsymbol{x'_0}$	0
$\boldsymbol{y'_0}$	0.014305829858888
$\boldsymbol{z'_0}$	0

Table 4-2: Initial conditions of the Halo orbit after conversion from the L2-centered reference frame to the Rotating Reference Frame

The propagated trajectory, using the values of the state vector from Table 4-2, has been plotted using MATLAB with the help of a variable order method of solving ordinary differential equations. The obtained plots of the trajectory in the X-Y plane, and in the 3D view are shown below in.

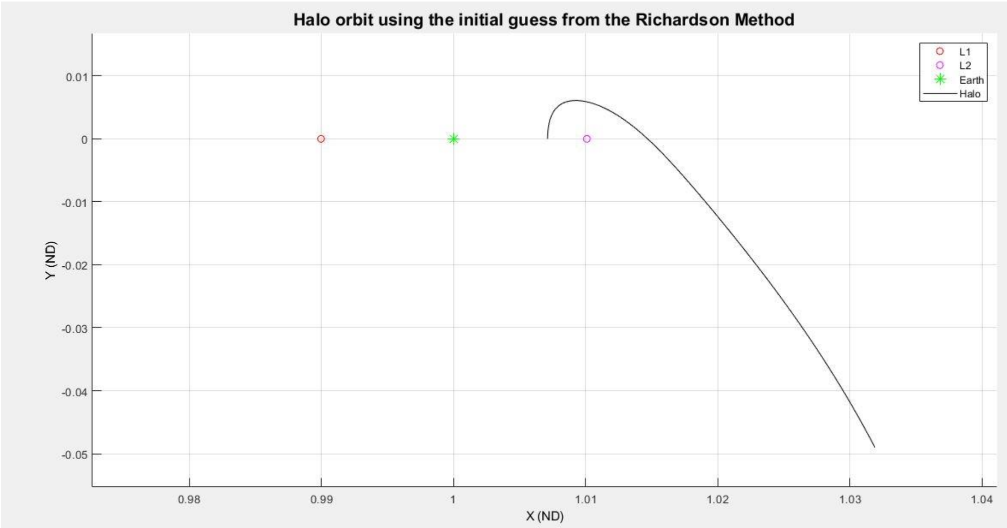

Figure 4.1: The X-Y plane of the trajectory obtained using the initial guess from the Richardson method

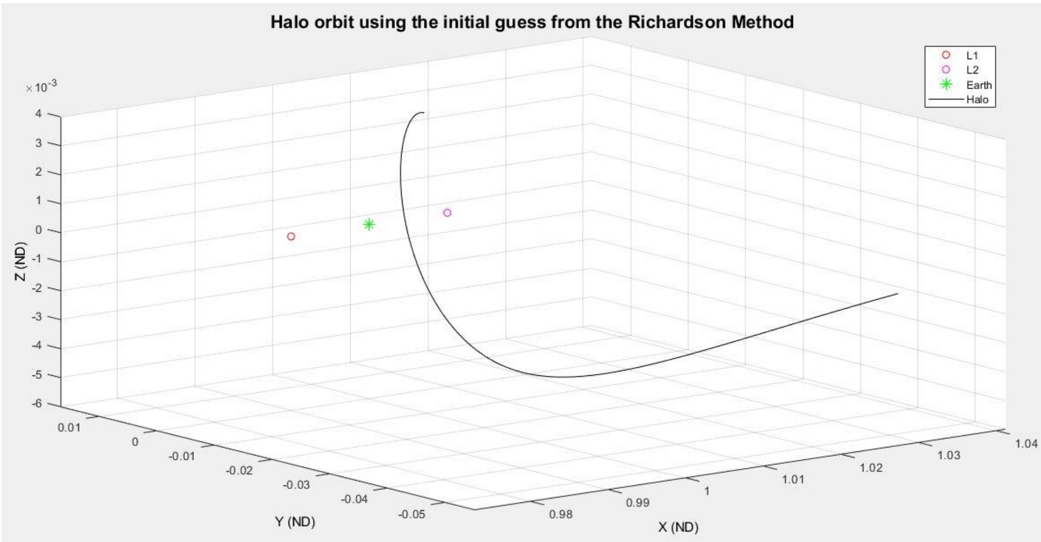

Figure 4.2: The 3D view of the trajectory obtained using the initial guess from the Richardson method

As seen in the Figure 4.1 and Figure 4.2, while the initial guess provides a basic insight into the dynamics of the CR3BP and how the trajectory evolves around the L2 point, it is not sufficient to obtain a more accurate, closed periodic orbit. Therefore, the initial state vector obtained from the third-order approximation method has to be pruned using a set of numerical integration methods so that the obtained orbit is a closed periodic orbit. This is done by using a differential corrector method, utilising the concept of state-transition matrix, explained in the sections below.

4.2 State Transition Matrix (STM)

Since the initial state vector for the trajectory of a halo orbit around L2, presented in Table 4-2, does not yield the desired closed periodic orbit in the CR3BP system, a set of numerical integration tools are used in order to determine a specific initial condition for the given system of bodies. This method of using numerical integration improves the initial guess obtained from Richardson's third-order approximation method by predicting its behaviour near the reference solution. This requires a matrix, called the state transition matrix, containing the information regarding the sensitivity of the dynamics of a particular state to perturbations in the initial guess [33]. Therefore, having an initial guess, there is a need to linearize the dynamical system, after which the periodic orbit can be numerically computed.

If $\bar{x}$ is the state vector in a given 3-dimensional space, then the non-linear dynamical system is given by the differential equation as shown below.

$$\bar{x} = \begin{bmatrix} \mathrm{x} \\ y \\ z \\ x' \\ y' \\ z' \end{bmatrix}_{RRF} \quad ; \quad \dot{\bar{x}} = f(\bar{x}) \tag{4-20}$$

Expanding the non-linear equation in a Taylor series results in the linearization of the system of the periodic orbit. The higher order terms are generally ignored in the expansion. Therefore, the equation is changed to a homogenous, linear equation dependent on a perturbation as given below.

$$\delta\dot{\bar{x}} = A(t)\delta\bar{x} \tag{4-21}$$

Where $\delta\bar{x} = [\delta\mathrm{x}, \delta y, \delta z, \delta x', \delta y', \delta z']^T$ is the perturbation relative to the reference guess and $A(t)$ is a [6x6] matrix called the State-Transition Matrix.

The STM, $A(t)$, can be represented as follows:

$$A(t) = \begin{bmatrix} 0_3 & I_3 \\ U & 2\Omega_3 \end{bmatrix} \quad \textbf{(4-22)}$$

The submatrices 0_3 and I_3 represent [3x3] null and identity matrices respectively.

$$0_3 = \begin{bmatrix} 0 & 0 & 0 \\ 0 & 0 & 0 \\ 0 & 0 & 0 \end{bmatrix} ;\ I_3 = \begin{bmatrix} 1 & 0 & 0 \\ 0 & 1 & 0 \\ 0 & 0 & 1 \end{bmatrix} \quad \textbf{(4-23)}$$

The submatrix Ω_3 is evaluated as,

$$\Omega_3 = \begin{bmatrix} 0 & 1 & 0 \\ -1 & 0 & 0 \\ 0 & 0 & 0 \end{bmatrix} ;\ 2\Omega_3 = \begin{bmatrix} 0 & 2 & 0 \\ -2 & 0 & 0 \\ 0 & 0 & 0 \end{bmatrix} \quad \textbf{(4-24)}$$

And finally, the submatrix U contains the second partial derivatives of each element with respect to the position states of the reference elements.

$$U = \begin{bmatrix} U_{xx} & U_{xy} & U_{xz} \\ U_{yx} & U_{yy} & U_{yz} \\ U_{zx} & U_{zy} & U_{zz} \end{bmatrix} ;\ U = \begin{bmatrix} \frac{\partial^2 U}{\partial x^2} & \frac{\partial^2 U}{\partial x \partial y} & \frac{\partial^2 U}{\partial x \partial z} \\ \frac{\partial^2 U}{\partial y \partial x} & \frac{\partial^2 U}{\partial y^2} & \frac{\partial^2 U}{\partial y \partial z} \\ \frac{\partial^2 U}{\partial z \partial x} & \frac{\partial^2 U}{\partial z \partial y} & \frac{\partial^2 U}{\partial z^2} \end{bmatrix} \quad \textbf{(4-25)}$$

Since the pseudo-potential function U has already been defined in equation (3-39), the individual elements of matrix U can be calculated by partial differentiation. The elements are mentioned below.

$$\frac{\partial^2 U}{\partial x^2} = 1 - \frac{(1-\mu)}{r^3_{S-s/c}} + \frac{3(1-\mu) * (x+\mu)^2}{r^5_{S-s/c}} - \frac{(\mu)}{r^3_{E-\frac{s}{c}}} + \frac{3(\mu) * (x-1+\mu)^2}{r^5_{E-\frac{s}{c}}} \quad \textbf{(4-26)}$$

$$\frac{\partial^2 U}{\partial y^2} = 1 - \frac{(1-\mu)}{r^3_{S-s/c}} + \frac{3(1-\mu) * (y)^2}{r^5_{S-s/c}} - \frac{(\mu)}{r^3_{E-\frac{s}{c}}} + \frac{3(\mu) * (y)^2}{r^5_{E-\frac{s}{c}}} \quad \textbf{(4-27)}$$

$$\frac{\partial^2 U}{\partial z^2} = -\frac{(1-\mu)}{r^3_{S-s/c}} + \frac{3(1-\mu) * (z)^2}{r^5_{S-s/c}} - \frac{(\mu)}{r^3_{E-\frac{s}{c}}} + \frac{3(\mu) * (z)^2}{r^5_{E-\frac{s}{c}}} \quad \textbf{(4-28)}$$

$$\frac{\partial^2 U}{\partial x \partial y} = \frac{\partial^2 U}{\partial y \partial x} = \frac{3(1-\mu)(x+\mu)y}{r_{S-s/c}^5} + \frac{3(\mu)(x-1+\mu)y}{r_{E-\frac{s}{c}}^5} \tag{4-29}$$

$$\frac{\partial^2 U}{\partial y \partial z} = \frac{\partial^2 U}{\partial z \partial y} = \frac{3(1-\mu)zy}{r_{S-s/c}^5} + \frac{3(\mu)zy}{r_{E-\frac{s}{c}}^5} \tag{4-30}$$

$$\frac{\partial^2 U}{\partial x \partial z} = \frac{\partial^2 U}{\partial z \partial x} = \frac{3(1-\mu)(x+\mu)z}{r_{S-s/c}^5} + \frac{3(\mu)(x-1+\mu)z}{r_{E-\frac{s}{c}}^5} \tag{4-31}$$

Using these values, the state transition matrix can be computed and can further be used to determine the required state vector (at time t) given the starting position and velocity i.e., initial state vector $\bar{x}$, and the perturbation $\delta\bar{x}$. Thus, the general solution can be calculated as given below.

A non-singular [6x6] matrix, $\psi(t)$, is assumed to satisfy the following equation.

$$\dot{\psi}(t) = A(t)\psi(t) \tag{4-32}$$

The general solution for equation (4-21) is now written in terms of $\psi(t)$ as,

$$\delta\bar{x}(t) = \psi(t)c \tag{4-33}$$

Where c is a constant vector. At $t = t_0$ (Initial time),

$$\delta\bar{x}(t_0) = \psi(t_0)c \tag{4-34}$$

From the above equation, the constant vector c can be calculated by calculating the inverse of $\psi(t_0)$.

$$c = \left(\psi(t_0)\right)^{-1}\delta\bar{x}(t_0) \tag{4-35}$$

Substituting equation (4-35) in equation (4-33) gives,

$$\delta\bar{x}(t) = \psi(t)\left(\psi(t_0)\right)^{-1}\delta\bar{x}(t_0) \tag{4-36}$$

The value of $\psi(t) * \left(\psi(t_0)\right)^{-1}$ is the state-transition matrix, represented by ϕ.

$$\phi(t, t_0) = \psi(t)\big(\psi(t_0)\big)^{-1} \quad \textbf{(4-37)}$$

Therefore, from equation (4-36), the final general solution can be represented as,

$$\delta\bar{x}(t) = \phi(t, t_0)\delta\bar{x}(t) \quad \textbf{(4-38)}$$

This equation aids in determining the change in state vector after some time t, given a small change or perturbation to the initial state vector. The value of the elements after any time t can be found by propagating the initial state vector from time t_0 to time t [27].

The state transition matrix can be evaluated at the initial time t_0 in order to check for its validity, i.e.,

$$\delta\bar{x}(t_0) = \phi(t_0, t_0)\delta\bar{x}(t_0) \quad \textbf{(4-39)}$$

Equation (4-39) implies that the value of the state transition matrix at the initial time is the identity matrix, implying that the subsequent systems of the state are sensitive to the initial state of the system.

$$\phi(t_0, t_0) = I \quad \textbf{(4-40)}$$

Another specific condition exists for equation (4-38), where $t = t_0 + period$, useful for determining the dynamics of the orbit after one complete rotation period (t_P). This state transition matrix is generally known as the Monodromy matrix.

$$\phi(t_0 + t_P, t_0) = \phi_{MONODROMY} \quad \textbf{(4-41)}$$

One of the applications of the State-Transition Matrix lies in the differential corrector algorithm, which is an efficient technique for determining specific initial conditions [33].

4.3 Differential Correction

Computation of periodic orbits of a system requires certain initial conditions. Since the closed-form solutions cannot be obtained analytically for the three-body system, an efficient methodology employing a set of numerical tools can be used to determine the trajectory of the body around the said system [34]. This section deals with a differential correction scheme, which is used in order to achieve a desired orbit, provided an initial condition. It works in conjunction with the application of State-Transition Matrices by predicting the amount of perturbation that needs to be applied to the initial conditions so that the final trajectory is desirable.

This method involves 2 main matrices, the constraint matrix and the free variable matrix. The free variable matrix comprises of elements which can be modified, such as the initial velocity components and the integration time, so that certain conditions are satisfied, while the constraint matrix consists of quantities that are under some constraint and need to be satisfied by the resultant, propagated trajectory, such as the final and initial positions and time of flight. The 2 matrices are represented as,

$$Free\ Variable\ Matrix = \bar{X}_0\ ; Constraint\ Matrix = F(\bar{X}_0) \quad \textbf{(4-42)}$$

In order to determine the proper set of free variables which satisfy the mission constraints, the initial state vector obtained by Richardson method is used as the initial free variable matrix, which is present in Table 4-2. Now, using the Taylor series expansion, equation (4-21) can be expanded for the initial guess as,

$$F(\bar{X}) = \quad F(\bar{X}_0) + \frac{\partial F(\bar{X}_0)}{\partial \bar{X}_0}(\bar{X} - \bar{X}_0) + .. \quad \textbf{(4-43)}$$

The higher order terms arising from the Taylor series expansion are neglected. And, it can be seen from the above equation that the second term in the Right-Hand Side is a function of the partial derivative of the constraint variables with respect to the free variables i.e., $\frac{\partial F(\bar{X}_0)}{\partial \bar{X}_0}$ is the Jacobian matrix of the system. It can also be represented by the below mentioned matrix, which is similar to equation (4-22).

$$DF(\bar{X}_0) = \frac{\partial F(\bar{X}_0)}{\partial \bar{X}_0} = \begin{bmatrix} \frac{\partial F_1}{\partial X_1} & \cdots & \frac{\partial F_1}{\partial X_f} \\ \vdots & \ddots & \vdots \\ \frac{\partial F_c}{\partial X_1} & \cdots & \frac{\partial F_c}{\partial X_f} \end{bmatrix} \tag{4-44}$$

Variables f and c signify the number of elements in the free variable and constraint matrices respectively, values for which are the same for this system in the CR3BP. Now, the equation (4-43) looks like,

$$F(\bar{X}) = F(\bar{X}_0) + DF(\bar{X}_0) * (\bar{X} - \bar{X}_0) \tag{4-45}$$

If the constraint equations are not satisfied, and if $F(\bar{X}) \neq 0,$ using the above equation, the initial condition for the next iteration, $(\bar{X})$, can be determined by calculating the inverse of the Jacobian matrix i.e.,

$$\bar{X} = (\bar{X}_0) - DF(\bar{X}_0)^{-1} * F(\bar{X}_0) \tag{4-46}$$

If the number of free variables (f) exceeds the number of constraint variables (c), the system is called an under determined system and hence, the equation (4-46) changes to the following:

$$\bar{X} = (\bar{X}_0) - DF(\bar{X}_0)^T (DF(\bar{X}_0) DF(\bar{X}_0)^T)^{-1} * F(\bar{X}_0) \tag{4-47}$$

In another possible case, if the number of constraint variables (c) exceeds the number of free variables (f), the equation (4-46) changes into:

$$\bar{X} = (\bar{X}_0) - (DF(\bar{X}_0)^T DF(\bar{X}_0))^{-1} DF(\bar{X}_0)^T * F(\bar{X}_0) \tag{4-48}$$

Till an error constraint vector (Equation (4-49)) is larger than the required value of error, the above equation helps in the computation of the final value of the required initial condition through an iterative process, where the elements of the Jacobian matrix keep changing because of the changes in the free variable and constraint matrices. This way, the initial conditions or the free variables of the subsequent iteration is dependent on the free and constraint variables of the present state. The defined error constraint vector should be larger than the Euclidean norm of the constraint vector ([31]) and is given by,

$$Tolerance\ \varepsilon = |F(\bar{X})| < 10^{-16} \quad \textbf{(4-49)}$$

The summary of the iterative process of differential correction has been given below:

1. Understanding the system and identifying the required free variables $(\bar{X})$ for constructing the halo orbit
2. Obtaining the first guess of the initial state vector from Richardson's third-order approximation method $(\bar{X}_0)$, which is the first free variable vector
3. Defining the constraints of the problem which need to be satisfied $F(\bar{X})$
4. Using the current free variable and constraint matrices to calculate the Jacobian matrix $DF(\bar{X}_0)$
5. Solving for the next set of free variables, $F(\bar{X})^{i+1}$, using the equation (4-46), where i represents the current iteration
6. Using equation (4-49) to determine the error of the constraint vector. If it is lower than the set value of tolerance, the solution has been achieved and $(\bar{X})$ of that particular state is the state vector used to construct the halo orbit. If not, the process needs to be repeated from step 5 till the method converges

Differential correction techniques can be used for solving a multitude of problems, including calculation of trajectories, generation of halo orbits, etc. Depending on the type of problem, there are many approaches which can be used. For the construction of Halo orbits, an option called the Single Shooting method has been elaborated in the following section.

4.3.1 Single Shooting Method

The shooting method is a differential correction method which is used for solving differential equations coupled with constraints by reducing it to a system of initial values, which specify how the system evolves with time [35]. The single shooting method involves the computation of trajectories, by finding the solution using an initial state vector, so that the final state vector or the constraint vector has been satisfied. The analysis of the single shooting method of differential correction is given below.

The first step of this method involves the propagation of the initial state vector using the equations of motion in the CR3BP for a given time t. Using the achieved final state after propagation, an insight into the current state of the system and initial state vector can be obtained so that a closer approach to the target/final state vector can be made by modifying the initial conditions accordingly. This simple objective of satisfying the set constraints in order to reach the desired value is the concept of the single shooting method. The said process can be done through 2 different cases of integration times, a fixed integration time where the integration time is kept a constant over the entire timeframe and a variable integration time where the integration time keeps varying through iterations.

This thesis deals with a single shooting method of differential correction using a fixed integration time, which is formulated as follows.

The free variables vector for the first iteration is written as equation (4-50), similar to equation (4-20).

$$\bar{X}_0 = \begin{bmatrix} \mathrm{x}_0 \\ y_0 \\ z_0 \\ \mathrm{x}'_0 \\ y'_0 \\ z'_0 \end{bmatrix} \tag{4-50}$$

Because of the fact that the only variables that can be modified in order to reach the desired final state are the initial velocity components, equation (4-50) can be rewritten as,

$$\bar{X}_0 = \begin{bmatrix} \mathrm{x}'_0 \\ y'_0 \\ z'_0 \end{bmatrix} = \begin{bmatrix} x'(t_{\mathbf{0}}) \\ y'(t_{\mathbf{0}}) \\ z'(t_{\mathbf{0}}) \end{bmatrix} \tag{4-51}$$

The final state of the system is defined as follows:

$$\bar{X}_d = \begin{bmatrix} \mathrm{x}_d \\ y_d \\ z_d \\ \mathrm{x}'_d \\ y'_d \\ z'_d \end{bmatrix} \quad \textbf{(4-52)}$$

Since only the final position states (After time T) determine the constraints of the problem,

$$\bar{X}_d = \begin{bmatrix} x_d \\ y_d \\ z_d \end{bmatrix} = \begin{bmatrix} x_d(t_0+T) \\ y_d(t_0+T) \\ z_d(t_0+T) \end{bmatrix} \quad \textbf{(4-53)}$$

The next step is to obtain the constraint vectors of the system using the desired final position states, which is given by,

$$F(\bar{X}_d(t_{\mathbf{0}}+T)) = \begin{bmatrix} x_d(t_0+T) - x_0 \\ y_d(t_0+T) - y_0 \\ z_d(t_0+T) - z_0 \end{bmatrix} \quad \textbf{(4-54)}$$

After having created the free variables and the constraint matrices, the Jacobian matrix of the system with respect to those 2 matrices is now constructed as the following.

$$DF(\bar{X}_0) = \begin{bmatrix} \frac{\partial F_1}{\partial X_1} & \cdots & \frac{\partial F_1}{\partial X_f} \\ \vdots & \ddots & \vdots \\ \frac{\partial F_c}{\partial X_1} & \cdots & \frac{\partial F_c}{\partial X_f} \end{bmatrix} = \begin{bmatrix} \frac{\partial x_d(t_0+T)}{\partial \mathrm{x}'_0} & \frac{\partial x_d(t_0+T)}{\partial y'_0} & \frac{\partial x_d(t_0+T)}{\partial z'_0} \\ \frac{\partial y_d(t_0+T)}{\partial \mathrm{x}'_0} & \frac{\partial y_d(t_0+T)}{\partial y'_0} & \frac{\partial y_d(t_0+T)}{\partial z'_0} \\ \frac{\partial z_d(t_0+T)}{\partial \mathrm{x}'_0} & \frac{\partial z_d(t_0+T)}{\partial y'_0} & \frac{\partial z_d(t_0+T)}{\partial z'_0} \end{bmatrix} \quad \textbf{(4-55)}$$

Using the above-mentioned Jacobian matrix which relates the initial velocity states of the system with the final position states of the system, the sensitivity of the final states of the system is quantified. Therefore, in order to complete this method, the differential corrector procedure explained in section 4.3 is carried out, giving out the required value of the initial state of the system.

The next section deals with the method of generation of the required Halo orbit using the differential corrector algorithm, given the initial condition.

4.4 Generation of Halo orbit

The periodic solution of a general halo orbit is found by applying the differential corrector for an estimate of the required initial condition, which is obtained through the third order approximation method, as seen in section 4.1. The aim is to obtain the required initial state vector so that it fulfils the constraints imposed by the desired trajectory.

Since halo orbits cross the y = 0 plane perpendicularly, it is said that the halo orbits are symmetrical around the y-plane [31]. Therefore, the components V_x and V_z of an initial state vector need to be zero in order to construct a closed periodic orbit. Now, the initial state vector can be written as,

$$\bar{X}_0 = \begin{bmatrix} \mathrm{x}_0 \\ 0 \\ z_0 \\ 0 \\ y'_0 \\ 0 \end{bmatrix} \tag{4-56}$$

This initial condition needs to be propagated till a point where the differential corrector can be applied. In an attempt to do this, the free variables and constraint matrices need to be determined. From the state vector given above, only the 3 values (x_0, z_0, y'_0) can be modified and therefore constitute the free variables vector.

$$\bar{X} = \begin{bmatrix} \mathrm{x}_0 \\ z_0 \\ y'_0 \end{bmatrix} \tag{4-57}$$

Since the values of (y_0, x'_0, z'_0) need to be equal to zero at the end of the time period as well, the desired final state vector is similar to the initial state vector.

$$\bar{X}_F = \begin{bmatrix} \mathrm{x}_F \\ 0 \\ Z_F \\ 0 \\ Y'_F \\ 0 \end{bmatrix} \tag{4-58}$$

The constraint vector is a function of velocities in the x and z directions. The value of the y-component can also be added, but since it is satisfied ($y = 0$) automatically after the time period, it is not necessary.

$$F(\bar{X}_d(t_{\mathbf{0}} + T)) = \begin{bmatrix} y_d(t_0 + T) - y_0 \\ x'_d(t_0 + T) - x'_0 \\ z'_d(t_0 + T) - z'_0 \end{bmatrix} = \begin{bmatrix} x'_d(t_0 + T) - x'_0 \\ z'_d(t_0 + T) - z'_0 \end{bmatrix} \quad \textbf{(4-59)}$$

Equations (4-57) and (4-59) signify that in order to achieve the 2 desired final states, 3 initial free variables can be modified. This is done by fixing one of the 2 free variables containing position states (x_0 and z_0). There are 2 possible conditions for which the Jacobian matrices need to be found. In the first condition, the value of x_0 is kept a constant, while in the second condition, the value of $z_{\mathbf{0}}$ is kept a constant. The Jacobian matrices are given by,

$$CASE\ 1{:}\ x_0 = CONSTANT;\ DF(\bar{X}_0) = \begin{bmatrix} \frac{\partial x'_d(t_0 + T)}{\partial z_0} & \frac{\partial x'_d(t_0 + T)}{\partial y'_0} \\ \frac{\partial z'_d(t_0 + T)}{\partial z_0} & \frac{\partial z'_d(t_0 + T)}{\partial y'_0} \end{bmatrix} \quad \textbf{(4-60)}$$

$$CASE\ 2{:}\ z_0 = CONSTANT;\ DF(\bar{X}_0) = \begin{bmatrix} \frac{\partial x'_d(t_0 + T)}{\partial x_0} & \frac{\partial x'_d(t_0 + T)}{\partial y'_0} \\ \frac{\partial z'_d(t_0 + T)}{\partial x_0} & \frac{\partial z'_d(t_0 + T)}{\partial y'_0} \end{bmatrix} \quad \textbf{(4-61)}$$

After calculating the values of the Jacobian matrices, the single shooting approach with the following steps needs to be implemented to get accurate initial conditions.

1. The initial guess obtained from the Richardson's third order method must be used
2. The free variables and the constraint matrices need to be defined using equations (4-57) and (4-59) according to the required application
3. The Jacobian matrices need to be determined using the free variables and the constraint vectors for either case (Equations (4-60) and (4-61))
4. Equation (4-46) needs to be used in order to determine the next initial state

5. Integration of the obtained initial condition of the current state must be done for half the time period (Till the halo orbit crosses the x-z plane)
6. The error in the values of the (y_0, x'_0, z'_0) need to be calculated from equation (4-49), since they need to be zero
7. The obtained error tolerance value needs to be compared with the accepted value of tolerance. The method is said to be converged if the obtained tolerance is lesser than the accepted tolerance. Else, Step 4 needs to be repeated until satisfactory tolerance is satisfied
8. The complete periodic orbit is constructed with the obtained value of the accurate initial conditions

The initial state vector obtained after differential correction is recorded in Table 4-3.

State Vector components (RRF)	Values (Non-Dimensional)
$\boldsymbol{x_0}$	1.006853340998547
$\boldsymbol{y_0}$	0
$\boldsymbol{z_0}$	0.003569385608856
$\boldsymbol{x'_0}$	0
$\boldsymbol{y'_0}$	0.014729952513454
$\boldsymbol{z'_0}$	0

Table 4-3: Initial conditions of the required Halo orbit after using differential correction (Single Shooting Method)

The time period of the Halo orbit before implementing the differential corrector is 178.955 days, whose formulation can be found in 7Appendix A. Now, the time period for the newly found initial conditions, after using the differential correction, is given by,

$$T = 3.0746075\ (ND) = 178.7257952\ DAYS \qquad \textbf{(4-62)}$$

If the initial state vector in Table 4-3 is propagated for half its time period ($T/2$), the obtained halo orbit is,

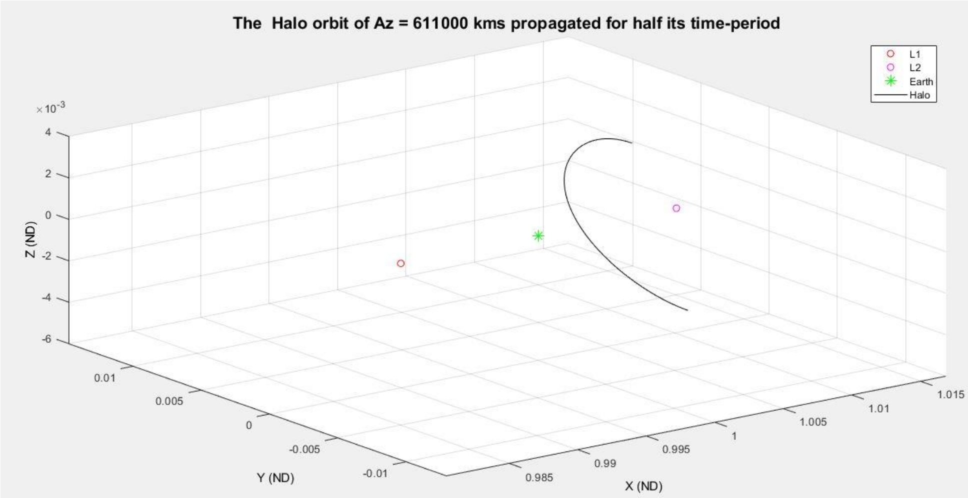

Figure 4.3: The initial conditions propagated for half the time-period (T/2), resulting in a partial halo

The complete, desired halo orbit of $A_z = 611000\, km$ has been obtained by propagating it for its entire time-period, whose figures have been given below.

The three-dimensional halo orbit is represented in the following figure:

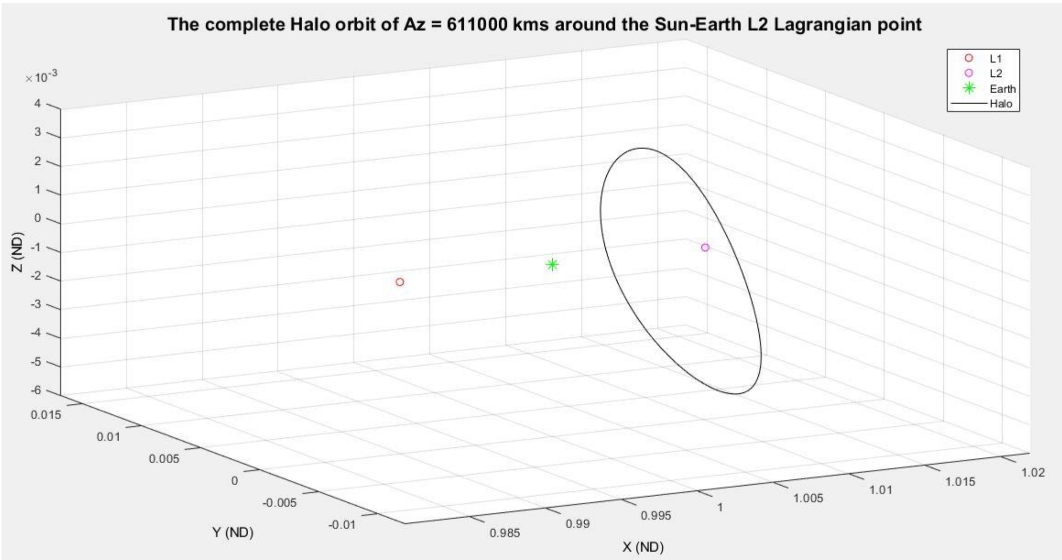

Figure 4.4: The 3D view of the complete periodic halo orbit of $A_z = 611000\ km$

The different planar views have also been given in subsequent figures for purposes of visualisation.

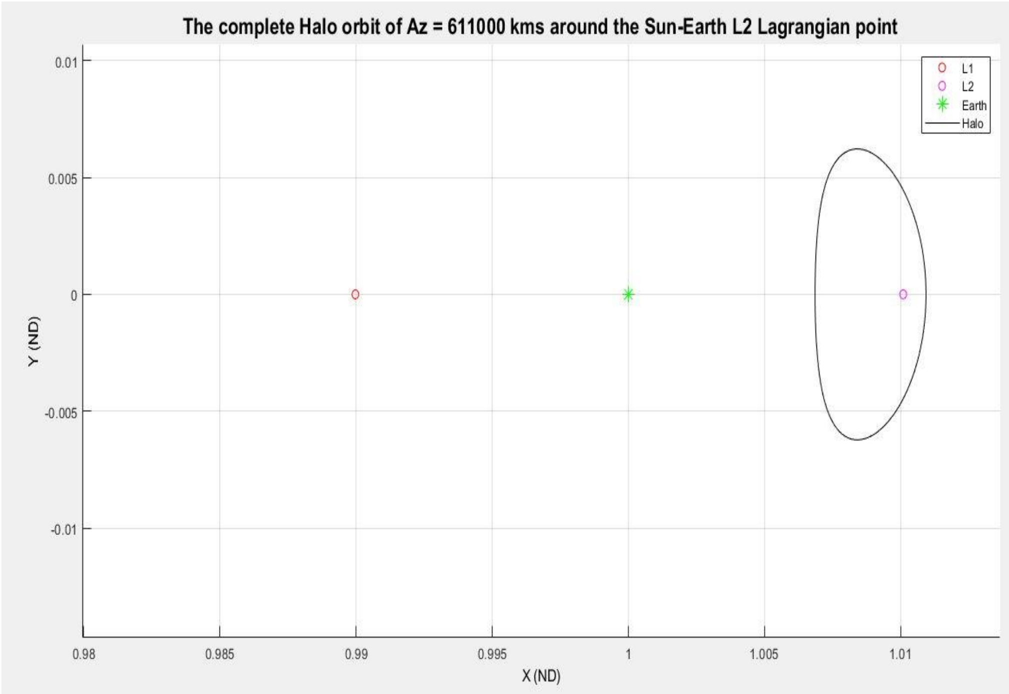

Figure 4.5: The desired halo orbit in the X-Y plane

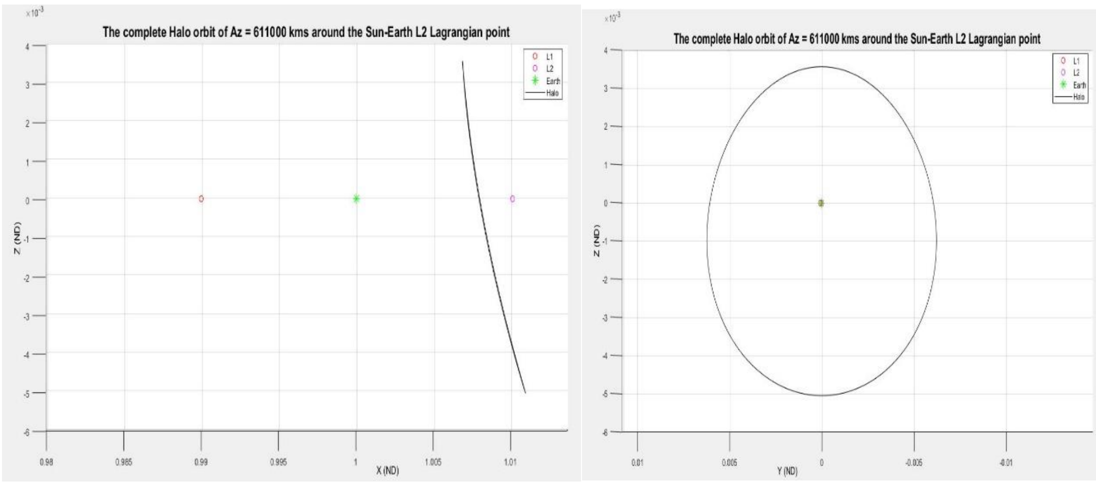

Figure 4.6: The X-Z (Left) and Y-Z (Right) views of the complete Halo orbit

4.5 Stablility of the Halo orbit

The stability of a halo orbit often plays a vital role in the design of space missions. Depending on the application, missions can either decide to opt for one particular halo orbit around one of the lagrangian points for its entire mission timeline or multiple periodic orbits depending on the mission constraints [29]. In general, if a mission is aiming for a specific periodic orbit for a long time, a stable periodic orbit is the suitable choice due to the fact that the spacecraft can stay in the vicinity of the orbit for a long time. Moreover, the station-keeping costs, used for the maintenance of the spacecraft in a particular orbit, for a stable orbit are much lower than that of unstable orbits [36]. The unstable periodic orbits are preferred when the mission involves low-energy transfers from/to a point near the vicinity of the periodic orbits around the libration points, due to the presence of stable and unstable manifolds. By this way, the overall cost of the transfer is reduced, making them viable options for transfers.

An approximation of the system's stability can be obtained by assessing the linear stability of the equations of motion in the CR3BP [37]. This is generally done by examining the monodromy matrix for a particular solution.

The monodromy matrix, as mentioned in section 4.2, is a specific condition of the State-Transition Matrix that is useful for determining the dynamics of the orbit after one complete rotation period (T). The stability of the halo orbits can be determined by studying the eigenvalues (λ_i) of this monodromy matrix. Computing the eigenvalues reflects the dynamics of the system and informs about the existence of spaces inside the system which are stable or unstable. The said eigenvalues are found using Floquet's theorem [36], and the different classifications of regions based on the eigenvalues are shown below:

- Stable region, if $|\lambda_i| < 1$
- Unstable region, if $|\lambda_i| > 1$
- Centre, if $|\lambda_i| = 1$

The stable regions can be defined as regions where the disturbances in the vicinity of the orbit remain inside that small area, without causing much disturbance to the original orbit, whereas the trajectory of the orbit can change due to slight perturbations in the unstable regions. After knowing how the eigenvalues of the monodromy matrix can define the flow in the vicinity of an orbit, it is now important to analyse the values of the eigenvalues. This is done using Lyapunov's theorem which states that, for every state in the system, there exists 3 reciprocal pairs of 6 eigenvalues [38].

Since the State-Transition Matrix and by extension, the monodromy matrix, are time-invariant, according to Lyapunov's theorem, if λ_i is an eigenvalue, then it can be said that ${\lambda_i}^{-1}$ is also one of the eigenvalues of the state-transition matrix [37]. Therefore, the following expression regarding the relation between the real eigenvalues has been found.

$$\lambda_i = {\lambda_{i+1}}^{-1} \; where \; i = 1,3,5 \qquad \textbf{(4-63)}$$

Because the halo orbit is periodic, one of the eigenvalues is 1, implying that another eigenvalue is also 1 [36]. The 4 other values of the eigenvalues include 2 pairs of real or complex values. This can be given by the below-mentioned equation, tying the presence of a conjugate, if a complex eigenvalue exists.

$$\lambda_i = {\lambda_{i+1}}^{-1} \; and \; \lambda_i = {\lambda_{i+1}}^{*} \qquad \textbf{(4-64)}$$

Therefore, the 3 pairs of eigenvalues available for a monodromy matrix of a state in the system are represented as,

1. 2 unity eigenvalues: $\lambda_1 = \lambda_2 \quad = 1$
2. 2 complex conjugate eigenvalues: $\lambda_3 = a + ib; \; \lambda_4 \quad = a - ib$
3. 2 real eigenvalues: $\lambda_5 = n; \; \lambda_6 \quad = 1/n$

The real eigenvalues usually determine the stable and unstable regions in a system and therefore determine the linear stability of the orbit. A parameter, called the stability index, has thus been used to characterise the linear stability of the orbit. It is given by,

$$v = \frac{1}{2}(\lambda_{max} + \frac{1}{\lambda_{max}}) \qquad \textbf{(4-65)}$$

where λ_{max} is the eigenvalue with the maximum magnitude of all the eigenvalues of the monodromy matrix. Certain definitions regarding the stability of the orbits can be derived using the above-mentioned equation.

1. If the magnitude of the stability index, v, is less than 1, then the halo orbit can be classified as a stable orbit, implying that the orbit would maintain its trajectory over extended periods of time

2. If the magnitude of the stability index, v, is more than 1, then the halo orbit can be classified as an unstable orbit, implying that the orbit could disintegrate from the original trajectory
3. If the magnitude of the stability index, v, is equal to 1, then the halo orbit is a marginally stable orbit

For a halo orbit of $A_z = 611000\, km$ around the Sun-Earth libration point, the monodromy matrix has been calculated, whose values are given below as a [6x6] matrix in Table 4-4.

709.2959	19.51513	263.3064	132.4083	154.1904	32.92234
-829.183	-21.9044	-307.558	-154.19	-180.62	-38.4355
176.3577	4.540889	66.42759	32.92234	38.43552	8.016642
2149.227	59.03522	798.8536	400.9151	467.9422	99.48667
-1521.44	-41.3336	-565.344	-284.332	-330.285	-70.3856
1413.97	38.73114	525.7694	263.3064	307.5583	66.42759

Table 4-4: The [6x6] monodromy matrix for the desired halo orbit near the L2 system

In order to find the stability of this orbit, the eigenvalue with the maximum magnitude in the monodromy matrix needs to be found.

$$Maximum\ value\ in\ the\ monodromy\ matrix = 2149.227 \qquad \textbf{(4-66)}$$

The corresponding eigenvectors obtained from the monodromy matrix has been recorded in the below table.

-0.22265	-1.7848e-06	-0.016148	-0.01614855326 – 2.4472e-11i	-1.784e-06	- 0.2227
0.25985	0.47239418	-1.272e-10	- 1.27187e-10 - 0.520833069733189i	-0.472394	- 0.2598
-0.05537	1.73156e-06	-0.354948	-0.35494789211 + 0.000000000067371i	1.731e-06	- 0.0553
-0.67399	0.14647859	-2.629e-11	-2.6297e-11 + 0.160715701875237i	-0.146478	0.6739
0.47814	5.24173e-06	0.6803377	0.680337705521656	5.241e-06	0.4781
-0.44377	-0.86913046	1.8964e-11 + 0.33733544i	1.8964e-11 - 0.337335443142346i	0.8691304	0.4437

Table 4-5: The eigenvectors of the [6x6] monodromy matrix for the desired halo orbit near the L2 system

The eigenvalues corresponding monodromy matrix are,

1. Real Eigenvalues ($\lambda_1$and λ_2): 8.873e+02 and 0.001127
2. Unit eigenvalues ($\lambda_3$and λ_4): 1 and 1
3. Complex conjugate eigenvalues ($\lambda_5$and λ_6): 0.7807 + 0.625i and 0.7807 - 0.625i

Substituting the value of λ_{max} in equation (4-65) determines the stability of the constructed Halo orbit.

$$v_1 = \frac{1}{2}\left(\lambda_1 + \frac{1}{\lambda_1}\right) > 1 \quad \textbf{(4-67)}$$

$$v_2 = \frac{1}{2}\left(\lambda_3 + \frac{1}{\lambda_3}\right) = 1 \quad \textbf{(4-68)}$$

$$v_3 = \frac{1}{2}\left(\lambda_5 + \frac{1}{\lambda_5}\right) < 1 \quad \textbf{(4-69)}$$

According to the values of the stability index and due to the linear stability criteria, it can be said that the halo orbit is marginally stable. This enables the creation of invariant manifolds around the desired halo orbit in the system so that it paves way of low-energy transfers from/to halo orbit.

4.6 Creation of Invariant Manifolds

Since the obtained halo orbit is marginally stable, there exists a transition region between states along the orbit where the orbit changes from stable to unstable. This paves way for random perturbations to create stable and unstable pathways around the orbit. There are 2 primary components, called stable and unstable manifolds, for each point on the orbit around a lagrangian point. While the stable components asymptotically shrink, the unstable components grow exponentially. This implies that if a spacecraft is on one of the stable manifolds, then it will be driven to the lagrangian point, and if a spacecraft is on one of the unstable manifolds, then it will be moving away from the original orbit, leaving the lagrangian point [27].

The monodromy matrix and the associated eigenvalues, given in section 4.5, aid in the determination of the invariant manifolds of the system. The eigenvectors corresponding to the stable and unstable eigenvalues of the monodromy matrix, present in Table 4-5, are tangents to their local manifolds [37]. Therefore, analysing the eigenvectors enables the creation of possible invariant manifolds for a particular state of the system.

The unstable direction is determined by obtaining the eigenvector which corresponds to the larger real eigenvalue i.e., the first column of Table 4-5.

$$v^u = \begin{bmatrix} -0.222653786698708 \\ 0.259859509865829 \\ -0.055374323666203 \\ -0.673998888063079 \\ 0.478147726193160 \\ -0.443770505447998 \end{bmatrix} \tag{4-70}$$

And similarly, the stable direction is determined by obtaining the eigenvector which corresponds to the lower real eigenvalue i.e., the last column of Table 4-5

$$v^s = \begin{bmatrix} -0.222653786708902 \\ -0.259859509884977 \\ -0.055374323670575 \\ 0.673998888044530 \\ 0.478147726216651 \\ 0.443770505433988 \end{bmatrix} \tag{4-71}$$

Using the above-mentioned eigenvectors, the initial state vectors can be computed in order to create the 2 invariant manifolds. The initial vector in order to propagate the manifolds for every point in the original halo orbit are found by,

$$\overline{X^u} = \bar{X}_0 \pm \epsilon v^u \qquad \textbf{(4-72)}$$

$$\overline{X^s} = \bar{X}_0 \pm \epsilon v^s \qquad \textbf{(4-73)}$$

where,

- $\overline{X^u}$ and $\overline{X^s}$ represent the required initial state vector for propagation
- $\bar{X}_0$ is the current state vector of the point in the halo orbit
- ϵ is a small perturbation, usually in the order of 1000 kms in the Sun-Earth system (1000/(1 AU) in Non-Dimensional terms)
- v^u and v^s are the required unstable and stable eigenvectors
- The '$\pm$' signifies the existence of 2 directions for a single manifold, one coming towards the system (Towards the Sun from L2) and another moving away from the system (Away from the Earth from L2)

This is the general methodology used for obtaining the invariant manifolds of an orbit around a system in the CR3BP. However, due to constant changes in the state transition matrix along the points in an unstable orbit, a more efficient manner of using the eigenvectors has also been discussed.

This technique involves the propagation of the eigenvectors of the monodromy matrix using the State-Transition Matrix, which changes exponentially along the orbit. For a particular time t_i the state transition matrix is calculated and represented as $\phi(t_0 + t_i, t_0)$. Using this expression, the required stable and unstable vectors can be calculated as,

$$v_i{}^u = \phi(t_0 + t_i, t_0)v^u \qquad \textbf{(4-74)}$$

$$v_i{}^s = \phi(t_0 + t_i, t_0)v^s \qquad \textbf{(4-75)}$$

Using the values of these vectors in the general expression given in equations (4-72) and (4-73), the initial conditions of the orbit for time t_i can be calculated as,

$$\overline{X_i{}^u} = \bar{X}_0 \pm \epsilon v_i{}^u \quad \textbf{(4-76)}$$

$$\overline{X_i{}^s} = \bar{X}_0 \pm \epsilon v_i{}^s \quad \textbf{(4-77)}$$

In order to maintain a consistent value of perturbation along the entire orbit, the vectors need to be normalized. Therefore, equations (4-76) and (4-77) can be rewritten as,

$$\overline{X_i{}^u} = \bar{X}_0 \pm \epsilon \frac{v_i{}^u}{|v_i{}^u|} \quad \textbf{(4-78)}$$

$$\overline{X_i{}^s} = \bar{X}_0 \pm \epsilon \frac{v_i{}^s}{|v_i{}^s|} \quad \textbf{(4-79)}$$

The unstable manifold can be constructed by propagating the initial state vector, $\overline{X_i{}^u}$, forward in time. The obtained unstable invariant manifolds of the desired halo orbit of $A_z = 611000\ km$ have been represented in the figures below.

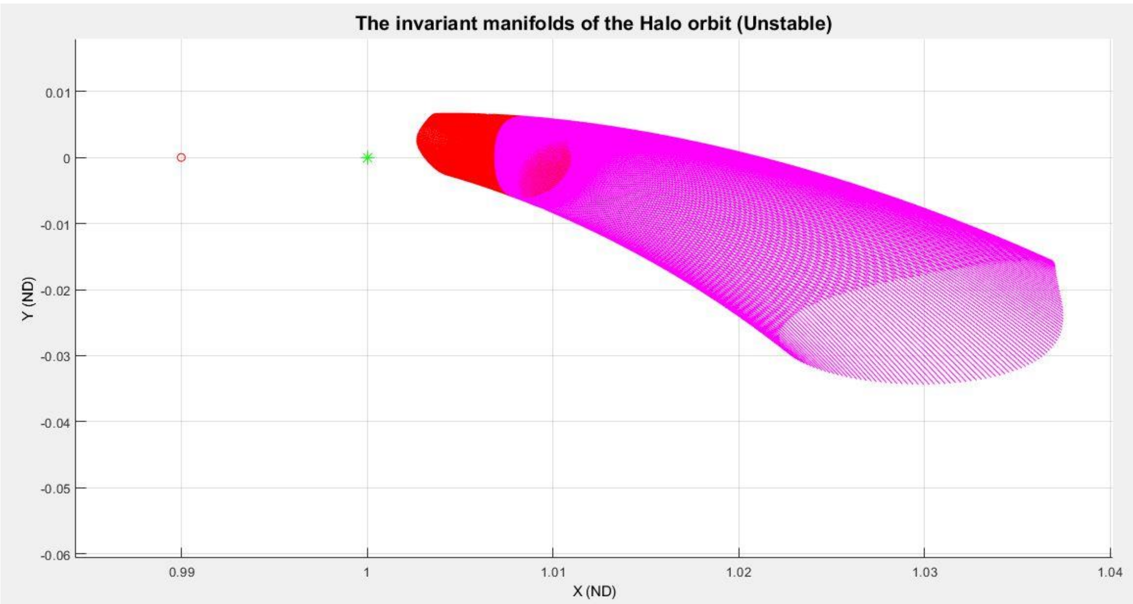

Figure 4.7: Unstable manifolds in the X-Y plane, for a halo orbit of A_z = 611000 km

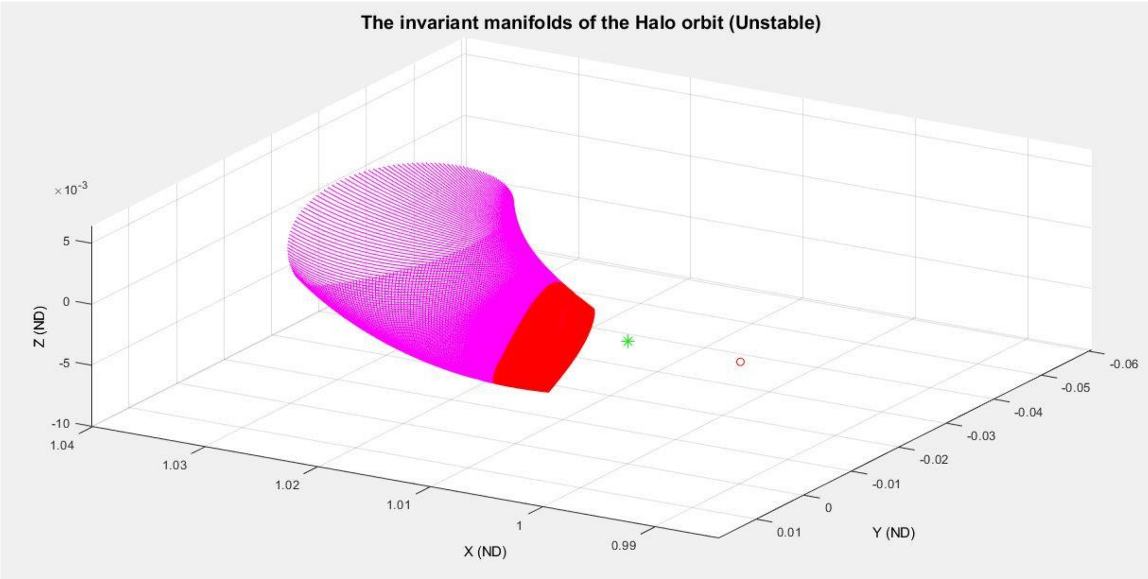

Figure 4.8: Three-Dimensional view of the unstable manifolds, for a halo orbit of A_z = 611000 km

In the above figures, the colour red represents all the unstable manifolds which are which are directed towards the sun and moving towards the Sun-Earth system, while pink represents all the unstable manifolds that are moving away from the Sun-Earth system. For a sense of clear visualisation, the manifolds in pink were propagated forward for a longer time than the manifolds in red.

The stable manifolds can be constructed by propagating the initial state vector, $\overline{X_\iota}^s$, backward in time. The obtained stable invariant manifolds of the desired halo orbit of $A_z = 611000\ km$ have been represented in the figures below.

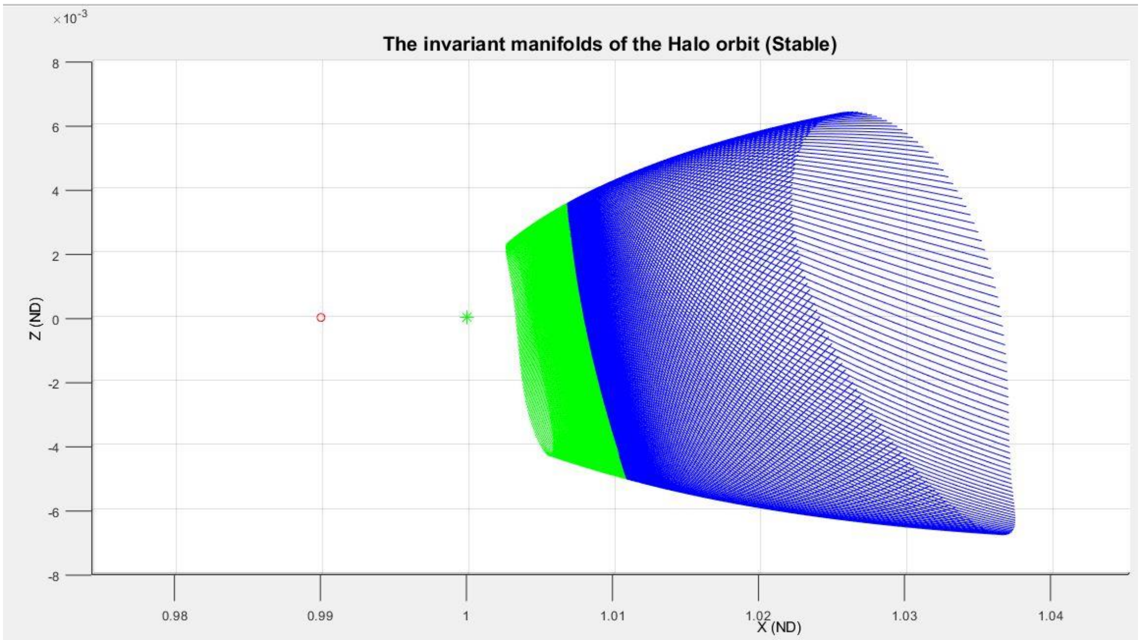

Figure 4.9: Stable manifolds in the X-Z plane, for a halo orbit of A_z = 611000 km

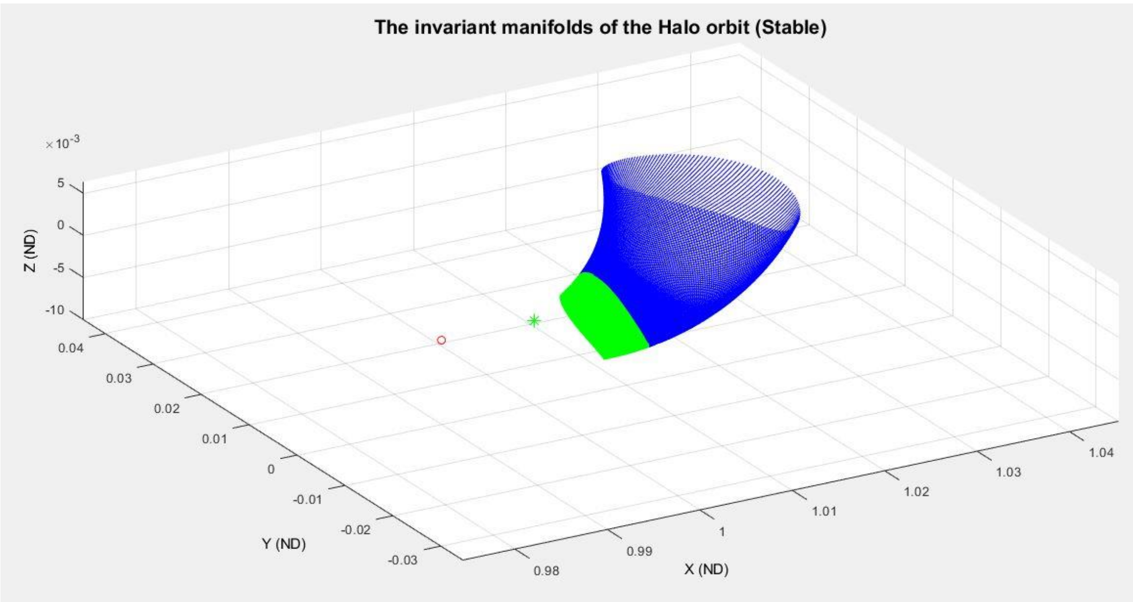

Figure 4.10: Three-Dimensional view of the stable manifolds, for a halo orbit of A_z = 611000 km

In the above figures, the colour green represents all the unstable manifolds which are which are directed towards the sun and moving towards the Sun-Earth system, while blue represents all the unstable manifolds that are moving away from the Sun-Earth system. For a sense of clear visualisation, the manifolds in blue were propagated backward for a longer time than the manifolds in green.

The figure below contains all the stable and unstable manifolds of the halo orbit, from where different possible scenarios for transfer trajectories, and ΔVs for different departure windows are analysed.

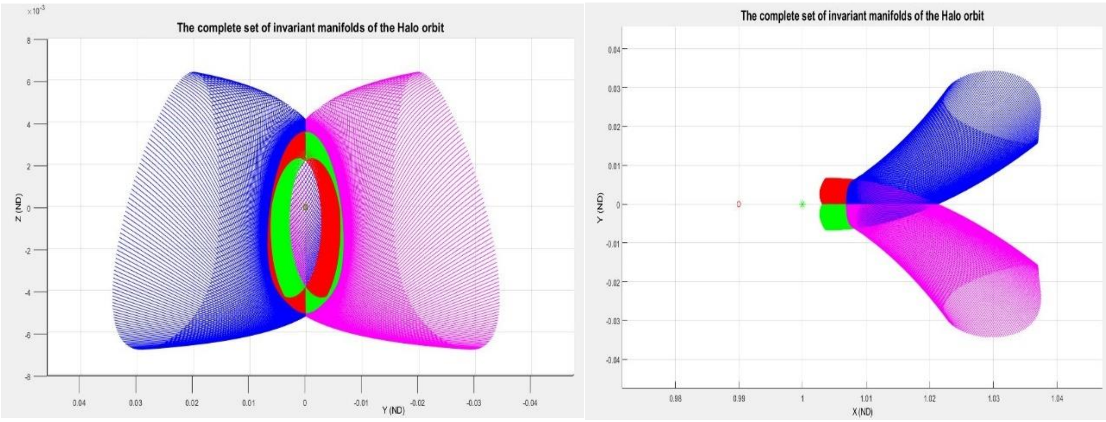

Figure 4.11: The invariant manifolds of the halo orbit in the Y-Z axis (Left) and X-Y axis (Right)

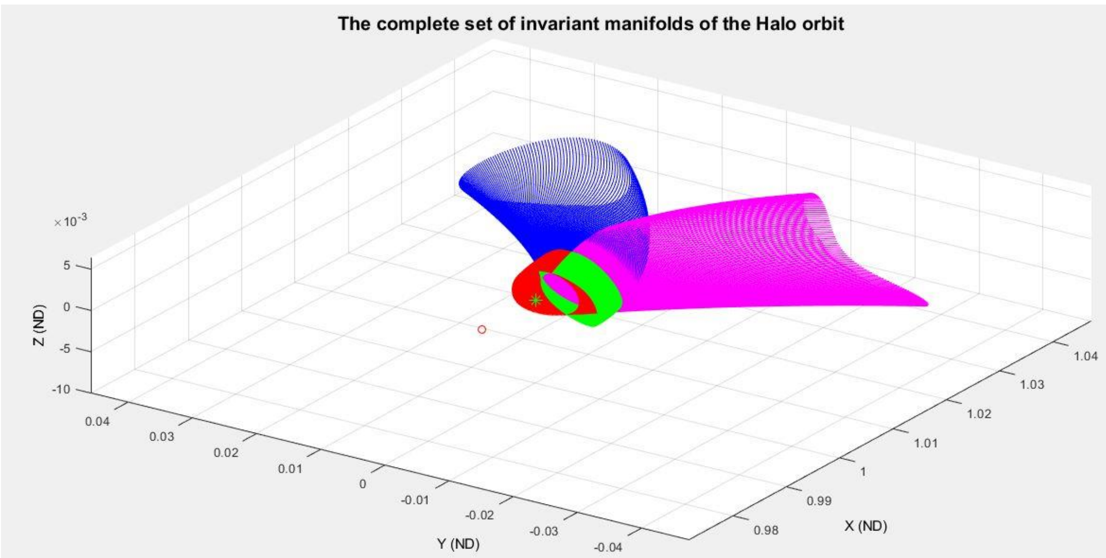

Figure 4.12:The Three-Dimensional view of the invariant manifolds of the halo orbit

5 Delta-V results and Transfer Trajectories

After obtaining the primary results of the required halo orbit of $A_z = 611000\ km$ and its associated manifolds using the techniques given in sections 4.4 and 4.6, one of the tasks now is to calculate and design trajectories which require low energy i.e., trajectories which require less than 1 km/s as the Δv in order to reach the selected asteroid, 2000SG344, in accordance with the mission constraints in section 1.1.1.

Since one of the main applications of halo orbits and its manifolds is in creating pathways for low-energy transfers, added to its low cost of station keeping [27], this section concentrates on calculating the Δv to reach the Asteroid from the obtained halo orbit and its unstable invariant manifolds. In order to compare the values obtained for different cases of departure points and different timeframes, this computation of Δv is split into 2 brief sections:

1. Direct transfer from the Halo orbit
2. Transfer using the unstable invariant manifolds

The comparison between the results of the 2 methods with the value of Δv obtained via a simple transfer from the L2 point, as obtained in Table 2-2, hopes to shine some light on the utility of periodic orbits around the libration points for usage beyond simple Earth-Moon transfers, and also hopes to open avenues of discussion for possible transfers to Near-Earth bodies.

For the purposes of this thesis, the departure timeframe is taken from the 1st of January, 2028 till the 31st of December, 2033, and the arrival timeframe has been selected from the 1st of January, 2028 till the 31st of December, 2034, as shown in equations (5-1) and (5-2). These extended periods of departure and arrival windows have been chosen in order to explore every possible Δv , less and more than 1 km/s, so that it can be ensured that all the possibilities for the Comet Interceptor mission were drawn and covered. This facilitates a deeper and a more lucid understanding of the transfer methodologies from the halo orbit and its manifolds.

$$Departure\ Time = [01, 01, 2028, 00:00\ AM] to\ [31, 12, 2033, 23:59\ PM] \quad \textbf{(5-1)}$$

$$Arrival\ Time = [01, 01, 2028, 00:00\ AM] to\ [31, 12, 2034, 23:59\ PM] \quad \textbf{(5-2)}$$

Furthermore, for purposes of clarity and computational simplicity, this thesis splits the departure timeframe into 6 individual timelines, i.e., every year, starting from 2028 to 2033, is a separate departure window. This will be explained further clearly in sections below.

5.1 Direct Transfer from the Halo orbit

After obtaining the value of Δv for a simple transfer between L2 lagrangian point and the Asteroid, the same techniques are now applied in order to calculate the values of Δv for transferring from a point in the halo orbit to the Asteroid. If the obtained values are lower than 1 km/s, then they can be considered as viable transfer paths and usable transfer windows.

In order to obtain meaningful values of Δv, it is imperative to convert the halo orbits from the Rotating Reference Frame into the Heliocentric Reference Frame. This is done by feeding the state vectors of the Halo orbit in the rotating reference frame into the formulae given in section 3.2.2.4, which deals with the conversion of reference frame from one form to the other. This also requires clear definitions of the departure window. As said in the previous section, the departure window is split into 6 separate timelines. It is split according to the time period of the halo orbit so that as the halo completes 1 revolution, an equivalent number of days would have passed in the revolution around the sun. This is explained using the statements below.

$$Time\ period\ of\ Halo = 178.955\ days \ \cong 179\ days \quad \textbf{(5-3)}$$

$$departure\ window\ 1 = [01, 01, 2028, 00:00\ AM] + 2 * (179\ days) \quad \textbf{(5-4)}$$

$$DEP\ window\ 1 = [01, 01, 2028, 00:00\ AM]\ to\ [25, 12, 2028, 00:00\ AM] \quad \textbf{(5-5)}$$

Subsequently, every other departure window starts at the end of its previous departure window and extends for a time twice the period of the halo. The consolidated departure windows are given below.

$$DEP\ window\ 1 = [01, 01, 2028, 00{:}\,00\ AM]\ to\ [25, 12, 2028, 00{:}\,00\ AM] \quad \textbf{(5-6)}$$

$$DEP\ window\ 2 = [25, 12, 2028, 00{:}\,00\ AM]\ to\ [18, 12, 2029, 00{:}\,00\ AM] \quad \textbf{(5-7)}$$

$$DEP\ window\ 3 = [18, 12, 2029, 00{:}\,00\ AM]\ to\ [11, 12, 2030, 00{:}\,00\ AM] \quad \textbf{(5-8)}$$

$$DEP\ window\ 4 = [11, 12, 2030, 00{:}\,00\ AM]\ to\ [04, 12, 2031, 00{:}\,00\ AM] \quad \textbf{(5-9)}$$

$$DEP\ window\ 5 = [04, 12, 2031, 00{:}\,00\ AM]\ to\ [26, 11, 2032, 00{:}\,00\ AM] \quad \textbf{(5-10)}$$

$$DEP\ window\ 6 = [26, 11, 2032, 00{:}\,00\ AM]\ to\ [19, 11, 2033, 00{:}\,00\ AM] \quad \textbf{(5-11)}$$

These departure dates are converted into one of the standard values of time called Modified Julian Day, which is used in astronomy to facilitate simplified chronological calculations [39]. The MJD of a date in the modern calendar format i.e., the Gregorian calendar format, is given as a function of the Julian day, JD.

$$MJD = JD - 2400000.5 \quad \textbf{(5-12)}$$

Where the JD is the number of days since noon on January 1, - 4712, i.e., January 1, 4713 BC, which is calculated by,

$$JD = 367Y - INT\left(\frac{7\left(Y + INT\left(\frac{M+9}{12}\right)\right)}{4}\right) - INT\left(\frac{3\left(INT\left(\frac{Y + \frac{M-9}{7}}{100}\right) + 1\right)}{4}\right) + INT\left(\frac{275M}{9}\right) + D + 1721028.5 + UT/24 \quad \textbf{(5-13)}$$

Where Y, M, D, and UT are the values of the year, month, day, and the universal time on the day (In hours, minutes, and seconds).

Using the above-mentioned departure windows, the conversion of the halo orbit can be done, and the figures for the converted halo orbit for one complete rotation of the halo orbit and for the entire departure window 1 (2 complete rotations of the halo orbit) have been given below.

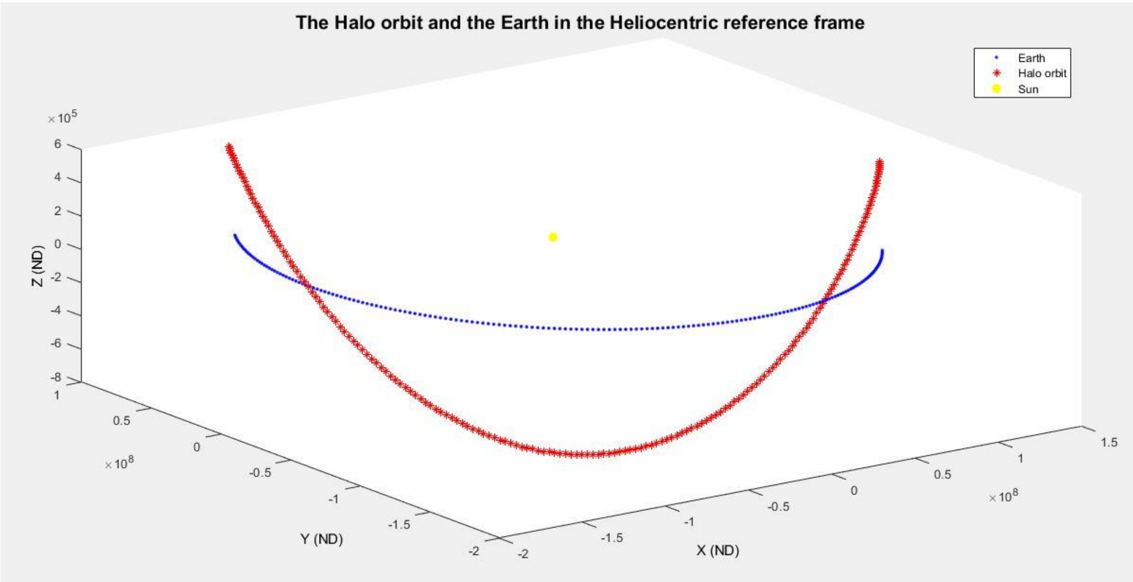

Figure 5.1: Halo orbit in the Heliocentric Reference Frame for 1 complete rotation of the halo (179 days) (3D view)

The movement of a spacecraft in the halo orbit, as it revolves around the sun can be clearly seen in the above figure.

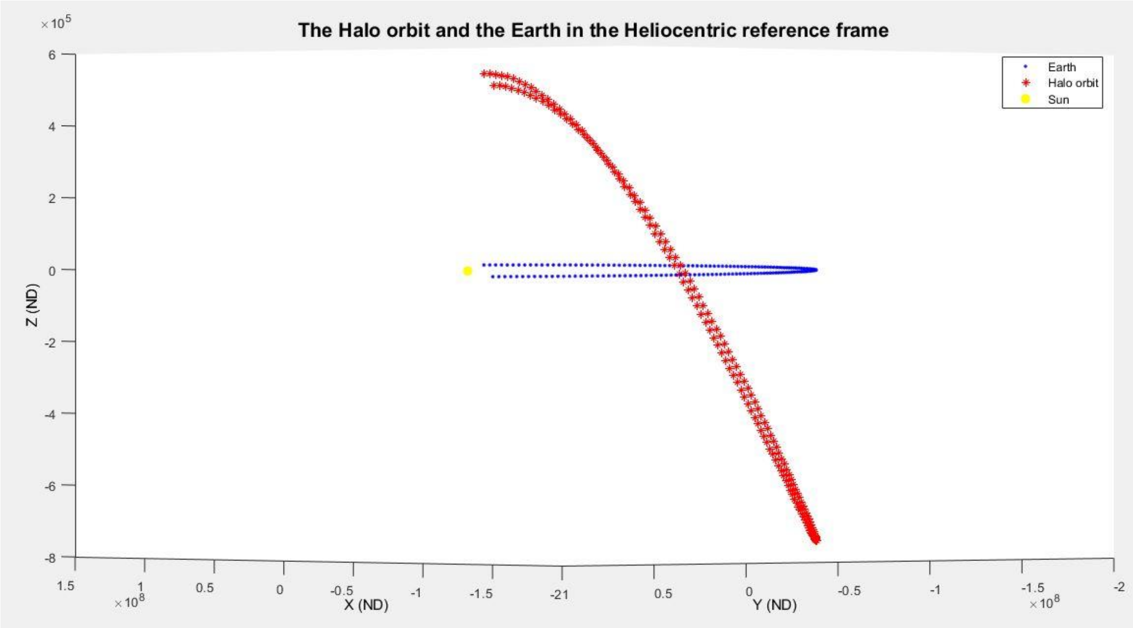

Figure 5.2: Halo orbit in the Heliocentric Reference Frame for 1 complete rotation of the halo (179 days)

If the halo orbit completes two full orbits, then the halo orbit in the Heliocentric Reference Frame is given in the figure below.

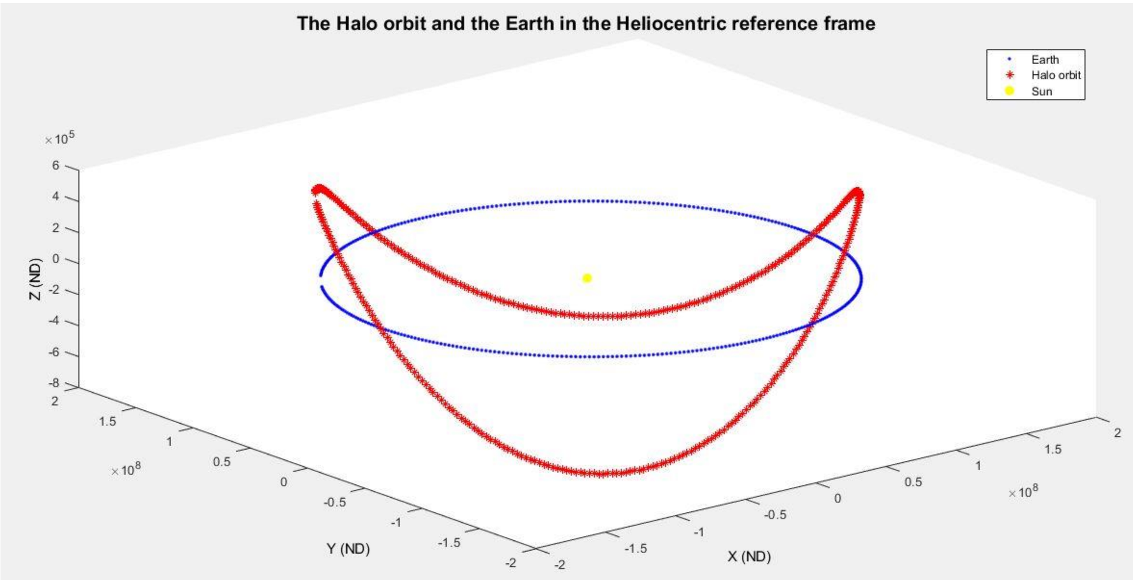

Figure 5.3: Halo orbit in the Heliocentric Reference Frame for the first departure window (359 days)

The shape of the halo orbit as it goes around the sun has during the departure window 1 can clearly be seen in the below-mentioned figure.

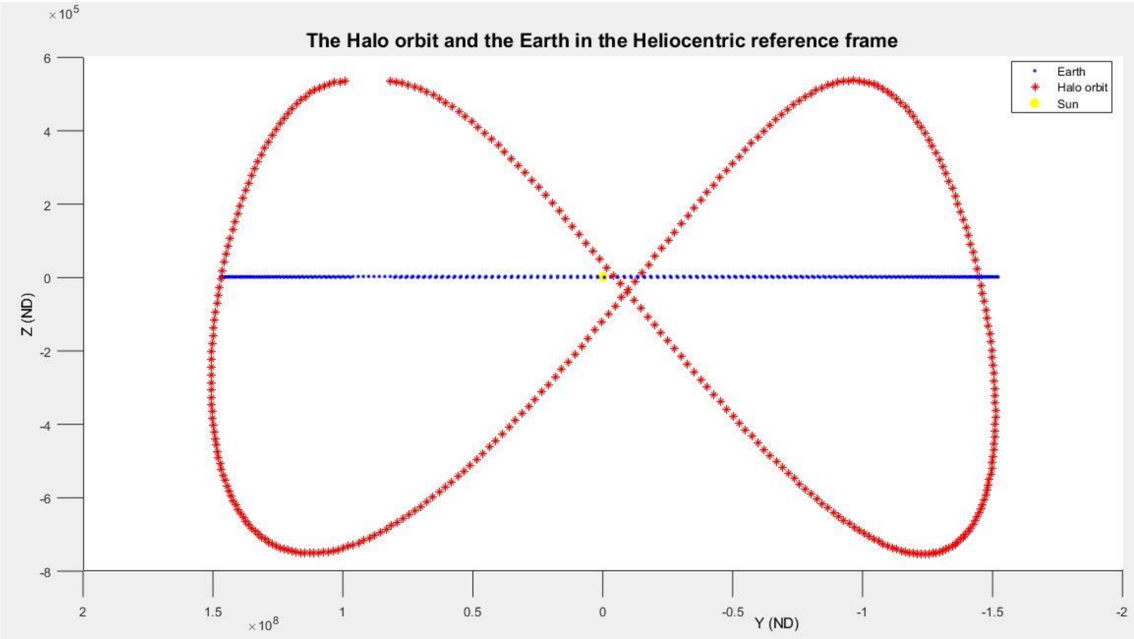

Figure 5.4: Halo orbit in the Heliocentric Reference Frame for the first departure window (359 days) (Demonstrating the shape)

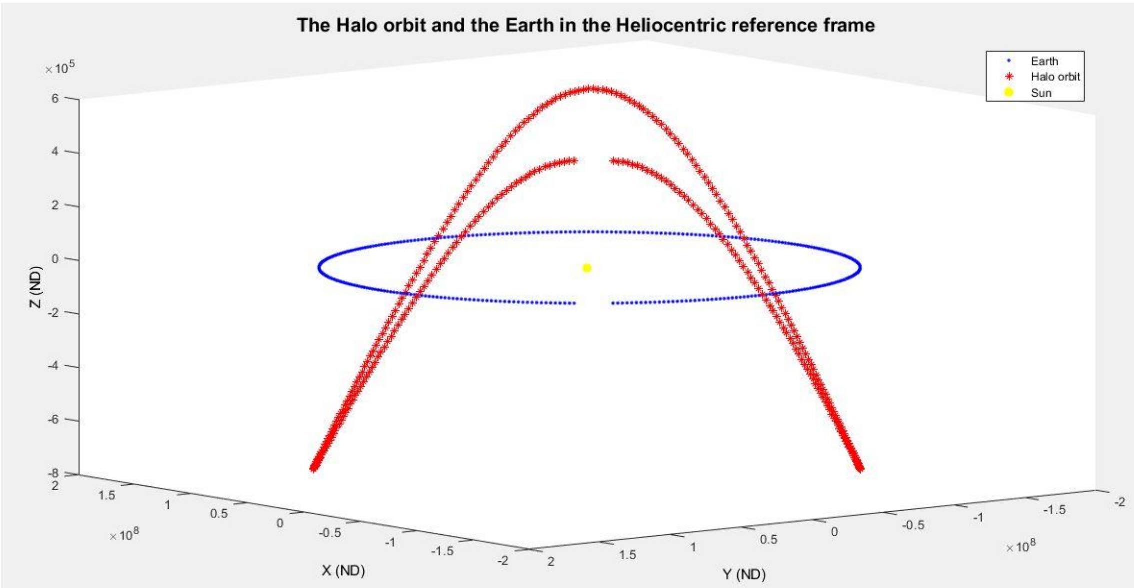

Figure 5.5: Halo orbit in the Heliocentric Reference Frame for the first departure window (359 days) (View of the start and end of window)

Figure 5.5 shows the start and stop of the departure window. The gap between them confirms that the 2 complete rotations of the halo orbit does not take 1 complete year, but takes 6 days fewer.

In a similar fashion, the halo orbits can be converted for the other 5 departure windows. Using the set of points of the converted halo orbits, transfers were propagated to the Asteroid using MATLAB and the values of Δv corresponding every departure day and every arrival day were found. For conciseness, the minimum values of Δv that can be achieved for every departure window have been presented in a table below. This also contains the departure and the arrival date at which the low-energy transfer is possible.

	DEP-1	DEP-2	DEP-3	DEP-4	DEP-5	DEP-6
Δv (km/s)	1.435672	0.925741	1.699188	1.790137	2.115779	3.720465
DEPARTURE DATE (MJD)	62011	62420	62740	62969	63326	63775
ARRIVAL DATE (MJD)	62336	62664	62999	63209	63609	64043

Table 5-1: Values of the Δv and the corresponding departure and arrival dates for transfer between the halo orbit and Asteroid for the 6 departure windows

From the table above, it can be clearly seen that, of the 6 departure windows, the required value of Δv is lower than 1 km/s and minimum at a date in the second departure window, with the departure on 11th October, 2029 (MJD 62420) and the arrival on 12th June, 2030 (MJD 62664).

A comparison can now be drawn stating that, while a simple transfer from the L2 lagrangian point would require a Δv of 1.2 km/s, as obtained in Table 2-2, a transfer from a point in the halo orbit could very well cost a lower amount Δv (0.92 km/s), reducing the effective cost of the complete transfer mission. The transfer between the point in the halo orbit and the Asteroid, 2000SG344 has been given clearly in the figures below.

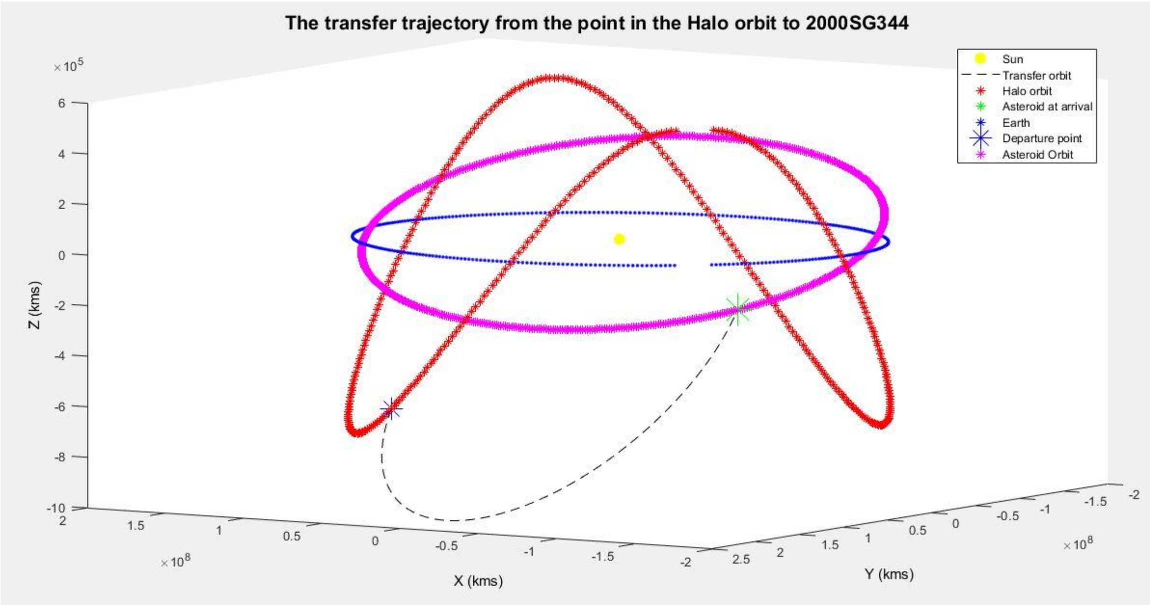

Figure 5.6: The transfer trajectory, along with the orbits of the Halo and Earth around the sun; (In picture: Blue star – Departure point at Halo orbit; Green star – Arrival point at Asteroid; Pink – Asteroid's orbit)

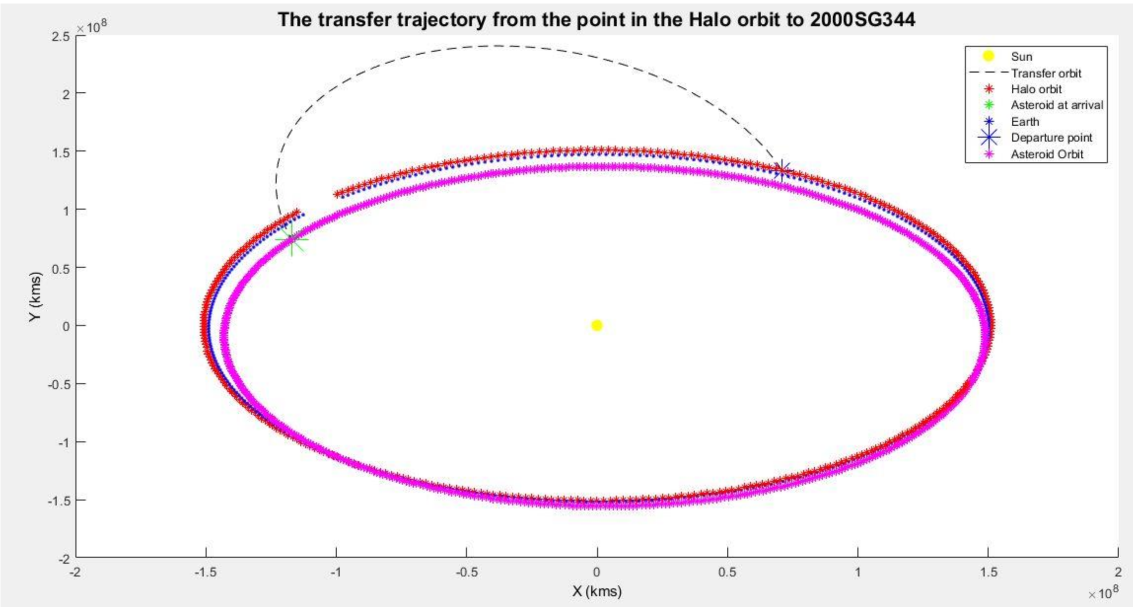

Figure 5.7: The transfer trajectory in the X-Y plane

This method is the direct transfer from the halo orbit. The next section aims to reduce the Δv further by looking at viable options of transfer from the unstable manifolds of the halo orbit in the given system.

5.2 Manifold to Asteroid transfer

Mission designs often use the manifolds of unstable halo orbits to transfer spacecrafts from/to the vicinity of the libration points with lesser fuel than what would be required for direct transfers. These are slightly more complex in terms of the computation due to the extra required procedure of having to calculate the manifolds emerging from every point of the halo orbit, and for every departure window. Since the spacecraft is departing from the halo orbits, this thesis concentrates only on the unstable manifolds, from where the spacecraft can leave the libration point. Therefore, a huge set of unstable manifolds have been obtained for every departure window and the associated Δv have been calculated.

Following a similar procedure to the one in 5.1, the 2 unstable manifolds (one moving towards the Sun-Earth system and another one moving away from the Sun-Earth system) from every point on the halo orbit, obtained in 4.6, need to be converted from the Rotating Reference Frame to the Heliocentric Reference Frame in order to calculate the Δv. The cases of the 2 unstable manifolds have been presented below.

5.2.1 Unstable Manifold 1 (Away from the Sun-Earth system)

One of the unstable manifolds moves away from the Sun-Earth system by using the equation (4-78). Calculating this unstable manifold at every point of the halo orbit for every departure window results in a massive collection of manifold state vectors. These state vectors are in turn used as the departure points for obtaining the Δv and the transfer trajectory. The converted unstable manifold 1 calculated for a point on the halo orbit during the first departure window has been given below. The (PLUS) in the title of the graphs denote the direction of the unstable manifolds i.e., going away from the Sun-Earth system.

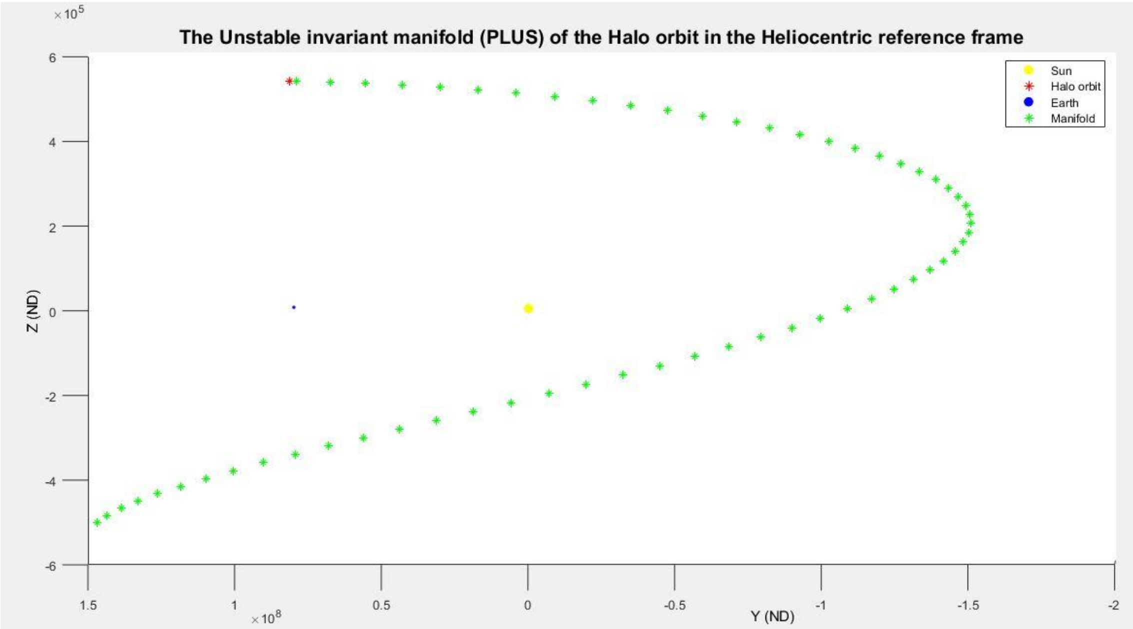

Figure 5.8: The unstable manifold of a point in the halo orbit in the Heliocentric Reference Frame (In picture: Red – Halo point from where the manifold is propagated; Green – Unstable manifold)

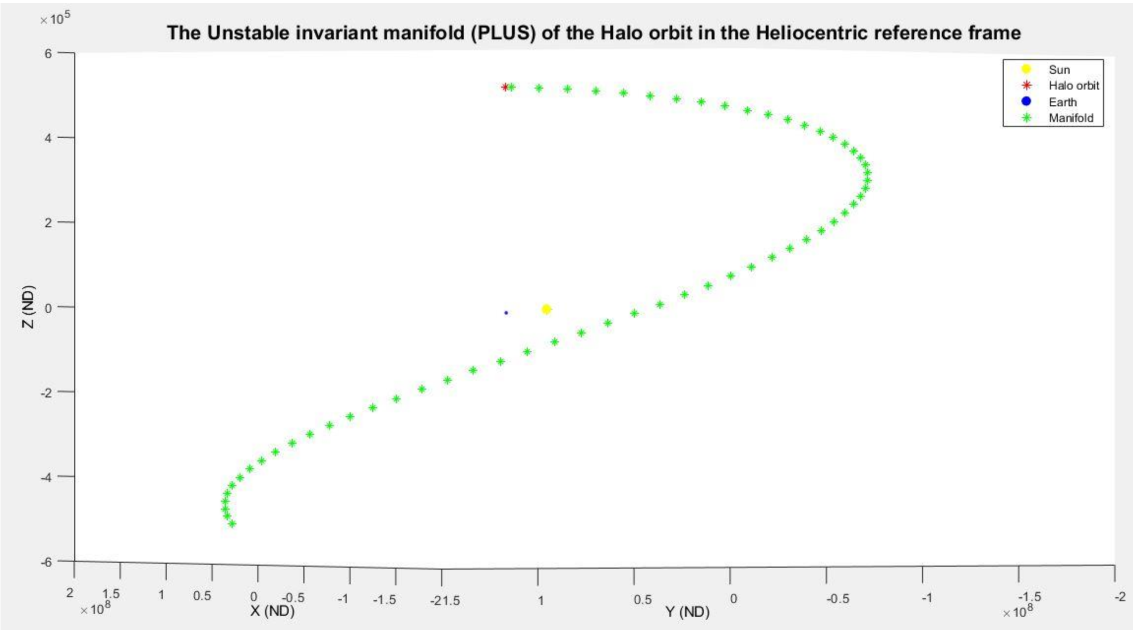

Figure 5.9: The 3D view of the unstable manifold of a point in the halo orbit in the Heliocentric Reference Frame

For example visualisation, the converted unstable manifolds, generated for 5 points on the halo orbit, have been given below. These images clearly show the number of departure points that can exist and the wealth of option the mission designer has when planning a mission from the vicinity of the libration points.

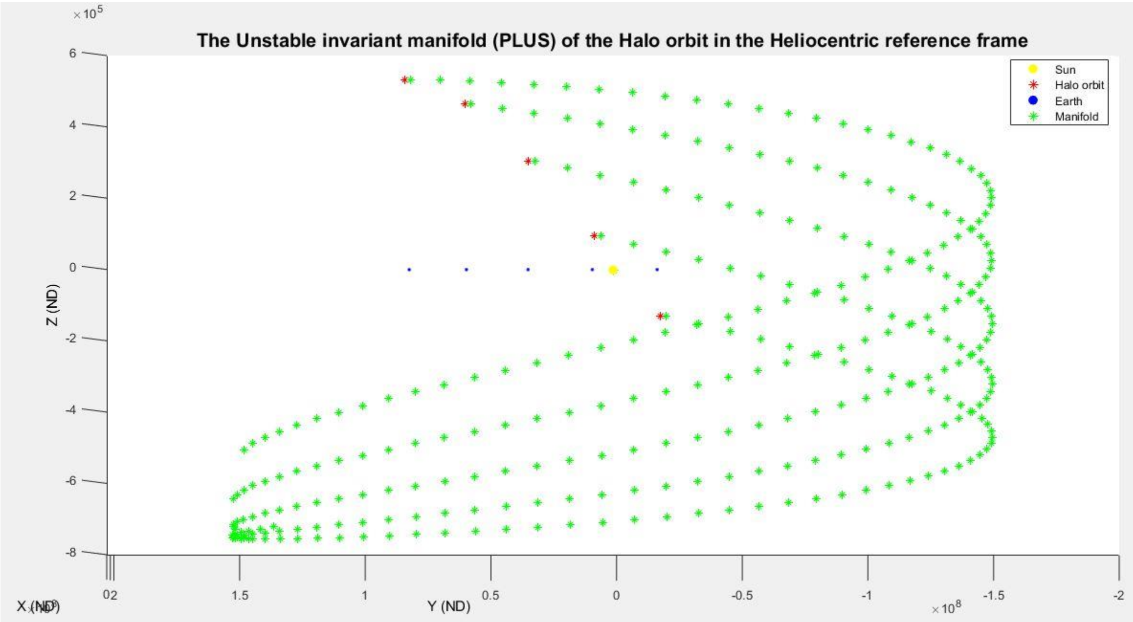

Figure 5.10: The Y-Z view of the unstable manifolds from 5 points of the Halo orbit in the Heliocentric Reference Frame

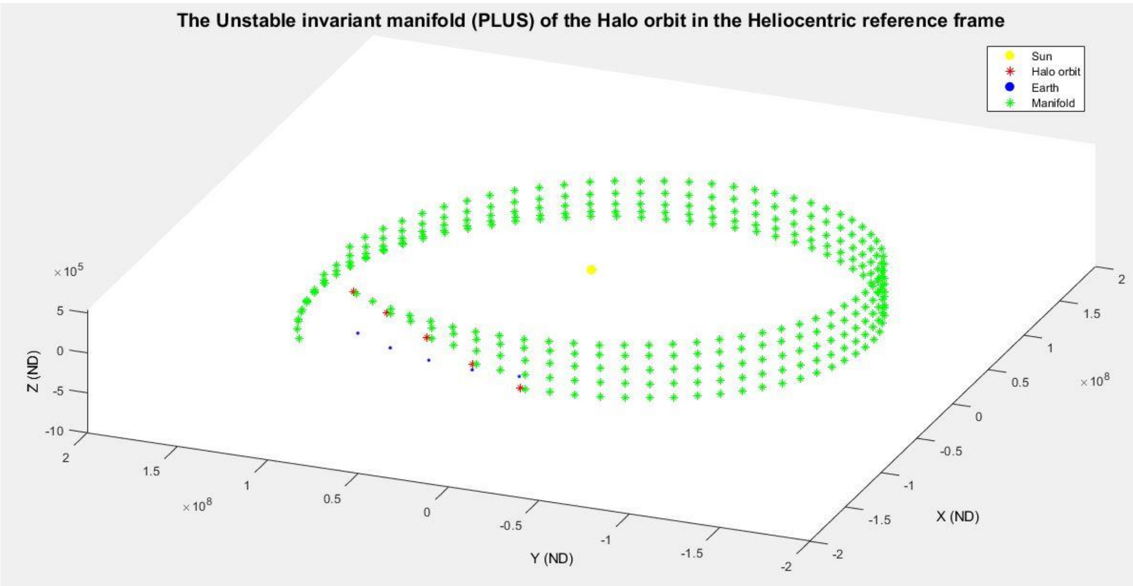

Figure 5.11: The 3D view of the unstable manifolds from 5 points of the Halo orbit in the Heliocentric Reference Frame

The Δv was calculated from every position of unstable manifold and the values lower than 1 km/s for all the 6 departure windows have been given below:

	DELTA-V (km/s)	DEPARTURE DATE (MJD)	ARRIVAL DATE (MJD)
DEP-1	0.926435	61981	62136
DEP-1	0.642833	61987	62116
DEP-2	0.840096	62343	62482
DEP-2	0.747405	62352	62459
DEP-3	1.225783	62693	62831
DEP-4	0.994633	63391	63634
DEP-4	0.973614	63392	63657
DEP-4	0.967422	63396	63670
DEP-4	0.96854	63401	63678
DEP-4	0.977827	63409	63683
DEP-5	0.982714	63661	63757
DEP-5	0.973543	63733	63952
DEP-5	0.971369	63737	63981
DEP-6	0.959475	63907	64087
DEP-6	0.902516	63837	64086

Table 5-2: The calculated minimum values of Δv, the associated departure and arrival dates for the points in the Unstable manifold 1, for every departure window

From the above table, it can be seen that values as low as 0.64 km/s can be reached via a transfer from the manifold. By this way, the usage of the invariant manifolds of a halo orbit can be justified. The transfer from the point in the unstable manifold 1 on 4th August, 2028 (MJD 61987) to the Asteroid, 2000SG344 on 11th December, 2028 (MJD 62116), has been given clearly in the figures below.

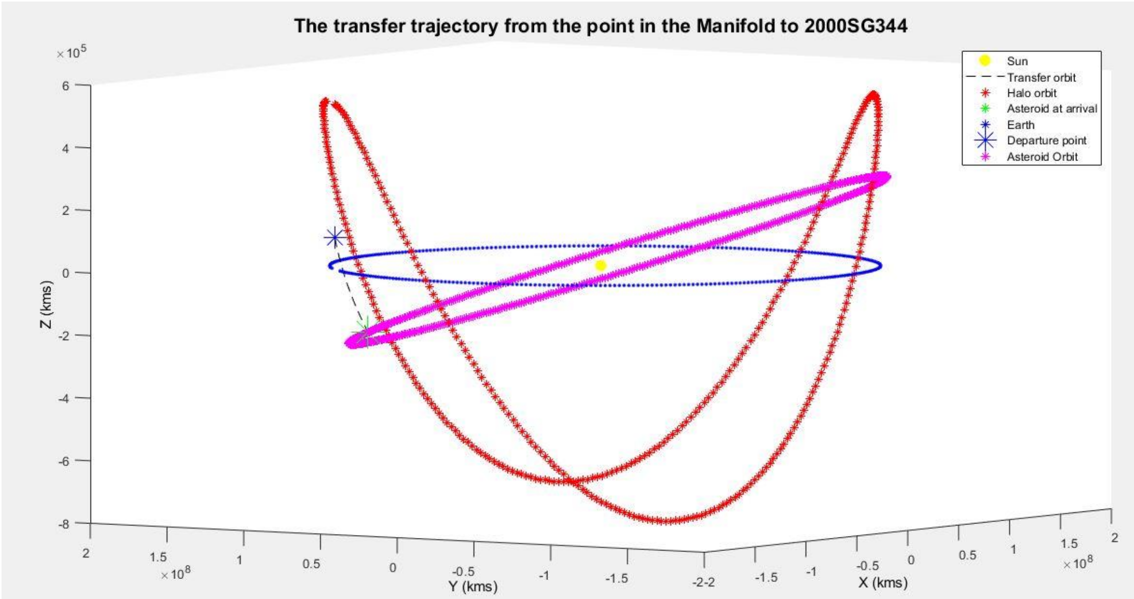

Figure 5.12: The transfer trajectory, along with the orbits of the Halo and Earth around the sun; (In picture: Blue star – Departure point at a point in the Unstable Manifold 1; Green star – Arrival point at Asteroid; Pink – Asteroid's orbit)

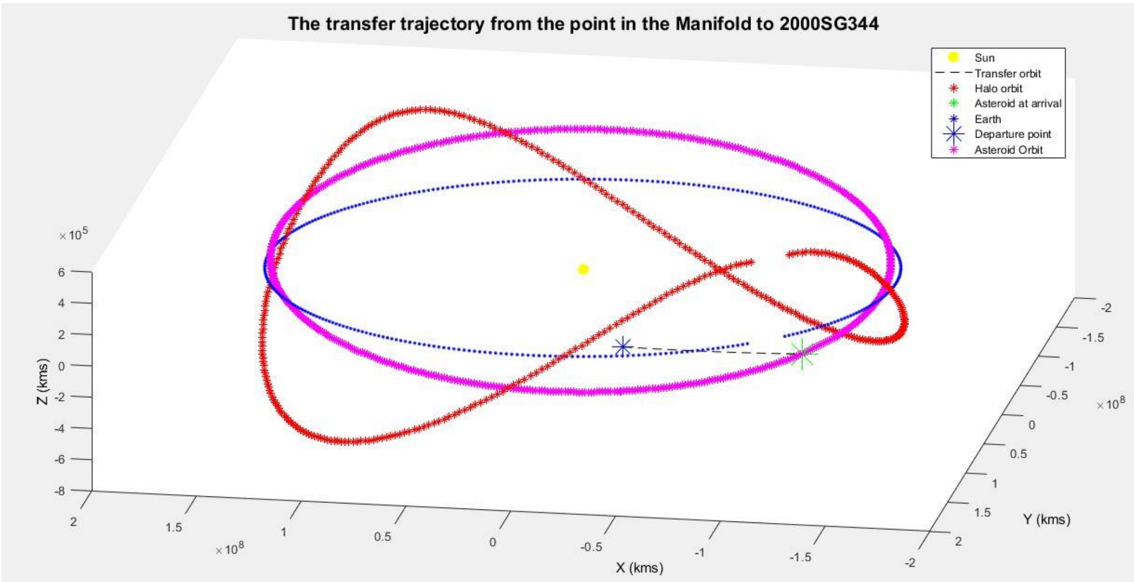

Figure 5.13: The transfer trajectory in the 3D view

The next subsection involves the transfers from the second unstable manifold to the Asteroid.

5.2.2 Unstable Manifold 2 (Towards from the Sun-Earth system)

One of the unstable manifolds moves towards from the Sun-Earth system using the equation (4-78). These are also used as points of departure in order to further delve into the applications of invariant manifolds. The converted unstable manifold 2 calculated for a point on the halo orbit during the first departure window has been given below. The (MINUS) in the title of the graphs denote the direction of the unstable manifolds i.e., coming towards from the Sun-Earth system

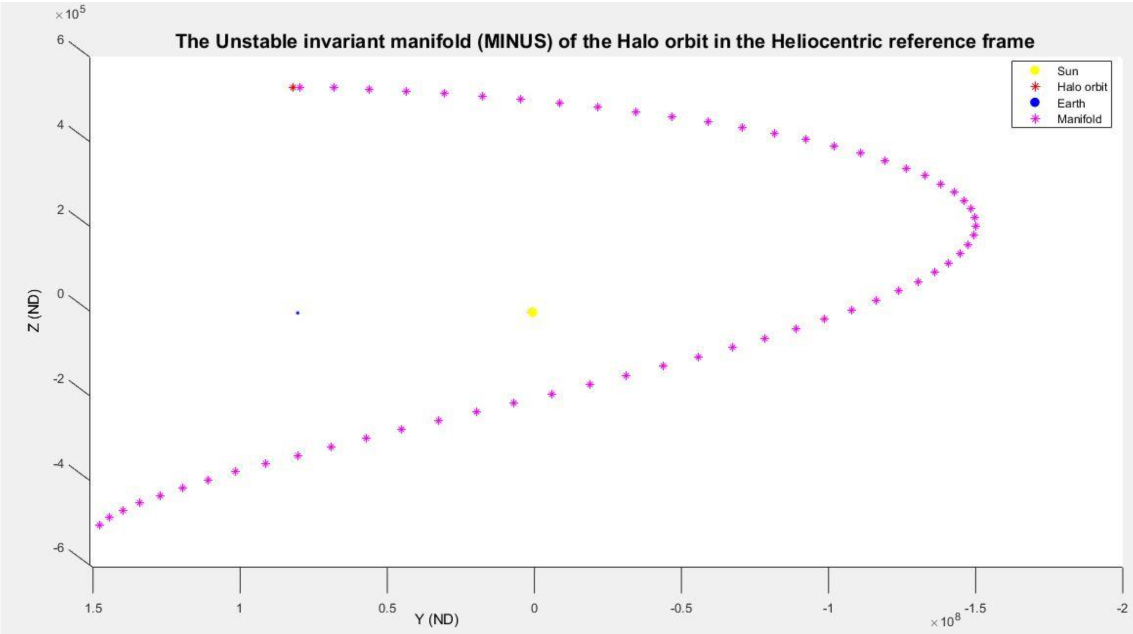

Figure 5.14: The unstable manifold of a point in the halo orbit in the Heliocentric Reference Frame (In picture: Red – Halo point from where the manifold is propagated; Pink – Unstable manifold 2)

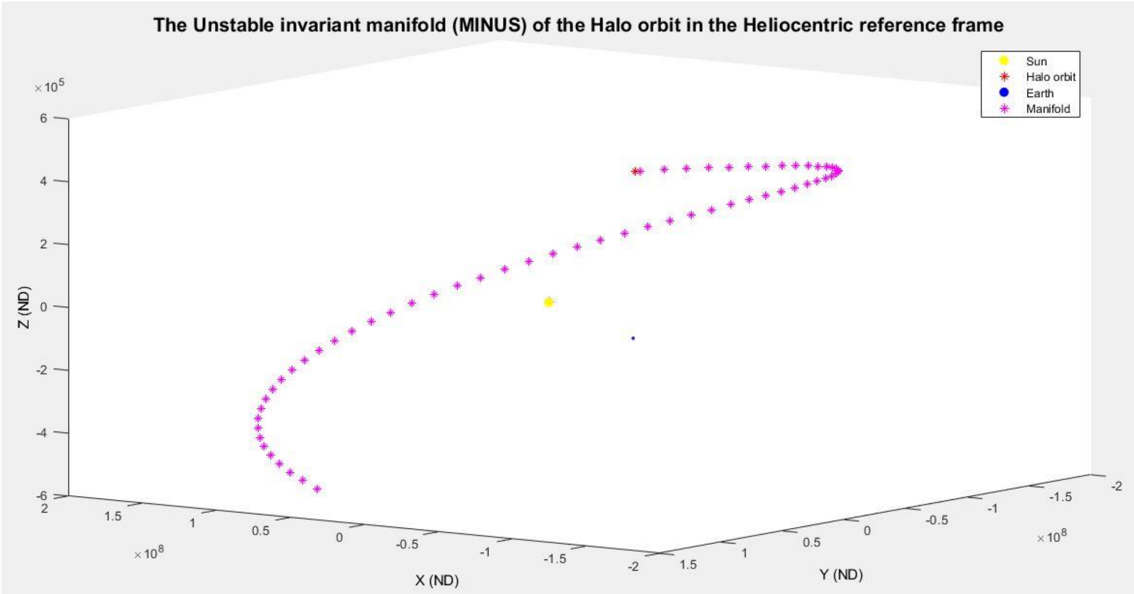

Figure 5.15: The 3D view of the unstable manifold 2 of a point in the halo orbit in the Heliocentric Reference Frame

Similar to unstable manifolds 2, the converted unstable manifolds 2, generated for 5 points on the halo orbit, have been given below.

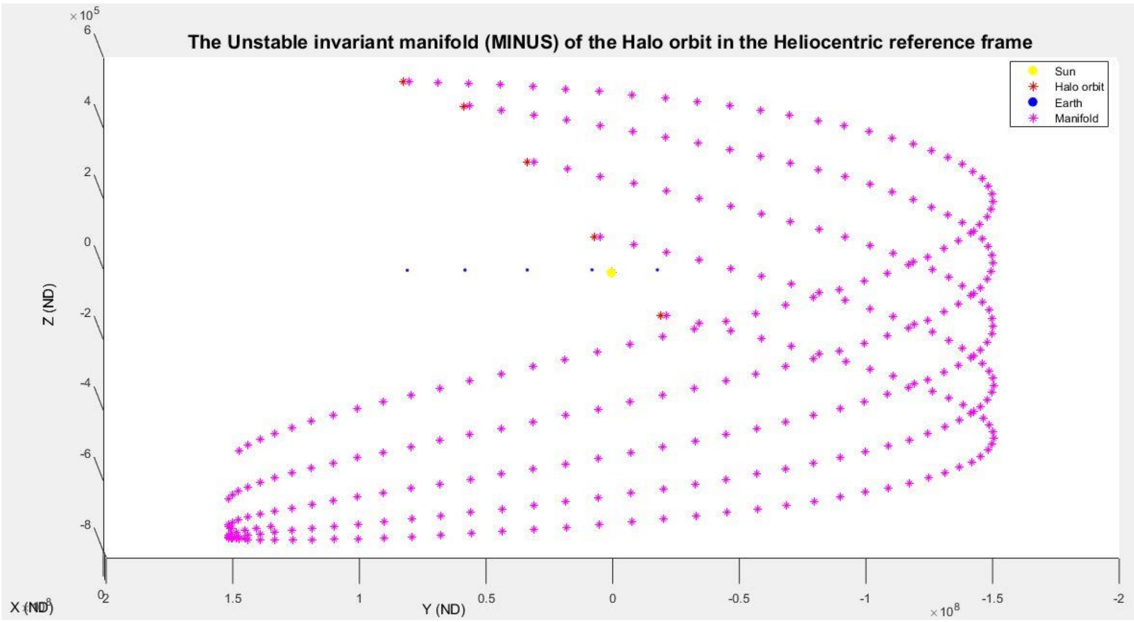

Figure 5.16: The Y-Z view of the unstable manifolds 2 from 5 points of the Halo orbit in the Heliocentric Reference Frame

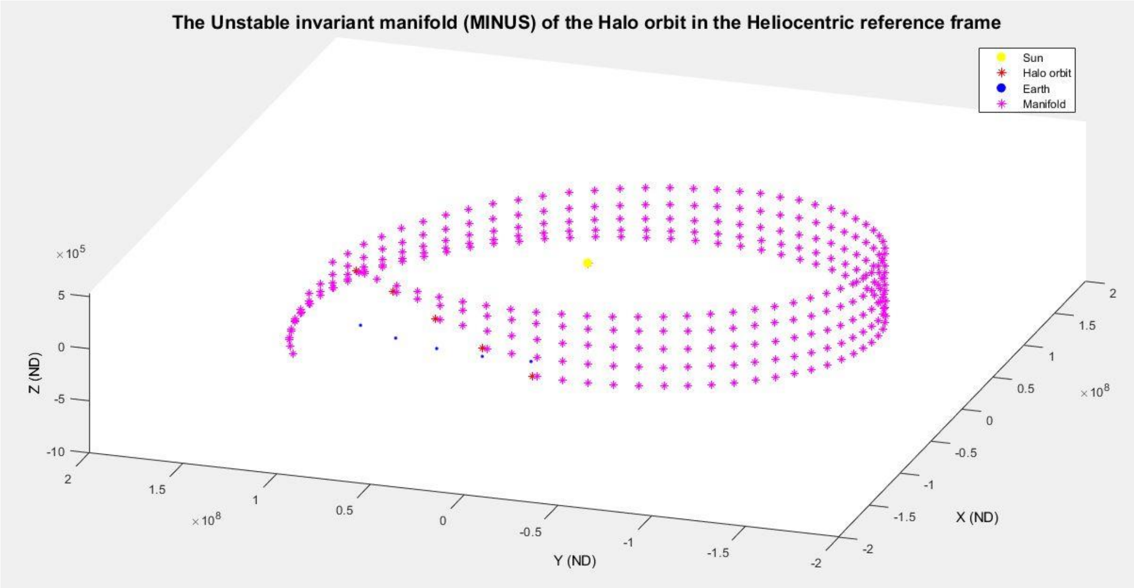

Figure 5.17: The 3D view of the unstable manifolds 2 from 5 points of the Halo orbit in the Heliocentric Reference Frame

The Δv was calculated from every position of unstable manifold 2 and the minimum values obtained for all the 6 departure windows have been given below:

	DELTA-V (km/s)	DEPARTURE DATE (MJD)	ARRIVAL DATE (MJD)
DEP-1	1.211982	62404	62682
DEP-1	1.196747	61838	61932
DEP-2	1.388121	62537	62674
DEP-3	1.147947	63141	63384
DEP-3	1.120564	63100	63383
DEP-3	1.246134	63062	63385
DEP-4	1.045356	63533	63727
DEP-4	2.017187	62991	63257
DEP-5	1.048303	63914	64073
DEP-6	1.023994	63808	64081
DEP-6	3.718473	63709	63985

Table 5-3: The calculated minimum values of Δv, the associated departure and arrival dates for the points in the Unstable manifold 2, for every departure window

From the above table, it can be seen that no value of Δv is lower than 1 km/s and therefore, transfer from the second unstable manifold to the Asteroid is not possible in the given departure and arrival windows, unless the mission constraint allows more expenditure of Δv.

6 Conclusions

The main goal of this thesis was to attempt to reach a Potentially Hazardous Asteroid as a possible secondary mission to the ESA Comet Interceptor mission, on the off chance that the detection of and transfer to a comet was unfeasible. This way, the thesis hoped to shed new light on the dynamics of the Near-Earth Asteroids, the Earth-Moon system, the evolution of the asteroids from the asteroid belt, low ΔV transfers to the NEAs, and the in-situ resource utilization and asteroid deflection techniques. Therefore, the thesis aimed at generating trajectories which require a ΔV lower than 1 km/s within the departure and arrival windows to go from the Sun-Earth L2 point to the selected Potentially hazardous asteroid.

The PHA that was selected was 2000SG344, from a list of PHAs arranged by decreasing Palermo scale. This Asteroid was selected from the larger section of PHAs due to its reachability from the L2 point with the least energy. The whole thesis was based on the premise that the obtained value of Δv could be lowered further with the help of Halo orbits and associated invariant manifolds.

In the subsequent chapter, the foundation and the basics of the CR3BP system, used for creating the halo orbits and the manifolds, were discussed, including the location of the libration points, several reference frames, and the methods to convert one reference frame into another. Using these, the halo orbit of desired amplitude was created using appropriate third-order approximation techniques, which were subjected to a correction algorithm, termed the ‘Differential Corrector’, which used the functionalities of a State-Transition Matrix.

After generating the Halo orbit, the corresponding invariant manifolds in the Rotating Reference Frame were constructed and explored in order to identify potential trajectories with much lower ΔV. This involved the study of the stability of the halo orbit and the techniques used for creation of the manifolds based on the monodromy matrix and associated eigenvalues.

The construction of these halo orbits and manifolds led way to the final section of the thesis, where the ΔV was calculated to reach the selected Asteroid from every point in the Halo orbit and its unstable invariant manifolds. In order to calculate that, the obtained halo orbits and manifolds in the Rotating Reference Frame were converted to Heliocentric Reference Frame using techniques presented in previous sections. Hence, the results were calculated and recorded using MATLAB, and were discussed and analysed in graphical and tabular formats, including an example trajectory from one of the manifolds.

From the results, it was seen that a transfer from the halo orbit and its manifolds could be achieved with lower ΔVs than direct transfers from the L2 lagrangian point, cementing the viability of the halo orbits and manifolds. This paves way for some future work in this area of dynamical systems.

6.1 Future Work

While this thesis presents a preliminary analysis of the transfers between the vicinity of the lagrangian point (Halo orbit and manifolds) and the Asteroid, the techniques involved in the thesis could be exploited and explored further in order to fine-tune the results. Also, this thesis limits its scope to a particular Potentially Hazardous Asteroid and a specific halo orbit and its manifolds. Analysing the transfers to various other PHAs and even Asteroids in the Asteroid belt from a multitude of halo orbits with different amplitudes would employ countless more unstable manifolds and subsequently, points of departure. This could pave way for a deeper understanding of the dynamics of the system and allows mission designers to understand more about ΔV optimization techniques. Although the results obtained in this thesis satisfy the aims, it is more necessary to validate the results using other visualisation techniques such as the NASA recommended GMAT (General Mission Analysis Tool) or STK (System ToolKit).

Another possible avenue of extension could be the construction of a return transfer trajectory i.e., from the Asteroid back to the vicinity of the libration point or the Earth. This can employ the use of stable manifolds, which bring the spacecraft towards the libration point. Manifold to Manifold transfer technology could possibly be addressed for optimizing the energy required.

Since this thesis does not address the station-keeping strategies in detail, discussing the techniques for possible maintenance across different libration points could be talked and discussed about. These are some of the works which can be done in order to prune this thesis and develop new insights about the dynamics of a CR3BP system.

REFERENCES

[1] Atkinson, Harry; Tickell, Crispin; Williams, D. (2000) *Report of the Task Force on Potentially Hazardous Near Earth Objects*. Available at: https://spaceguardcentre.com/wp-content/uploads/2014/04/full_report.pdf.

[2] Hartmann, W. K. et al. (1981) *Basaltic volcanism on the terrestrial planets*. Edited by H. Lunar and Planetary Institute. Pergamon, New York.

[3] Chapman, Clark R; Morrison, D. (1994) 'Impacts on the Earth by asteroids and comets: assessing the hazard', *Nature*, pp. 33–40.

[4] Alvarez, L; Alvarez, W; Asaro, F; Michel, H. V. (1980) 'No Title', *Science 208*, pp. 1095–1108.

[5] Jedicke, R., Bolin, B. T., Bottke, W. F., Chyba, M., Fedorets, G., Granvik, M., Jones, L. and Urrutxua, H. (2018) 'Earth's Minimoons: Opportunities for Science and Technology', *Frontiers in Astronomy and Space Sciences*, 5(May). doi: 10.3389/fspas.2018.00013.

[6] *ESA, Comet Interceptor* (2020). Available at: https://www.cosmos.esa.int/web/comet-interceptor/home (Accessed: 6 August 2020).

[7] *Comet Interceptor* (2019). Available at: https://www.cometinterceptor.space/# (Accessed: 7 August 2020).

[8] *ESA* (2019). Available at: http://www.esa.int/Science_Exploration/Space_Science/ESA_s_new_mission_to_intercept_a_comet (Accessed: 7 August 2020).

[9] *ESA - F Mission Call - Technical Annex* (2018) *ESA Publications Division*. Available at: https://www.cosmos.esa.int/documents/1731240/1731261/Call_for_Fast_missions_Annex.pdf/fde18523-e7d6-9191-b852-556aa07e44b9.

[10] *TYPES OF COMET* (2020) *COMETWATCH*. Available at: http://www.cometwatch.co.uk/comet-info/types-of-comet-2/#:~:text=Long period

comets can have,difficult to detect and catalogue. (Accessed: 12 August 2020).

[11] Kim, M. and Hall, C. D. (2001) 'AAS 01-324 LYAPUNOV AND HALO ORBITS ABOUT L 2', pp. 1–19.

[12] Howell, K. C. (2001) 'Families of Orbits in the Vicinity of the Collinear Libration Points', *The Journal of the Astronautical Sciences*, 49(1), pp. 107–125.

[13] Chen, H., Kawakatsu, Y. and Hanada, T. (2016) 'Phasing Delta-V for transfers from Sun – Earth halo orbits to the Moon', *Acta Astronautica*. Elsevier, 127, pp. 464–473. doi: 10.1016/j.actaastro.2016.05.003.

[14] Qian, Y., Yang, X., Jing, W. and Zhang, W. (2018) 'An improved numerical method for constructing Halo / Lissajous orbits in a full solar system model', *Chinese Journal of Aeronautics*. Chinese Society of Aeronautics and Astronautics, 31(6), pp. 1362–1374. doi: 10.1016/j.cja.2018.03.006.

[15] *NEODYS DATABASE* (2020) *ESA*. Available at: https://newton.spacedys.com/neodys/ (Accessed: 24 March 2020).

[16] *NEO Basics* (2018) *NASA*. Available at: https://cneos.jpl.nasa.gov/about/neo_groups.html (Accessed: 21 May 2020).

[17] *POTENTIALLY HAZARDOUS OBJECT* (2020). Available at: https://en.wikipedia.org/wiki/Potentially_hazardous_object (Accessed: 19 July 2020).

[18] *Discovery Statistics* (2020) *NASA*. Available at: https://cneos.jpl.nasa.gov/stats/totals.html (Accessed: 21 July 2020).

[19] *Palermo Technical Impact Hazard Scale* (2019) *NASA*. Available at: https://cneos.jpl.nasa.gov/sentry/palermo_scale.html (Accessed: 9 August 2020).

[20] Lancaster, E. R. and Blanchard, R. C. (1969) 'A Unified Form of Lambert's Theorem', p. 18.

[21] *NEODyS - NEA ELEMENTS* (2020) *ESA*. Available at: https://newton.spacedys.com/neodys/index.php?pc=5 (Accessed: 21 January

2020).

[22] Heggie, D. C. (2005) ‘The Classical Gravitational N -Body Problem’, *School of Mathematics, University of Edinburgh*, 2.

[23] Weisstein, E. W. (2019) *Integral of Motion*, *MathWorld*. Available at: https://mathworld.wolfram.com/IntegralofMotion.html (Accessed: 14 August 2020).

[24] Curtis, H. (2005) *Orbital Mechanics for Engineering Students*. 2008th edn. Burlington, MA: Elsevier B.H.

[25] Marchal, C., Yoshida, J. and Yi-Sui, S. (1984) ‘Three-body problem’, *Celestial Mechanics*. doi: 10.1007/BF01235792.

[26] Marchal, C. (1990) *The Three-Body Problem*. Elsevier.

[27] Vallado, D. A. and Mcclain, W. D. (2013) ‘Fundamentals of Astrodynamics and Applications’, 4th, p. 1138.

[28] *NASA Solar System Exploration - What is a Lagrange Point?* (2019) *NASA Science*. Available at: https://solarsystem.nasa.gov/resources/754/what-is-a-lagrange-point/ (Accessed: 13 August 2020).

[29] Wakker, K. F. (2015) *FUNDAMENTALS OF ASTRODYNAMICS*. January 20. Delft, The Netherlands: Institutional Repository, Library, TU Delft.

[30] *Jacobi Integral* (2020) *Wikipedia*. Available at: https://en.wikipedia.org/wiki/Jacobi_integral (Accessed: 15 August 2020).

[31] LARA, C. S. (2018) *Preliminary Design of Near Rectilinear Orbits around the Moon as Operational Orbit for the Future Deep Space Gateway*. CRANFIELD UNIVERSITY.

[32] Richardson, D. L. (1980) ‘Analytic construction of periodic orbits about the collinear points’, *Celestial Mechanics*, 22(3), pp. 241–253. doi: 10.1007/BF01229511.

[33] Kakoi, M. (2005) *TRANSFERS BETWEEN THE EARTH-MOON AND SUN-*

EARTH SYSTEMS USING MANIFOLDS AND TRANSIT ORBITS. Purdue University.

[34] Celletti, A., Pucacco, G. and Stella, D. (2015) 'Lissajous and Halo Orbits in the Restricted Three-Body Problem. Journal of Nonlinear Science', *Journal of Nonlinear Science*, 25(2), pp. 343–370.

[35] Press, WH; Teukolsky, SA; Vetterling, WT; Flannery, B. (2007) 'Section 18.1. The Shooting Method', in *Numerical Recipes: The Art of Scientific Computing*. 3rd edn. New York: Cambridge University Press.

[36] Patterson, C. E. (2005) *REPRESENTATIONS OF INVARIANT MANIFOLDS FOR APPLICATIONS IN SYSTEM-TO-SYSTEM TRANSFER DESIGN*. Purdue University.

[37] Galanos, G. (2019) *Near Rectilinear Halo Orbit in the vicinity of L1 Point in the Earth-Moon System*. CRANFIELD UNIVERSITY.

[38] Bosanac, N. (2016) *Leveraging natural dynamical structures to explore multi-body systems*. Purdue University.

[39] NETWORK, C. (2020) *MODIFIED JULIAN DAY CONVERTER*. Available at: http://www.csgnetwork.com/julianmodifdateconv.html (Accessed: 12 August 2020).

[40] *RISK PAGE* (2020) *ESA Publications Division*. Available at: http://neo.ssa.esa.int/risk-page (Accessed: 1 July 2020).

7 APPENDICES

Appendix A Analytical construction of periodic orbits by Richardson Method

The third-order solution for periodic motion about the collinear lagrange points is found to be,

$$x = a_{21}A_x^2 + a_{22}A_z^2 - A_x\cos(\tau_1) + (a_{23}A_x^2 - a_{24}A_z^2)\cos(2\tau_1) + (a_{31}A_x^3 - a_{32}A_xA_z^2)\cos(3\tau_1) \tag{7-1}$$

$$y = kA_x\sin(\tau_1) + ((b_{21}A_x^2 - b_{22}A_z^2)\sin(2\tau_1) + (b_{31}A_x^3 - b_{32}A_xA_z^2)\sin(3\tau_1) \tag{7-2}$$

$$z = \delta_n A_z\cos(\tau_1) + \delta_n d_{21}A_xA_z(\cos(2\tau_1) - 3) + \delta_n(d_{32}A_zA_x^2 - d_{31}A_z^3)\cos(3\tau_1) \tag{7-3}$$

Where δ_n, called the switch function, determines the property of the family of periodic orbits (Northern family/Southern family) around the particular libration point.

$$\delta_n = 2 - n\,; n = 1, 3 \tag{7-4}$$

The values of the initial conditions are obtained by formulating these below-mentioned values for a given value of the Amplitude A_z of Halo orbit.

The linearized frequency, λ, is the root of the following equation:

$$\lambda^4 + (C_2 - 2)\lambda^2 - (C_2 - 1)(1 + 2C_2) = 0 \tag{7-5}$$

Where C_2 is gotten from equation (4-5). This value of the linearized frequency is utilized in the frequency correction formulae as given below.

$$S_1 = \frac{2\lambda}{2\lambda(\lambda(1 + k^2) - 2k)}\{1.5c_3[2a_{22}(k^2 - 2) - a_{24}(k^2 + 2) + 2kb_{22} + 5d_{21}] - \left(\frac{3}{8}\right)c_4(12 - k^2)\} \tag{7-6}$$

$$S_2 = \frac{1}{2\lambda(\lambda(1+k^2)-2k)}\{1.5c_3[2a_{21}(k^2-2)-a_{23}(k^2+2)-2kb_{21}] - \left(\frac{3}{8}\right)c_3(3k^4-8k^2+8)\} \tag{7-7}$$

where

$$k = \frac{2\lambda}{\lambda^2+1-c_2} \tag{7-8}$$

There are terms which relate the 2 amplitudes, A_x and A_z, for an amplitude-constraint relationship. Those are defined as:

$$l_1 = a_1 + 2\lambda^2 s_1\,;\; l_1 = a_2 + 2\lambda^2 s_2 \tag{7-9}$$

where

$$a_1 = 1.5c_3(2a_{21}+a_{23}+5d_{21}) - \left(\frac{3}{8}\right)c_4(12-k^2) \tag{7-10}$$

$$a_2 = 1.5c_3(a_{24}-2a_{22}) + \left(\frac{9}{8}\right)c_4 \tag{7-11}$$

The expressions for other constants ($a_{ij}, b_{ij}, d_{ij}, etc.$) used in the above-mentioned formulae for determining the properties of the halo orbit around L2 are given below:

The values for a_{ij}:

$$a_{21} = \left(\frac{3c_3(k^2-2)}{4(1+2c_2)}\right) \tag{7-12}$$

$$a_{22} = \left(\frac{3c_3}{4(1+2c_2)}\right) \tag{7-13}$$

$$a_{23} = \frac{-3c_3\lambda}{4kd_1}(3k^3\lambda - 6k(k-\lambda) + 4) \quad \textbf{(7-14)}$$

$$a_{23} = \frac{-3c_3\lambda}{4kd_1}(2 + 3\lambda k) \quad \textbf{(7-15)}$$

$$a_{31} = \frac{-9\lambda}{4d_2}[4c_3(ka_{23} - b_{21}) + kc_4(4 + k^2)] + \left(\frac{9\lambda^2 + 1 - c_2}{2d_2)}\right)[3c_3(2a_{23} - kb_{21}) + c_4(2 + 3k^2)] \quad \textbf{(7-16)}$$

$$a_{31} = \frac{-1}{d_2}\{\frac{9\lambda}{4}[4c_3(ka_{24} - b_{22}) + kc_4] + 1.5(9\lambda^2 + 1 - c_2)[c_3(kb_{22} + d_{21} - 2a_{24}) - c_4]\} \quad \textbf{(7-17)}$$

The values for b_{ij}:

$$b_{21} = \frac{-3c_3\lambda}{2d_1}(3\lambda k - 4) \quad \textbf{(7-18)}$$

$$b_{22} = \left(\frac{3c_3\lambda}{d_1}\right) \quad \textbf{(7-19)}$$

$$b_{31} = \frac{-3}{8d_2}\{8\lambda[3c_3(kb_{21} - 2a_{23}) - c_4(2 + 3k^2)] + (9\lambda^2 + 1 + 2c_2)[4c_3(ka_{23} - b_{21}) + kc_4(4 + k^2)]\} \quad \textbf{(7-20)}$$

$$b_{32} = \frac{1}{d_2}\{9\lambda[c_3(kb_{22} + d_{21} - 2a_{24}) - c_4] + 1.5(9\lambda^2 + 1 + 2c_2)[4c_3(ka_{24} - b_{22}) + kc_4]\} \quad \textbf{(7-21)}$$

The values for d_{ij}:

$$d_{21} = \frac{-c_3}{2\lambda^2} \quad \textbf{(7-22)}$$

$$d_{31} = \left(\frac{3}{64\lambda^2}(4c_3 a_{24} + c_4)\right) \quad \textbf{(7-23)}$$

$$d_{32} = \frac{3}{64\lambda^2}[4c_3(a_{23} - d_{21}) + c_4(4 + k^2)] \quad \textbf{(7-24)}$$

$$d_1 = \frac{3\lambda^2}{k}[k(6\lambda^2 - 1) - 2\lambda \quad] \quad \textbf{(7-25)}$$

$$d_2 = \frac{8\lambda^2}{k}[k(11\lambda^2 - 1) - 2\lambda \quad] \quad \textbf{(7-26)}$$

In order to determine the value for frequency correction, it becomes necessary to mention the amplitude-constraint relationship using the parameters mentioned above.

$$l_1 {A_x}^2 + l_2 {A_z}^2 + \Delta = 0 \quad \textbf{(7-27)}$$

where

$$\Delta = \lambda^2 - c_2 \quad \textbf{(7-28)}$$

The quantity for frequency correction, as mentioned in equation (4-13), after the removal of the secular terms is now given by,

$$\omega = 1 + \omega_2 \quad \textbf{(7-29)}$$

$$\omega_2 = s_1 {A_x}^2 + s_2 {A_z}^2 \quad \textbf{(7-30)}$$

With this value of the frequency correction, the values of the initial velocity vector are determined using the set of equations mentioned below.

$$\dot{x}_0 = A_x \sin(\tau_1) - 2(a_{23}A_x^2 - a_{24}A_z^2)\sin(2\tau_1) - 3(a_{31}A_x^3 - a_{32}A_xA_z^2)\sin(3\tau_1) \tag{7-31}$$

$$\dot{y} = kA_x \cos(\tau_1) + 2(b_{21}A_x^2 - b_{22}A_z^2)\cos(2\tau_1) + 3(b_{31}A_x^3 - b_{32}A_xA_z^2)\cos(3\tau_1) \tag{7-32}$$

$$\dot{z} = -\delta_n A_z \sin(\tau_1) - 2\,\delta_n d_{21}A_xA_z(\sin(2\tau_1)) - 3\delta_n(d_{32}A_zA_x^2 - d_{31}A_z^3)\sin(3\tau_1) \tag{7-33}$$

The final values are found by multiplying $\dot{x}, \dot{y}, \dot{z}$ with the frequency correction value, i.e.,

$$\dot{x}_0 = \dot{x}_0 * \omega * \lambda \tag{7-34}$$

$$\dot{y}_0 = \dot{y}_0 * \omega * \lambda \tag{7-35}$$

$$\dot{z}_0 = \dot{z}_0 * \omega * \lambda \tag{7-36}$$

Setting a zero-phase angle ($\phi = 0$) and τ = 0, the initial conditions of the trajectory of the halo orbit can be found.

The time-period of the halo orbit is found as,

$$t_p = \frac{2\pi}{\omega * \lambda} = 3.07855101\ (ND) = 178.955\ DAYS \tag{7-37}$$

For a given halo amplitude A_z= 611000 kms around L2, in the Sun-Earth system, the values of the required constants to determine the initial state vector are mentioned in Table A-1.

CONSTANTS	VALUE
γ_l	0.01009348
λ	2.05699240
k	3.18719821
Δ	0.29078410
c_2	3.94043365
c_3	-2.97981197
c_4	2.97021283
s_1	-0.74439396
s_2	0.12505002
l_1	-14.82800461
l_2	1.67364247
a_1	-8.52861869
a_2	0.61541466
d_1	293.17924866
d_2	1497.9394807
a_{21}	-2.05300884
a_{22}	-0.25164873
a_{23}	0.89627619
a_{24}	0.10660115
a_{31}	0.78063667
a_{32}	0.08369678
b_{21}	0.49135647
b_{22}	-0.06272050
b_{31}	0.85528247
b_{32}	0.02043351
d_{21}	0.35212226
d_{31}	0.01882887
d_{32}	0.39402506

Table A-1: Values of the constants in the Richardson method for a halo orbit of A_z= 611000 km in the Sun-Earth system

Appendix B Database of Potentially Hazardous Asteroids

B.1 Table of PHA properties

The table consisting some of the physical and dynamical properties (Name, Diameter, Date and Time of predicted impact, Impact Probability, Palermo Scale, and timespan of detected impacts) has been given below. The table was obtained from [40].

Object Name	Diameter [m]	Date/Time	IP max	PS max	Years
2010RF12	8*	2095-09-05 23:50	1/14	-3.20	2095-2118
1979XB	700*	2113-12-14 18:06	1/1.79E6	-3.27	2056-2113
2000SG344	40*	2071-09-16 00:58	1/1183	-3.38	2069-2118
99942	375	2068-04-12 15:13	1/531914	-3.67	2068-2116
2008JL3	30*	2027-05-01 09:06	1/6993	-3.68	2027-2116
2009JF1	13*	2022-05-06 08:12	1/4166	-3.72	2022
2018VP1	2.4*	2020-11-02 01:13	1/193	-3.77	2020-2097
2007KE4	30*	2029-05-26 00:23	1/10834	-3.82	2026-2115
2012QD8	90*	2047-03-08 23:17	1/172117	-3.91	2042-2113
2011DU9	16*	2046-02-23 20:44	1/1742	-3.98	2046-2059
2020FT3	80*	2089-08-05 20:47	1/54644	-4.11	2089-2118
2007FT3	400*	2024-10-02 21:40	1/1.46E7	-4.14	2013-2118
2006JY26	8*	2074-05-03 00:48	1/152	-4.16	2073-2117
2013VW13	20*	2080-11-08 16:21	1/3968	-4.17	2063-2097
2007DX40	40*	2056-08-18 05:15	1/31545	-4.20	2030-2118
2014GN1	40*	2061-09-16 20:14	1/49751	-4.21	2061-2070
2017US	22*	2110-09-22 07:11	1/1788	-4.22	2085-2118
2018JD	16*	2067-05-08 13:29	1/2127	-4.26	2067-2114
2001VB	700*	2023-07-23 07:16	1/2.56E8	-4.28	2023
2008EX5	60*	2083-10-09 17:02	1/43103	-4.30	2059-2090
2007VE8	29*	2062-11-06 02:54	1/9615	-4.32	2062
2005QK76	30*	2030-02-26 08:15	1/59171	-4.32	2030-2107
2020MJ	30*	2102-06-12 10:45	1/13550	-4.34	2082-2107

2017SH33	700*	2026-04-30 08:44	1/1.91E8	-4.36	2026-2093
2015YJ	8*	2059-12-14 08:15	1/1017	-4.39	2042-2118
2010CR5	400*	2062-01-01 02:05	1/1.78E7	-4.41	2051-2075
2020CQ1	6*	2070-02-03 04:36	1/236	-4.42	2070-2118
2016DK1	12*	2043-02-18 02:17	1/2544	-4.42	2043-2118
2009BE	21*	2083-01-25 02:21	1/5181	-4.43	2037-2118
2009TD17	10*	2039-05-08 11:40	1/1666	-4.45	2039-2118
1994GK	50*	2061-04-03 15:23	1/62111	-4.46	2039-2073
2005ED224	60*	2023-03-11 08:25	1/568181	-4.48	2018-2064
2017WT28	8*	2104-11-24 16:32	1/355	-4.49	2080-2117
2016WG	80*	2076-06-23 07:13	1/383141	-4.51	2076-2101
2018TY4	8*	2033-10-05 16:22	1/3115	-4.52	2033
2017YM1	30*	2091-12-16 12:48	1/18975	-4.55	2048-2110
2020OB	70*	2116-07-23 09:37	1/197238	-4.56	2114-2116
2008CC71	40*	2066-02-27 12:17	1/31645	-4.61	2034-2082
2019LU1	50*	2056-06-05 11:12	1/425531	-4.61	2056-2070
2011AM37	4*	2048-01-11 10:09	1/188	-4.65	2048-2118
2020KD3	19*	2089-05-26 08:59	1/5208	-4.65	2076-2114
2014CR13	25*	2108-02-11 19:52	1/11520	-4.67	2096-2118
2017SF20	8*	2034-09-26 12:42	1/3184	-4.68	2034-2036
2008UB7	60*	2060-10-31 18:29	1/258397	-4.68	2048-2101
2017FO63	70*	2097-11-13 18:32	1/471698	-4.68	2097-2108
2012MF7	15*	2046-06-21 21:10	1/7575	-4.69	2046-2104
2019TU	22*	2099-01-27 20:48	1/8333	-4.69	2090-2116
2014WA201	15*	2075-11-16 03:23	1/5347	-4.69	2074-2084
2010QG2	38	2051-09-05 09:14	1/145137	-4.70	2051-2070
2011XC2	90*	2056-12-02 09:55	1/925925	-4.70	2056-2108
2012HG2	14*	2071-02-10 04:08	1/2967	-4.72	2052-2119
2010UK	15*	2068-10-15 10:25	1/4032	-4.73	2068-2118
2017LD	11*	2066-06-10 07:32	1/2096	-4.74	2053-2118
2016WN55	400*	2032-09-12 17:37	1/1.09E8	-4.75	2026-2114
2008FF5	80*	2060-03-27 18:10	1/1.9E6	-4.75	2060
2008HJ	25*	2081-05-02 12:04	1/13003	-4.77	2077-2116

2008ST7	50*	2094-09-10 01:44	1/85470	-4.78	2062-2116
2016RD34	10*	2051-05-18 21:48	1/2816	-4.82	2051-2118
2006DM63	16*	2031-02-24 05:54	1/18050	-4.83	2028-2113
2018GR4	13*	2058-03-07 07:09	1/4926	-4.85	2058-2118
2018DQ	5*	2027-02-21 16:52	1/7812	-4.85	2027-2118
2013TP4	12*	2026-10-01 07:49	1/40160	-4.86	2026
2011UM169	30*	2102-10-24 12:30	1/46728	-4.88	2099-2107
2008EZ84	21*	2073-03-09 23:41	1/12836	-4.90	2072-2118
2000SB45	50*	2088-10-08 03:04	1/72992	-4.92	2068-2118
2019QR3	13*	2078-08-31 22:36	1/6060	-4.92	2073-2089
2006CM10	160*	2092-08-12 11:24	1/3.68E6	-4.94	2092
2007TC14	130*	2082-10-22 10:11	1/3.31E6	-4.94	2082
2007WP3	70*	2105-11-12 07:32	1/273972	-4.98	2098-2114
2014JU15	40*	2086-04-28 19:52	1/84033	-4.99	2068-2116
2010GM23	341	2105-04-15 03:59	1/84745	-4.99	2086-2118
2019WG2	40*	2114-11-24 08:12	1/68493	-5.00	2093-2118
2016NL39	11*	2075-06-28 07:42	1/3058	-5.01	2055-2118
2015XA378	24*	2107-12-20 18:55	1/33557	-5.02	2084-2116
2019WU2	40*	2093-11-04 16:02	1/107874	-5.05	2080-2109
2012EK5	28*	2095-03-24 11:40	1/46296	-5.05	2070-2111
2020DF3	50*	2074-02-22 06:52	1/628930	-5.05	2067-2115
2006SC	30*	2053-09-13 14:41	1/98039	-5.06	2047-2106
1995CS	29*	2042-02-03 14:40	1/174216	-5.06	2042-2062
2019JO1	12*	2052-04-28 02:02	1/21881	-5.07	2044-2053
2020FA5	210*	2049-10-31 01:31	1/4.48E7	-5.07	2049-2118
2002RB182	100*	2110-09-27 05:15	1/775193	-5.09	2036-2118
2013EV27	14*	2038-02-28 23:44	1/29411	-5.10	2038-2078
2002GM5	180*	2064-10-03 10:18	1/9.26E6	-5.11	2064-2113
2011VG9	130*	2104-11-03 20:47	1/3.58E6	-5.11	2104-2117
2017OE7	20*	2114-08-23 12:24	1/10090	-5.12	2113-2114
2006QN111	60*	2079-08-16 11:20	1/319488	-5.12	2079
2016EO28	5*	2035-02-28 09:50	1/2754	-5.13	2035-2113
2017VL2	22*	2098-11-09 16:25	1/19841	-5.13	2074-2118

2012ES10	60*	2059-03-05 10:45	1/1.29E6	-5.13	2054-2064
2002UV36	16*	2087-10-26 07:55	1/11376	-5.14	2044-2087
2011SO189	18*	2056-09-24 11:51	1/32258	-5.14	2056-2102
2017RV2	20*	2094-09-10 07:28	1/16474	-5.15	2072-2117
2011ES4	26*	2055-09-02 16:44	1/56497	-5.16	2031-2115
2018NL	29*	2060-06-29 00:29	1/81967	-5.16	2060-2115
2019FE	50*	2106-03-18 05:27	1/190114	-5.19	2095-2106
2017GG8	21*	2066-03-31 12:17	1/44642	-5.19	2066-2078
2009TH8	40*	2097-10-21 13:51	1/111482	-5.19	2068-2111
2010JH110	20*	2092-06-03 17:12	1/18903	-5.22	2071-2102
2014JR24	5*	2069-05-01 22:19	1/800	-5.23	2069-2117
2020BW5	18*	2046-06-12 18:29	1/54054	-5.24	2046-2110
2006HF6	50*	2070-04-19 01:49	1/331125	-5.24	2053-2110
2020KN2	19*	2063-06-08 09:04	1/33557	-5.25	2063-2116
2011OB26	28*	2115-08-11 23:18	1/46296	-5.25	2096-2118
1996TC1	60*	2067-09-26 05:02	1/917431	-5.26	2054-2072
2009WP6	16*	2074-11-16 09:58	1/46082	-5.26	2067-2117
2006JE	60*	2106-05-02 07:22	1/833333	-5.27	2094-2112
2008PK9	80*	2057-08-10 18:32	1/3.12E6	-5.30	2037-2067
2020MO1	70*	2059-07-03 04:25	1/2.2E6	-5.31	2059
2017PY26	120*	2111-08-19 03:33	1/3.25E6	-5.31	2092-2117
2014ML67	50*	2027-07-03 19:51	1/3.66E6	-5.31	2023-2108
2016VB1	7*	2093-11-05 01:24	1/1647	-5.32	2065-2118
2010MY112	372	2030-12-23 03:23	1/1.4E8	-5.32	2018-2101
2016PM38	22*	2020-07-01 02:08	1/632911	-5.33	2020
2008TE	10*	2023-09-25 11:08	1/38022	-5.34	2023-2117
2020DJ1	40*	2114-07-30 21:10	1/158227	-5.35	2068-2117
2013GM3	20*	2073-04-13 21:14	1/36231	-5.36	2028-2117
2020BK3	14*	2091-01-20 21:00	1/16949	-5.36	2091-2105
2010VQ	10*	2034-10-07 14:44	1/15267	-5.37	2034-2117
2002MN	80*	2071-06-15 16:02	1/980392	-5.37	2036-2110
2009BR5	140*	2078-07-19 06:30	1/6.41E6	-5.37	2059-2111
2013WM	60*	2047-11-20 11:34	1/4.31E6	-5.37	2047-2105

2016JB18	11*	2117-04-14 08:37	1/4587	-5.38	2085-2118
2014UD57	24*	2086-10-21 05:08	1/56497	-5.39	2076-2118
2012BA77	24*	2025-10-10 01:47	1/353356	-5.39	2025-2107
2013BL18	23*	2086-01-14 07:26	1/67567	-5.39	2070-2092
2020OX4	40*	2088-07-18 14:12	1/454545	-5.39	2067-2116
2011MX	15*	2081-06-19 08:11	1/22371	-5.40	2070-2092
2001CA21	600*	2045-10-12 01:42	1/1.25E9	-5.40	2015-2105
2016CY135	50*	2108-03-10 10:22	1/179533	-5.41	2103-2115
2006BC8	30*	2103-07-27 11:11	1/123915	-5.41	2050-2118
2010HV20	465	2116-05-05 13:51	1/8.47E6	-5.41	2116
2014OM207	5*	2101-07-25 21:36	1/1234	-5.42	2101
2014YN	25*	2110-11-10 12:46	1/37878	-5.44	2090-2118
2010KV7	13	2034-05-21 06:52	1/116009	-5.44	2034-2118
2018JN	30*	2100-04-24 08:20	1/109170	-5.44	2100-2118
2019SJ	11*	2095-09-16 20:50	1/8403	-5.44	2055-2118
2019LW4	12*	2083-06-08 18:50	1/13698	-5.44	2083-2117
2007KO4	80*	2046-11-23 22:02	1/2.54E6	-5.44	2015-2114
2020GZ2	8*	2049-04-20 00:48	1/13550	-5.46	2049-2054
2011BL45	13*	2071-08-01 11:59	1/12738	-5.47	2050-2117
2015KG158	8*	2071-05-14 21:29	1/5291	-5.48	2045-2117
2005XA8	27*	2076-12-05 17:43	1/108695	-5.48	2063-2092
2007DS7	24*	2075-02-17 10:09	1/91743	-5.48	2048-2116
2018GG	40*	2095-04-11 02:27	1/347222	-5.48	2086-2095
2017HG4	10*	2086-04-17 10:25	1/7092	-5.49	2046-2115
2008YO2	30*	2107-12-24 21:56	1/172711	-5.49	2052-2114
2005EL70	60*	2034-03-05 23:20	1/5.59E6	-5.49	2034-2058
2009OW6	30*	2080-08-20 07:31	1/110132	-5.50	2074-2118
2012SY49	24*	2048-09-28 18:30	1/233100	-5.51	2031-2114
2020JK	60*	2118-05-19 01:00	1/671140	-5.51	2057-2118
2010VW194	18*	2079-11-12 19:47	1/34482	-5.52	2042-2117
2011EB74	15*	2054-03-16 12:20	1/31545	-5.53	2033-2118
2009FZ10	28*	2115-03-16 20:18	1/103734	-5.53	2111-2115
2001GP2	15*	2063-10-07 00:14	1/19685	-5.54	2043-2117

2018XQ2	8*	2091-01-06 08:43	1/4545	-5.54	2065-2118
2019HS3	14*	2055-04-21 19:39	1/132802	-5.54	2055-2083
2020HL1	30*	2055-05-22 18:42	1/305810	-5.55	2055-2066
2020OR4	26*	2093-01-20 03:09	1/222222	-5.55	2093-2117
2020LV	30*	2112-06-22 00:19	1/88495	-5.56	2099-2116
2012WS3	23*	2117-05-23 07:05	1/51020	-5.56	2082-2118
2012VE77	19*	2033-11-17 12:49	1/256410	-5.57	2033-2035
2002TY59	29*	2110-10-03 10:54	1/86206	-5.58	2074-2118
2011SM173	10*	2058-09-22 03:55	1/21645	-5.58	2058-2112
2015WN1	19*	2092-11-11 22:25	1/47619	-5.59	2041-2118
2002VU17	40*	2099-11-17 07:02	1/295857	-5.59	2084-2099
2008LD	6*	2092-05-30 04:21	1/2036	-5.60	2054-2118
2017FN1	2.7*	2033-03-20 22:58	1/3906	-5.60	2033-2084
2018NW	10*	2117-07-09 03:36	1/16181	-5.60	2046-2118
2019SX	4*	2077-09-21 08:08	1/2659	-5.61	2046-2116
2016BA15	16*	2056-07-18 21:13	1/94339	-5.61	2054-2114
2013WZ44	26*	2117-11-25 20:37	1/98039	-5.62	2111-2117
2016CD30	10*	2070-01-31 17:21	1/18939	-5.63	2056-2097
2005CC37	100*	2117-01-13 15:48	1/2.02E6	-5.65	2117
2017UL7	50*	2041-03-19 22:55	1/2.45E6	-5.65	2041-2054
2014MO68	80*	2108-08-07 01:34	1/1.3E6	-5.66	2088-2108
2018SD2	7*	2088-09-20 04:47	1/4464	-5.67	2069-2118
2000WJ107	80*	2114-11-19 23:43	1/1.41E6	-5.69	2100-2118
2010XB	4*	2036-11-30 06:03	1/9900	-5.69	2036-2067
2009FJ	40*	2117-03-15 04:55	1/217864	-5.70	2058-2117
2012BY1	25*	2043-01-25 16:51	1/526315	-5.70	2043-2117
2018PZ21	16*	2064-07-27 19:57	1/58139	-5.71	2052-2110
2004VM24	28*	2078-11-13 02:48	1/165562	-5.71	2049-2117
2020ED	15*	2096-04-15 17:41	1/29850	-5.72	2096-2117
2006HX57	30*	2065-05-09 12:17	1/330033	-5.72	2065-2071
2007CC27	15*	2088-02-12 14:34	1/37735	-5.72	2059-2105
2016NL56	600*	2078-02-14 22:16	1/1.3E7	-5.72	2039-2118
2015ME131	400*	2027-08-18 22:08	1/2.7E9	-5.72	2019-2105

2011BG10	19*	2051-01-24 09:50	1/163934	-5.73	2051-2074
2019AW2	30*	2072-12-27 15:49	1/377358	-5.73	2072
443104 2013XK22	50*	2101-06-20 07:39	1/568181	-5.74	2101-2118
2017YO3	8*	2049-12-19 19:49	1/19960	-5.75	2049-2098
2019NO2	8*	2102-07-04 02:17	1/7194	-5.75	2102-2117
2011BF40	40*	2083-06-27 12:03	1/740740	-5.75	2083
2004GE2	190*	2106-05-03 01:54	1/2.72E7	-5.75	2106-2109
2008ST	14*	2116-09-25 15:46	1/15723	-5.76	2047-2118
2019UT	9*	2106-10-25 12:55	1/11312	-5.76	2103-2118
2014QC391	11*	2100-09-07 05:56	1/16286	-5.77	2078-2118
2012LJ	27*	2072-11-10 21:45	1/387596	-5.77	2051-2072
2011FQ6	10*	2075-03-23 23:31	1/21141	-5.78	2051-2115
2019SC	13*	2051-09-16 03:35	1/95238	-5.79	2051
2010XN69	20*	2055-01-08 09:26	1/100603	-5.81	2020-2118
2015MN11	40*	2081-06-26 12:40	1/1.56E6	-5.81	2061-2116
2019NF7	9*	2080-07-07 22:35	1/15128	-5.82	2080
2013RO30	7*	2090-09-04 21:19	1/8264	-5.82	2044-2105
2008KO	50*	2052-06-01 14:24	1/3.12E6	-5.82	2049-2061
2010CS19	9*	2104-02-13 15:56	1/9174	-5.83	2104-2116
2018HJ2	40*	2114-03-10 09:03	1/401606	-5.83	2114
2018FE4	40*	2098-09-26 04:22	1/1.09E6	-5.85	2085-2101
2018CM	10*	2072-02-08 09:40	1/24875	-5.86	2054-2117
2017RZ17	300*	2029-11-26 15:27	1/1.35E9	-5.86	2019-2114
2017AE21	40*	2025-05-09 20:11	1/2.76E6	-5.87	2024-2114
2018BN6	16*	2089-07-22 17:07	1/64935	-5.87	2073-2117
2019AU6	17*	2097-01-13 16:47	1/66225	-5.88	2064-2118
2006UU17	18*	2103-10-21 20:27	1/71942	-5.88	2075-2107
2020CO2	16*	2087-07-20 03:36	1/111856	-5.88	2048-2118
2017QC36	190*	2024-02-20 12:13	1/1.09E10	-5.88	2024-2091
2015BW516	10*	2061-01-29 19:45	1/42735	-5.89	2046-2081
2019JR2	14*	2114-05-01 19:05	1/45662	-5.89	2079-2118
2010HS20	80*	2071-07-01 10:03	1/3.24E6	-5.90	2057-2071

2018TB	40*	2103-10-08 12:22	1/448430	-5.90	2103
2018TP5	25*	2091-10-04 12:14	1/216450	-5.90	2074-2113
2000LG6	6*	2094-05-26 22:32	1/2840	-5.91	2082-2118
2013NH6	80*	2060-06-29 19:36	1/1.03E7	-5.91	2060
2018NJ	10*	2083-07-10 02:54	1/18248	-5.92	2083-2116
2005VN5	14*	2071-11-12 13:38	1/48780	-5.92	2047-2118
2010JL88	16*	2082-05-18 21:19	1/99009	-5.92	2042-2118
2017NT5	90*	2115-01-12 05:47	1/7.69E6	-5.92	2050-2117
2019UH9	30*	2078-03-18 19:58	1/1.1E6	-5.92	2078-2118
2010TW149	24*	2093-10-07 00:35	1/278551	-5.93	2058-2113
2016TY55	15*	2082-10-20 04:44	1/52356	-5.94	2074-2118
2007XZ9	40*	2068-11-28 00:30	1/980392	-5.95	2056-2110
2012TV	30*	2081-04-02 17:04	1/746268	-5.95	2059-2118
2004PU42	16*	2085-08-17 01:26	1/70422	-5.96	2071-2118
2014GY44	30*	2080-03-29 01:12	1/467289	-5.96	2069-2101
2011DV10	40*	2093-02-18 04:51	1/862068	-5.96	2093
2017FB1	70*	2106-03-04 11:08	1/6.17E6	-5.97	2098-2106
2016SA2	8*	2111-09-26 14:02	1/10204	-5.98	2107-2118
2016DA31	4*	2031-09-04 20:11	1/15698	-5.98	2020-2118
2019FA	6*	2036-03-14 11:17	1/30864	-6.00	2036-2111
1999RZ31	60*	2056-09-05 02:01	1/2.57E6	-6.00	2056
2009FG	28*	2077-12-24 13:00	1/340136	-6.00	2022-2118
2007UO6	12*	2031-10-17 06:01	1/155520	-6.00	2031-2113
2014AD16	12*	2087-01-08 08:34	1/38167	-6.01	2087-2100
2020FN3	50*	2106-04-09 07:36	1/943396	-6.02	2086-2116
2010UB	40*	2116-10-29 07:32	1/581395	-6.02	2116
2014HN197	400*	2031-01-04 05:27	1/1.83E8	-6.02	2024-2118
2016LP10	4*	2023-06-10 10:39	1/66225	-6.02	2023-2118
2020HQ4	14*	2077-04-12 14:33	1/62111	-6.03	2059-2118
2009VA	7*	2025-11-06 20:14	1/49751	-6.04	2025-2048
2010UH	14*	2115-07-14 11:48	1/39215	-6.06	2047-2118
2016RR1	10*	2102-09-03 22:44	1/21367	-6.06	2063-2118
2016NK22	6*	2111-07-14 06:03	1/5555	-6.06	2082-2118

2007TL16	20*	2090-10-06 07:26	1/181488	-6.07	2074-2104
2007PR25	150*	2094-08-18 23:54	1/6.37E7	-6.07	2094-2113
2017SA20	8*	2047-04-22 01:48	1/37037	-6.08	2031-2118
2018GE2	14*	2112-10-31 09:53	1/45662	-6.08	2060-2118
2010TW54	11*	2117-10-09 17:44	1/25316	-6.08	2074-2118
2017RZ15	13*	2106-09-04 20:20	1/47393	-6.08	2067-2118
2014FX32	30*	2076-03-12 03:29	1/735294	-6.08	2076-2115
2013GA55	10*	2114-04-06 00:56	1/25125	-6.08	2070-2114
2020BA14	100*	2055-02-25 12:29	1/2.95E7	-6.08	2055
2009CZ1	40*	2058-02-19 01:02	1/3.5E6	-6.08	2058-2074
2011DS	14*	2080-02-24 17:57	1/67567	-6.09	2065-2116
2011CU46	29*	2080-08-11 21:19	1/746268	-6.09	2015-2118
2007EV	30*	2117-03-18 16:58	1/507614	-6.10	2086-2118
2011CW46	40*	2021-08-14 22:44	1/1.2E7	-6.10	2021-2113
2009HS44	17*	2111-09-17 12:53	1/172117	-6.10	2111
2011WN69	21*	2109-11-23 12:37	1/366300	-6.10	2038-2117
2001BA16	24*	2041-01-15 01:29	1/409836	-6.11	2040-2111
2017YO5	21*	2117-12-24 12:24	1/132100	-6.11	2077-2117
2010UY7	7*	2092-10-28 05:02	1/9803	-6.12	2066-2118
2020BB5	4*	2107-01-23 02:04	1/3355	-6.12	2092-2118
2011AK37	30*	2097-01-16 21:53	1/666666	-6.12	2097
2019KJ4	12*	2066-06-03 13:55	1/71428	-6.13	2059-2118
2010GH7	8	2111-04-02 12:37	1/31746	-6.13	2099-2118
2019WE	15*	2044-11-22 20:27	1/280898	-6.13	2044-2081
2015BE511	7*	2078-01-27 11:00	1/16233	-6.13	2057-2111
2017VJ	40*	2118-11-01 08:47	1/1.07E6	-6.13	2109-2118
2017HJ61	6*	2029-04-22 15:35	1/91743	-6.13	2026-2033
2014MA68	23*	2026-05-03 12:30	1/1.23E6	-6.14	2019-2117
2005WG57	70*	2029-08-21 04:25	1/1.15E7	-6.14	2029-2107
2008EV84	30*	2041-03-07 15:52	1/1.39E6	-6.14	2041-2106
2018BL11	8*	2107-01-22 18:56	1/20408	-6.15	2102-2118
2012DJ54	7*	2068-02-24 13:55	1/18450	-6.16	2068-2118
2018EE9	19*	2115-03-09 15:19	1/219780	-6.16	2067-2118

2016CK137	12*	2059-02-03 13:08	1/110987	-6.17	2040-2118
2016AF9	130*	2083-12-23 13:57	1/9.8E7	-6.17	2083
2013FU13	13*	2088-03-12 18:33	1/56818	-6.18	2070-2111
2019DP	40*	2109-08-30 13:51	1/699300	-6.18	2065-2118
2005AU3	23*	2097-01-05 06:53	1/324675	-6.18	2070-2118
2019AH3	9*	2060-01-06 05:48	1/101522	-6.18	2060-2068
2019BZ	11*	2078-07-28 06:53	1/58823	-6.19	2077-2118
2016TQ18	19*	2110-10-01 03:58	1/166666	-6.19	2086-2110
2019XS	50*	2105-11-10 08:27	1/2.04E6	-6.19	2079-2118
2018VA8	15*	2099-11-09 16:58	1/117233	-6.19	2098-2116
2005SO1	29*	2110-09-21 11:08	1/490196	-6.20	2108-2110
2020FZ2	30*	2118-03-29 03:49	1/1.37E6	-6.20	2110-2118
2015SG	18*	2105-08-17 08:11	1/143266	-6.21	2105
2020DK	22*	2106-02-09 05:15	1/276243	-6.21	2077-2118
2019BU1	20*	2062-01-21 18:55	1/602409	-6.21	2056-2062
2009HW67	22*	2079-04-24 14:14	1/699300	-6.21	2046-2079
1994GV	11*	2051-04-11 15:59	1/84033	-6.22	2024-2113
2017MZ8	110*	2020-10-18 20:28	1/4E8	-6.22	2020-2118
2012VS76	15*	2084-11-16 16:06	1/131406	-6.22	2081-2118
2015EO	17*	2074-09-12 08:51	1/266666	-6.22	2048-2077
2012BL14	8*	2031-01-19 16:52	1/242130	-6.22	2014-2118
2001UD5	120*	2107-10-10 03:39	1/2.08E7	-6.23	2060-2110
2005NX55	140*	2021-01-06 01:32	1/3.98E8	-6.23	2011-2117
2006BM8	30*	2113-01-21 22:58	1/645161	-6.24	2098-2118
2020AO1	60*	2049-01-13 17:17	1/1.79E7	-6.24	2049
2017QM33	10*	2084-08-25 03:58	1/93457	-6.24	2078-2107
2016GK2	10*	2096-03-26 17:37	1/42194	-6.25	2086-2118
2015XR169	6*	2062-12-13 16:24	1/22779	-6.25	2049-2118
2020HB3	30*	2118-05-05 06:14	1/735294	-6.25	2105-2118
2017TW5	14*	2072-10-18 20:25	1/211864	-6.25	2072-2115
2012VJ38	7*	2077-11-14 15:42	1/19531	-6.27	2031-2115
2017SM33	600*	2021-03-18 09:26	1/4.76E10	-6.27	2021-2043
2017YV8	12*	2099-12-19 05:43	1/62893	-6.28	2061-2117

2005TM173	60*	2048-11-16 05:08	1/4.69E6	-6.28	2008-2114
2016EM156	9*	2116-03-19 15:10	1/30211	-6.29	2108-2116
2018LH16	220*	2025-12-06 11:56	1/7.75E8	-6.29	null
2008CT1	11*	2116-02-06 09:30	1/62111	-6.29	2030-2118
2019GD4	10*	2084-02-03 22:52	1/54644	-6.30	2065-2118
2018VS6	15*	2083-11-09 08:12	1/180180	-6.30	2083-2118
2009BF58	13*	2083-01-22 05:31	1/81967	-6.31	2055-2118
2020FA1	20*	2118-09-08 08:27	1/145772	-6.32	2102-2118
2012XM16	25*	2081-12-20 01:00	1/671140	-6.32	2081-2114
2007YS56	25*	2113-12-26 15:13	1/344827	-6.33	2084-2115
2009RR	27*	2108-09-17 08:30	1/632911	-6.33	2098-2118
2001SB170	120*	2095-03-17 18:52	1/3.76E7	-6.33	2063-2101
2017UJ43	10*	2060-11-06 15:26	1/84033	-6.34	2050-2114
2012BA102	18*	2117-01-26 10:11	1/139664	-6.34	2104-2117
2011TO	20*	2064-09-27 09:27	1/411522	-6.34	2063-2099
2018VC7	12*	2049-11-12 07:15	1/149031	-6.35	2049-2118
2016CG18	7*	2062-08-07 04:22	1/30581	-6.35	2062-2118
2013HT14	20*	2077-04-16 13:35	1/793650	-6.36	2043-2095
2016AB166	50*	2108-01-13 08:04	1/4.31E6	-6.36	2106-2115
2020GB1	15*	2073-04-06 19:34	1/198412	-6.37	2049-2118
2012BU1	10*	2102-01-14 09:07	1/54347	-6.37	2071-2118
2008XU2	27*	2039-11-25 01:25	1/1.77E6	-6.37	2039
2020BY4	21*	2072-01-30 20:40	1/1.06E6	-6.37	2055-2118
2009WR52	8*	2060-11-22 13:08	1/39370	-6.38	2031-2118
2014GQ17	14*	2067-06-13 08:51	1/149253	-6.39	2052-2116
2019GK21	26*	2099-04-08 22:15	1/621118	-6.39	2099-2107
2018BD	3*	2032-01-18 12:30	1/24630	-6.40	2032-2098
2018DZ3	18*	2110-03-04 19:18	1/250000	-6.40	2068-2113
2017UP43	19*	2111-10-29 21:09	1/230414	-6.41	2110-2118
2013RS43	14*	2073-09-17 10:54	1/157480	-6.42	2073-2118
2015UR67	20*	2091-10-25 02:36	1/409836	-6.42	2091-2115
2007US51	13*	2114-11-01 16:41	1/134952	-6.42	2062-2118
2007YM	22*	2042-12-01 15:07	1/591715	-6.43	2011-2118

2019UE4	10*	2064-10-21 03:00	1/145560	-6.43	2064-2118
2016WY	5*	2097-11-11 09:56	1/9174	-6.44	2094-2118
2019VH	10*	2065-10-24 19:16	1/117096	-6.44	2057-2109
2006CD	290*	2032-07-04 15:00	1/3.76E8	-6.44	2008-2092
2018XR4	15*	2079-12-16 14:17	1/294117	-6.44	2062-2117
2014OX3	10*	2116-07-24 17:50	1/70921	-6.44	2116
2018QE	10*	2068-10-11 01:02	1/77519	-6.45	2036-2118
2018FE3	13*	2118-03-17 09:22	1/83333	-6.45	2118
2009JL2	23*	2057-05-13 16:22	1/1.07E6	-6.45	2055-2118
2020GE	8*	2089-04-27 13:19	1/36496	-6.46	2089-2118
2020JS1	19*	2022-06-21 05:56	1/1E7	-6.46	2022-2105
2013BR27	10*	2092-01-17 02:33	1/83333	-6.46	2067-2110
2011BU59	21*	2118-01-17 04:55	1/363636	-6.46	2089-2118
2011YQ1	27*	2113-12-16 02:59	1/729927	-6.46	2113
2015ET	16*	2076-03-08 02:11	1/370370	-6.46	2076-2117
2018LM	30*	2116-06-01 12:12	1/694444	-6.47	2116
2005TA	13*	2110-10-06 13:52	1/77519	-6.48	2097-2118
2016JA6	19*	2099-05-03 04:03	1/396825	-6.48	2081-2117
2011AY22	13*	2106-01-17 18:29	1/169779	-6.48	2051-2118
2014SR261	15*	2058-09-19 03:09	1/606060	-6.48	2058-2118
2020DO2	15*	2113-02-12 11:21	1/408163	-6.48	2071-2113
2008DA4	60*	2091-02-12 08:21	1/5.95E6	-6.49	2091-2100
2017SD33	400*	2085-07-21 22:58	1/1E9	-6.49	null
2006WV29	18*	2096-06-05 00:07	1/448430	-6.49	2036-2116
2017AT20	13*	2028-06-24 06:06	1/917431	-6.50	2028-2115
2017WL15	24*	2114-05-22 19:41	1/990099	-6.50	2058-2115
2007HB15	10*	2055-04-25 12:23	1/110253	-6.51	2055-2118
2011EB	15*	2070-02-27 17:20	1/294985	-6.51	2070-2077
2018EB4	29*	2099-03-16 19:26	1/1.39E6	-6.51	2099-2103
2019YM	22*	2117-12-21 04:58	1/826446	-6.51	2041-2117
2004VZ14	30*	2076-11-01 21:40	1/2.16E6	-6.52	2076-2118
2009MG1	50*	2118-06-16 06:06	1/5.88E6	-6.52	2079-2118
2017DG16	5*	2084-02-25 01:22	1/12836	-6.53	2066-2105

2006WZ184	22*	2117-11-26 05:10	1/348432	-6.53	2070-2117
2018RF5	12*	2103-09-02 13:54	1/111234	-6.53	2101-2103
2013AB65	11*	2113-01-13 10:12	1/217864	-6.53	2087-2118
2007UD6	8*	2067-10-18 22:41	1/49999	-6.54	2058-2113
2012UU158	15*	2070-10-20 05:12	1/378787	-6.54	2040-2078
2017QF3	9*	2046-02-16 12:03	1/278551	-6.54	2035-2118
2016TQ2	18*	2110-10-04 13:12	1/467289	-6.54	2110-2117
2020GO1	10*	2109-04-02 21:16	1/74626	-6.55	2064-2116
2019PG	27*	2115-07-13 19:21	1/662251	-6.55	2092-2115
2017KC36	12*	2037-05-25 04:49	1/574712	-6.55	2037-2054
2009TU	12*	2086-10-09 23:01	1/217864	-6.55	2086-2118
2010JH80	40*	2082-05-05 10:42	1/1.05E7	-6.55	2074-2095
2007UN12	6*	2098-10-19 22:21	1/17953	-6.56	2069-2118
2016RP41	110*	2022-12-22 11:38	1/3.83E8	-6.56	2019-2111
2010FD	22*	2085-03-08 17:11	1/649350	-6.56	2043-2085
2015TL21	18*	2078-10-05 19:03	1/757575	-6.56	2061-2103
2020GA3	30*	2089-04-23 05:00	1/3.45E6	-6.56	2054-2118
2009WQ25	60*	2094-10-27 14:43	1/9.9E6	-6.56	2058-2094
2019DG1	16*	2118-03-16 22:11	1/205761	-6.57	2097-2118
2017RC	9*	2115-08-30 10:08	1/66666	-6.57	2084-2118
2017FW90	8*	2118-10-03 08:56	1/35587	-6.58	2101-2118
2007EO88	18*	2110-09-19 21:23	1/358422	-6.58	2073-2117
2011QF48	30*	2067-08-26 23:59	1/4.31E6	-6.58	2067
2007EH26	50*	2117-09-16 02:44	1/6.99E6	-6.58	2109-2118
2012PB20	40*	2098-02-10 06:03	1/1.55E6	-6.59	2087-2116
2014XM7	90*	2115-12-27 13:51	1/1.99E7	-6.60	2115
2016JB29	40*	2090-06-13 03:20	1/2.96E6	-6.60	2090-2117
2011SE191	30*	2118-09-23 12:56	1/2.04E6	-6.60	2106-2118
2014WA	8*	2049-11-16 03:32	1/144717	-6.61	2049-2091
2018LF16	280*	2023-08-07 15:01	1/3.83E9	-6.62	2023-2118
2010TD	15*	2080-09-27 11:53	1/606060	-6.62	2072-2091
2019XV	5*	2100-10-30 10:39	1/14104	-6.63	2055-2117
2012EP10	5*	2096-02-21 13:06	1/14749	-6.63	2056-2118

2013PG10	10*	2064-02-10 22:05	1/145137	-6.63	2056-2116
2011YC63	6*	2034-12-30 01:31	1/185528	-6.63	2034-2048
2017AA21	21*	2028-02-06 02:10	1/5.68E6	-6.64	2020-2118
2014MB6	20*	2075-07-08 21:19	1/1.03E6	-6.64	2052-2075
2010UJ	20*	2024-11-13 14:41	1/2.01E6	-6.65	2019-2118
2014SR223	16*	2063-09-27 15:12	1/847457	-6.65	2063
2011BP40	29*	2039-03-07 14:15	1/2.84E6	-6.66	2019-2101
2019TK5	12*	2065-09-28 08:34	1/238663	-6.66	2061-2110
2020MP1	21*	2105-06-26 13:18	1/584795	-6.66	2105
2017RN16	5*	2104-09-11 21:45	1/22172	-6.66	2060-2117
2017UK3	13*	2115-10-27 15:49	1/224215	-6.66	2114-2115
2008VM	3*	2031-11-04 17:36	1/30030	-6.67	2016-2031
2010UC7	43	2118-11-06 08:56	1/3.32E6	-6.67	2104-2118
2016CH30	9*	2103-02-16 03:23	1/83333	-6.70	2100-2112
2008YV32	19*	2102-01-11 00:17	1/490196	-6.70	2085-2117
2015XP	25*	2067-12-04 01:52	1/1.65E6	-6.71	2067
2019YV1	30*	2113-12-20 06:09	1/1.43E6	-6.72	2101-2115
2017RK2	9*	2083-09-26 06:23	1/104602	-6.72	2083
2008LE	40*	2021-05-26 22:45	1/4.93E6	-6.72	2021-2111
2020FK6	9*	2081-03-12 14:47	1/153374	-6.72	2054-2118
2015DQ224	5*	2049-02-17 14:44	1/65789	-6.72	2041-2065
2019UL	6*	2112-10-09 13:39	1/26881	-6.73	2088-2117
2016XP23	400*	2110-11-01 20:15	1/1.96E9	-6.73	2110
2019AB	20*	2108-01-05 13:06	1/680272	-6.74	2073-2115
2012CL17	26*	2108-02-07 05:28	1/2.48E6	-6.74	2095-2118
2020AW	6*	2072-01-17 09:20	1/55248	-6.75	2063-2118
2019RT3	30*	2087-09-11 01:16	1/2.39E6	-6.75	2087-2118
2018RB2	12*	2102-09-06 14:36	1/206611	-6.75	2089-2118
2001HJ31	60*	2116-04-11 17:21	1/8.06E6	-6.75	2116
2017UE52	90*	2022-04-16 17:47	1/7.69E8	-6.75	2020-2117
2010JA43	478	2023-01-07 08:05	1/6.37E8	-6.75	2014-2117
2015FA345	50*	2024-03-15 17:36	1/7.35E7	-6.76	2024-2116
2008OO1	40*	2107-07-23 14:01	1/5.03E6	-6.76	2107

2017QU34	8*	2083-08-26 04:02	1/141442	-6.76	2083-2111
2010MA113	903	2068-08-02 10:34	1/1.21E10	-6.76	2068-2118
2015TG24	16*	2110-10-14 07:47	1/431034	-6.78	2102-2118
2003UQ25	50*	2093-03-17 11:59	1/1.25E7	-6.78	2093
2009HC	40*	2113-04-11 08:21	1/2.3E6	-6.79	2095-2114
2019ED1	11*	2073-03-01 10:51	1/281690	-6.79	2070-2109
2017QT1	15*	2050-01-30 17:08	1/2.18E6	-6.79	2050-2077
1997UA11	30*	2073-10-24 02:08	1/3.4E6	-6.80	2073
2017UA45	23*	2112-10-13 21:20	1/763358	-6.81	2099-2118
2020HF	30*	2110-04-16 20:33	1/2.18E6	-6.81	2067-2117
2016LG10	28*	2108-06-06 00:27	1/1.59E6	-6.81	2108-2113
2013NE24	12*	2093-07-11 14:34	1/282485	-6.81	2073-2113
2009EW	19*	2081-03-06 09:45	1/1.05E6	-6.81	2066-2082
2011CL50	11*	2059-02-16 16:36	1/220750	-6.82	2036-2119
2017SU17	9*	2093-09-24 15:43	1/119331	-6.82	2053-2118
2018FL29	3*	2026-11-20 16:39	1/153846	-6.83	2024-2118
2017UC52	50*	2067-11-28 01:39	1/1.77E7	-6.83	2067-2112
2017DA120	300*	2024-09-13 15:17	1/5.59E9	-6.83	2024-2106
2016AU193	30*	2109-12-31 16:12	1/5.03E6	-6.83	2109
2017DW119	16*	2029-01-16 07:31	1/5.41E6	-6.84	2029-2067
2012KP24	18*	2032-05-28 13:58	1/3.73E6	-6.84	2032
2007SN6	40*	2059-09-18 15:13	1/1E7	-6.84	2022-2059
2011UL169	8*	2057-10-25 16:02	1/173310	-6.85	2057-2073
2006DN	50*	2056-04-22 02:15	1/7.75E6	-6.86	2056-2098
2014AG51	4*	2072-08-27 10:36	1/30395	-6.86	2049-2113
2004BN41	25*	2116-02-12 01:36	1/1.13E6	-6.87	2086-2116
2018VT5	7*	2097-11-05 06:01	1/83333	-6.87	2085-2118
1997TC25	40*	2096-09-28 05:17	1/3.7E6	-6.87	2096-2117
2018LT5	40*	2039-12-16 09:49	1/2.91E7	-6.87	2039-2083
2016NP56	20*	2058-01-14 00:16	1/1.35E6	-6.88	2024-2112
2018LB	23*	2092-05-31 12:14	1/1.27E6	-6.88	2075-2118
2004RU109	18*	2038-09-14 06:03	1/2.31E6	-6.88	2038-2053
1993UA	29*	2111-10-21 04:58	1/1.69E6	-6.89	2111

2010RA91	70*	2104-03-24 13:22	1/2.08E7	-6.89	2104-2115
2020GZ1	14*	2040-04-01 03:35	1/1.66E7	-6.89	2040
2020HW7	13*	2044-12-06 16:44	1/1.12E6	-6.90	2044-2117
2019DX	15*	2098-03-04 18:59	1/636942	-6.90	2051-2105
2018GG4	20*	2058-04-16 09:30	1/3.57E6	-6.90	2058-2070
2015FF36	18*	2073-05-21 09:37	1/1.04E6	-6.91	2064-2117
2018YH2	90*	2038-07-14 09:39	1/1.45E8	-6.91	2031-2113
2018VP6	13*	2088-11-07 21:00	1/529100	-6.91	2087-2118
2017DC120	150*	2021-01-29 16:39	1/2.24E9	-6.91	null
2017TA5	13*	2117-10-08 13:54	1/313479	-6.92	2078-2117
2014UX34	120*	2084-10-18 20:20	1/2.74E8	-6.92	2084
2016EV84	16*	2073-03-11 13:52	1/892857	-6.93	2056-2080
2009WW7	6*	2108-11-20 01:13	1/44642	-6.93	2050-2117
2014TL	10*	2111-10-01 18:50	1/179856	-6.93	2072-2118
2015VP64	8*	2087-11-09 11:15	1/279329	-6.93	2068-2117
2010NH	26*	2092-06-30 20:24	1/2.24E6	-6.94	2089-2107
2006WM3	80*	2113-12-20 10:58	1/2.7E7	-6.94	2113
2010CA	50*	2022-08-07 07:29	1/8.13E7	-6.94	2022
2017UG52	400*	2047-06-19 07:39	1/9.09E9	-6.94	2047-2103
2013RR43	30*	2050-09-08 18:03	1/1.24E7	-6.94	2039-2057
2017BG92	6*	2072-01-17 18:04	1/81967	-6.95	2072-2118
2004DA53	9*	2111-02-25 15:03	1/139860	-6.96	2095-2117
2009YR	9*	2060-09-20 03:01	1/194931	-6.97	2060-2118
2020HN	7*	2065-03-14 19:36	1/110253	-6.97	2055-2118
2020KU	7*	2079-05-24 12:23	1/110619	-6.97	2070-2108
2018QS	20*	2084-08-13 11:10	1/1.46E6	-6.97	2084-2116
2012CU	23*	2100-02-01 19:18	1/1.67E6	-6.97	2040-2108
2017KQ27	24*	2117-06-06 13:24	1/1.77E6	-6.97	2117
2006SR131	9*	2072-09-24 18:06	1/210084	-6.98	2045-2117
2007TX22	8*	2060-10-12 06:07	1/174520	-6.98	2044-2090
2019VD	12*	2105-11-12 22:51	1/352112	-6.98	2073-2110
2015UH52	23*	2075-10-21 02:33	1/2.6E6	-6.98	2075-2115
2011UC64	9*	2093-10-24 11:59	1/271739	-6.98	2093-2118

2008BC15	17*	2094-07-22 19:34	1/1.71E6	-6.98	2072-2095
2014QN266	20*	2078-08-23 17:34	1/1.14E6	-6.99	2078-2108
2013TV132	18*	2111-10-05 01:08	1/751879	-6.99	2091-2115
2013PS13	12*	2096-08-12 09:19	1/666666	-6.99	2096-2116
2008EA9	10*	2081-12-21 06:32	1/184162	-7.00	2053-2114
2010NN	8*	2060-07-03 07:41	1/186915	-7.00	2049-2117
2017HZ4	24*	2106-05-30 23:40	1/1.49E6	-7.01	2091-2107
2018AU18	11*	2046-11-16 22:26	1/1.02E6	-7.01	2046-2116
1991BA	7*	2023-01-18 01:41	1/505050	-7.01	2014-2118
2020CQ	13*	2112-02-01 12:32	1/709219	-7.02	2051-2112
2018DN4	8*	2023-02-22 12:26	1/5.49E6	-7.02	2023
2013UR1	10*	2050-10-21 19:12	1/1.36E6	-7.05	2043-2067
2010FN	17*	2082-10-12 20:25	1/909090	-7.06	2079-2117
2014CE	14*	2112-02-03 06:56	1/675675	-7.06	2108-2118
2019QE7	16*	2097-08-24 08:01	1/961538	-7.07	2097-2116
2011YC40	4*	2028-12-27 12:17	1/185528	-7.07	2028-2050
2019KL	18*	2052-05-25 07:51	1/4.2E6	-7.07	2052-2115
2016GU2	50*	2113-04-01 22:05	1/7.41E7	-7.07	2113
2008GM2	8*	2093-04-03 06:26	1/108932	-7.08	2069-2118
2017VV12	9*	2062-11-15 21:53	1/331125	-7.08	2062-2115
2015QS8	15*	2116-08-25 06:19	1/826446	-7.08	2116
2015CL13	26*	2090-02-15 16:09	1/4.48E6	-7.08	2090-2106
2009FP32	10*	2117-04-03 11:11	1/334448	-7.08	2073-2117
2019DF2	400*	2118-01-31 23:05	1/5.03E9	-7.08	2064-2118
2018RQ4	15*	2098-11-21 02:08	1/666666	-7.09	2088-2102
2002XV90	30*	2113-12-12 01:19	1/3.33E6	-7.09	2078-2114
2009FZ4	30*	2022-09-20 06:17	1/3.22E7	-7.09	2014-2118
2015WP2	3*	2089-11-19 22:15	1/31948	-7.09	2077-2116
2018FY2	25*	2046-02-26 03:20	1/1.58E7	-7.09	2046-2102
2017RP16	13*	2065-09-08 02:38	1/990099	-7.10	2065-2112
2012BK14	11*	2061-01-12 08:04	1/253164	-7.12	2019-2116
2018HW1	24*	2108-04-21 23:53	1/1.95E6	-7.12	2105-2116
2010UR7	12*	2086-10-28 16:08	1/704225	-7.12	2079-2086

2020BH3	21*	2104-01-24 19:24	1/1.67E6	-7.13	2059-2106
2019BO	8*	2078-01-15 22:55	1/257731	-7.13	2044-2105
2007DC	11*	2059-02-07 22:48	1/602409	-7.14	2040-2117
2007EN88	18*	2104-03-13 11:47	1/1.49E6	-7.14	2068-2110
2005UL6	40*	2069-11-02 03:55	1/1.96E7	-7.14	2069-2072
2018CA15	22*	2038-02-05 16:11	1/8.13E6	-7.15	2028-2108
2019UC14	80*	2068-11-13 23:48	1/1.35E8	-7.15	2068
2017SC33	120*	2029-03-03 11:17	1/1.08E10	-7.15	2029-2084
2005TH50	9*	2077-10-02 17:54	1/238663	-7.16	2055-2097
2018BC	5*	2089-01-10 13:32	1/43478	-7.17	2083-2118
2018VC	19*	2112-10-28 22:42	1/1.18E6	-7.18	2109-2118
2016WU	12*	2109-05-16 03:48	1/456621	-7.18	2089-2115
2017RU2	25*	2093-10-02 03:45	1/3.16E6	-7.18	2093
2018EZ2	17*	2107-03-15 17:41	1/1.3E6	-7.18	2107-2118
2012BW13	13*	2095-01-27 14:37	1/763358	-7.18	2072-2118
2004XB45	20*	2035-12-18 01:58	1/8.47E6	-7.18	2035-2087
2011MD	6	2113-06-05 07:51	1/158227	-7.19	2106-2118
2018PU23	8*	2097-06-13 10:26	1/168634	-7.19	2072-2118
2002EM7	50*	2117-03-09 06:30	1/1.19E7	-7.19	2105-2117
2018WJ	10*	2045-11-17 22:12	1/2.44E6	-7.19	2045-2075
2016FZ13	8*	2109-03-23 09:00	1/129533	-7.20	2108-2117
2019GS19	27*	2102-04-12 21:22	1/5.65E6	-7.20	2089-2102
2001YN2	40*	2079-12-16 04:55	1/1.69E7	-7.20	2020-2091
2007EZ25	28*	2097-03-04 05:11	1/9.01E6	-7.21	2063-2097
2019CZ1	50*	2115-01-24 16:13	1/3.66E7	-7.21	2114-2115
2014HJ198	18*	2034-04-21 14:34	1/1.63E7	-7.21	2034-2111
2017TB	5*	2095-10-03 14:38	1/72992	-7.22	2053-2118
2009TB	5*	2029-09-30 06:58	1/224719	-7.22	2014-2112
2019CJ4	29*	2116-08-19 23:04	1/4.81E6	-7.22	2075-2116
2007CS5	40*	2108-07-22 16:12	1/9.01E6	-7.23	2094-2117
2003DW10	21*	2046-03-02 09:04	1/4.39E6	-7.23	2046-2068
2007UT3	25*	2075-08-29 00:09	1/4.69E6	-7.23	2054-2103
2004FU162	7*	2029-03-31 20:44	1/970873	-7.23	2019-2118

2013BR15	30*	2100-01-02 18:01	1/1.01E7	-7.23	2090-2110
2006UQ216	12*	2102-02-15 06:17	1/448430	-7.25	2064-2115
2008WO2	4*	2092-11-18 23:20	1/36231	-7.25	2065-2116
2013XU21	21*	2055-12-12 18:16	1/5.41E6	-7.25	2055
2013YB	1.8*	2023-12-24 03:04	1/63291	-7.26	2022-2063
2013VD17	13*	2117-11-12 16:15	1/840336	-7.26	2075-2117
2018WH1	7*	2080-11-22 22:29	1/176056	-7.27	2076-2111
2019NP5	11*	2116-06-26 21:53	1/331125	-7.27	2106-2116
2018WH	4*	2053-11-16 05:30	1/89285	-7.27	2053-2118
2010TN55	14*	2111-10-12 22:54	1/2.26E6	-7.27	2062-2117
2012TU231	20*	2111-10-13 20:50	1/2.27E6	-7.28	2111-2117
2016SU2	10*	2110-09-26 15:30	1/549450	-7.28	2102-2118
2006UC64	40*	2085-04-18 18:27	1/2.15E7	-7.28	2069-2102
2014CH13	50*	2100-07-06 05:50	1/1.58E7	-7.29	2024-2116
2006BF56	4*	2106-01-28 16:08	1/152439	-7.29	2092-2118
2017WE28	16*	2039-11-23 21:29	1/5.29E6	-7.30	2038-2086
2019MT2	18*	2109-07-07 03:59	1/2.12E6	-7.30	2079-2110
2010HP20	11*	2063-04-18 14:41	1/201612	-7.32	2021-2118
2014FE	11*	2064-03-17 19:12	1/2.07E6	-7.32	2034-2081
2019QU3	6*	2060-08-09 06:42	1/290697	-7.33	2060-2117
2008XC1	70*	2111-12-18 12:13	1/4.59E7	-7.33	2085-2111
2008UA202	5*	2066-10-12 01:48	1/78125	-7.34	2042-2118
2018MC5	30*	2111-08-21 05:14	1/4.98E6	-7.34	2111-2116
2010DG77	315	2052-01-11 00:03	1/3.29E9	-7.34	2024-2117
2006GU2	10*	2084-10-09 18:19	1/485436	-7.35	2022-2117
2017MD1	40*	2068-02-07 09:50	1/2.75E7	-7.35	2067-2103
2020CF2	11*	2108-02-11 22:31	1/440528	-7.37	2096-2117
2019TC2	10*	2113-10-01 04:41	1/500000	-7.37	2097-2118
2012SU9	13*	2111-01-11 14:05	1/1E6	-7.38	2082-2111
2008EM68	11*	2026-03-12 05:27	1/3.29E6	-7.38	2013-2118
2005UA1	19*	2036-10-19 18:39	1/1.06E7	-7.38	2036-2066
2015BY3	11*	2033-07-11 01:09	1/5.81E6	-7.38	2033-2085
2020BH	8*	2114-01-01 22:00	1/205338	-7.39	2104-2117

2005BS1	12*	2024-01-14 10:34	1/5.41E6	-7.40	2016-2041
2003WT153	9*	2048-08-30 22:21	1/609756	-7.41	2044-2113
2015VK1	18*	2103-11-01 22:52	1/3.57E6	-7.41	2077-2111
2016VA18	7*	2022-08-02 09:17	1/5.62E6	-7.42	2020-2118
2018LR3	20*	2096-06-17 23:59	1/2.44E6	-7.42	2077-2118
2006HE2	18*	2081-10-06 10:13	1/2.07E6	-7.42	2069-2115
2020CK2	5*	2073-02-08 06:53	1/141043	-7.42	2057-2118
2016TC57	14*	2112-10-14 09:42	1/1.14E6	-7.42	2112
2008BN16	23*	2083-01-21 22:34	1/1.07E7	-7.42	2067-2085
2008CJ	12*	2106-02-02 01:49	1/740740	-7.43	2033-2106
2018YW2	50*	2069-01-17 23:02	1/5.56E7	-7.43	2069
2008UA92	12*	2078-11-01 17:51	1/1.18E6	-7.43	2078
2019GF3	50*	2099-03-23 14:41	1/1.28E8	-7.43	2093-2099
2017OO1	40*	2115-07-22 15:16	1/2.09E7	-7.44	2115-2118
2008SH148	21*	2049-10-17 03:40	1/9.17E6	-7.44	2011-2118
2018LV3	17*	2061-06-13 23:15	1/5.56E6	-7.44	2061
2011FA23	6*	2063-03-31 07:05	1/414937	-7.44	2025-2110
2016WN7	9*	2095-11-22 02:53	1/500000	-7.45	2095-2118
2004XG29	30*	2112-12-12 22:35	1/5.65E6	-7.46	2089-2117
2015YM1	7*	2096-06-16 15:49	1/306748	-7.46	2096-2117
2014JV79	30*	2022-11-14 08:01	1/1.33E8	-7.46	2020-2113
2015GB1	17*	2052-04-17 06:46	1/5.08E6	-7.47	2031-2109
2007VH189	80*	2042-06-05 12:04	1/3.75E8	-7.47	2013-2045
2018FK5	8*	2087-10-03 05:24	1/558659	-7.48	2080-2110
2011SE58	11*	2055-09-27 16:09	1/2.43E6	-7.48	2042-2063
2009WJ6	11*	2049-11-20 12:42	1/3.16E6	-7.48	2049-2056
2010RM80	9*	2108-09-05 17:02	1/390625	-7.49	2090-2118
2009TM8	7*	2099-10-18 16:55	1/255754	-7.49	2079-2118
2008HC38	21*	2029-04-23 02:40	1/2.6E7	-7.49	2029
2018JL1	16*	2114-05-15 15:39	1/1.61E6	-7.50	2112-2114
2010VN1	8*	2054-11-02 23:15	1/862068	-7.50	2046-2066
2001SD286	30*	2080-09-23 05:15	1/1.52E7	-7.51	2080
2014HE199	30*	2039-04-13 21:43	1/7.09E7	-7.51	2030-2092

2018FQ3	7*	2114-03-20 06:13	1/302114	-7.52	2070-2118
2006UJ185	9*	2116-11-01 16:34	1/787401	-7.52	2049-2116
2018RR1	4*	2103-09-07 03:06	1/49019	-7.53	2083-2117
2019FU1	12*	2098-03-26 10:39	1/2.66E6	-7.53	2090-2106
2018EV3	13*	2081-03-05 06:09	1/2.7E6	-7.54	2081-2116
2018BP6	40*	2074-02-03 04:18	1/6.02E7	-7.54	2074-2115
2011AE3	15*	2058-01-03 02:11	1/2.26E6	-7.55	2018-2117
2016EG28	10*	2099-03-04 16:05	1/1.18E6	-7.55	2079-2113
2012HE31	23*	2094-09-12 23:38	1/6.71E6	-7.56	2046-2117
2009MU	40*	2099-06-24 01:15	1/3.69E7	-7.56	2096-2109
2017FO128	110*	2111-03-16 12:32	1/3.98E8	-7.56	2111
2016DK2	6*	2069-02-21 08:33	1/598802	-7.56	2069
2016UB26	40*	2066-03-14 10:42	1/6.02E7	-7.56	2066
2015VO142	6*	2078-12-06 13:16	1/207468	-7.57	2046-2118
2018XX2	21*	2106-12-09 16:39	1/6.33E6	-7.57	2106
2012CR	160*	2025-05-20 19:06	1/6.45E9	-7.58	2025
2013QM48	12*	2097-08-23 13:44	1/1.15E6	-7.58	2096-2118
2019NK1	4*	2114-07-03 19:09	1/64935	-7.58	2089-2118
2017SS12	13*	2089-09-24 18:24	1/2.19E6	-7.58	2071-2113
2016TT	22*	2095-09-27 05:50	1/7.58E6	-7.58	2083-2096
2006QK33	70*	2116-08-23 04:13	1/8.62E7	-7.58	2116
2019PO1	9*	2116-08-08 16:41	1/438596	-7.59	2085-2118
2000SZ162	13*	2070-06-22 13:52	1/1.41E6	-7.59	2070-2118
2004FY3	30*	2116-03-19 14:53	1/1.52E7	-7.59	2083-2116
2012XL55	14*	2025-12-08 23:46	1/2.42E7	-7.59	2025-2052
2019FB1	10*	2113-04-02 22:09	1/769230	-7.60	2110-2117
2017DB120	90*	2061-03-26 07:42	1/3.39E8	-7.60	2039-2065
2017HJ	11*	2092-04-16 04:47	1/2.14E6	-7.60	2070-2118
2019SG1	10*	2064-09-25 05:37	1/3.12E6	-7.60	2064
2015FH37	40*	2115-03-30 12:29	1/3.76E7	-7.60	2114-2115
2019WU	14*	2108-12-05 05:38	1/2.01E6	-7.61	2069-2112
2011UR63	25*	2110-10-19 04:08	1/9.8E6	-7.61	2110
2016PR66	80*	2026-05-11 10:19	1/1.07E9	-7.62	2026-2111

2008VL	11*	2085-10-28 18:45	1/990099	-7.62	2025-2118
2019NL4	21*	2074-07-06 08:23	1/1.32E7	-7.62	2074
2014WE6	3*	2104-11-07 08:44	1/41841	-7.63	2104-2118
2014HY198	4*	2065-05-06 14:00	1/166666	-7.63	2041-2118
2011EL40	18*	2073-03-06 05:18	1/9.52E6	-7.63	2073-2095
2016NJ56	40*	2036-12-17 15:06	1/6.13E7	-7.64	2036-2057
2008KT	8*	2098-11-18 21:14	1/409836	-7.65	2092-2117
2008VS4	50*	2030-01-01 02:10	1/1.47E8	-7.65	2014-2100
2019AF14	200*	2028-06-10 08:17	1/1.09E10	-7.65	null
2014HV2	23*	2116-04-29 06:59	1/8.2E6	-7.66	2095-2116
2014HB177	8*	2085-05-03 22:38	1/584795	-7.67	2059-2103
2015HO182	19*	2046-04-10 22:48	1/1.42E7	-7.67	2046-2113
2016DY30	2.8*	2036-02-26 00:13	1/338983	-7.67	2036-2118
2005GQ33	60*	2081-10-25 08:28	1/2.55E8	-7.67	2017-2118
2015HQ182	40*	2020-11-12 13:02	1/2.9E8	-7.68	2015-2118
1993HP1	14*	2065-04-26 15:40	1/3.42E6	-7.68	2065-2112
2015EG7	12*	2093-03-23 07:39	1/2.45E6	-7.68	2090-2118
2016WR55	8*	2115-11-29 07:49	1/719424	-7.68	2092-2115
2016FC1	5*	2082-03-11 08:31	1/495049	-7.69	2082-2088
2019NX5	5*	2069-06-23 00:07	1/294117	-7.70	2069-2118
2016JO38	40*	2112-09-24 01:58	1/3.34E7	-7.70	2112
2017DP109	15*	2086-03-02 03:50	1/4.61E6	-7.70	2057-2086
2018WE	8*	2057-11-20 08:57	1/1.69E6	-7.70	2057-2106
2009WZ53	50*	2084-05-22 14:10	1/1.52E8	-7.70	2020-2109
2018EL4	30*	2110-03-08 19:06	1/1.41E7	-7.72	2102-2115
2004ME6	110*	2071-07-12 00:58	1/5.43E8	-7.72	2040-2105
2019KT	17*	2110-05-29 17:33	1/5.18E6	-7.73	2110
2010XB73	140*	2037-06-01 17:01	1/1.08E9	-7.74	2023-2038
2016TQ54	12*	2096-10-02 20:57	1/2.23E6	-7.74	2082-2118
2016VF18	4*	2077-10-20 06:58	1/205338	-7.75	2031-2077
2017YM14	10*	2074-12-25 14:56	1/3.66E6	-7.75	2056-2074
2018WA3	9*	2055-11-28 19:29	1/4.35E6	-7.76	2055-2060
2020DG4	8*	2094-02-18 10:05	1/847457	-7.78	2094-2118

2015VN64	11*	2088-11-03 17:21	1/3.29E6	-7.78	2086-2096
2019CM5	9*	2099-02-02 02:54	1/1.02E6	-7.79	2065-2115
2018TS6	8*	2104-10-03 01:21	1/757575	-7.79	2068-2115
2010CK19	9*	2116-08-19 13:25	1/757575	-7.80	2089-2116
2014KS76	17*	2089-05-18 00:13	1/5.18E6	-7.80	2089-2114
2019TD	5*	2060-09-29 07:48	1/636942	-7.80	2042-2060
2003YS70	6*	2110-01-11 06:36	1/256410	-7.81	2052-2117
2018ST1	30*	2090-09-30 23:48	1/3.64E7	-7.81	2090
2019VE4	9*	2112-10-29 21:06	1/1.11E6	-7.82	2068-2116
2016JN38	5*	2072-04-30 14:14	1/1.06E6	-7.82	2039-2118
2014HJ197	3*	2050-04-20 13:45	1/156250	-7.83	2045-2118
2017WE29	30*	2051-08-22 07:58	1/3.32E7	-7.83	2034-2117
2004FM4	40*	2116-03-22 10:26	1/6.13E7	-7.83	2116
2018PA25	40*	2032-02-02 18:26	1/3.45E8	-7.84	2029-2112
2020AC1	7*	2117-01-02 03:00	1/581395	-7.85	2093-2117
2019BB5	16*	2109-02-12 15:46	1/4.33E6	-7.85	2109
2018RJ3	10*	2070-09-08 03:17	1/2.26E6	-7.85	2070
2016BE	70*	2117-02-04 08:14	1/1.44E8	-7.85	2117
2017KH5	11*	2067-05-26 09:49	1/5.03E6	-7.85	2067-2074
2018BH1	30*	2095-09-15 22:16	1/4.61E7	-7.86	2066-2095
2007EE126	28*	2092-07-24 22:42	1/7.19E7	-7.86	2065-2092
2013NR13	25*	2114-07-14 21:48	1/1.55E7	-7.87	2114
2011CF22	2.4*	2094-02-07 01:09	1/106157	-7.87	2031-2118
2013CY	8*	2098-11-29 14:15	1/740740	-7.88	2058-2116
2019UB8	6*	2057-10-30 11:31	1/1.1E6	-7.88	2053-2118
2006DO62	7*	2053-02-21 23:50	1/1.87E6	-7.88	2050-2112
2019WV1	8*	2111-11-22 14:30	1/934579	-7.89	2078-2117
2007VJ3	40*	2112-10-29 03:35	1/5.65E7	-7.89	2112
2016GS134	10*	2070-03-31 14:14	1/3.3E6	-7.90	2054-2101
2017KB3	30*	2117-11-22 06:59	1/3.32E7	-7.90	2084-2117
2010VO139	18*	2065-11-11 06:46	1/2.31E7	-7.90	2022-2117
2017RX17	19*	2085-09-05 19:38	1/1.99E7	-7.91	2040-2108
2019BX1	8*	2085-01-09 15:06	1/1.18E6	-7.92	2085-2115

2014UY57	13*	2090-10-15 02:33	1/4E6	-7.92	2072-2097
2019GP21	4*	2039-04-01 03:26	1/1.03E6	-7.92	2039-2118
2009WQ52	8*	2037-11-19 14:47	1/5.46E6	-7.92	2037
2014LJ	7*	2069-05-18 13:31	1/943396	-7.93	2055-2118
2009VT1	4*	2046-10-19 08:18	1/534759	-7.93	2046-2118
2017XY2	13*	2108-06-13 08:04	1/3.39E6	-7.93	2108
2020CW	1.1*	2046-02-01 02:57	1/68027	-7.93	2046-2076
2020NY	21*	2090-07-09 22:45	1/1.49E7	-7.93	2080-2090
2015DD54	29*	2116-03-04 10:11	1/1.93E7	-7.95	2114-2116
2008TS10	6*	2078-09-21 08:53	1/591715	-7.96	2068-2118
2016WT	4*	2117-11-19 07:29	1/224719	-7.96	2070-2117
2005UC3	13*	2109-10-05 05:46	1/3.41E6	-7.97	2068-2118
2015KH160	18*	2087-10-08 20:12	1/4.29E7	-7.97	2087-2117
2017RJ2	11*	2108-09-17 22:34	1/4.52E6	-7.98	2099-2118
2019VB5	1.6*	2053-05-14 20:10	1/57142	-7.99	2052-2116
2015HE1	14*	2098-04-21 07:57	1/7.81E6	-7.99	2098-2117
2016HF3	40*	2078-05-19 21:36	1/8E7	-8.00	2078
2019QB1	11*	2032-08-19 19:29	1/2.28E7	-8.00	2032-2053
2005CM7	21*	2032-08-11 02:01	1/8E7	-8.00	2028-2118
2016FV7	80*	2083-03-30 18:59	1/1.93E9	-8.00	2083
2013XS21	5*	2079-12-12 11:11	1/454545	-8.01	2076-2111
2011EM40	9*	2054-09-12 21:13	1/4.03E6	-8.01	2054-2118
2017UL5	19*	2116-10-24 08:41	1/8.62E6	-8.02	2100-2116
2020GY2	70*	2093-05-03 08:12	1/4.12E8	-8.02	2093
2018CN	18*	2082-02-07 23:47	1/2.87E7	-8.02	2082
2017UF	9*	2082-10-16 07:38	1/6.99E6	-8.02	2066-2082
2008CM74	9*	2100-07-17 13:08	1/1.21E6	-8.03	2075-2109
2007FP3	7*	2106-03-16 04:52	1/1.07E6	-8.03	2050-2118
2015VL64	8*	2097-11-02 16:39	1/1.46E6	-8.05	2081-2118
2005VP	27*	2053-11-01 05:30	1/6.25E7	-8.05	2053-2094
2016UQ36	10*	2041-10-24 15:42	1/9.9E6	-8.05	2041-2050
2016WF7	6*	2113-11-21 06:10	1/657894	-8.06	2102-2113
2016FE15	6*	2068-03-28 04:49	1/1.81E6	-8.07	2066-2116

2017WY27	9*	2116-11-25 19:31	1/1.94E6	-8.08	2068-2118
2008KN11	80*	2045-06-20 09:45	1/1.29E9	-8.08	2045
2018GD2	5*	2111-10-16 18:10	1/357142	-8.09	2094-2118
2018FG1	12*	2107-03-22 16:38	1/4.57E6	-8.09	2075-2117
2013GW38	7*	2098-04-07 10:52	1/1.42E6	-8.09	2070-2113
2017UK52	14*	2027-04-30 13:54	1/1.31E8	-8.09	2022-2118
2014HD198	4*	2025-05-02 07:51	1/3.69E6	-8.09	2018-2118
2009ST171	15*	2066-09-30 03:45	1/1.11E7	-8.10	2066
2019TN5	7*	2041-09-30 18:22	1/6.54E6	-8.10	2041
2010YD	26	2052-03-05 01:48	1/2.26E7	-8.12	2052-2091
2015FU344	2.3*	2066-03-16 10:58	1/158478	-8.13	2066-2110
2007WT3	50*	2101-11-08 01:26	1/3.25E8	-8.13	2101-2105
2015PS228	6*	2080-03-11 08:31	1/787401	-8.14	2080-2110
2017BE30	20*	2100-01-22 14:28	1/2.81E7	-8.14	2100
2019QS	40*	2096-02-20 20:57	1/2.06E8	-8.14	2096
2014KC45	5*	2066-05-26 23:27	1/869565	-8.15	2066-2118
2020DN3	15*	2107-02-25 02:48	1/1.22E7	-8.15	2104-2117
2018GN	20*	2109-09-28 15:29	1/3.79E7	-8.15	2109
2017UL6	1.4*	2069-10-27 10:32	1/42372	-8.16	2062-2114
2017UW5	6*	2081-10-11 00:14	1/2.01E6	-8.16	2081-2115
2020GV2	15*	2078-04-10 02:23	1/1.95E7	-8.16	2062-2078
2016XL23	5*	2080-11-29 13:47	1/917431	-8.18	2080-2098
2017TU1	21*	2104-08-05 07:12	1/2.38E7	-8.19	2104-2116
2014EU	10*	2101-12-10 22:38	1/2.93E6	-8.20	2083-2111
2016EL1	10*	2087-09-06 12:00	1/8.26E6	-8.20	2037-2109
2014WC201	21*	2102-12-05 16:16	1/2.59E7	-8.21	2102-2117
2019LA2	16*	2109-12-04 18:16	1/1.71E7	-8.21	2109-2116
2020FG	9*	2107-03-22 19:36	1/4.57E6	-8.21	2093-2118
2009QR	12*	2042-08-24 08:12	1/1.22E7	-8.22	2042-2115
2016JG38	50*	2055-10-23 21:20	1/3.69E9	-8.22	2055-2109
2019YA3	18*	2095-04-22 13:06	1/1.82E7	-8.23	2095-2103
2020FU2	7*	2098-03-20 15:24	1/2.1E6	-8.23	2098-2115
2014KW76	9*	2115-05-29 14:38	1/3.66E6	-8.23	2081-2116

2019RQ2	29*	2105-01-11 23:25	1/7.41E7	-8.23	2105
2018WA1	3*	2101-11-06 16:35	1/229885	-8.24	2061-2118
2010XU	30*	2116-11-14 18:09	1/3.8E7	-8.24	2074-2116
2015JC1	14*	2094-05-12 05:04	1/1.37E7	-8.24	2070-2102
2016TG94	4*	2114-10-10 07:38	1/429184	-8.25	2096-2118
2019SO6	26*	2109-02-08 05:24	1/1.32E8	-8.26	2077-2109
2014QJ365	11*	2118-08-27 01:47	1/5.95E6	-8.27	2095-2118
2011CF66	12*	2092-02-19 00:40	1/5.41E6	-8.27	2023-2118
2012WR10	7*	2087-09-02 20:07	1/1.5E6	-8.28	2081-2115
2015SK7	6*	2100-09-21 18:22	1/1.66E6	-8.28	2059-2112
2017FB102	15*	2054-03-20 02:37	1/2.94E7	-8.30	2054-2113
2014OP2	5*	2071-07-25 14:31	1/2E6	-8.31	2071-2079
2010GV23	11*	2096-04-06 02:10	1/4.26E6	-8.32	2096-2118
2010RK53	10*	2029-09-08 16:31	1/1.88E7	-8.32	2024-2029
2017VF14	7*	2093-11-13 16:45	1/2.88E6	-8.32	2080-2099
2020KS	25*	2090-11-29 23:12	1/4.5E7	-8.33	2055-2104
2017FW158	8*	2104-11-22 19:25	1/3.68E6	-8.33	2063-2117
2020AR1	13*	2072-01-08 11:59	1/1.51E7	-8.34	2072-2089
2015FC345	10*	2111-07-16 18:01	1/3.86E6	-8.35	2074-2117
2010XQ	30*	2036-12-04 21:55	1/4.46E8	-8.35	2034-2104
2012UE	7*	2053-10-20 13:58	1/6.62E6	-8.35	2040-2066
2016FA14	12*	2072-03-28 22:48	1/1.91E7	-8.35	2072-2082
2020BY1	19*	2049-01-16 10:26	1/1.14E8	-8.35	2049
2016BQ15	30*	2098-02-06 12:17	1/2.12E8	-8.35	2072-2098
2019VA	8*	2090-11-02 23:40	1/3.11E6	-8.37	2090-2112
2017UQ7	30*	2096-10-22 18:06	1/1.42E8	-8.37	2096
2020FD	10*	2043-03-19 00:35	1/3.42E7	-8.37	2027-2106
2012DY13	9*	2074-08-23 21:01	1/1.04E7	-8.37	2074-2116
2016TH	5*	2081-03-31 09:32	1/1.01E6	-8.38	2072-2118
2017YE8	28*	2112-12-25 17:59	1/8.4E7	-8.38	2112-2117
2019EH1	3*	2064-08-21 03:58	1/1.1E6	-8.38	2046-2118
2018BX5	6*	2113-01-16 03:20	1/1.15E6	-8.39	2087-2117
2014WR362	12*	2078-11-21 07:31	1/1.56E7	-8.39	2078

2019DM1	9*	2088-02-27 11:54	1/8.62E6	-8.39	2072-2091
2019YV4	12*	2049-12-25 08:38	1/5.05E7	-8.39	2049-2062
2015XH55	5*	2092-12-01 23:21	1/1.1E6	-8.40	2092-2118
2020HV5	25*	2037-06-12 20:12	1/1.83E8	-8.41	2037-2105
2004OD4	15*	2100-07-17 00:29	1/1.25E7	-8.41	2100-2116
2017WF30	18*	2028-02-21 18:32	1/1.68E8	-8.42	2024-2116
2017TD6	13*	2106-10-21 00:09	1/1.08E7	-8.42	2081-2106
2019QF	9*	2069-08-23 09:00	1/9.71E6	-8.42	2062-2118
2019JZ2	16*	2041-05-04 03:50	1/1.56E8	-8.43	2041
2019JK	9*	2053-04-29 12:53	1/2.17E7	-8.44	2053
2006BO7	5*	2067-05-31 02:24	1/1.7E6	-8.45	2060-2083
2013UJ5	9*	2061-08-07 03:49	1/1.03E7	-8.46	2055-2061
2014DK10	10*	2099-02-21 11:41	1/8.26E6	-8.46	2073-2118
2019DF	4*	2059-02-25 15:22	1/1.64E6	-8.46	2051-2110
2006YE	12*	2074-01-15 00:52	1/1.14E7	-8.47	2065-2106
2019WH4	6*	2113-11-26 23:50	1/9.01E6	-8.47	2113
2018BQ6	12*	2044-02-01 15:00	1/3.4E7	-8.47	2044-2059
2010UE	4*	2032-10-14 10:49	1/5.78E6	-8.47	2032-2044
2011AZ36	40*	2081-02-18 16:05	1/2.65E8	-8.48	2049-2108
2017UM52	5*	2057-04-16 11:11	1/1.51E6	-8.48	2056-2116
2007BB	10*	2076-01-17 04:11	1/6.13E6	-8.49	2076-2085
2018DU1	10*	2078-03-02 16:22	1/8.93E6	-8.50	2078-2113
2011UA64	14*	2113-10-20 06:09	1/1.99E7	-8.50	2113
2016EP84	12*	2088-01-29 20:43	1/8.93E6	-8.51	2084-2111
2003UM3	9*	2086-10-13 02:07	1/7.63E6	-8.51	2026-2117
2015FN36	60*	2117-03-16 03:56	1/1.01E9	-8.51	2117
2018LD1	19*	2112-09-19 09:27	1/3.46E7	-8.52	2112
2016AZ193	17*	2038-01-05 22:36	1/8.62E7	-8.52	2024-2094
2012TP20	10*	2069-10-02 08:59	1/9.26E6	-8.53	2064-2117
2012RU16	27*	2077-07-20 19:58	1/1.06E8	-8.53	2077-2118
2008US	1.9*	2026-04-17 23:56	1/1.3E6	-8.53	2010-2087
2018BP3	6*	2115-01-24 02:33	1/2.09E6	-8.54	2099-2115
2020HN3	4*	2118-10-22 06:19	1/684931	-8.55	2080-2118

2014MG68	90*	2060-11-02 03:58	1/6.45E9	-8.55	2060
2015HD1	12*	2047-04-21 05:15	1/5.24E7	-8.55	2047-2060
2009XQ2	30*	2031-12-17 04:09	1/7.94E9	-8.57	2031-2083
2011FQ16	11*	2114-03-27 04:11	1/7.58E6	-8.59	2066-2114
2008CB6	14*	2103-04-28 17:57	1/1.54E7	-8.60	2087-2106
2007VD8	9*	2086-11-03 01:15	1/1.29E7	-8.60	2028-2096
2019KY3	17*	2104-06-01 23:01	1/5.71E7	-8.61	2104
2019BV2	28*	2102-08-05 03:17	1/1.81E8	-8.62	2102
2018DB	11*	2088-08-06 13:31	1/2.23E7	-8.63	2068-2109
2020FM1	5*	2109-03-17 17:54	1/1.44E6	-8.64	2089-2115
2017VC14	8*	2111-11-17 19:08	1/5.71E6	-8.65	2075-2112
2008EL68	10*	2061-03-07 08:41	1/1.09E7	-8.66	2024-2114
2019JY2	4*	2059-11-08 21:40	1/2.6E6	-8.66	2059-2118
2008UY91	60*	2037-04-24 08:02	1/1.52E9	-8.66	2014-2106
2017JB2	5*	2095-04-28 08:50	1/1.96E6	-8.69	2092-2103
2012BN123	80*	2074-01-02 02:34	1/1.7E9	-8.70	2074
2004XO63	22*	2065-12-15 00:04	1/9.62E7	-8.70	2065
2017FX158	6*	2118-03-20 08:33	1/2.37E6	-8.70	2118
2020KD1	9*	2042-05-23 08:23	1/3.45E7	-8.70	2042-2061
2009XR1	5*	2038-01-24 00:56	1/5.41E6	-8.71	2033-2088
2020KU2	24*	2105-10-15 21:04	1/1.4E8	-8.71	2105
2013VJ13	60*	2099-10-30 09:27	1/1.6E9	-8.71	2099
2016TM	11*	2093-06-10 22:08	1/1.33E7	-8.72	2093-2111
2009EJ1	8*	2039-11-09 05:56	1/2.22E7	-8.72	2037-2118
2019QD	6*	2112-08-21 17:05	1/5.56E6	-8.73	2095-2112
2018XX3	4*	2088-12-10 14:21	1/1.3E6	-8.74	2088-2103
2019JX1	5*	2100-05-02 20:20	1/4.22E6	-8.74	2100-2104
2007XB23	14*	2045-12-11 12:03	1/4.78E7	-8.76	2045
2019JH7	4*	2114-05-17 11:02	1/1.48E6	-8.78	2114-2118
2016VZ17	11*	2030-08-19 22:34	1/1.64E8	-8.80	2027-2118
2006WV	13*	2101-11-23 08:25	1/3.92E7	-8.80	2091-2110
2017SA21	8*	2056-09-27 16:06	1/1.9E7	-8.82	2056
2018WG2	3*	2103-05-21 13:08	1/952380	-8.85	2077-2115

2012GD	15*	2058-06-12 03:09	1/7.46E7	-8.85	2036-2106
2008UM1	1.6*	2021-10-22 06:43	1/3.47E6	-8.85	2011-2073
2017YE7	7*	2022-12-30 21:04	1/2.57E8	-8.85	2022
2020KJ4	4*	2106-05-27 02:38	1/1.13E6	-8.87	2096-2106
2016JA	11*	2118-09-27 09:19	1/1.66E7	-8.87	2074-2118
2018XW3	19*	2098-12-08 12:32	1/1.08E8	-8.88	2042-2098
2018CK	18*	2072-01-31 09:16	1/1.69E8	-8.88	2083-2088
2016LE10	14*	2072-06-06 18:46	1/7.25E7	-8.89	2072
2011AZ22	7*	2095-01-09 18:10	1/8.93E6	-8.90	2034-2110
2020BA13	6*	2101-01-27 18:01	1/6.13E6	-8.91	2062-2105
2010VR139	17*	2021-10-06 14:20	1/4.65E8	-8.92	2012-2068
2018LE1	10*	2102-05-26 20:54	1/1.62E7	-8.92	2102-2112
2009SD15	15*	2081-09-14 22:42	1/8.62E7	-8.92	2081-2105
2009VZ39	8*	2053-01-30 21:23	1/2.71E7	-8.93	2016-2118
2016NC56	14*	2114-07-08 11:30	1/5.1E7	-8.93	2114
2010UZ7	40*	2111-10-17 17:25	1/8.55E8	-8.96	2111
2016AQ164	4*	2035-01-10 07:48	1/1.32E7	-8.98	2035
2019AK12	11*	2113-01-14 03:50	1/4.22E7	-8.98	2113
2019UX12	6*	2108-10-26 18:01	1/7.46E6	-8.99	2107-2108
2019UN8	4*	2105-05-30 02:04	1/5.05E6	-8.99	2093-2114
2008JD33	30*	2030-02-21 05:25	1/9.43E7	-9.00	2011-2117
2012CS46	10*	2106-02-27 10:24	1/1.86E7	-9.00	2106-2116
2011AD3	18*	2035-01-06 13:05	1/4.2E8	-9.01	2032-2116
2015HE183	8*	2090-04-20 05:33	1/2.21E7	-9.02	2090
2019ED	15*	2104-04-05 05:17	1/4.42E7	-9.03	2104
2016UR36	11*	2107-04-08 03:19	1/5.46E7	-9.03	2097-2116
2016YY	29*	2101-12-11 10:32	1/5.15E8	-9.04	2101
2020BY11	9*	2114-01-25 07:13	1/2.26E7	-9.05	2114-2118
2017UQ6	13*	2109-01-18 09:59	1/3.46E7	-9.07	2109-2117
2010XC	6*	2049-11-27 22:16	1/1.33E8	-9.08	2049
2017YK14	7*	2022-12-19 22:52	1/8.55E9	-9.09	2022-2096
2012BP123	13*	2021-09-02 11:05	1/4.93E8	-9.12	2021-2110
2019SE11	24*	2053-09-19 12:39	1/8.7E8	-9.12	2042-2092

2020DM3	20*	2109-07-03 04:54	1/2.85E8	-9.12	2109
2008JL24	4*	2093-01-03 17:02	1/2.94E6	-9.13	2083-2116
2007VF189	8*	2077-11-14 00:01	1/2.37E7	-9.14	2072-2081
2019TP5	30*	2078-10-17 02:59	1/1.74E9	-9.14	2078
2020HY8	100*	2073-04-20 07:08	1/3.03E10	-9.14	2073
2019SQ8	80*	2094-04-20 22:00	1/1E10	-9.15	2094
2020MA1	29*	2097-07-07 06:52	1/3.47E8	-9.16	2097
2008XK	13*	2056-12-01 04:08	1/1.87E8	-9.16	2026-2092
2008YD3	21*	2022-01-27 08:48	1/1.65E9	-9.17	2022-2068
2013EC20	6*	2112-03-08 15:48	1/5.26E6	-9.18	2075-2112
2018KY2	13*	2115-05-27 03:04	1/1.04E8	-9.18	2075-2115
2011CA7	3*	2062-02-19 17:27	1/3.46E6	-9.19	2062-2097
2009EH1	10*	2056-03-09 22:34	1/6.58E7	-9.19	2056
2010XP	18*	2064-12-06 10:24	1/1.68E8	-9.20	2047-2115
2019FT1	14*	2113-03-24 02:28	1/8.47E7	-9.21	2104-2113
2014HM199	50*	2070-04-08 17:04	1/3.58E9	-9.24	2070
2014HK197	17*	2062-09-07 04:24	1/8.77E8	-9.27	2062-2097
2014HN2	19*	2082-03-23 00:40	1/1.83E8	-9.28	2082-2117
2008VB4	8*	2038-09-05 05:00	1/1.36E8	-9.29	2011-2102
1993KA2	6*	2060-11-10 00:23	1/3.73E7	-9.30	2060-2084
2008UC202	8*	2116-04-26 14:47	1/1.59E7	-9.31	2116
2019SM8	5*	2061-10-01 13:25	1/2.81E7	-9.33	2061
2018XF2	20*	2104-12-06 16:13	1/2.79E8	-9.35	2053-2104
2015RU178	9*	2055-09-09 15:49	1/1.92E8	-9.37	2044-2055
2014JU79	100*	2041-10-03 00:39	1/3.11E10	-9.38	2041
2019SU2	3*	2096-09-19 06:13	1/5.43E6	-9.40	2069-2104
2017FA159	7*	2021-06-21 13:19	1/8.26E8	-9.41	2019-2118
2012EZ1	6*	2107-11-07 03:42	1/2.36E7	-9.43	2107
2017TT3	26*	2104-06-15 13:26	1/6.33E8	-9.44	2075-2104
2005TK50	6*	2106-03-15 19:54	1/3.22E7	-9.44	2027-2117
2016JY5	13*	2093-04-29 18:56	1/1.19E8	-9.45	2080-2099
2020KC5	12*	2106-06-01 12:33	1/9.9E7	-9.47	2105-2106
2017SG33	60*	2070-09-08 03:03	1/1.1E10	-9.47	2051-2111

2016FF14	14*	2117-03-31 14:12	1/1.3E8	-9.48	2093-2117
2017BK30	13*	2085-02-11 16:21	1/1.66E8	-9.48	2085
2020FP5	4*	2116-03-23 13:41	1/6.45E6	-9.51	2110-2118
2016QY84	18*	2063-08-26 10:31	1/4.17E6	-9.52	2024-2118
2019TJ5	16*	2103-10-11 01:41	1/3.24E8	-9.52	2086-2103
2015KW157	24*	2026-04-07 11:30	1/2.97E9	-9.53	2026-2078
2005WN3	4*	2024-04-15 09:42	1/6.58E7	-9.53	2024
2017UK1	14*	2108-10-13 10:31	1/1.52E8	-9.56	2098-2112
2014WU200	6*	2111-12-03 06:00	1/1.45E7	-9.60	2105-2112
2016WQ1	9*	2105-09-21 19:19	1/6.85E7	-9.60	2046-2109
2014HE197	25*	2049-09-01 05:56	1/5.95E9	-9.61	2028-2105
2013RZ53	2.1*	2103-02-04 04:19	1/1.52E6	-9.64	2093-2117
2019SK9	13*	2099-09-22 13:09	1/3.32E8	-9.64	2099
2019GC6	17*	2113-04-18 18:43	1/2.78E8	-9.65	2113
2016EN157	8*	2054-03-11 00:48	1/2.04E8	-9.68	2054
2016EU84	6*	2115-03-01 18:16	1/2.04E7	-9.69	2109-2115
2019CY1	26*	2060-02-21 03:39	1/3.13E9	-9.71	2060
2015PL57	25*	2112-07-08 03:29	1/6.94E8	-9.72	2112
2014HC196	29*	2060-03-25 21:45	1/2.81E9	-9.73	2048-2112
2010SK13	12*	2084-02-24 22:26	1/4.48E8	-9.73	2084
2019GK3	4*	2103-03-31 17:30	1/1.26E7	-9.74	2103-2118
1994ES1	7*	2061-10-02 08:41	1/1.27E8	-9.75	2061
2017UJ2	2.4*	2112-06-22 16:05	1/2.97E6	-9.76	2079-2116
2018YO2	4*	2090-12-23 22:26	1/1.1E7	-9.79	2066-2112
2011SL189	40*	2092-01-25 21:27	1/6.37E9	-9.82	2092-2100
2020LO	15*	2065-06-03 20:48	1/7.09E8	-9.85	2061-2065
2017WW1	4*	2055-11-22 09:37	1/5.32E7	-9.85	2055
2014UU56	8*	2115-10-20 14:12	1/7.41E7	-9.86	2078-2115
2016AF2	10*	2072-03-26 07:45	1/2.12E8	-9.88	2072-2087
2019UO8	5*	2106-10-27 20:27	1/1.13E8	-10.01	2106-2116
2014OQ392	110*	2114-06-10 07:15	1/3E10	-10.02	2103-2114
2016DB	7*	2063-02-14 16:03	1/2.04E8	-10.03	2059-2063
2019SX8	6*	2110-09-30 01:21	1/6.1E7	-10.05	2110-2116

2018DO3	5*	2040-02-14 23:48	1/6.71E8	-10.08	2040-2115
2017FW128	12*	2072-04-10 13:32	1/5.41E8	-10.09	2072-2118
2008WJ14	19*	2042-11-19 21:09	1/2.87E9	-10.09	2042-2080
2007WW3	60*	2039-11-15 05:23	1/4.67E10	-10.11	2039-2067
2017WE30	1.5*	2047-11-27 02:28	1/1.89E7	-10.17	2038-2100
2019UN13	1.3*	2111-11-01 04:11	1/3.34E6	-10.28	2111
2014WZ365	26*	2105-12-12 22:08	1/4.59E9	-10.29	2105
2010VP139	12*	2034-04-25 03:17	1/6.58E8	-10.37	2014-2090
2018AT2	10*	2115-01-11 10:19	1/4.37E8	-10.38	2115
2011BH40	40*	2094-02-03 04:29	1/4.46E10	-10.40	2094
2017KJ32	6*	2105-07-17 03:33	1/1.21E8	-10.43	2105
2003SQ222	4*	2101-09-28 10:21	1/7.14E7	-10.44	2101
2017BF136	20*	2049-02-01 17:44	1/2.28E10	-10.44	2049
2015KH158	22*	2098-05-16 12:49	1/7.41E9	-10.45	2097-2098
2016PA79	50*	2064-09-23 16:49	1/3.13E10	-10.46	2064
2016VH	16*	2115-10-24 09:36	1/1.32E9	-10.46	2115
2019EF	16*	2097-08-31 21:09	1/4.52E9	-10.48	2097
2008EK68	4*	2032-03-03 16:21	1/1.37E9	-10.49	2032-2118
2020DW	3*	2108-12-23 19:54	1/2.94E7	-10.52	2108
2014HR197	14*	2035-10-29 16:28	1/6.06E9	-10.53	2035-2080
2019SU1	7*	2116-03-13 12:46	1/2.68E8	-10.55	2116
2020HM6	17*	2090-04-20 08:36	1/5.03E9	-10.55	2090
2016TB57	21*	2096-11-06 23:14	1/3.55E9	-10.56	2096-2112
2019VS4	12*	2102-11-06 13:45	1/1.22E9	-10.56	2102-2117
2015HZ182	12*	2036-03-18 12:12	1/1.35E10	-10.56	2036-2101
2020BA15	12*	2051-01-28 07:21	1/4.69E9	-10.61	2051-2053
2019TX	7*	2101-10-05 17:41	1/3.89E8	-10.72	2101
2009SH1	5*	2118-09-16 04:45	1/4.93E7	-10.73	2075-2118
2020DV	16*	2072-01-31 23:30	1/5.99E9	-10.73	2072-2117
2018PV24	4*	2087-08-14 14:30	1/1.64E8	-10.80	2087
2018DP3	7*	2108-02-17 03:58	1/3.8E8	-10.91	2034-2110
2012WQ3	29*	2081-05-09 08:01	1/8.62E10	-10.91	2081
2020HE7	6*	2102-04-21 21:13	1/4.69E8	-10.95	2086-2111

2017CY32	7*	2047-01-30 22:34	1/5.78E9	-10.95	2047-2093
2018WE1	22*	2074-11-25 03:36	1/2.72E10	-10.98	2074
2020AY1	30*	2103-04-01 07:54	1/3.27E10	-11.03	2103
2019BZ3	6*	2092-01-27 10:57	1/1.31E9	-11.13	2092
2010WW8	15*	2081-11-22 12:37	1/6.67E9	-11.33	2051-2081
2017RW17	4*	2116-09-17 15:10	1/6.85E8	-11.37	2116
2017BD6	7*	2083-01-25 11:31	1/3.39E9	-11.44	2083-2093
2017VN2	12*	2110-11-21 03:52	1/1.14E10	-11.65	2110
2016VR4	6*	2107-11-10 10:41	1/3.09E9	-11.68	2107
2018TT6	2.9*	2117-10-06 14:30	1/7.94E9	-11.73	2117
2019AS5	1.2*	2110-01-09 03:22	1/1.05E8	-11.89	2085-2110
2016CO248	11*	2061-02-07 14:37	1/3.95E10	-11.96	2061
2019HR2	6*	2063-04-23 19:51	1/3.58E10	-12.52	2063-2096
2015HM182	6*	2067-11-13 00:09	1/5.21E10	-12.64	2067-2102
2017YD2	6*	2081-12-27 13:06	1/5.78E10	-12.75	2055-2103

Table B-1: Potentially Hazardous Asteroid properties database

The asterisk (*) implies that the diameter of the Potentially Hazardous Asteroid is determined using the value of its absolute magnitude (H), as given below.

$$Diameter\ (m) = \frac{1.329 * 10^6}{0.14^{0.5}}(10^{-0.2H}) \quad \textbf{(7-38)}$$

B.2 Table of Keplerian Elements of the PHAs

Using [21], the Keplerian elements of the list of PHAs in Table B-1 were obtained. This includes the epoch at which the observations were made (in Modified Julian Day (MJD)), and the regular Keplerian elements (Semi-major axis (a), eccentricity (e), Inclination (i), Right Ascension of the Ascending Node (RAAN), Argument of Perigee(om), and Mean Anomaly)

Object Name	Epoch (MJD)	a (AU)	e	i (°)	RAAN (°)	Om (°)	Mean Anomaly (°)
2010RF12	59000	1.06053	0.188224	0.882882	163.8307	267.6007	261.9137
1979XB	59000	2.561657	0.747997	25.38296	81.96633	78.50534	313.1827
2000SG344	59000	0.97744	0.066958	0.112203	191.9125	275.3467	35.68057
99942	59000	0.922571	0.191475	3.336855	204.0484	126.687	248.1482
2008JL3	59000	2.157424	0.54361	0.89732	40.26674	155.5622	299.3471
2009JF1	59000	1.892947	0.738182	6.149536	45.56982	281.3488	73.22485
2018VP1	59000	1.587421	0.429796	3.241162	39.8156	315.1251	300.8012
2007KE4	59000	2.386062	0.577302	9.302618	64.7893	195.4345	184.3536
2012QD8	59000	1.914003	0.698035	5.579542	348.7522	87.77044	311.8507
2011DU9	59000	1.937568	0.514056	3.414071	155.1234	328.303	166.2868
2020FT3	59000	1.430756	0.363052	1.535787	136.0609	124.3819	355.3389
2007FT3	59000	1.129202	0.30769	26.86029	9.835025	277.3465	296.0125
2006JY26	59000	1.01031	0.083105	1.438559	43.4747	273.6619	227.4963
2013VW13	59000	1.672147	0.574188	3.529566	227.6549	101.4277	33.06831
2007DX40	59000	1.534661	0.537564	0.44298	326.8518	276.8194	320.4996
2014GN1	59000	2.657223	0.750101	2.962792	193.066	80.36101	141.6201
2017US	59000	0.829535	0.229492	0.906499	200.0505	357.1821	359.0864
2018JD	59000	1.566553	0.357512	10.86135	47.46748	187.8017	15.58094
2001VB	59000	2.409765	0.897439	9.058321	303.549	226.9753	342.7081
2008EX5	59000	1.360784	0.391481	3.384645	16.20893	66.18773	297.7917
2007VE8	59000	2.497161	0.588018	7.223465	43.78625	352.5318	63.43025
2005QK76	59000	1.400944	0.519035	22.93376	337.4525	266.2866	357.6856
2020MJ	0	0	0	0	0	0	0
2017SH33	59000	2.334342	0.454664	65.89242	225.8788	179.7458	264.9273
2015YJ	59000	1.263467	0.522854	0.120575	264.8205	79.02323	89.19687
2010CR5	59000	3.051903	0.806726	3.987318	298.0103	75.09187	8.203871
2020CQ1	59000	1.437224	0.321657	2.804053	134.3601	342.7396	75.3437
2016DK1	59000	1.362573	0.330875	0.767969	336.3206	125.7995	271.7429
2009BE	59000	1.460827	0.443156	0.980884	125.5298	62.45735	93.65608
2009TD17	59000	1.126774	0.220027	0.078696	217.9818	83.14817	13.40901

1994GK	59000	1.955	0.604823	5.677288	14.44366	112.6687	218.267
2005ED224	59000	1.910904	0.659815	31.92092	170.1489	277.567	292.6334
2017WT28	59000	0.899942	0.13091	5.773281	243.0613	35.89302	114.159
2016WG	59000	1.831699	0.742102	0.220033	294.5018	231.6816	131.4068
2018TY4	59000	2.410576	0.609749	2.712882	12.49713	329.0512	164.7917
2017YM1	59000	1.716777	0.437268	15.52363	83.98338	339.781	40.14429
2020OB	0	0	0	0	0	0	0
2008CC71	59000	1.448981	0.366972	1.870881	339.0932	222.5918	350.3971
2019LU1	59000	1.525345	0.875477	7.34434	75.63613	316.8474	164.929
2011AM37	59000	1.100424	0.147321	2.629071	291.2187	129.2861	84.25851
2020KD3	0	0	0	0	0	0	0
2014CR13	59000	1.484859	0.460985	7.459188	141.6414	292.524	199.4824
2017SF20	59000	1.806009	0.492696	3.072966	183.1954	137.284	50.40324
2008UB7	59000	1.235047	0.593551	2.023082	219.4996	287.8202	114.8168
2017FO63	59000	2.362702	0.84333	2.114466	254.5367	43.45162	302.6884
2012MF7	59000	1.474226	0.383196	1.967749	90.96984	127.4713	180.1724
2019TU	59000	1.502032	0.426759	0.709664	130.0397	302.0767	102.9851
2014WA201	59000	1.421977	0.422502	5.335183	53.42327	294.6077	123.1854
2010QG2	59000	1.66652	0.515873	4.702687	342.7533	64.75691	167.9025
2011XC2	59000	2.001732	0.580544	28.79726	70.65545	306.5954	12.4628
2012HG2	59000	1.189086	0.181713	0.11153	143.4826	26.27103	120.5328
2010UK	59000	0.86663	0.218605	4.922397	203.3599	36.59145	102.3461
2017LD	59000	1.394786	0.277863	0.067978	78.86594	196.1134	281.5525
2016WN55	59000	0.834808	0.369685	12.31775	340.6344	242.8141	104.8665
2008FF5	59000	2.274455	0.966037	2.548609	14.58585	20.69234	206.1887
2008HJ	59000	1.632177	0.406684	0.925087	47.46722	204.1696	273.9836
2008ST7	59000	1.935517	0.513446	2.449172	347.7996	321.79	138.7343
2016RD34	59000	1.046302	0.034673	1.957837	349.5915	11.07136	159.8694
2006DM63	59000	0.695759	0.49657	1.752737	335.6445	18.15989	339.3643
2018GR4	59000	0.936024	0.111118	1.004373	167.5958	232.8823	285.6107
2018DQ	59000	1.713173	0.683388	0.395744	152.3199	263.735	25.36626
2013TP4	59000	1.88032	0.759583	6.314846	188.6866	73.54201	228.2747
2011UM169	59000	1.697688	0.525323	6.267874	210.6997	114.9058	340.1708

2008EZ84	59000	1.010864	0.150766	13.09832	169.4969	268.2566	86.26939
2000SB45	59000	1.560091	0.397056	3.677385	195.4363	216.5772	14.74291
2019QR3	59000	1.535001	0.43062	9.094423	158.3634	235.6638	119.7282
2006CM10	59000	2.134355	0.701228	18.31219	143.0991	92.26373	192.2535
2007TC14	59000	2.091005	0.806397	4.65719	220.8839	272.6006	47.71854
2007WP3	59000	1.485817	0.44672	10.67757	229.1289	115.7103	358.9777
2014JU15	59000	0.726046	0.466552	9.104524	38.58899	20.24841	74.51778
2010GM23	59000	1.316865	0.442201	4.394101	204.7817	81.22776	222.7973
2019WG2	59000	1.277797	0.304561	23.35074	240.5396	124.4608	159.7231
2016NL39	59000	1.342342	0.247118	0.790201	281.7393	341.8806	195.0195
2015XA378	59000	1.831179	0.6393	0.225986	74.64167	91.96333	267.6841
2019WU2	59000	1.681498	0.486519	3.283783	222.9608	125.5094	110.8396
2012EK5	59000	1.814208	0.555485	9.956683	4.320283	240.8395	109.1811
2020DF3	59000	1.450833	0.634963	36.58725	153.4766	258.108	84.76853
2006SC	59000	1.113035	0.350023	10.42802	350.8051	265.2169	299.3048
1995CS	59000	1.941604	0.774208	2.604433	134.9693	253.0101	143.9658
2019JO1	59000	1.205239	0.58639	5.07431	218.1403	248.2133	338.5689
2020FA5	59000	1.916984	0.800327	6.566086	39.41694	242.0292	2.863432
2002RB182	59000	2.541688	0.651436	0.23073	166.5846	253.0838	119.9797
2013EV27	59000	1.978871	0.568752	4.256203	340.1988	127.3701	230.371
2002GM5	59000	2.127499	0.697955	7.31143	13.27979	274.7815	284.6244
2011VG9	59000	2.28837	0.777702	1.272448	236.041	65.90887	187.2808
2017OE7	59000	1.399642	0.280588	0.653463	308.4013	18.40851	246.1842
2006QN111	59000	2.489164	0.596007	11.72923	143.7513	171.819	187.0724
2016EO28	59000	1.28805	0.306199	2.432423	159.4259	305.5712	356.1687
2017VL2	59000	1.265186	0.239703	12.49732	226.9467	147.6693	306.2863
2012ES10	59000	1.886926	0.757655	6.791233	345.8256	73.78189	82.58106
2002UV36	59000	2.453112	0.598462	2.867198	32.58371	356.1132	205.7607
2011SO189	59000	1.995569	0.566176	4.44702	2.267033	306.9392	42.11741
2017RV2	59000	1.545766	0.365518	0.21317	172.1533	149.8974	160.5472
2011ES4	59000	1.090126	0.241839	3.363573	339.8955	273.5291	338.6257
2018NL	59000	1.826024	0.449196	8.43579	277.6232	15.32983	274.9153
2019FE	59000	1.917517	0.52587	2.643239	177.4211	317.067	175.3375

2017GG8	59000	1.878716	0.533107	5.522603	191.1782	309.0381	97.45875
2009TH8	59000	2.047435	0.592136	4.91211	30.89509	50.00081	213.1536
2010JH110	59000	2.33633	0.565851	0.744064	72.4343	165.4784	289.5802
2014JR24	59000	1.066419	0.118344	0.929674	48.88924	246.4271	126.3658
2020BW5	59000	1.330136	0.344474	0.52581	276.3237	282.2273	42.60212
2006HF6	59000	1.411097	0.550106	6.609054	29.32614	86.90948	188.9852
2020KN2	0	0	0	0	0	0	0
2011OB26	59000	1.654367	0.476691	1.765748	138.6946	234.9902	30.98959
1996TC1	59000	1.860517	0.719947	14.46679	4.080452	259.7806	135.3666
2009WP6	59000	1.131272	0.741461	2.771317	54.38159	228.0677	312.9232
2006JE	59000	1.789709	0.759004	15.08058	43.00331	286.4425	294.173
2008PK9	59000	1.638202	0.724726	27.41797	318.2912	108.1597	203.1341
2020MO1	0	0	0	0	0	0	0
2017PY26	59000	1.62479	0.616178	16.94959	145.6005	268.776	98.26317
2014ML67	59000	2.634144	0.760366	1.576943	283.4573	80.42391	123.1509
2016VB1	59000	0.754912	0.318791	1.222342	41.0369	176.1394	349.2066
2010MY112	59000	1.070508	0.244139	38.51126	82.98644	327.8583	261.1117
2016PM38	59000	2.442878	0.583954	2.106627	279.4665	358.5316	7.671424
2008TE	59000	1.517629	0.452325	0.304518	1.061818	297.5104	112.6905
2020DJ1	59000	1.498874	0.49107	5.830351	307.2018	282.6231	24.06156
2013GM3	59000	0.835601	0.286918	0.013363	337.6787	11.70095	352.2908
2020BK3	59000	1.158246	0.316887	9.819975	120.3924	280.0401	149.5027
2010VQ	59000	0.860448	0.198002	0.356294	28.90382	198.2542	161.3651
2002MN	59000	1.815051	0.498354	1.047971	85.23396	131.5521	138.2242
2009BR5	59000	2.027474	0.660075	3.837895	300.4963	277.6318	314.9946
2013WM	59000	2.085307	0.915781	4.133087	239.1545	41.18284	72.82309
2016JB18	59000	1.12331	0.14893	1.891274	208.3981	304.6611	207.3218
2014UD57	59000	1.365885	0.350139	0.654547	214.1264	119.6299	210.6936
2012BA77	59000	2.360509	0.633109	1.188536	196.6501	228.2633	119.8594
2013BL18	59000	1.993192	0.591474	7.524405	294.9518	121.0241	237.6464
2020OX4	0	0	0	0	0	0	0
2011MX	59000	1.430969	0.397445	13.47029	268.1336	297.3836	109.0303
2001CA21	59000	1.533762	0.751551	4.808388	43.92222	221.6554	33.30832

2016CY135	59000	1.475081	0.353462	1.103749	173.4903	26.54235	113.2783
2006BC8	59000	1.226953	0.431381	6.891013	303.2939	91.24481	243.672
2010HV20	59000	2.621011	0.787772	6.439528	98.95384	216.3423	125.7891
2014OM207	59000	2.428972	0.583408	2.247476	122.7165	168.6461	198.8892
2014YN	59000	0.892314	0.134149	1.208751	239.3604	15.89118	1.647291
2010KV7	59000	1.217478	0.219595	0.316712	254.7217	37.15815	135.261
2018JN	59000	2.162884	0.541067	3.617833	214.3559	344.7514	241.1759
2019SJ	59000	1.056996	0.197338	11.05931	353.6126	272.5702	298.2347
2019LW4	59000	1.080101	0.19648	12.08564	77.56341	262.6309	252.6268
2007KO4	59000	1.102862	0.161566	25.16443	61.11123	299.3067	340.8709
2020GZ2	0	0	0	0	0	0	0
2011BL45	59000	1.037729	0.020968	3.048838	134.7706	155.1533	139.5847
2015KG158	59000	1.138328	0.276816	2.231836	54.11442	97.45763	107.2327
2005XA8	59000	1.417693	0.436643	5.347439	254.09	111.2994	236.5388
2007DS7	59000	1.1795	0.399703	8.450064	148.3804	270.9096	174.1385
2018GG	59000	2.176279	0.605728	7.171191	22.98908	229.1366	228.4261
2017HG4	59000	0.862314	0.186725	2.983669	210.7452	204.802	103.342
2008YO2	59000	1.670777	0.590144	1.42558	92.72665	78.28962	83.29443
2005EL70	59000	2.488708	0.931979	16.1774	166.0316	221.8	331.6184
2009OW6	59000	1.954992	0.482176	0.118194	95.87424	229.7339	341.7173
2012SY49	59000	1.527501	0.557247	1.194255	5.922255	84.3833	355.6516
2020JK	0	0	0	0	0	0	0
2010VW194	59000	1.822154	0.466052	2.017422	50.85257	339.5734	323.5824
2011EB74	59000	0.948992	0.166303	10.68378	355.9014	295.362	247.5603
2009FZ10	59000	2.131006	0.597948	6.468438	177.5027	304.7244	228.0766
2001GP2	59000	1.037346	0.073867	1.279873	196.7101	111.2695	298.7562
2018XQ2	59000	0.856976	0.177884	0.076816	111.7238	148.0623	125.0583
2019HS3	59000	2.471475	0.830353	5.931359	216.2086	251.5589	113.0811
2020HL1	0	0	0	0	0	0	0
2020OR4	0	0	0	0	0	0	0
2020LV	0	0	0	0	0	0	0
2012WS3	59000	1.11111	0.279271	3.872014	241.4628	86.25952	211.7746
2012VE77	59000	1.64248	0.555123	8.083787	235.3332	254.0022	186.2405

2002TY59	59000	1.018341	0.233361	6.611775	9.775603	259.2234	134.5983
2011SM173	59000	2.492415	0.651478	0.524918	175.7452	237.5469	61.17213
2015WN1	59000	1.405435	0.369844	0.502839	231.9251	124.9153	286.7808
2002VU17	59000	2.453776	0.623665	1.491788	55.41154	309.7871	203.3472
2008LD	59000	0.891906	0.15477	6.540104	250.8299	201.4596	238.2644
2017FN1	59000	1.466718	0.577696	2.248151	0.443921	271.5927	258.8404
2018NW	59000	1.161055	0.339608	36.74423	285.7154	271.6688	236.3118
2019SX	59000	1.168338	0.483364	1.120849	178.5225	282.4526	150.3008
2016BA15	59000	1.543092	0.550392	1.443282	115.1212	96.87599	67.5128
2013WZ44	59000	1.607435	0.462739	11.50189	242.8595	125.8652	90.0554
2016CD30	59000	1.768792	0.496891	5.863127	131.8171	314.1155	316.1946
2005CC37	59000	2.212616	0.561874	6.137532	112.9994	345.9131	243.4089
2017UL7	59000	2.211832	0.66428	2.486717	180.9146	290.6449	266.6308
2014MO68	59000	2.398165	0.599318	2.545415	317.559	22.93653	199.8915
2018SD2	59000	0.930257	0.111379	3.676886	1.803743	138.0398	185.2625
2000WJ107	59000	1.947659	0.557373	5.990169	237.7499	127.5082	81.86091
2010XB	59000	1.775314	0.652908	1.486309	248.5435	92.52523	25.0028
2009FJ	59000	2.207905	0.567115	0.886978	353.5463	150.7014	156.7984
2012BY1	59000	2.115827	0.672508	0.521346	320.7194	237.8957	242.5954
2018PZ21	59000	0.857197	0.257444	3.151686	309.101	214.571	237.1822
2004VM24	59000	1.139931	0.429509	2.925908	231.2169	277.2003	233.0349
2020ED	59000	2.044487	0.522286	1.133743	26.42448	167.938	21.00674
2006HX57	59000	1.808103	0.495126	0.196939	111.2495	160.0752	269.0086
2007CC27	59000	1.687753	0.49323	2.123486	323.9427	125.3862	40.16896
2016NL56	59000	1.385244	0.682151	4.681308	14.05449	80.58998	35.58353
2015ME131	59000	0.805522	0.205007	30.22731	315.3076	162.3336	130.5779
2011BG10	59000	2.501909	0.621687	3.380905	125.4258	37.92574	122.1729
2019AW2	59000	2.008519	0.581893	8.813484	96.58509	306.7489	192.6439
443104 2013XK22	0	0	0	0	0	0	0
2017YO3	59000	0.752563	0.348816	8.64812	267.9923	19.529	51.41514
2019NO2	59000	2.355817	0.576732	1.468902	101.0716	159.2402	95.22974
2011BF40	59000	2.802971	0.726212	5.505116	300.8001	264.5724	345.9176

2004GE2	59000	2.040201	0.706426	2.15489	44.2148	261.0699	173.1176
2008ST	59000	0.964036	0.125865	1.907219	189.4705	291.1999	16.42242
2019UT	59000	1.986885	0.552441	3.547957	211.7612	222.682	66.10098
2014QC391	59000	1.563593	0.39705	2.140911	345.124	37.63807	319.1229
2012LJ	59000	2.324974	0.698903	0.687587	239.0614	96.31697	77.18397
2011FQ6	59000	0.97986	0.351607	5.156187	183.0463	246.4594	242.5192
2019SC	59000	2.529241	0.658064	0.443641	171.7609	234.3891	53.72261
2010XN69	59000	1.897836	0.497629	2.02816	99.10649	22.07646	210.0897
2015MN11	59000	2.039204	0.704178	5.710174	277.6457	86.37227	233.0523
2019NF7	59000	2.455627	0.587723	7.297009	286.1742	11.41216	81.34204
2013RO30	59000	1.919376	0.487868	8.337039	162.2893	156.7648	198.7149
2008KO	59000	2.155666	0.735919	14.73932	72.47916	270.7453	270.2095
2010CS19	59000	1.74001	0.440623	4.180937	143.5945	340.5172	181.9317
2018HJ2	59000	2.486993	0.61596	3.123419	168.9556	8.003747	200.5167
2018FE4	59000	1.64607	0.605071	19.20719	183.6774	92.4971	346.3996
2018CM	59000	2.002357	0.532033	1.498328	138.6359	31.34895	285.1572
2017RZ17	59000	1.904463	0.506785	11.08738	29.58847	67.59673	312.455
2017AE21	59000	1.990753	0.537749	5.962173	265.1324	145.3168	92.72071
2018BN6	59000	1.112447	0.343607	2.094942	300.1429	93.42685	52.1875
2019AU6	59000	0.983618	0.281945	0.348875	302.0044	278.0734	74.20028
2006UU17	59000	2.329797	0.586797	2.909137	208.8165	151.5601	302.0845
2020CO2	59000	1.753296	0.576576	0.521432	302.4728	278.6001	23.77299
2017QC36	59000	0.792447	0.312498	20.03518	137.5922	355.6721	190.7144
2015BW516	59000	2.017113	0.555557	1.945715	310.9764	222.4849	299.1321
2019JR2	59000	1.274784	0.444879	8.308822	40.73375	90.55764	310.8636
2010HS20	59000	2.207675	0.553846	2.216363	99.69418	158.7664	17.38861
2018TB	59000	2.393539	0.581916	3.613414	14.39529	341.1622	164.2761
2018TP5	59000	1.682495	0.472431	2.739167	11.30309	308.9608	290.9368
2000LG6	59000	0.917297	0.11066	2.830549	72.54229	8.157076	86.73544
2013NH6	59000	1.244708	0.587319	24.15798	98.38575	69.91562	35.12709
2018NJ	59000	1.539587	0.344727	4.67394	107.7498	192.8763	350.7658
2005VN5	59000	0.945347	0.232757	2.062357	48.22941	116.1633	213.7383
2010JL88	59000	1.423322	0.50352	0.095281	268.8023	51.37964	297.1962

2017NT5	59000	1.868281	0.675992	6.03961	293.5692	88.93879	26.89542
2019UH9	59000	1.559776	0.68534	1.68869	179.4696	102.0176	139.015
2010TW149	59000	1.88696	0.614122	4.570634	195.3808	104.0549	277.0289
2016TY55	59000	1.031094	0.153172	4.208732	206.9395	264.3223	95.13141
2007XZ9	59000	2.042846	0.585609	3.043778	247.5993	126.2565	114.23
2012TV	59000	1.50225	0.572061	5.542194	193.4972	269.9332	26.76757
2004PU42	59000	1.574609	0.443698	0.991005	146.9466	232.5127	335.0612
2014GY44	59000	1.18874	0.391255	10.19073	188.6799	271.6424	319.3488
2011DV10	59000	2.840945	0.690249	8.123595	159.6351	293.02	345.039
2017FB1	59000	2.120388	0.740055	5.11467	348.9441	80.52994	31.25406
2016SA2	59000	1.176401	0.184817	4.763321	183.0496	134.5365	349.2321
2016DA31	59000	1.237697	0.443496	0.022785	338.6049	271.2907	350.7047
2019FA	59000	1.342418	0.298844	1.099275	174.2555	320.3887	301.5422
1999RZ31	59000	2.586166	0.601325	2.973818	163.184	179.9223	354.874
2009FG	59000	1.968098	0.529062	0.033083	46.28084	78.31172	36.1754
2007UO6	59000	2.274427	0.597647	2.391598	23.50715	320.5754	252.5137
2014AD16	59000	1.401651	0.368109	0.345153	130.4375	27.68888	279.9183
2020FN3	59000	1.013278	0.208322	0.897048	20.73128	270.1119	337.9121
2010UB	59000	2.052998	0.518717	3.395434	215.0535	199.7882	87.47408
2014HN197	59000	2.767667	0.757006	4.00299	269.6096	171.1428	156.3268
2016LP10	59000	2.28774	0.648051	0.668016	79.27102	241.3344	41.69896
2020HQ4	0	0	0	0	0	0	0
2009VA	59000	1.15075	0.209603	12.27387	224.4047	238.2432	160.9251
2010UH	59000	1.359322	0.306449	0.631528	295.0408	40.67692	45.14779
2016RR1	59000	1.666178	0.399144	5.33534	340.5483	345.8225	271.6708
2016NK22	59000	1.497342	0.352984	2.713557	111.0634	213.4481	27.34991
2007TL16	59000	1.461126	0.400236	10.50305	12.92193	303.9408	82.62688
2007PR25	59000	1.966409	0.846042	3.520951	153.8106	292.5749	216.3199
2017SA20	59000	1.099901	0.191733	0.12873	34.99226	248.9455	173.9057
2018GE2	59000	1.08628	0.22636	0.47503	42.35347	74.92236	18.43998
2010TW54	59000	1.043382	0.234192	3.84556	196.2847	85.93595	84.2447
2017RZ15	59000	0.957604	0.256755	2.043086	162.0398	62.41027	61.85177
2014FX32	59000	1.783077	0.482302	3.782292	172.2523	320.7727	232.7992

2013GA55	59000	1.644543	0.455115	0.475922	206.846	298.7345	158.937
2020BA14	59000	2.175762	0.656338	6.770997	157.4018	67.24534	19.10494
2009CZ1	59000	2.227182	0.659699	2.196231	150.3218	66.30741	128.1456
2011DS	59000	1.035018	0.229343	0.277408	346.389	71.39543	357.5147
2011CU46	59000	1.39874	0.531158	8.006734	140.0411	270.0498	255.9225
2007EV	59000	1.090821	0.307764	8.167712	357.3541	268.6176	156.6429
2011CW46	59000	1.049253	0.156266	30.36814	322.1386	77.31256	318.7759
2009HS44	59000	2.573704	0.70171	2.438315	209.1315	73.2017	238.7398
2011WN69	59000	2.505645	0.779323	6.033593	243.1333	89.61588	64.28928
2001BA16	59000	0.94011	0.137563	5.774893	115.4443	243.293	190.2356
2017YO5	59000	1.800213	0.459078	5.831471	91.82715	344.7114	7.804082
2010UY7	59000	0.896814	0.150302	0.456911	40.07816	210.3555	236.6872
2020BB5	59000	1.408417	0.382623	0.874799	305.9811	120.369	101.2643
2011AK37	59000	2.837707	0.660162	3.619726	118.7678	321.8998	349.0767
2019KJ4	59000	0.82091	0.263862	0.187627	356.4142	59.12645	326.3445
2010GH7	59000	1.400228	0.299719	3.536751	191.9255	335.5478	54.28411
2019WE	59000	1.726538	0.461346	0.436139	240.0773	215.2222	70.84536
2015BE511	59000	2.604058	0.630295	0.363148	126.1922	332.8114	103.4251
2017VJ	59000	1.331272	0.399794	4.478969	218.0713	107.1046	278.2167
2017HJ61	59000	1.832868	0.568826	0.783731	212.6553	293.9477	108.4059
2014MA68	59000	1.525451	0.348578	1.438504	57.85431	180.2362	70.60695
2005WG57	59000	1.79664	0.492051	0.42649	161.6245	212.3099	25.09703
2008EV84	59000	2.524961	0.613794	12.98865	350.1838	205.8825	12.14756
2018BL11	59000	1.675989	0.495397	2.071359	302.4773	122.9996	48.9501
2012DJ54	59000	1.176078	0.230091	1.989567	336.8533	120.1057	210.4378
2018EE9	59000	2.175909	0.655043	1.221198	171.9458	287.8448	262.3309
2016CK137	59000	1.173312	0.34629	0.793821	314.6726	95.40786	189.7186
2016AF9	59000	2.513018	0.902643	22.66857	97.18305	224.3153	50.30833
2013FU13	59000	1.728864	0.425485	0.760292	177.3487	349.1348	64.82102
2019DP	59000	1.072811	0.248789	10.36512	336.4319	91.04701	109.1163
2005AU3	59000	1.244214	0.47198	3.764165	105.0485	266.8237	73.55336
2019AH3	59000	1.229399	0.564386	3.894605	285.4896	284.5563	330.516
2019BZ	59000	1.087112	0.271669	6.736681	305.1092	92.20921	124.255

2016TQ18	59000	2.497852	0.601112	3.602826	7.089821	339.2971	338.414
2019XS	59000	1.004771	0.326996	4.182576	49.70334	250.1002	272.7457
2018VA8	59000	1.357678	0.39956	8.329595	226.9755	111.3296	24.97903
2005SO1	59000	2.167018	0.577324	5.236786	358.7901	315.6133	227.6576
2020FZ2	59000	1.906065	0.712883	2.127588	11.47526	268.8743	6.286945
2015SG	59000	2.290531	0.56107	0.497029	339.5897	354.2509	133.4584
2020DK	59000	0.68898	0.499468	2.805279	323.266	13.12686	336.3616
2019BU1	59000	1.841401	0.573742	5.418983	121.9103	295.5629	211.7928
2009HW67	59000	2.049529	0.751967	2.352097	216.0952	260.0679	296.1192
1994GV	59000	2.005789	0.520658	0.45376	20.21593	153.9602	77.39991
2017MZ8	59000	2.667815	0.678842	4.700903	15.72369	348.2129	227.3644
2012VS76	59000	0.990952	0.38623	0.805943	242.3181	284.4469	161.4626
2015EO	59000	1.299445	0.462248	4.511826	349.7512	271.1881	148.9735
2012BL14	59000	1.723164	0.653056	6.829878	119.3904	269.9476	271.6539
2001UD5	59000	2.281031	0.665362	2.54306	17.83787	291.7293	157.929
2005NX55	59000	1.624997	0.616039	27.38249	105.9518	276.425	38.02579
2006BM8	59000	1.54195	0.530201	5.197573	121.7054	281.9865	203.6499
2020AO1	59000	1.91038	0.627555	4.196344	294.635	252.1992	35.31748
2017QM33	59000	1.941932	0.633332	2.40301	335.3594	279.1862	25.1454
2016GK2	59000	1.562783	0.430983	0.933158	7.701879	127.3559	69.73585
2015XR169	59000	1.216151	0.346623	0.043114	264.7712	251.5253	78.58341
2020HB3	0	0	0	0	0	0	0
2017TW5	59000	1.900598	0.607239	0.515931	33.24224	61.76473	342.4131
2012VJ38	59000	1.358891	0.286136	0.386199	52.46437	24.47221	260.7915
2017SM33	59000	2.062005	0.498983	16.88187	180.4448	38.49508	54.39223
2017YV8	59000	0.89786	0.256671	3.113607	268.4816	51.88913	55.33783
2005TM173	59000	2.843397	0.687202	1.465849	239.5132	175.0324	351.628
2016EM156	59000	1.97379	0.514755	1.995566	0.735117	202.8126	178.2951
2018LH16	59000	1.994331	0.233272	1.46645	62.88397	244.6964	235.2917
2008CT1	59000	0.911849	0.450012	0.642916	137.119	124.2796	336.4698
2019GD4	59000	1.799041	0.467011	0.381279	320.2404	197.8337	184.7987
2018VS6	59000	1.132348	0.366945	5.497629	226.6512	87.39328	156.169
2009BF58	59000	1.512017	0.377646	0.984576	303.2408	145.1496	52.05943

2020FA1	59000	1.029577	0.033511	3.525856	170.3736	129.4179	311.3599
2012XM16	59000	2.363826	0.633637	2.185654	91.06574	41.30989	9.435494
2007YS56	59000	0.942766	0.283974	6.244176	274.564	63.67373	293.7474
2009RR	59000	1.41045	0.466579	6.097131	174.1746	256.5819	114.9369
2001SB170	59000	1.360663	0.463807	34.50989	356.5904	261.3986	326.7505
2017UJ43	59000	1.170164	0.265011	2.903201	45.12835	67.2968	327.28
2012BA102	59000	1.546306	0.395608	2.365539	306.7331	142.9293	136.7593
2011TO	59000	0.926411	0.279858	2.232215	185.4072	57.32692	355.3688
2018VC7	59000	0.872507	0.189795	0.803205	60.19613	132.1957	196.1698
2016CG18	59000	0.982709	0.092205	5.704353	316.8713	276.8675	67.30806
2013HT14	59000	2.09908	0.719401	5.781348	30.40231	88.16899	138.8714
2016AB166	59000	1.51895	0.639302	16.41307	112.0444	260.6614	148.9392
2020GB1	0	0	0	0	0	0	0
2012BU1	59000	1.614187	0.442716	0.425148	294.4803	133.8308	46.89898
2008XU2	59000	2.455822	0.616548	2.953624	62.44064	334.1934	4.452454
2020BY4	59000	2.028613	0.699329	1.7302	131.8497	82.03404	26.83036
2009WR52	59000	1.033595	0.155244	4.243282	61.01187	269.945	75.12288
2014GQ17	59000	0.853711	0.247086	0.091455	79.23765	330.7246	53.59551
2019GK21	59000	0.860792	0.340193	5.924523	19.53859	46.63936	254.3294
2018BD	59000	1.053266	0.287105	2.408696	298.0764	273.6723	6.619394
2018DZ3	59000	2.075035	0.531754	5.505727	344.6459	206.3399	263.0679
2017UP43	59000	1.375925	0.332597	3.920397	35.50886	312.303	241.1154
2013RS43	59000	1.457064	0.333367	0.938323	359.358	24.18413	278.1963
2015UR67	59000	2.625509	0.646523	1.138613	219.4884	136.2569	35.67338
2007US51	59000	2.18983	0.631868	1.470901	39.19254	298.3869	328.861
2007YM	59000	2.569274	0.620574	0.972031	59.29313	11.74827	6.917702
2019UE4	59000	1.371574	0.41489	1.136773	210.0281	107.505	167.0934
2016WY	59000	0.846539	0.173189	1.925706	236.0014	2.43278	8.442646
2019VH	59000	1.938436	0.495519	5.40305	211.5446	160.841	85.11218
2006CD	59000	1.894591	0.436779	9.035562	105.0387	299.2865	205.2405
2018XR4	59000	1.143915	0.357183	10.21468	84.45437	88.38791	18.74068
2014OX3	59000	2.003567	0.563527	1.921682	122.8016	123.3169	37.04432
2018QE	59000	1.313852	0.246747	0.182888	107.7226	249.4184	47.41954

2018FE3	59000	0.885086	0.209505	6.879685	176.8912	225.0057	349.0663
2009JL2	59000	1.854605	0.471711	17.85292	52.93962	204.9536	126.7925
2020GE	0	0	0	0	0	0	0
2020JS1	0	0	0	0	0	0	0
2013BR27	59000	1.551693	0.459333	2.567582	296.8736	120.8637	313.9892
2011BU59	59000	1.255686	0.394288	3.500198	116.6697	279.6235	276.7003
2011YQ1	59000	1.933641	0.548116	1.720044	266.4993	128.011	65.68344
2015ET	59000	2.032835	0.579386	0.598931	353.9151	124.4945	300.5184
2018LM	59000	0.869274	0.197256	7.090249	72.20032	20.7953	313.8138
2005TA	59000	1.281539	0.25052	2.777556	13.85477	34.58571	17.38057
2016JA6	59000	1.0876	0.27634	16.01044	222.2184	269.3059	273.9606
2011AY22	59000	2.114248	0.599224	0.473237	307.1391	218.9036	6.749615
2014SR261	59000	1.877511	0.585015	0.388061	182.9178	105.177	94.54785
2020DO2	59000	1.823924	0.714524	9.970218	144.4505	260.1823	62.59092
2008DA4	59000	2.427313	0.624863	4.21535	146.5073	317.5828	98.99337
2017SD33	59000	2.121517	0.528708	8.155933	311.6325	293.9771	358.6283
2006WV29	59000	1.383415	0.559211	1.215769	75.53235	81.60853	76.7339
2017AT20	59000	1.052893	0.247985	4.198004	270.3804	93.6116	124.3753
2017WL15	59000	1.225481	0.416051	25.15689	240.4014	89.68311	353.0027
2007HB15	59000	1.255094	0.255943	1.108867	37.30708	226.3428	91.23317
2011EB	59000	2.295711	0.597283	2.506092	160.3312	322.7759	244.2276
2018EB4	59000	2.321951	0.619204	1.455777	3.030054	217.5817	215.7386
2019YM	59000	2.161178	0.670717	2.225339	88.83596	70.88757	36.94463
2004VZ14	59000	1.53362	0.526392	4.579593	41.46089	280.4498	97.04278
2009MG1	59000	1.995802	0.626047	6.798186	87.2492	102.2717	334.6981
2017DG16	59000	1.387762	0.315749	3.398636	336.0169	212.8817	341.6592
2006WZ184	59000	1.365608	0.328112	0.845723	249.3852	128.0313	189.1392
2018RF5	59000	2.395183	0.582556	1.760403	339.9288	345.2661	171.8538
2013AB65	59000	1.810555	0.74973	2.439842	113.6199	252.4977	29.13771
2007UD6	59000	1.230971	0.242184	1.693078	205.7269	131.512	111.0841
2012UU158	59000	1.098607	0.372472	5.958365	26.73047	261.954	274.581
2017QF3	59000	1.253958	0.439621	2.387095	148.1242	272.4426	308.3434
2016TQ2	59000	1.863104	0.563627	10.21637	11.2755	296.2723	174.5587

2020GO1	0	0	0	0	0	0	0
2019PG	59000	1.751895	0.431813	2.990812	290.6291	336.1464	144.8157
2017KC36	59000	2.085186	0.573146	6.043192	243.947	312.6606	12.40523
2009TU	59000	1.725729	0.558695	1.556519	198.7869	106.46	270.4086
2010JH80	59000	2.090464	0.779107	21.61441	227.9879	252.9541	135.9128
2007UN12	59000	1.053346	0.060812	0.235632	215.9655	134.7363	269.1094
2016RP41	59000	1.929358	0.330402	4.271183	318.5402	44.21641	134.2952
2010FD	59000	2.87548	0.631612	0.345171	22.41641	162.6666	32.87477
2015TL21	59000	2.603738	0.677047	0.569045	220.1939	97.95248	47.33761
2020GA3	0	0	0	0	0	0	0
2009WQ25	59000	2.520512	0.71874	4.559758	40.53939	291.0033	240.055
2019DG1	59000	2.220776	0.54983	0.824521	356.3255	171.3806	134.062
2017RC	59000	1.543787	0.418668	1.513604	337.0133	306.2294	177.3521
2017FW90	59000	1.033426	0.145989	3.173377	10.4226	85.8291	82.58713
2007EO88	59000	1.13278	0.337388	5.934672	356.1743	270.1806	299.3699
2011QF48	59000	2.127545	0.636909	21.50547	154.0751	113.1167	309.1653
2007EH26	59000	1.89329	0.666783	5.617251	355.8688	269.4555	7.475304
2012PB20	59000	1.054119	0.094886	5.839053	142.9044	49.98827	194.2579
2014XM7	59000	2.021365	0.548953	10.66068	95.11628	33.38474	308.9204
2016JB29	59000	1.971347	0.494953	6.27834	82.19868	199.1084	150.922
2011SE191	59000	2.578921	0.656427	10.33057	5.172651	309.9789	42.66327
2014WA	59000	2.043644	0.539619	4.816914	53.81803	32.15283	312.9644
2018LF16	59000	1.909162	0.401611	15.47648	166.2902	188.779	220.4972
2010TD	59000	2.176105	0.675916	3.228161	187.8621	100.22	19.37362
2019XV	59000	1.100552	0.09763	0.343986	46.02605	356.461	176.3762
2012EP10	59000	1.050266	0.116005	1.032605	347.9976	105.8695	293.6588
2013PG10	59000	1.078279	0.226691	0.106818	3.846414	210.7269	104.1552
2011YC63	59000	1.532513	0.596111	10.40733	98.15078	270.1031	183.2929
2017AA21	59000	1.904163	0.471395	2.290549	332.0624	172.6415	92.70788
2014MB6	59000	2.824117	0.650097	1.279964	107.2009	134.4143	95.3588
2010UJ	59000	0.941961	0.09814	0.357213	125.2469	77.59098	11.11528
2014SR223	59000	2.56938	0.658661	1.710309	186.5379	122.9378	146.0881
2011BP40	59000	1.122567	0.153444	0.916347	164.8022	236.4416	17.2489

2019TK5	59000	1.02088	0.200053	1.504564	215.0793	264.8924	143.3126
2020MP1	0	0	0	0	0	0	0
2017RN16	59000	1.20178	0.281945	1.988075	169.9176	108.4122	64.67629
2017UK3	59000	1.981027	0.589125	1.013308	37.08372	52.91801	320.699
2008VM	59000	1.392027	0.397878	6.42584	41.81298	62.74795	347.8286
2010UC7	59000	1.87924	0.56708	5.181579	224.1622	237.1485	242.3226
2016CH30	59000	0.932777	0.178408	0.485509	346.2561	270.1825	183.2026
2008YV32	59000	1.529618	0.413993	1.095095	114.5176	39.68447	348.7823
2015XP	59000	1.884301	0.493057	4.868656	71.65051	24.88288	256.9561
2019YV1	59000	1.016514	0.114498	8.658426	88.21028	274.2923	227.7701
2017RK2	59000	2.008686	0.509089	0.424694	193.6315	183.6021	335.2997
2008LE	59000	1.44822	0.267903	1.938333	200.9291	33.21954	325.7616
2020FK6	59000	1.154828	0.443253	6.779076	352.3446	80.77971	111.1165
2015DQ224	59000	0.779407	0.526032	11.01806	149.0163	215.0536	337.4658
2019UL	59000	0.832746	0.206795	1.355692	17.33322	197.6143	96.81556
2016XP23	59000	2.460182	0.644878	37.93497	38.02255	319.3879	337.7009
2019AB	59000	1.932684	0.523841	5.047747	103.9992	33.79638	178.3011
2012CL17	59000	1.854327	0.70311	4.381049	319.8482	81.93541	122.7747
2020AW	59000	0.808276	0.233877	0.357791	321.3323	315.6708	30.00087
2019RT3	59000	1.807178	0.45133	4.601954	348.0671	340.312	113.4603
2018RB2	59000	1.378361	0.325585	9.216202	342.8726	312.2133	49.93341
2001HJ31	59000	2.069438	0.587338	2.839847	20.72277	132.6028	160.9388
2017UE52	59000	1.912482	0.32728	2.332786	32.31791	359.0882	357.2901
2010JA43	59000	1.609063	0.366773	35.41521	292.605	237.5258	7.29441
2015FA345	59000	2.339307	0.577511	4.690333	357.9005	157.478	169.219
2008OO1	59000	2.432021	0.614266	9.337711	304.1918	314.3048	54.97154
2017QU34	59000	2.212588	0.621632	3.135452	154.8962	120.1302	314.0389
2010MA113	59000	2.565209	0.650473	40.60611	309.6675	26.22724	140.8264
2015TG24	59000	0.746361	0.443407	3.986555	21.95762	151.3281	301.8866
2003UQ25	59000	2.5403	0.680979	2.131276	187.2057	276.8028	23.89085
2009HC	59000	1.039312	0.125692	3.778215	203.7877	269.9172	257.5834
2019ED1	59000	0.901423	0.328528	5.342282	341.5344	53.85261	255.1616
2017QT1	59000	2.526543	0.746155	1.113975	310.698	101.2497	237.6778

1997UA11	59000	2.361042	0.617979	3.302468	212.4142	138.4717	92.23977
2017UA45	59000	0.922052	0.166707	4.208334	202.1381	50.38178	103.903
2020HF	0	0	0	0	0	0	0
2016LG10	59000	1.785468	0.462448	4.674974	255.3094	324.3261	253.5035
2013NE24	59000	2.787204	0.661396	0.407465	320.268	289.6547	179.7407
2009EW	59000	1.257703	0.389233	10.71307	345.8762	258.258	310.1593
2011CL50	59000	0.886059	0.144574	0.18798	12.17949	293.461	252.6754
2017SU17	59000	1.226237	0.294269	1.641612	182.6286	112.1118	29.59707
2018FL29	59000	1.692736	0.51262	0.102972	52.4021	64.50128	19.22826
2017UC52	59000	2.506613	0.66316	3.520933	73.36267	35.26577	219.5599
2017DA120	59000	1.298593	0.473251	26.20131	348.8884	351.326	234.9625
2016AU193	59000	1.720023	0.667614	12.31299	100.7253	264.4437	5.449211
2017DW119	59000	2.42302	0.584041	0.381609	305.8122	186.8064	316.5572
2012KP24	59000	1.498221	0.369449	18.46993	67.45846	221.4837	112.8373
2007SN6	59000	2.337135	0.690789	4.757465	356.7902	286.7306	210.3224
2011UL169	59000	1.460761	0.377638	6.812351	212.3261	132.8724	334.1554
2006DN	59000	1.379451	0.275441	0.265822	96.62422	101.1842	264.0362
2014AG51	59000	1.875108	0.591026	0.091806	144.7852	258.2438	191.5243
2004BN41	59000	2.062164	0.520337	0.400552	330.9232	145.9561	189.0698
2018VT5	59000	1.456017	0.394539	2.703913	43.65647	305.9303	344.2859
1997TC25	59000	2.602164	0.618629	0.17135	39.64859	300.8604	154.3718
2018LT5	59000	1.784687	0.642066	8.351862	84.6607	83.38317	320.2601
2016NP56	59000	1.155317	0.156725	6.696751	113.5445	232.5581	3.369728
2018LB	59000	0.824956	0.319271	0.87983	79.51265	318.6452	116.1127
2004RU109	59000	1.532513	0.489376	5.848156	171.3255	250.716	75.39416
1993UA	59000	2.013704	0.524112	4.629697	26.82221	330.2539	103.5928
2010RA91	59000	1.166838	0.349028	5.613203	183.6126	272.6956	188.2992
2020GZ1	0	0	0	0	0	0	0
2020HW7	0	0	0	0	0	0	0
2019DX	59000	1.822201	0.531089	1.180562	346.0867	230.4621	166.6463
2018GG4	59000	2.531404	0.655117	5.233265	30.64622	233.7971	179.278
2015FF36	59000	2.087559	0.533375	0.177056	6.097062	205.4765	251.6663
2018YH2	59000	1.131517	0.221228	14.38175	111.9948	261.267	131.4035

2018VP6	59000	2.377107	0.61365	3.724513	47.00045	318.362	161.1134
2017DC120	59000	2.047964	0.450925	3.392197	277.9796	199.982	53.5423
2017TA5	59000	1.800638	0.484413	8.413101	14.58021	320.3084	46.40825
2014UX34	59000	1.722275	0.64852	32.94336	206.1271	89.86869	196.1706
2016EV84	59000	0.866002	0.177904	13.58795	351.3455	16.13657	242.6817
2009WW7	59000	1.090765	0.262023	2.526213	57.14005	273.7193	144.1027
2014TL	59000	1.13284	0.339193	3.243139	187.9055	90.66022	300.841
2015VP64	59000	2.091681	0.69858	0.714447	44.1514	274.8481	198.8647
2010NH	59000	2.087894	0.5407	7.505397	280.4295	325.77	113.0556
2006WM3	59000	1.992027	0.551658	2.018609	89.80197	36.5449	271.0498
2010CA	59000	1.318387	0.45977	9.900533	134.5334	93.13694	251.8954
2017UG52	59000	1.025197	0.596298	42.00191	262.9729	337.745	44.61495
2013RR43	59000	1.759801	0.639297	2.010454	165.1472	93.25084	338.0681
2017BG92	59000	1.252048	0.25793	0.350306	337.0006	98.66567	169.4306
2004DA53	59000	0.883575	0.330219	5.136334	336.5314	50.00708	299.9894
2009YR	59000	0.942625	0.110142	0.699824	87.16542	127.9545	33.79697
2020HN	0	0	0	0	0	0	0
2020KU	0	0	0	0	0	0	0
2018QS	59000	1.81699	0.480162	0.862908	147.4824	134.1861	276.4317
2012CU	59000	1.743998	0.506137	0.310344	172.4525	268.213	236.5102
2017KQ27	59000	2.333693	0.589691	4.773269	256.8325	30.14907	294.228
2006SR131	59000	1.354608	0.337867	0.632031	184.8211	121.2559	279.1149
2007TX22	59000	1.545173	0.42084	2.689109	19.62675	48.44085	188.2612
2019VD	59000	2.638277	0.65831	0.355877	229.1431	211.7063	41.44349
2015UH52	59000	0.852706	0.385659	4.743527	26.50671	225.6482	45.37583
2011UC64	59000	1.071576	0.462769	3.927889	211.5212	288.0479	216.3514
2008BC15	59000	2.174451	0.709073	3.387657	309.4458	264.0973	291.5723
2014QN266	59000	1.052628	0.092314	0.488416	171.1119	61.61525	211.2673
2013TV132	59000	2.190437	0.556905	1.789697	192.0377	152.5876	24.70138
2013PS13	59000	1.477088	0.582163	0.900862	139.5532	270.791	256.1034
2008EA9	59000	1.048956	0.074413	0.43984	124.2263	343.4658	134.1244
2010NN	59000	1.77915	0.44758	2.256133	282.4933	331.4628	72.49563
2017HZ4	59000	0.910032	0.216718	1.792453	67.55356	312.2073	52.12427

2018AU18	59000	2.349837	0.597036	0.097115	71.60379	12.19072	243.2854
1991BA	59000	2.096354	0.667777	2.09032	117.9495	73.4848	218.1577
2020CQ	59000	2.276003	0.616654	12.55337	313.3995	227.8185	24.14728
2018DN4	59000	2.098663	0.667317	3.759673	333.9826	107.0137	281.4166
2013UR1	59000	2.230785	0.727603	2.702784	29.7761	272.4001	7.021333
2010FN	59000	0.989677	0.211475	0.124082	161.5906	126.0318	41.8101
2014CE	59000	1.369952	0.45757	6.043741	133.0315	281.2373	11.63422
2019QE7	59000	1.899774	0.507233	3.421338	331.9622	319.1133	117.6122
2011YC40	59000	1.434745	0.418835	6.423295	96.06232	298.7295	349.6138
2019KL	59000	1.681344	0.452052	19.12505	64.41681	224.5252	151.8003
2016GU2	59000	2.051497	0.958312	10.00564	15.79907	21.75011	161.3011
2008GM2	59000	1.052012	0.157388	4.098975	195.0747	278.305	159.534
2017VV12	59000	1.618167	0.405154	0.199982	246.8839	192.791	73.66451
2015QS8	59000	2.074197	0.506157	6.796287	151.5462	176.0146	214.5306
2015CL13	59000	1.627091	0.492587	11.06073	327.1618	238.7512	177.1154
2009FP32	59000	1.973733	0.595141	0.990344	16.75212	237.3598	355.4775
2019DF2	59000	2.528095	0.676783	28.15707	128.8366	333.3721	125.752
2018RQ4	59000	1.608828	0.402347	0.351092	262.5013	130.938	284.9201
2002XV90	59000	1.577671	0.375784	9.989444	78.98149	356.3683	292.1872
2009FZ4	59000	1.29859	0.40884	3.374913	357.1098	276.1753	155.7537
2015WP2	59000	1.43441	0.457045	1.718722	58.06247	287.9008	256.6853
2018FY2	59000	2.548985	0.740657	1.225432	49.69361	38.49568	207.3486
2017RP16	59000	1.124769	0.328856	2.369773	166.3995	90.53974	154.8102
2012BK14	59000	0.977707	0.182426	1.554279	115.7847	255.9113	319.4239
2018HW1	59000	1.097963	0.136327	6.872838	32.07521	120.8196	345.7805
2010UR7	59000	2.285797	0.619599	3.622845	217.0386	129.5681	286.9049
2020BH3	59000	1.565008	0.397714	0.439613	155.2283	358.1357	51.78754
2019BO	59000	1.635987	0.421449	2.789692	295.6203	150.0603	247.1325
2007DC	59000	1.354787	0.325965	0.411512	174.7453	278.2881	182.2865
2007EN88	59000	2.175071	0.59058	8.957706	353.5695	135.739	52.25485
2005UL6	59000	2.525294	0.619959	0.282255	265.8003	90.60744	230.9309
2018CA15	59000	2.756467	0.621467	2.260088	136.335	354.6651	182.6085
2019UC14	59000	2.10313	0.673623	1.939682	52.86456	73.58635	48.22973

2017SC33	59000	2.019976	0.604418	49.20123	346.3236	268.1365	16.54445
2005TH50	59000	0.837749	0.224041	0.630891	177.3797	36.64478	181.69
2018BC	59000	1.048391	0.069717	2.864771	297.225	212.7471	45.33161
2018VC	59000	1.126355	0.169169	3.701417	36.58769	304.322	157.8006
2016WU	59000	1.036358	0.174702	8.410536	54.67882	272.9188	193.6799
2017RU2	59000	2.025518	0.522836	0.350236	30.44765	357.7874	328.285
2018EZ2	59000	1.952645	0.510512	4.971509	173.9164	27.40793	284.2292
2012BW13	59000	1.889767	0.540455	1.096352	310.5059	223.9371	63.41874
2004XB45	59000	1.550541	0.5815	3.161885	84.92398	86.1198	335.7553
2011MD	59000	1.056265	0.037069	2.445637	271.5946	5.959545	78.43144
2018PU23	59000	0.963486	0.084072	0.827641	144.6236	330.1434	174.026
2002EM7	59000	0.920726	0.363155	1.556927	345.9232	58.99389	307.0793
2018WJ	59000	2.265122	0.699096	1.712768	57.06675	75.68032	148.5715
2016FZ13	59000	0.944292	0.149985	4.178385	183.8697	238.6304	307.7019
2019GS19	59000	1.977703	0.587297	6.590277	23.09116	117.9412	161.8049
2001YN2	59000	2.499098	0.719343	1.608524	81.89695	290.4759	249.7628
2007EZ25	59000	2.129808	0.718251	5.454675	167.4453	268.411	106.9233
2019CZ1	59000	2.429358	0.773154	6.529576	136.5346	260.5967	139.4301
2014HJ198	59000	2.132037	0.739131	6.02786	214.7873	262.9434	1.212296
2017TB	59000	1.041197	0.209612	1.123273	190.5813	273.1898	111.2768
2009TB	59000	1.603459	0.43081	5.85317	7.592253	314.8554	108.4761
2019CJ4	59000	1.202507	0.379455	3.241987	327.009	86.07607	42.08831
2007CS5	59000	0.980438	0.172719	0.751293	125.2637	261.4207	345.3265
2003DW10	59000	1.44616	0.36066	2.193988	342.1553	221.0928	310.5667
2007UT3	59000	0.773241	0.398756	0.605606	155.4348	26.27252	72.82907
2004FU162	59000	0.827279	0.391378	4.169474	191.0518	139.6739	72.29022
2013BR15	59000	1.555194	0.520316	1.954612	102.8352	284.9407	320.6316
2006UQ216	59000	1.103662	0.16248	0.473524	217.7548	247.575	206.033
2008WO2	59000	1.025068	0.188169	2.010198	238.1149	85.73604	109.8858
2013XU21	59000	2.445829	0.619715	4.386623	80.28577	34.30867	240.2977
2013YB	59000	1.251933	0.336425	2.711753	91.80883	67.33575	178.2945
2013VD17	59000	2.281183	0.602993	4.761235	231.7059	138.5341	333.0709
2018WH1	59000	0.863604	0.157679	4.743986	64.39535	197.8261	112.5175

2019NP5	59000	0.79628	0.293014	2.711529	280.0233	188.621	269.919
2018WH	59000	1.211697	0.276318	1.889897	235.1279	116.6882	91.7053
2010TN55	59000	2.284696	0.786928	0.254699	35.17216	243.1517	297.3127
2012TU231	59000	1.744253	0.45323	9.609606	19.23163	327.5368	123.537
2016SU2	59000	0.897032	0.419775	4.763235	182.9541	50.07023	202.6007
2006UC64	59000	2.00907	0.699641	6.064348	211.2371	269.0834	259.1535
2014CH13	59000	1.138687	0.148535	3.62596	110.5407	115.3576	359.2624
2006BF56	59000	2.339991	0.79869	0.961137	125.2374	102.6422	343.6864
2017WE28	59000	1.108798	0.26685	6.714527	61.17789	278.9721	107.5268
2019MT2	59000	1.957652	0.517445	10.19733	104.5144	217.1049	107.4723
2010HP20	59000	2.06294	0.549825	7.881941	208.9372	320.9931	158.0717
2014FE	59000	1.915375	0.688111	2.192565	359.1344	88.87717	140.4078
2019QU3	59000	1.869694	0.459204	0.541741	310.9374	11.93218	110.7211
2008XC1	59000	2.052184	0.578268	4.474159	86.32404	43.67035	311.7398
2008UA202	59000	1.033139	0.068483	0.263084	21.11153	300.9017	77.95793
2018MC5	59000	1.373154	0.264863	1.029928	323.3102	354.4278	47.77032
2010DG77	59000	2.091359	0.539752	14.81567	291.3521	195.1286	152.6643
2006GU2	59000	1.07975	0.256496	3.386374	197.0355	266.2869	280.5311
2017MD1	59000	1.943198	0.578585	0.065891	166.8605	28.50942	50.86242
2020CF2	59000	1.194753	0.190106	1.152401	329.606	141.6758	103.4161
2019TC2	59000	1.282544	0.35817	8.506212	187.1897	107.9386	201.2366
2012SU9	59000	0.929528	0.359915	0.494309	323.4362	264.344	301.0987
2008EM68	59000	1.743498	0.64953	5.535338	350.2555	268.7397	86.40073
2005UA1	59000	2.121231	0.614603	0.432329	255.9284	72.91769	274.8575
2015BY3	59000	1.419334	0.552569	2.912933	288.9564	92.81921	95.68187
2020BH	59000	1.302749	0.242958	0.597413	106.9848	354.2002	98.37443
2005BS1	59000	1.959711	0.566017	2.64513	113.4762	308.614	231.3967
2003WT153	59000	0.893332	0.178098	0.381224	52.52689	151.4929	80.61498
2015VK1	59000	0.977479	0.426759	11.96021	38.08735	241.9317	334.8664
2016VA18	59000	1.115498	0.170531	1.089483	18.13031	318.9733	58.68601
2018LR3	59000	1.20118	0.186595	0.469983	303.3323	8.729696	140.9856
2006HE2	59000	1.064549	0.156676	1.181538	200.31	90.8025	240.0726
2020CK2	59000	1.474589	0.341019	2.070845	140.3374	339.5484	70.56044

2016TC57	59000	2.176269	0.547467	4.463221	20.88326	339.7543	52.09423
2008BN16	59000	2.207263	0.684663	5.497712	307.5548	98.86473	291.1562
2008CJ	59000	2.390711	0.564177	2.232517	131.7969	3.109492	121.6338
2018YW2	59000	1.996979	0.507509	4.989662	118.0452	8.213249	173.1772
2008UA92	59000	2.61658	0.606233	3.054926	39.50673	351.6045	267.8186
2019GF3	59000	2.213363	0.841773	9.260382	192.511	234.9044	142.5016
2017OO1	59000	0.894366	0.137556	20.02635	298.3046	186.1358	309.6446
2008SH148	59000	2.657626	0.641404	3.540651	202.6792	200.1824	244.672
2018LV3	59000	2.002016	0.525562	8.996298	83.08497	216.621	239.0445
2011FA23	59000	2.028937	0.587771	2.160869	190.8551	56.69358	47.06443
2016WN7	59000	0.881481	0.182303	8.277422	239.857	35.58972	222.6374
2004XG29	59000	1.41013	0.313589	0.1538	302.1929	110.6116	100.957
2015YM1	59000	1.041025	0.204729	5.236109	86.29468	270.2911	134.7127
2014JV79	59000	1.079833	0.135702	16.34737	233.0291	113.901	41.17277
2015GB1	59000	1.75507	0.438641	2.417395	27.61986	200.4241	65.77209
2007VH189	59000	2.615756	0.726188	5.886298	75.13322	250.526	359.4667
2018FK5	59000	1.09373	0.296511	12.22275	9.54447	269.7819	265.8124
2011SE58	59000	1.89359	0.612122	1.207608	5.39397	70.80825	100.8497
2009WJ6	59000	1.767344	0.633405	5.040431	238.6528	263.0709	153.3531
2010RM80	59000	1.176027	0.199385	2.364142	344.9644	304.431	262.2801
2009TM8	59000	1.559313	0.408624	2.322411	205.5485	220.3462	136.2671
2008HC38	59000	1.279103	0.480495	1.500876	213.3404	272.2954	167.2376
2018JL1	59000	0.980706	0.177774	5.148975	54.69488	287.4009	308.5716
2010VN1	59000	1.630787	0.465628	3.359354	40.59572	307.4245	233.2358
2001SD286	59000	2.08842	0.565448	6.298586	181.7983	131.4176	81.83666
2014HE199	59000	2.392041	0.632101	5.258109	24.754	125.1281	247.5351
2018FQ3	59000	1.823266	0.508065	7.850764	179.0032	314.2414	335.4156
2006UJ185	59000	1.695141	0.579995	0.901235	39.8301	73.94864	37.78045
2018RR1	59000	1.075438	0.141371	0.668459	352.3523	277.1529	258.0746
2019FU1	59000	2.160532	0.711938	2.401977	10.21181	90.39604	148.1575
2018EV3	59000	1.910413	0.513556	15.53543	164.9282	324.0699	315.2852
2018BP6	59000	2.061294	0.582286	8.415868	135.3007	51.39229	269.9014
2011AE3	59000	0.983797	0.153026	8.51134	282.5619	80.9524	308.6421

2016EG28	59000	1.809812	0.571259	8.110298	344.4959	112.3237	284.551
2012HE31	59000	1.382163	0.392788	0.532164	10.80098	274.8258	320.8264
2009MU	59000	2.284873	0.610213	7.293228	93.9619	224.8371	47.83142
2017FO128	59000	1.740137	0.519247	17.11013	174.9695	300.9893	159.7989
2016DK2	59000	2.402881	0.714529	0.884335	159.1843	283.2377	62.82067
2016UB26	59000	2.529069	0.706298	4.67437	12.91183	88.16938	310.6466
2015VO142	59000	1.07468	0.125945	0.284332	95.26367	20.46362	336.1775
2018XX2	59000	2.009637	0.555415	7.351149	77.0088	315.8046	197.9228
2012CR	59000	1.783181	0.384799	2.187062	156.4839	33.8234	159.6302
2013QM48	59000	1.149465	0.221728	7.422169	330.6883	290.5619	223.9408
2019NK1	59000	1.556308	0.390952	3.004688	281.2211	317.7414	186.6889
2017SS12	59000	1.227676	0.342467	1.198952	1.26947	283.7278	30.74535
2016TT	59000	1.801735	0.506826	4.753655	184.2176	130.3858	201.9632
2006QK33	59000	2.658216	0.601196	14.87103	150.5888	192.917	63.42804
2019PO1	59000	1.03582	0.061021	1.120919	328.2711	250.2724	7.879422
2000SZ162	59000	0.928848	0.167738	0.888922	12.55323	132.9187	213.0981
2004FY3	59000	1.975047	0.55736	5.427637	359.5287	128.952	312.4115
2012XL55	59000	1.721762	0.644904	2.37763	77.26966	89.83772	90.08017
2019FB1	59000	1.76131	0.450874	3.853004	12.97058	203.6235	170.7952
2017DB120	59000	1.984321	0.405009	3.498765	201.3173	12.1463	36.49962
2017HJ	59000	1.293348	0.505684	1.207253	28.10444	83.45502	82.08233
2019SG1	59000	2.425314	0.695888	2.373009	183.6504	245.2629	54.38837
2015FH37	59000	1.328878	0.553026	10.26865	8.849606	276.1265	102.3806
2019WU	59000	2.333307	0.611216	0.650499	73.1659	28.97276	44.03769
2011UR63	59000	2.238683	0.593659	4.066868	207.8655	132.0317	216.2203
2016PR66	59000	2.175382	0.446669	5.559312	193.373	74.8448	84.4669
2008VL	59000	2.421026	0.615995	2.684319	216.4662	143.5098	35.48684
2019NL4	59000	2.044506	0.578617	7.366054	285.7882	300.7131	125.6598
2014WE6	59000	0.968924	0.13625	0.339066	52.56827	251.5907	24.01925
2014HY198	59000	1.083659	0.194966	2.613038	227.0161	77.96281	78.75737
2011EL40	59000	2.447655	0.704481	1.347794	187.2354	269.1377	162.1667
2016NJ56	59000	1.254533	0.141304	3.286489	252.3771	6.153288	295.9923
2008KT	59000	1.01109	0.084802	1.984116	240.5944	102.1656	202.2771

2008VS4	59000	1.966073	0.458296	1.279488	194.9648	213.0204	70.93524
2019AF14	59000	1.580112	0.118085	27.7399	87.57962	72.16235	216.8237
2014HV2	59000	2.043754	0.571276	4.293917	39.41587	229.6341	17.59486
2014HB177	59000	1.11476	0.194836	3.465345	45.32547	251.6231	5.129483
2015HO182	59000	2.689037	0.620472	1.659087	314.3608	207.4239	67.30241
2016DY30	59000	1.116735	0.51069	0.753292	157.9087	249.5898	267.591
2005GQ33	59000	2.336547	0.729751	1.547856	73.58353	36.57135	103.865
2015HQ182	59000	1.10763	0.229079	3.540385	241.1233	162.0132	294.7608
1993HP1	59000	1.99551	0.508995	7.996678	36.89809	152.1242	230.1481
2015EG7	59000	1.976082	0.566738	0.163587	175.5405	57.25152	300.1185
2016WR55	59000	1.615256	0.532487	5.255674	66.46458	69.07949	232.8799
2016FC1	59000	2.062459	0.638815	1.246949	352.2138	112.5883	167.0236
2019NX5	59000	0.917244	0.116179	0.457593	112.201	355.18	185.4338
2016JO38	59000	1.429555	0.344657	1.702399	4.55192	311.8102	84.22497
2017DP109	59000	2.36054	0.612377	3.019188	162.1192	39.28756	314.2904
2018WE	59000	1.804711	0.548476	0.06842	292.5882	182.8399	210.5944
2009WZ53	59000	1.138364	0.24228	32.76046	61.54931	111.4776	152.8643
2018EL4	59000	1.063948	0.197348	3.18132	168.5321	270.9506	75.85914
2004ME6	59000	2.414432	0.586426	9.547755	112.0223	210.427	74.83521
2019KT	59000	2.43475	0.615709	1.074488	72.81371	210.6033	88.35349
2010XB73	59000	5.520049	0.794872	2.412583	221.1321	231.8007	255.762
2016TQ54	59000	0.942734	0.289335	1.366825	7.720992	243.589	85.40039
2016VF18	59000	2.814064	0.685045	0.779436	229.6885	136.326	277.3042
2017YM14	59000	2.37499	0.70597	2.34526	278.8187	102.2065	250.4241
2018WA3	59000	1.819634	0.597368	4.51394	66.51853	287.1631	238.7572
2020DG4	59000	1.309943	0.313749	0.598508	166.3361	291.2548	94.26589
2015VN64	59000	1.841545	0.590727	3.641454	223.3027	108.1788	316.2484
2019CM5	59000	1.637728	0.40038	0.400548	115.6177	11.94788	228.9926
2018TS6	59000	0.898385	0.214078	8.915905	189.688	46.04357	95.4015
2010CK19	59000	0.986846	0.150067	2.256151	328.5373	278.9102	93.71206
2014KS76	59000	0.928184	0.270498	1.09612	62.2856	51.33941	4.172362
2019TD	59000	1.879673	0.501006	3.242011	186.6125	143.5667	104.2048
2003YS70	59000	1.287647	0.23686	0.353448	271.3675	195.8489	80.33746

2018ST1	59000	2.43481	0.628536	3.678166	189.0209	214.4322	151.4496
2019VE4	59000	2.433974	0.592321	0.561858	221.1088	155.3533	59.43517
2016JN38	59000	1.925807	0.683042	4.443731	41.89862	89.75742	207.6667
2014HJ197	59000	1.021601	0.166488	0.826527	214.5687	255.7083	51.97233
2017WE29	59000	2.303219	0.528573	0.485579	270.7776	122.5705	267.0819
2004FM4	59000	2.020713	0.595585	2.697453	185.205	290.0448	242.7019
2018PA25	59000	1.353498	0.532979	11.33111	132.4208	78.99643	94.41571
2020AC1	59000	0.859884	0.219723	6.002142	282.4723	38.41121	307.2727
2019BB5	59000	0.83585	0.276104	1.542724	335.3118	307.9999	131.7557
2018RJ3	59000	1.32876	0.306492	6.093964	165.4315	129.0077	73.2394
2016BE	59000	1.819288	0.469332	9.697355	314.7548	199.0172	267.8485
2017KH5	59000	1.770929	0.548095	7.847066	65.09195	245.4132	81.4661
2018BH1	59000	2.216103	0.618367	0.26798	38.019	7.204779	275.423
2007EE126	59000	3.316767	0.893985	8.375953	169.3505	249.8137	73.94562
2013NR13	59000	2.050613	0.528554	5.539635	113.3502	135.2509	135.516
2011CF22	59000	1.719376	0.618604	1.046449	138.0606	276.1916	67.96318
2013CY	59000	1.114045	0.134182	0.780427	302.5753	149.5757	114.3735
2019UB8	59000	1.533174	0.448509	0.20551	54.7414	39.30179	89.11465
2006DO62	59000	1.83419	0.488763	1.381839	334.6157	216.3234	255.1737
2019WV1	59000	1.275821	0.328245	0.740137	64.48955	290.2426	164.9424
2007VJ3	59000	2.126848	0.615795	12.70104	36.97338	300.0606	32.42404
2016GS134	59000	1.868326	0.532054	0.089769	44.61854	96.86939	240.9561
2017KB3	59000	1.078724	0.203927	18.96167	58.86317	76.2441	331.0828
2010VO139	59000	2.069182	0.70335	7.72281	229.7323	92.35761	89.94665
2017RX17	59000	1.965605	0.660378	4.133259	345.5294	275.6612	14.14557
2019BX1	59000	1.268701	0.231672	3.087441	111.3522	337.7662	2.042616
2014UY57	59000	2.349488	0.583886	0.208399	64.49605	299.7503	203.9962
2019GP21	59000	1.698883	0.493988	0.333525	197.1702	298.5855	207.495
2009WQ52	59000	2.558242	0.665493	5.610249	60.03962	50.67156	194.1921
2014LJ	59000	1.078516	0.1389	1.052711	78.16773	91.84375	192.4857
2009VT1	59000	1.984884	0.503073	0.268714	216.943	178.454	282.4575
2017XY2	59000	1.043814	0.170814	12.13349	261.7844	263.98	46.26311
2020CW	59000	1.094261	0.613764	5.894599	131.9029	120.0337	56.90931

2020NY	0	0	0	0	0	0	0
2015DD54	59000	1.958203	0.492846	0.950165	349.3237	178.9483	328.062
2008TS10	59000	1.257524	0.201562	1.45665	5.453926	345.7755	108.6055
2016WT	59000	1.555131	0.446825	1.188265	55.82482	304.3529	316.7548
2005UC3	59000	2.177875	0.543315	0.240769	28.02667	328.9643	204.298
2015KH160	59000	2.718706	0.869703	9.010946	241.0085	247.311	53.52084
2017RJ2	59000	1.961522	0.621527	1.560453	176.3512	248.3563	337.7022
2019VB5	59000	1.018751	0.203725	0.310884	54.99957	85.66824	124.3329
2015HE1	59000	1.423519	0.492662	3.467685	212.2032	79.23434	332.7319
2016HF3	59000	2.060185	0.49997	6.190123	58.79102	185.4886	129.056
2019QB1	59000	2.076678	0.561375	2.676467	327.1181	316.1287	104.6197
2005CM7	59000	1.719496	0.632357	4.896823	136.2606	270.824	320.56
2016FV7	59000	2.034374	0.876971	10.14209	13.76826	303.7193	142.4548
2013XS21	59000	1.914017	0.494823	3.080076	80.40895	341.1526	164.3003
2011EM40	59000	1.150624	0.371419	0.555358	173.9193	263.1131	221.5429
2017UL5	59000	2.263945	0.562656	3.399091	30.97668	348.0634	278.0552
2020GY2	0	0	0	0	0	0	0
2018CN	59000	1.824889	0.661546	3.549412	321.0879	263.5426	318.6178
2017UF	59000	2.538831	0.769522	0.577017	23.55071	271.0121	244.3064
2008CM74	59000	1.089024	0.1468	0.854806	321.4911	242.8137	248.1801
2007FP3	59000	1.413333	0.403625	0.236049	352.2222	119.8593	337.7919
2015VL64	59000	0.908822	0.28841	0.71332	51.57684	225.4098	192.9802
2005VP	59000	2.3551	0.592837	5.507293	222.779	134.0274	21.7075
2016UQ36	59000	1.807246	0.508756	4.666761	211.4285	132.7412	187.4683
2016WF7	59000	0.873455	0.238046	0.646755	76.30141	208.5848	226.4437
2016FE15	59000	1.439296	0.465904	0.454891	17.4335	96.84148	178.6154
2017WY27	59000	1.076452	0.246924	5.201301	243.0168	90.57904	150.859
2008KN11	59000	1.709243	0.529022	5.272014	89.36664	246.0481	103.7164
2018GD2	59000	1.031642	0.173836	9.672212	22.24546	271.0091	302.221
2018FG1	59000	1.073621	0.295496	6.54688	1.023321	271.6094	291.0227
2013GW38	59000	2.004833	0.546419	2.30135	18.11919	137.3144	196.9939
2017UK52	59000	1.29809	0.437582	2.38433	227.028	71.09922	315.9958
2014HD198	59000	2.102848	0.641917	0.985721	220.2675	69.61524	343.9967

2009ST171	59000	2.576561	0.608516	3.743939	186.5455	205.9694	202.3207
2019TN5	59000	2.348728	0.617	0.798333	190.8682	138.5958	73.72499
2010YD	59000	2.042455	0.538325	0.438656	93.92363	39.7581	72.68434
2015FU344	59000	1.746656	0.488653	0.89555	176.4146	311.7304	107.8452
2007WT3	59000	2.360845	0.720319	5.177661	226.7092	103.1083	179.2335
2015PS228	59000	1.056719	0.083902	0.438889	272.8024	327.4983	220.3678
2017BE30	59000	2.239486	0.664466	5.942206	304.7828	110.3627	11.46305
2019QS	59000	2.443507	0.770731	4.11736	163.3295	261.8869	59.63319
2014KC45	59000	1.517884	0.394952	0.039694	109.0253	185.7981	55.99329
2020DN3	59000	1.574542	0.526172	2.079696	337.0893	103.5819	72.30028
2018GN	59000	2.424529	0.735408	1.595512	25.05636	255.6389	192.5498
2017UL6	59000	1.100849	0.254609	3.153502	214.7262	262.0504	32.89983
2017UW5	59000	2.512441	0.663919	3.255695	208.7921	127.418	244.4324
2020GV2	0	0	0	0	0	0	0
2016XL23	59000	2.101431	0.5577	1.865732	248.8886	145.5947	61.37793
2017TU1	59000	0.794538	0.436452	0.409186	328.6272	196.4706	149.3908
2014EU	59000	1.292611	0.280577	0.330485	186.6035	288.8395	115.5348
2016EL1	59000	1.788424	0.658124	4.012426	165.036	87.1907	258.4713
2014WC201	59000	1.198057	0.389766	2.029854	253.5509	261.7834	24.5335
2019LA2	59000	1.126183	0.33505	20.45895	251.4287	268.0948	353.6331
2020FG	59000	2.372901	0.649372	1.824486	182.9375	50.02304	9.764325
2009QR	59000	1.342752	0.267149	3.419807	150.4769	209.7006	315.7848
2016JG38	59000	1.555081	0.436787	3.494352	29.45868	288.1332	350.7828
2019YA3	59000	0.939396	0.269387	1.5431	257.6566	62.25756	275.8956
2020FU2	59000	1.926463	0.565593	5.6719	1.019355	121.7256	41.29465
2014KW76	59000	1.682394	0.561226	2.335239	67.44786	102.0169	293.972
2019RQ2	59000	2.743844	0.714605	0.437387	335.9003	79.50496	47.46536
2018WA1	59000	0.872329	0.139164	1.81196	233.4222	8.374095	128.4207
2010XU	59000	1.331343	0.29423	0.706463	324.4489	49.29095	95.41272
2015JC1	59000	1.393896	0.518919	6.376953	231.7696	266.8701	60.34394
2016TG94	59000	1.69812	0.446126	1.210103	198.6816	140.135	245.6848
2019SO6	59000	2.319188	0.832922	1.105502	4.99651	241.1615	82.85653
2014QJ365	59000	1.619951	0.478161	1.343945	155.3742	115.981	307.7722

2011CF66	59000	1.023062	0.311369	1.018937	338.2085	274.6484	278.6214
2012WR10	59000	1.085313	0.111599	0.307653	224.2208	146.878	274.2819
2015SK7	59000	2.373489	0.619719	2.377398	359.5596	317.0704	110.2382
2017FB102	59000	2.01987	0.520095	5.618857	179.6786	332.9615	48.29164
2014OP2	59000	2.45556	0.618677	2.05126	122.2895	141.5576	195.0666
2010GV23	59000	0.92959	0.203063	3.622837	198.5007	233.8143	220.4031
2010RK53	59000	1.346892	0.31365	6.092204	346.0604	311.0065	105.5568
2017VF14	59000	1.456966	0.445011	0.441166	65.35104	279.8736	187.0465
2020KS	0	0	0	0	0	0	0
2017FW158	59000	2.350617	0.664469	0.080325	8.400676	107.6869	330.8858
2020AR1	59000	1.780702	0.48366	0.211393	344.8771	162.2165	47.09439
2015FC345	59000	1.270293	0.273442	0.522077	178.7571	60.38765	190.8359
2010XQ	59000	2.749464	0.634499	7.232346	73.40454	12.09808	26.03168
2012UE	59000	1.886889	0.572491	1.167222	27.75592	60.29602	320.6079
2016FA14	59000	1.801938	0.586464	4.263827	189.6415	286.4203	279.5794
2020BY1	59000	2.034036	0.637657	4.646567	297.5402	108.4944	60.43612
2016BQ15	59000	2.090656	0.696297	0.932904	135.1538	87.91465	138.2147
2019VA	59000	2.159733	0.552235	2.026205	220.47	200.7458	60.03875
2017UQ7	59000	1.08253	0.419525	8.516133	209.9433	74.49371	167.5548
2020FD	59000	1.212068	0.486333	1.174753	358.0685	278.0692	12.03044
2012DY13	59000	1.459117	0.573599	2.832936	151.0843	269.4431	278.7049
2016TH	59000	1.037576	0.259473	2.324866	191.517	276.0847	97.93906
2017YE8	59000	1.353714	0.457226	10.50058	93.55617	279.8845	229.5289
2019EH1	59000	1.382591	0.487447	0.603304	340.2003	262.8894	244.8898
2018BX5	59000	1.316815	0.332866	0.092817	164.9928	259.2419	230.3636
2014WR362	59000	2.231237	0.593318	9.148342	239.628	142.7029	243.936
2019DM1	59000	2.337064	0.694326	0.614364	350.5899	95.66739	138.4548
2019YV4	59000	2.575097	0.740118	3.634585	94.55891	283.5156	47.51308
2015XH55	59000	1.047048	0.21187	5.188828	70.71295	268.6271	136.4519
2020HV5	0	0	0	0	0	0	0
2004OD4	59000	2.038063	0.514468	4.359517	294.6051	336.086	171.2276
2017WF30	59000	1.337168	0.314463	1.027171	285.004	199.3984	191.4203
2017TD6	59000	1.194203	0.332183	1.915969	26.83066	77.75244	317.1073

2019QF	59000	2.437356	0.60495	2.197174	150.7686	145.3518	79.90684
2019JZ2	59000	1.413573	0.617232	13.77493	223.7751	257.3987	261.2087
2019JK	59000	1.983774	0.632893	13.5515	219.7204	286.4679	156.0082
2006BO7	59000	1.435916	0.4033	0.340421	294.6881	248.0704	97.45708
2013UJ5	59000	2.311001	0.597306	0.335804	190.7527	162.6886	323.986
2014DK10	59000	1.821537	0.507591	11.54481	152.6243	315.9279	211.642
2019DF	59000	2.375021	0.652124	2.874714	156.8237	55.49281	113.7615
2006YE	59000	1.744757	0.440365	0.32177	252.7379	211.3108	293.8125
2019WH4	59000	2.507551	0.60433	3.52635	243.4305	197.2585	42.68506
2018BQ6	59000	1.945595	0.523743	4.418853	132.1419	34.29071	299.3908
2010UE	59000	2.821072	0.728825	3.156368	22.91522	296.6301	19.60803
2011AZ36	59000	2.000243	0.467199	1.291676	244.4756	209.2447	119.6433
2017UM52	59000	1.035212	0.060187	2.982131	30.03153	73.39166	103.3642
2007BB	59000	0.933878	0.140779	3.533501	297.6591	300.9873	192.7834
2018DU1	59000	0.887089	0.233792	1.163409	344.1767	309.2683	137.6692
2011UA64	59000	2.276545	0.621239	6.367644	28.98993	303.7187	194.2283
2016EP84	59000	1.190479	0.173307	0.819294	287.4736	195.4639	124.199
2003UM3	59000	1.371166	0.440299	1.50721	17.70901	284.6656	162.2943
2015FN36	59000	1.901584	0.712934	9.040225	357.7571	81.36385	11.622
2018LD1	59000	1.845763	0.508855	0.226369	31.56088	279.0121	267.1712
2016AZ193	59000	0.933155	0.248128	0.343578	127.5658	201.5445	71.03856
2012TP20	59000	1.386908	0.32628	0.651705	207.9594	117.4929	269.8089
2012RU16	59000	2.475433	0.618067	0.386642	309.7751	359.2065	357.3414
2008US	59000	1.549647	0.595915	6.141797	207.694	90.49386	32.15772
2018BP3	59000	1.149947	0.257995	1.420851	306.9343	103.3494	12.61106
2020HN3	0	0	0	0	0	0	0
2014MG68	59000	2.182457	0.575524	1.836352	273.0831	65.37974	286.8228
2015HD1	59000	2.308964	0.645416	5.338972	210.901	57.74865	153.4593
2009XQ2	59000	1.169538	0.565606	6.794554	270.9866	282.6941	54.44958
2011FQ16	59000	2.126307	0.529315	1.428832	186.446	334.6233	352.6174
2008CB6	59000	1.602472	0.406871	0.309366	240.2003	300.6623	8.947995
2007VD8	59000	2.287788	0.594998	3.161614	43.09401	319.3992	232.9216
2019KY3	59000	2.274477	0.656192	3.294855	73.96793	241.7507	92.32152

2019BV2	59000	1.314118	0.499715	0.655098	134.7827	82.13807	284.2403
2018DB	59000	1.57739	0.555405	0.26304	54.18177	177.3329	28.57264
2020FM1	59000	1.136672	0.264916	1.842704	358.519	98.30401	112.1958
2017VC14	59000	2.051177	0.568224	2.456035	234.6413	225.1962	298.9315
2008EL68	59000	1.018271	0.04626	0.905274	352.1657	260.7093	253.5474
2019JY2	59000	1.089189	0.272698	0.983607	226.484	268.003	38.54695
2008UY91	59000	2.285436	0.676883	31.60824	213.7048	266.721	110.9085
2017JB2	59000	1.020536	0.051229	5.232156	222.8554	279.4479	69.66522
2012BN123	59000	2.548035	0.573199	8.931683	103.7025	350.7241	24.03884
2004XO63	59000	2.526626	0.617559	1.92336	264.6782	184.2755	296.418
2017FX158	59000	1.777963	0.468687	5.167362	178.8891	327.1303	136.685
2020KD1	0	0	0	0	0	0	0
2009XR1	59000	1.607021	0.400591	0.432524	256.8435	210.6412	39.73943
2020KU2	0	0	0	0	0	0	0
2013VJ13	59000	1.861474	0.582402	10.21542	37.57738	292.15	230.0829
2016TM	59000	1.152403	0.168744	0.36771	350.7926	327.8967	21.52346
2009EJ1	59000	1.599717	0.474543	0.024473	309.831	151.3082	223.8573
2019QD	59000	2.350103	0.653336	2.993609	149.7114	238.332	66.39834
2018XX3	59000	1.031979	0.125039	4.257131	260.3566	101.5506	207.9916
2019JX1	59000	1.008131	0.400086	17.02661	221.6135	246.2745	91.51024
2007XB23	59000	1.041276	0.054318	8.530112	260.2655	193.0466	252.1003
2019JH7	59000	0.991184	0.292426	0.845983	56.55275	288.7067	303.1899
2016VZ17	59000	2.129688	0.554158	1.603598	249.249	117.0461	62.66937
2006WV	59000	1.530352	0.533246	2.157927	56.60775	80.64917	18.94011
2017SA21	59000	2.31244	0.582655	4.223355	185.4215	152.3054	279.494
2018WG2	59000	1.107667	0.237646	0.816504	63.58891	79.99764	52.31493
2012GD	59000	1.968012	0.508511	0.528549	80.65129	152.5627	332.0956
2008UM1	59000	2.494979	0.703633	5.214727	207.3515	116.1968	345.8019
2017YE7	59000	1.811292	0.670066	4.345195	279.0162	268.8735	337.8643
2020KJ4	0	0	0	0	0	0	0
2016JA	59000	1.014579	0.269279	0.049512	12.17845	98.94552	80.0253
2018XW3	59000	1.443641	0.454999	2.546202	255.7421	110.6043	333.5433
2018CK	59000	1.83091	0.577471	3.413544	311.5705	112.8526	355.4188

2016LE10	59000	2.419514	0.61954	3.246193	257.337	42.22862	12.04146
2011AZ22	59000	2.044962	0.576172	7.387484	109.4055	312.438	85.47122
2020BA13	59000	1.899243	0.519078	5.648865	127.2655	321.3976	57.69879
2010VR139	59000	1.43382	0.301713	0.369763	155.8483	232.0285	213.2618
2018LE1	59000	1.022397	0.205819	1.804837	245.4256	262.1424	55.45589
2009SD15	59000	2.341116	0.620899	2.903191	356.4943	304.2917	6.950748
2009VZ39	59000	1.42196	0.349263	3.010197	51.94159	39.57286	59.6019
2016NC56	59000	2.169005	0.616529	5.540071	289.1399	296.5896	91.97556
2010UZ7	59000	2.199127	0.630636	5.449047	208.359	113.7785	354.0384
2016AQ164	59000	1.915586	0.577624	5.301331	289.7252	120.8974	250.6866
2019AK12	59000	1.704081	0.541912	11.94249	113.5945	292.7605	242.7058
2019UX12	59000	1.014666	0.26717	8.594924	212.9672	77.62891	280.7863
2019UN8	59000	2.580184	0.723991	0.354353	18.39849	300.0054	62.39183
2008JD33	59000	2.14952	0.549433	2.962078	73.56751	121.0855	306.4965
2012CS46	59000	1.266768	0.278318	0.491471	218.2736	348.7783	256.9354
2011AD3	59000	2.757215	0.679011	1.611484	295.3153	122.1675	21.25417
2015HE183	59000	2.187872	0.617601	3.123814	213.3833	299.9943	220.4896
2019ED	59000	0.891382	0.124499	1.141454	135.8736	215.741	339.4161
2016UR36	59000	2.049536	0.669757	0.455976	18.5805	97.45682	64.32252
2016YY	59000	2.6125	0.666642	10.3739	82.15611	308.1417	303.9081
2020BY11	59000	1.935798	0.565786	1.789665	306.7948	122.6969	60.66762
2017UQ6	59000	0.943754	0.109554	0.59053	333.3554	229.7789	130.4713
2010XC	59000	1.423578	0.320717	1.193449	247.8581	213.079	197.2476
2017YK14	59000	1.205466	0.180338	2.9304	273.7148	182.6039	299.1454
2012BP123	59000	1.122148	0.155748	2.595117	148.5184	272.9512	54.67754
2019SE11	59000	2.191529	0.514027	8.537151	177.9307	197.5312	71.58324
2020DM3	59000	2.560999	0.680849	5.366185	335.0613	240.4006	13.18297
2008JL24	59000	1.038226	0.106595	0.550684	225.7383	282.0451	212.9592
2007VF189	59000	1.206848	0.385165	6.980616	51.79893	83.58029	122.5347
2019TP5	59000	1.894169	0.661818	8.779566	204.9811	262.0751	67.60657
2020HY8	0	0	0	0	0	0	0
2019SQ8	59000	2.321994	0.672123	2.91547	39.96564	235.9315	87.25343
2020MA1	0	0	0	0	0	0	0

2008XK	59000	2.324881	0.613984	5.574721	75.02834	40.87331	79.22284
2008YD3	59000	2.266596	0.541316	0.303331	133.7727	315.5463	127.9916
2013EC20	59000	1.112255	0.12086	1.303563	165.6544	33.25736	37.49133
2018KY2	59000	2.026132	0.549728	7.416871	65.47431	223.1459	239.9408
2011CA7	59000	1.079936	0.288296	0.118765	306.8289	282.98	44.33831
2009EH1	59000	1.174175	0.350427	0.989033	156.7493	94.71878	252.4665
2010XP	59000	2.9754	0.664982	1.71659	78.17488	17.01883	298.7321
2019FT1	59000	2.044709	0.551873	4.517394	183.2896	316.6141	157.1017
2014HM199	59000	2.03861	0.408228	4.578916	14.94819	174.2743	46.44666
2014HK197	59000	1.927482	0.566556	5.004013	31.53668	254.285	80.39063
2014HN2	59000	0.926457	0.11823	1.234462	198.8946	207.3068	106.7788
2008VB4	59000	2.35241	0.614539	0.065891	188.4563	172.1889	84.26869
1993KA2	59000	2.229005	0.77042	3.154766	236.4117	264.6193	60.68933
2008UC202	59000	1.01086	0.068665	7.451489	37.32246	91.88009	67.22956
2019SM8	59000	1.532499	0.518724	4.644081	188.5564	256.037	100.004
2018XF2	59000	2.502873	0.618584	0.968046	254.7095	151.739	139.8384
2015RU178	59000	2.29406	0.682382	6.2485	167.7764	106.7956	142.1338
2014JU79	59000	1.209539	0.241675	5.958137	356.7005	54.08176	21.47833
2019SU2	59000	2.360272	0.606853	0.93179	179.2145	141.3928	76.32057
2017FA159	59000	1.389032	0.318321	0.582193	136.6228	85.29615	321.3886
2012EZ1	59000	2.002817	0.596758	0.501271	153.6257	308.2527	340.6044
2017TT3	59000	1.447388	0.370803	0.707317	95.14303	220.2529	214.4684
2005TK50	59000	1.918624	0.621844	4.876812	15.95129	74.11584	166.9869
2016JY5	59000	1.087238	0.211215	4.634823	220.282	277.5311	275.4556
2020KC5	0	0	0	0	0	0	0
2017SG33	59000	2.0805	0.456455	5.143955	188.9866	116.6247	341.2159
2016FF14	59000	1.752938	0.486083	1.346837	12.37785	129.7015	302.1289
2017BK30	59000	2.615756	0.632813	1.189927	140.744	24.18431	277.2932
2020FP5	59000	1.27555	0.293055	5.348252	182.6582	304.3104	78.34663
2016QY84	59000	1.163185	0.154364	1.975414	162.2557	128.5346	30.74073
2019TJ5	59000	2.60299	0.647696	2.692669	18.90529	316.6165	62.03063
2015KW157	59000	3.613187	0.677579	3.703564	52.76779	162.3305	266.8596
2005WN3	59000	2.694085	0.746655	0.282315	239.9557	256.0472	93.56619

2017UK1	59000	1.0437	0.202604	7.334109	199.911	88.67157	237.142
2014WU200	59000	1.027986	0.07151	1.266385	265.6933	226.5062	43.16501
2016WQ1	59000	1.805232	0.467547	0.23426	230.0987	160.7124	171.9526
2014HE197	59000	2.161761	0.587524	3.193506	185.1008	102.7326	311.7283
2013RZ53	59000	1.016232	0.027407	2.128214	343.0715	65.24722	156.7691
2019SK9	59000	2.525311	0.69145	3.301479	4.08641	295.4169	70.90839
2019GC6	59000	1.103517	0.174875	1.25352	211.5604	63.87075	297.3626
2016EN157	59000	1.94533	0.565478	4.867759	170.6285	305.5173	214.061
2016EU84	59000	0.920578	0.095091	3.198318	169.0963	206.1116	70.97454
2019CY1	59000	1.572007	0.49494	1.91732	322.9406	254.9827	210.0789
2015PL57	59000	1.120489	0.144108	1.63061	112.6278	115.2639	92.29223
2014HC196	59000	2.485809	0.567393	3.675982	47.77042	116.8111	211.9155
2010SK13	59000	2.455561	0.71436	1.045981	0.970315	80.85643	175.5048
2019GK3	59000	1.10965	0.138479	1.707651	194.184	304.485	39.24769
1994ES1	59000	1.408882	0.586971	0.896229	352.6228	279.3492	212.0732
2017UJ2	59000	1.12172	0.183578	0.524801	28.31732	297.4652	115.0803
2018YO2	59000	1.232994	0.21708	0.996123	94.04737	334.9365	31.40705
2011SL189	59000	2.347554	0.566802	1.383285	347.4823	63.49279	135.5657
2020LO	0	0	0	0	0	0	0
2017WW1	59000	1.497787	0.457577	9.664089	59.72764	63.8679	111.0543
2014UU56	59000	1.10277	0.262643	0.321587	201.3997	100.9807	359.3172
2016AF2	59000	0.885012	0.213921	0.586479	46.8141	275.9277	225.131
2019UO8	59000	2.191441	0.778411	0.319574	41.41296	250.4446	80.02483
2014OQ392	59000	2.427247	0.467192	6.55555	81.59382	247.2654	190.0703
2016DB	59000	0.891475	0.324662	2.887674	146.3853	232.8989	126.4997
2019SX8	59000	1.529198	0.382498	4.874012	186.1303	140.8345	144.2638
2018DO3	59000	1.788501	0.572928	4.399151	148.2887	284.3419	4.414506
2017FW128	59000	1.320994	0.274417	0.644082	56.55336	179.6951	5.238704
2008WJ14	59000	3.787765	0.703532	12.55083	233.5637	183.3827	215.1493
2007WW3	59000	3.195231	0.667121	6.496193	51.0335	344.4106	69.37557
2017WE30	59000	1.946694	0.649288	3.434926	64.64386	77.10336	316.1673
2019UN13	59000	1.449408	0.421973	1.504694	217.5084	241.7858	94.36101
2014WZ365	59000	0.788658	0.42802	1.33968	261.7022	321.3881	179.3796

2010VP139	59000	1.204801	0.3067	2.692122	48.78463	290.1007	120.4337
2018AT2	59000	1.868792	0.479	4.059202	110.2895	344.4476	340.5849
2011BH40	59000	2.015959	0.718654	3.296337	109.9485	119.7046	75.06844
2017KJ32	59000	0.906469	0.134656	2.178339	238.8187	207.7898	329.2271
2003SQ222	59000	1.504314	0.518238	3.556075	4.384091	280.9002	40.44749
2017BF136	59000	1.095135	0.49743	27.69799	131.3934	111.9012	272.2324
2015KH158	59000	2.018481	0.52284	4.945962	251.8385	42.79062	254.7835
2016PA79	59000	2.667162	0.561388	1.038954	1.317893	323.2732	314.2615
2016VH	59000	1.353754	0.2731	2.727741	211.7505	158.2769	113.6309
2019EF	59000	1.514414	0.589386	7.850208	159.1311	269.7491	269.0501
2008EK68	59000	1.476496	0.393255	3.929387	344.0539	129.6438	316.8583
2020DW	59000	0.859735	0.168988	0.063473	89.42448	216.6281	338.138
2014HR197	59000	1.599807	0.588775	3.177964	30.98152	277.8876	336.2198
2019SU1	59000	1.011638	0.088291	7.749159	352.928	259.9701	339.271
2020HM6	0	0	0	0	0	0	0
2016TB57	59000	1.102215	0.123156	0.298361	294.8246	147.8367	359.0346
2019VS4	59000	2.029994	0.513082	3.499122	223.3316	188.7937	67.97506
2015HZ182	59000	1.669553	0.395012	4.4262	211.7156	303.3087	156.5827
2020BA15	59000	1.58211	0.468752	9.334719	127.9493	302.4995	81.54234
2019TX	59000	1.35868	0.329118	1.500274	10.64557	51.09569	123.1279
2009SH1	59000	1.195672	0.244091	3.29188	354.5761	295.3909	106.2717
2020DV	59000	2.338536	0.59683	0.37177	238.5109	225.607	38.14824
2018PV24	59000	1.076137	0.221471	3.629523	142.229	269.7575	153.5034
2018DP3	59000	1.524399	0.301997	3.670269	147.5359	24.14415	64.52903
2012WQ3	59000	2.365427	0.773567	3.265112	51.20118	271.9579	36.15036
2020HE7	0	0	0	0	0	0	0
2017CY32	59000	2.106594	0.656297	3.788466	132.1301	72.72326	17.31367
2018WE1	59000	1.096125	0.358733	6.272625	242.7251	84.43295	169.1061
2020AY1	59000	0.88048	0.221915	1.03032	31.58705	294.9741	293.4327
2019BZ3	59000	2.295255	0.580824	10.64354	127.3584	338.4258	143.3795
2010WW8	59000	1.472279	0.313119	1.786362	252.2848	178.7078	112.2595
2017RW17	59000	1.972524	0.585638	0.970344	173.1572	241.8974	336.1042
2017BD6	59000	2.295707	0.584089	5.040427	125.573	335.5449	351.2824

2017VN2	59000	0.894739	0.206001	1.39029	251.908	295.813	243.6097
2016VR4	59000	2.448877	0.610622	6.164323	47.54864	330.4524	340.1594
2018TT6	59000	1.197992	0.201116	5.955695	192.0361	225.0883	63.17393
2019AS5	59000	1.34794	0.392301	0.701429	106.748	294.3618	350.7051
2016CO248	59000	0.932803	0.160326	4.771755	139.8805	240.0553	23.97833
2019HR2	59000	1.245347	0.325625	0.648714	32.14177	110.0583	324.5855
2015HM182	59000	1.192534	0.207777	2.760487	220.6821	277.8177	22.9185
2017YD2	59000	0.845007	0.316108	1.90796	277.4942	313.7755	297.6392

Table B-2: PHAs with their Keplerian Elements

It can be noticed that for some asteroids (41 out of 1060), the Keplerian elements are mentioned as zero. This is because of a lack of information in [21]. However, this lack of data for the said asteroids do not have a profound effect on this thesis.